UNIVERSITY OF OKLAHOMA

GRADUATE COLLEGE

# SUBSURFACE AND OUTCROP ORGANIC GEOCHEMISTRY OF THE EAGLE FORD SHALE (CENOMANIAN-CONIACIAN) IN WEST, SOUTHWEST, CENTRAL, AND EAST TEXAS

A DISSERTATION

SUBMITTED TO THE GRADUATE FACULTY

in partial fulfillment of the requirements for the

Degree of

DOCTOR OF PHILOSOPHY

By

ANDREA ANTONIETTA MICELI ROMERO
Norman, Oklahoma
2014

SUBSURFACE AND OUTCROP ORGANIC GEOCHEMISTRY OF THE EAGLE FORD SHALE (CENOMANIAN-CONIACIAN) IN WEST, SOUTHWEST, CENTRAL, AND EAST TEXAS

A DISSERTATION APPROVED FOR THE
CONOCOPHILLIPS SCHOOL OF GEOLOGY AND GEOPHYSICS

BY

_____
Dr. R. Paul Philp, Chair

_____
Dr. Deepak Devegowda

_____
Dr. Arthur D. Donovan

_____
Dr. Roger M. Slatt

_____
Dr. Michael J. Soreghan

*To Alessandro and Oswaldo*

## Acknowledgements

I would like to express my sincere appreciation to Dr. R. Paul Philp, my research advisor and committee chairman, for all his time, guidance, mentoring and support throughout the past seven years, and particularly during these last four years of my PhD research.

I also would like to thank the members of my committee, Dr. Deepak Devegowda, Dr. Arthur D. Donovan, Dr. Roger M. Slatt and Dr. Michael J. Soreghan for their encouragement and support, and for their time and valuable suggestions in reviewing this manuscript.

I wish to extend my gratitude to BP America, especially to the Global Unconventional Exploration & Resource Access Team for providing the main financial support for this project and for considering me to participate in this multidisciplinary research. I also gratefully acknowledge the Oklahoma Geological Foundation for awarding me the Suzanne Takken Memorial Award, and to the ConocoPhillips School of Geology and Geophysics for awarding me the Student Research Grant. These contributions significantly supported this research.

My sincere thanks to Dr. Stephen C. Ruppel and Mr. James Donnelly from the Core Research Center at the Bureau of Economic Geology in Austin, Texas for providing part of the core samples analyzed in this research. I also would like to thank Swift Energy, Encana Corporation, and Mrs. Andrea Cicero from Newfield Exploration Company who helped providing several core and liquids samples analyzed in the present study.

I want to thank Mr. Anthony McClain, Dr. T. Scott Staerker, Mr. Aris Pramudito, and Mr. Weiguo Li from BP America, and to Christopher Lowery and Matthew Corbett for their assistance in providing samples, for their help during field trips, and for the interesting scientific discussions. I also want to thank Mrs. Raquel Cepeda from BP for being a great mentor and friend.

Special thanks for Mr. Brian J. Cardott for training me in organic petrography, especially in vitrinite reflectance measurements, and for providing valuable data for this project. Thank you for your time, disposition, and patience.

I am deeply grateful with all the staff at the Organic Geochemistry Laboratory, especially with Mr. Jon Allen, who always had the patience and dedication for helping me in innumerable ways to successfully complete my laboratory work. I also wish to extend this acknowledgement to the rest of the staff at the laboratory, including Dr. Anh Do and Mr. Larry Hyde.

My deepest appreciation is for Dr. Thanh Nguyen. I will never be able to thank you enough for all the help you provided me during all these years. It has been an honor meeting you I am grateful for your invaluable contribution for this project. I admire your positive attitude, patience and dedication to teach.

I want to thank the staff of the School of Geology and Geophysics, for their assistance, kindness, and for always cheering my days. I also want to thank Mrs. Jody Foote, for all her help in the Youngblood Energy Library, and for also being a friend. I will miss y'all.

Thanks to my classmates and colleagues, especially to Kirellos Sefein for helping me from the distance and for his kind disposition to assist me when I needed it.

I want to thank my very dear friends Richard Brito, Norelis Rodriguez, Coralie Biache, Yoscel Shannon, and Gabriela Lugo for all their support and infinite help, especially during the course of this project.

I want to recognize and thank my parents, Gladys Romero and Francesco Miceli for their love, encouragement, and support. Thank you for being a great example for every aspect of my life. No se sabe ser hijo hasta que se es padre, ahora entiendo y aprecio mucho más todos los sacrificios que han hecho por amor a mi. Los amo.

My most special thanks are for my husband Oswaldo Davogustto, for his infinite patience, love, help, support, and sacrifice, especially during the past year. Thank you for your strength, and for always encouraging me and believing in me. Te amo. I also want to thank my son Alessandro for giving me the motivation to become a better person each day, for your amazing and innocent spirit, and for your beautiful smile, you are the greatest accomplishment of my life. This is for both of you.

I thank God everyday for these gifts, for his infinite kindness and for all the stones He puts in my paths.

# Table of Contents

# List of Tables

# List of Figures

## Abstract

A comprehensive organic geochemical analysis was performed to a suite of outcrops and core samples from the Eagle Ford Shale Group from West, Southwest, Central and East Texas with the aim of determining variations in organic matter source, thermal maturity and depositional environments. Oils and condensates produced from Eagle Ford Shale and San Miguel reservoirs were analyzed to determine the origin of these liquids. A total of 180 samples were subjected to total organic carbon (TOC) and Rock Eval analysis for geochemical screening, and one sample from each location was analyzed for vitrinite reflectance (%$R_o$). Rock samples with good source rock potential (TOC>1.0% wt.) were selected for biomarker and isotope analyses. These analyses were carried out by means of gas chromatography (GC), gas chromatography-mass spectrometry (GC-MS), and gas chromatography-isotope ratio mass spectrometry (GC-IRMS).

TOC and Rock Eval parameters show that the Eagle Ford Shale has excellent source rock potential and is dominated by Type II kerogen indicating a marine origin. Distributions of regular steranes, hopanes and monoaromatic steroids (MAS) point towards a marine carbonate depositional environment. Aryl isoprenoids suggest the occurrence of intermittent photic zone anoxia (PZA). In addition *n*-alkanes, steranes distribution, and the tentative identification of gammacerane suggest deposition under hypersaline conditions in West and East Texas. Biomarker parameters indicate that in East Texas the Eagle Ford Shale was partly sourced by terrigenous organic matter, reflecting the influence of the Harris Delta. Thermal maturity parameters indicate that the Eagle Ford Shale is immature to marginally mature in West and Central Texas, and

show a progressive increase in maturity increase towards the southeast following the regional dip. In East Texas, the Eagle Ford Shale is in the main stage of oil generation.

Geochemical logs show a minimal range of vertical variation within the Eagle Ford Shale Group. The Lower Eagle Ford Shale Formation has the highest TOC and hydrogen index (HI) values and in particular, the Lozier Canyon Member is the most organic-rich. Pristane and phytane (Pr/Ph) and biomarker ratios suggest the establishment of stronger anoxic conditions during deposition of the Lower Eagle Ford Shale Formation compared to the Upper Eagle Ford Shale, where the latter may have received an additional siliciclastic and terrigenous organic matter input. In East Texas, Pr/Ph ratios indicate deposition under oxic-suboxic conditions for the entire Eagle Ford Shale interval analyzed. Isotope data indicates a marine organic matter source for the Eagle Ford Shale Group, but $\delta^{13}C$ values do not show significant organic facies, depositional environment, or thermal maturity changes.

Geochemical data were correlated with an already established sequence stratigraphic framework for the Eagle Ford Shale Group in order to identify relationships between organic geochemical trends and stratigraphic sequences. In this study, these observations reached a general interpretation and it is recommended they be further refined by high-resolution organic geochemistry studies.

# CHAPTER I

## 1. INTRODUCTION

The Eagle Ford Shale (Cenomanian-Coniacian) is one of the most actively explored and produced shale-gas plays in the United States. This mixed siliciclastic/carbonate unit has proved to be the source rock for oil and gas in conventional reservoirs across Texas (Liro et al., 1994). The Eagle Ford Shale Play trends northeast for about 400 miles (640 Km) from the Mexican border into East Texas (Figure 1). It is approximately 50 miles wide (80 Km) and has a variable thickness from 660 ft (~200 m) in the Maverick Basin, to approximately 12 to 17 ft (~4 to 21m) in the San Marcos Arch, to about 450 ft (~150 m) in the center of the East Texas Basin (Hentz and Ruppel, 2010; RRC, 2013). In northwest Texas, the Eagle Ford Shale produces oil from about 5,000 feet (~1,500 m) deep. In the southwest, the Eagle Ford Shale produces mainly dry gas from about 12,000 feet deep (~3,600 m; Figure 1; EIA, 2010; Durham, 2013; RRC, 2013). Up-to-date there are about 22 active fields within the Eagle Ford trend. Gas, condensate, and oil production from the Eagle Ford Shale has been rapidly increasing since its development as an unconventional play in 2008. As of August 2013, hydrocarbon production has reached over 1 million barrels of oil equivalent per day (boe/d; RRC, 2013).

The Upper Cretaceous Eagle Ford Shale has worldwide age equivalent units, which comprise an important fraction of the hydrocarbon source rocks in the world. Deposition of organic rich rocks during the Cretaceous period was influenced by variations in different factors such as tectonism, volcanism, atmospheric and ocean chemistry, climate, sea-level, and sediment supply (Dean and Arthur, 1998). The Eagle

Ford Shale was deposited during a major transgressive episode on a carbonate platform south of the Western Interior Seaway during the Late Cretaceous. During this time, North America experienced warm climatic conditions, which when combined with the series of events leading to onset of the Oceanic Anoxic Event 2 (OAE2), significantly contributed on making the Eagle Ford Shale an organic-rich source rock (Robinson and Kirschbaum, 1995).

Several studies have demonstrated the stratigraphic and geochemical heterogeneities present in shales and shale-gas systems, previously thought to have no significant vertical or lateral variations. The understanding of these changes is essential to improve the efficiency of hydrocarbon prediction and production in unconventional reservoirs. Recent studies of the Eagle Ford Shale from outcrop and subsurface data have added significant value to the understanding of this play (Adams and Carr, 2010; Donovan and Staerker, 2010; Hentz and Ruppel, 2010; Harbor, 2011; Fairbanks, 2012; Donovan et al., 2012, 2013a, 2013b). However, few studies have reported detailed organic geochemical data and interpretations beyond Rock Eval pyrolysis and organic carbon content (Robison, 1997; Liro et al., 1994; Edman and Pitman, 2010; Lewan et al., 2012). The present research provides a comprehensive regional organic geochemical analysis of the Eagle Ford Shale including GC, GC-MS, GC-IRMS in addition to the traditional Rock Eval and TOC screening data, emphasizing the uses and applications of biomarker and isotope analysis in shale-gas studies. In order to achieve this, outcrop and core samples from the Eagle Ford Shale as well as oil and condensate samples produced from the Eagle Ford Shale and the San Miguel Formations were analyzed using several organic geochemistry techniques. The main objective of this research was

to geochemically characterize the Eagle Ford Shale and to determine if the liquid samples available were generated from this source rock. This study will improve our understanding of the lateral and vertical variability of the Eagle Ford Shale in outcrop and subsurface, and the value of organic geochemistry for evaluating unconventional shale-gas plays as an aid in sequence stratigraphic studies.

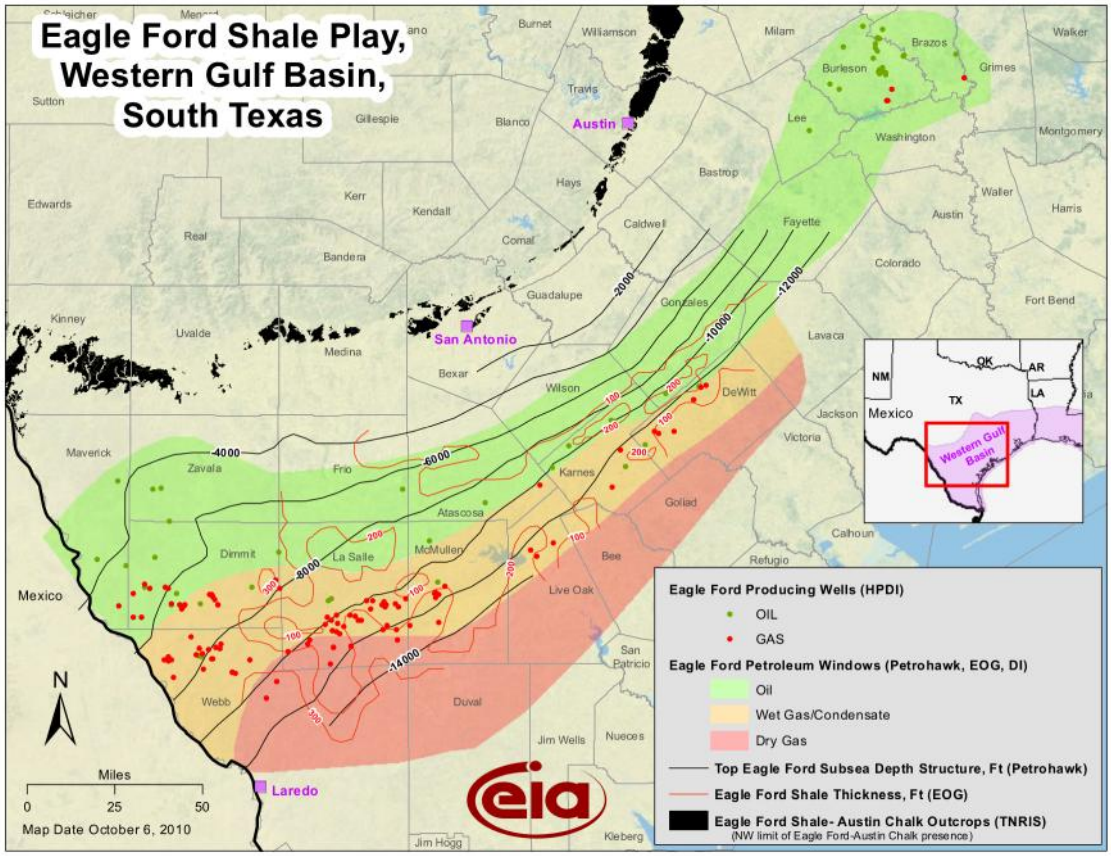


**Figure 1. Composite map of the Eagle Ford Shale in Southwest Texas, showing production, depth, thickness, and thermal maturity of this gas-shale play (EIA, 2010)**

## 1.1 Geologic Framework

### 1.1.1 Regional Geology

The Eagle Ford Shale was deposited during the Late Cretaceous in the Gulf of Mexico Coastal Plain. In Texas, the Gulf of Mexico Coastal Plain is delineated by important structural features that have influenced sediment deposition over geologic time. From west to east these structures correspond to the Maverick Basin of the Rio Grande Embayment, San Marcos Arch, East Texas Basin, and Sabine Uplift (Hentz and Ruppel, 2010; Donovan et al., 2012; Figure 2). A chronostratigraphic chart for South Texas (Figure 3) illustrates the major formations deposited during Cretaceous time. Hill (1887) defined two major successions for the Cretaceous, named Comanche and Gulfian Series. The Sligo, Pearsall, Glen Rose, Edwards, Georgetown, Del Rio and Buda formations comprise the carbonate-dominated Comanche Series, whereas the Eagle Ford, Austin, Anacacho, San Miguel, Olmos, and Escondido formations correspond to the siliciclastic-dominated Gulfian Series (Figure 3; Hill, 1887; Donovan et al., 2012).

The Comanche Platform was developed during the Albian and Early Cenomanian time across Central Texas. This carbonate platform was rimmed by reef build-ups corresponding to the Stuart City Reef Trend (Edwards, Georgetown, Del Rio and Buda formations), and it was centered in the San Marcos Arch. In South Texas, the South Texas Submarine Plateau formed (Gardner et al., 2013; Donovan et al., 2012). Throughout the Middle to Late Cenomanian, differential subsidence generated the Maverick and East Texas Basins (Figure 4a). During this time, a major marine transgression started the accumulation of organic-rich carbonate mudstones

corresponding to the Eagle Ford Shale Group (Hentz and Ruppel, 2010; Donovan et al., 2012). Donovan et al. (2012) presented an idealized cross section of the Comanche Platform to describe the inherited seafloor paleobathymetry at the beginning of Eagle Ford Shale deposition (Figure 4b). These authors proposed shallow water depths of 100 to 200 ft (~30 to 60 m) in most of the Comanche Platform, and water depths of 400 to 600 ft (~120 to 180 m) for the deeper portions of the seaway including the South Texas Submarine Plateau, Rio Grande Embayment, and the Texas Basin.

The stratigraphic characteristics of the Eagle Ford Shale Group vary across the region, since deposition of these units was influenced by several structural and physiographic features. The following sections will describe in detail the stratigraphic variations of the Eagle Ford Shale from Southwest, Central, and East Texas, based on recent studies published on this shale-gas play.

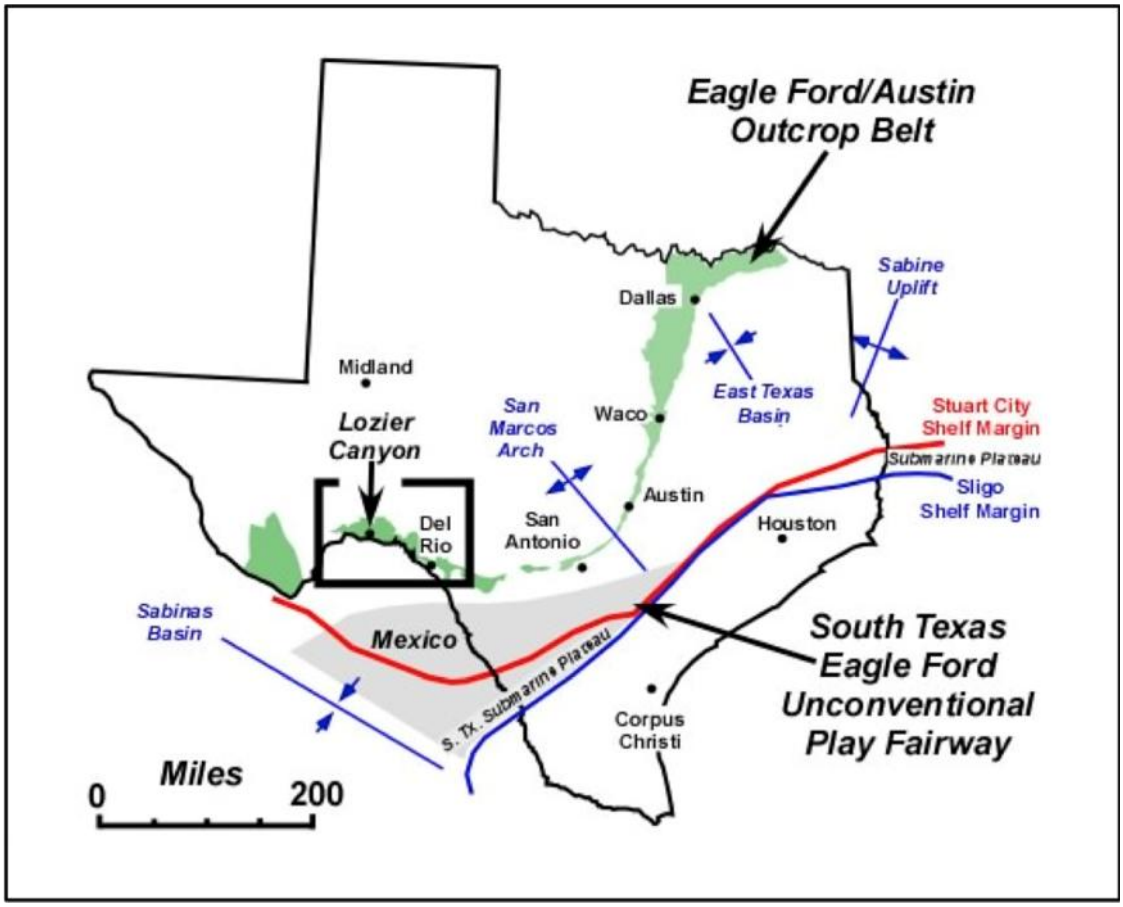


**Figure 2. Texas map showing the main structural and physiographic features influencing the Gulf of Mexico Coastal Plain (modified from Donovan et al., 2013a)**

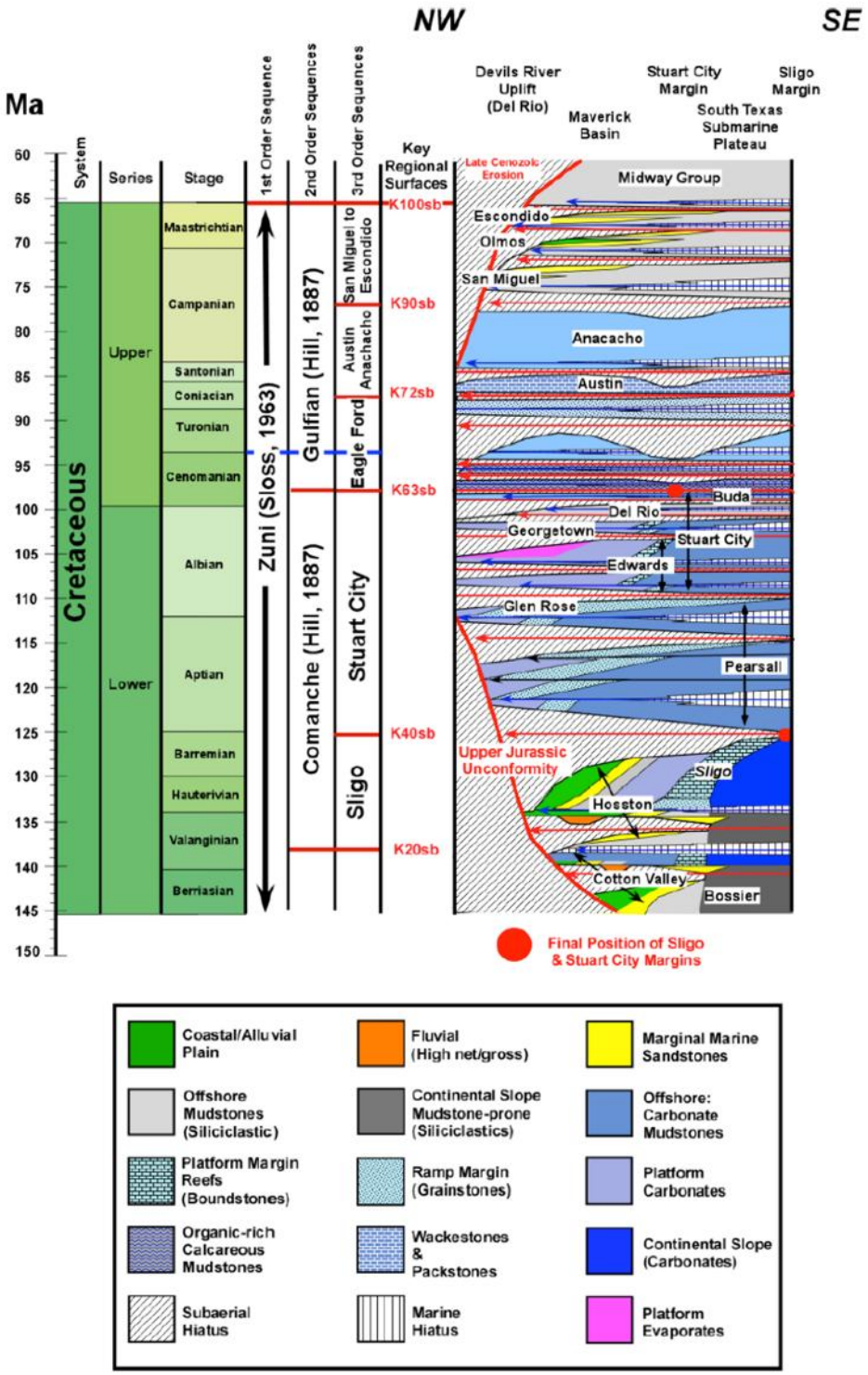


**Figure 3. Generalized chronostratigraphic chart for the Cretaceous of South Texas (modified from Donovan et al., 2012)**

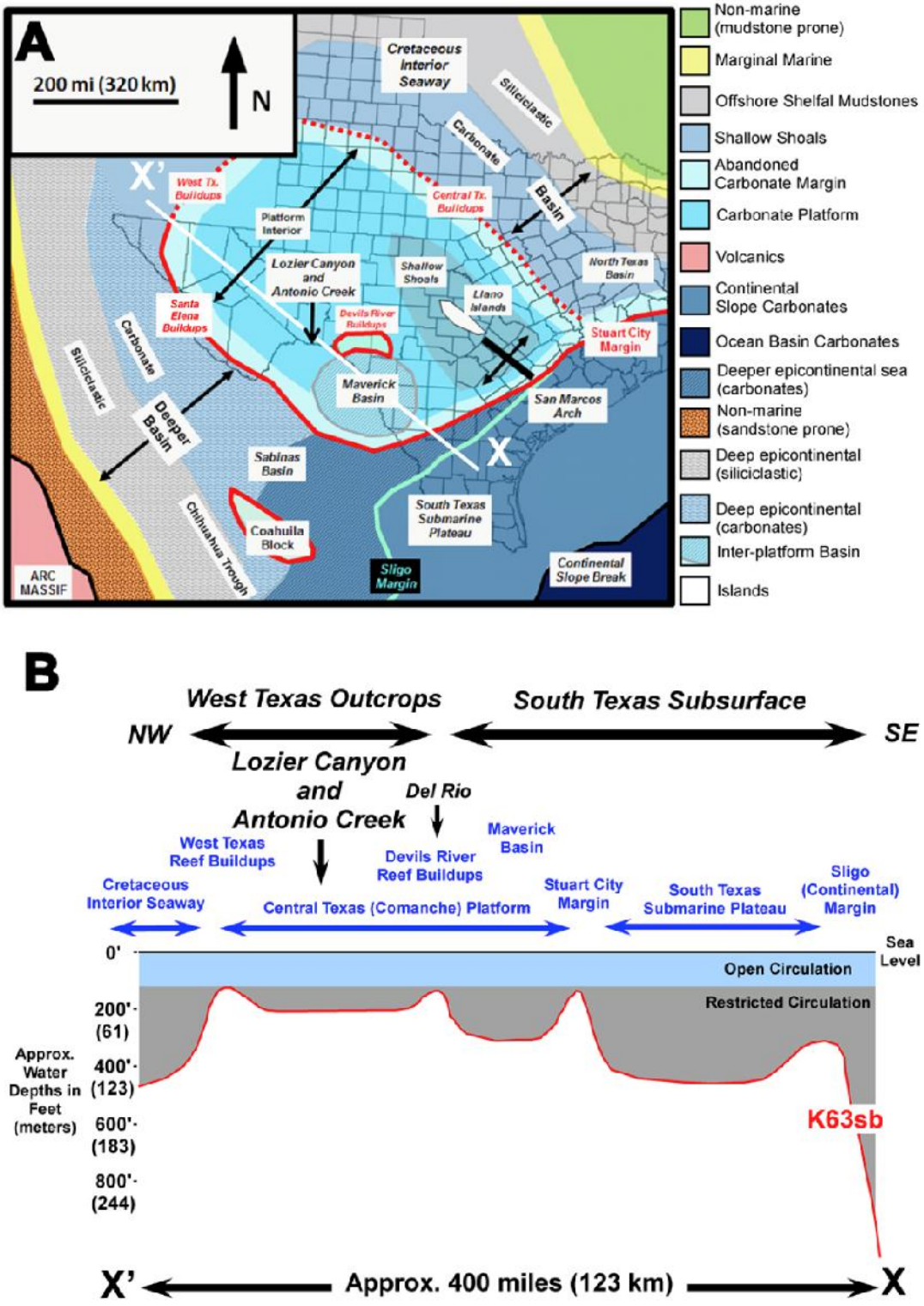


**Figure 4. Generalized A) Paleogeography of the Comanche Platform; B) Cross section X-X' illustrating inherited seafloor paleobathymetry during Late Cenomanian time (from Gardner et al., 2013)**

### 1.1.2 West and South Texas Eagle Ford Shale Geology

Donovan and Staerker (2010) summarized the different subdivisions that have been proposed to describe Eagle Ford Shale in West Texas, and raised attention to dual and arbitrary terminology that has been used to describe this interval west and east of the Devils River. Because of the different, and sometimes confusing nomenclature published on the Eagle Ford Shale, Donovan et al. (2013a) encouraged the use of the name Eagle Ford and not Boquillas for the strata located between the Buda and Austin Chalk formations in Texas, and proposed a new facies subdivision to standardize the Eagle Ford Group stratigraphic terminology (Donovan et al., 2013a; 2013b).

The Eagle Ford Shale outcrop belt trends in a northeast direction from El Paso in West Texas towards San Antonio, where the outcrops follow the edge of the East Texas Basin northward to the Oklahoma state line and eastward into Arkansas (Liro et al., 1994). In Terrell County, West Texas, the Lozier Canyon outcrop is a northeast-facing cutbank approximately 2000 ft long (~610 m) and 250 ft high (~76 m), which provides an excellent panoramic view of the complete Eagle Ford Group, the overlain Austin Chalk and the underlying Buda Limestone (Donovan and Staerker, 2010; Donovan et al., 2012; Donovan et al., 2013a and b). Donovan et al. (2012) referred to the Eagle Ford succession at Lozier Canyon as the Eagle Ford Group. These authors proposed a vertical facies succession for this unit based on their field observations and previous studies from other investigators. This succession, from base to top comprises the following five facies (Donovan et al., 2012; 2013a and b):

Facies A: Light gray hummocky cross-stratified limestones (grainstones) separated by thin calcareous mudstone beds.

Facies B: Black organic-rich calcareous mudstones with scattered limestones (packstone/grainstone) interbeds.

Facies C: Medium gray thick-bedded limestones (packstones) with mudstone interbeds.

Facies D: Pale yellow-ochre, echinoid-bearing marls and nodular limestones.

Facies E: Yellow ochre, thin-bedded limestones (grainstones) interbedded with calcareous mudstones.

Donovan et al. (2012; 2013a and b) further subdivided these five facies into 16 sub-units, which helped them define four unconformity-bounded depositional sequences (Figure 5). The Eagle Ford Group is divided into Lower and Upper formations by a regional unconformity at the contact between facies B and C. The Lower Eagle Ford Formation contains two depositional sequences, the Lozier Canyon and the Antonio Creek members, separated at the contact between sub-facies B2 and B3. Likewise, the Upper Eagle Ford Formation also contains two depositional sequences; the Scott Ranch and Langtry members divided at the contact between facies C and D.

At the Lozier Canyon outcrop, the Lozier Canyon Member (Figure 5) consists of interbedded grainstones and mudstones (subunits A1-A4) of approximately 18 to 20 ft (~6 m) overlain by about 30 ft (~9 m) of organic-rich mudstones and mudstones with hummocky-stratified grainstones (subunits B1 and B2). The Antonio Creek Member is characterized by bentonite-rich, dark gray mudstones, which show a marked decrease in organic content (Donovan et al., 2013b). The Scott Ranch Member is composed of interbedded light gray limestones and medium gray mudstones. Its basal section contains organic-poor, clay-rich mudstones and limestones (subunit C1), while the

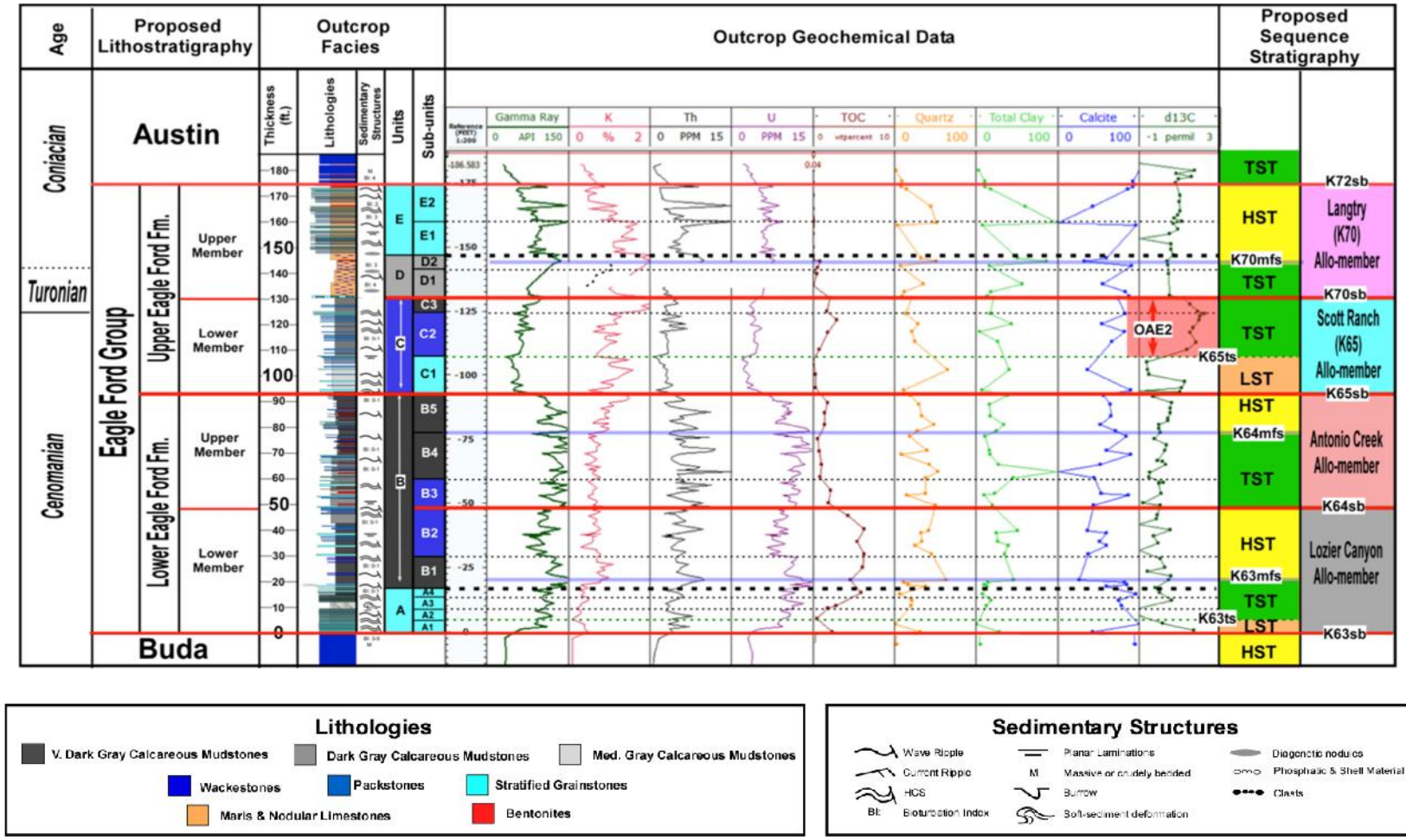


**Figure 5. Sequence stratigraphic and facies subdivision proposed by Donovan et al. (2014) for the Eagle Ford Group at the Lozier Canyon outcrop based on petrophysical and geochemical data (from Donovan et al., 2014)**

upper section (subunit C2) is characterized by high organic content, and a $\delta^{13}C$ excursion that corresponds to the Oceanic Anoxic Event 2 (OAE2) and the Cenomanian-Turonian boundary. The top of this member contains a clay-rich, low organic content interval (subunit C3) marked by the end of the $\delta^{13}C$ excursion (Donovan et al., 2012; 2013b). From base to top, the Langtry Member consists of pebble-size clasts, highly bioturbated yellowish-ochre echinoid-rich packstones (subunit D1), and wackestones (subunit D2) overlain by interbedded carbonate mudstones and hummocky-bedded packstones (subunit E). In addition, this member is also bentonite-rich, containing 2 to 6-inches-thick (5 to 15 cm) bentonite beds (Donovan et al., 2013b).

Based on geophysical and geochemical logs, Donovan et al. (2012; 2013a) were able to identify the same depositional sequences described at the Lozier Canyon outcrop in the South Texas subsurface (Figure 6). At the Fasken "A" #1 well (Webb County, Texas) the Eagle Ford Group is about 300 (~91 m) thick. However, in this area the Lozier Canyon and Scott Ranch members have a larger stratigraphic thickness compared to the equivalent units at the Lozier Canyon location. Moreover, the Lozier Canyon Member displays the highest organic content and corresponds to the main unconventional reservoir zone. Donovan et al. (2012; 2013a) identified a "marker beds" interval towards the base of the Upper Eagle Ford Formation characterized by high-clay, low-carbonate content, low gamma ray and resistivity, and a distinct density and neutron logs separation. Both, the Antonio Creek and Langtry members show a distinctive high gamma ray signature as a result of high bentonite content. In addition, a $\delta^{13}C$ excursion within the Scott Ranch Member could be observed at the occurrence of the OAE2 and the Cenomanian-Turonian boundary.

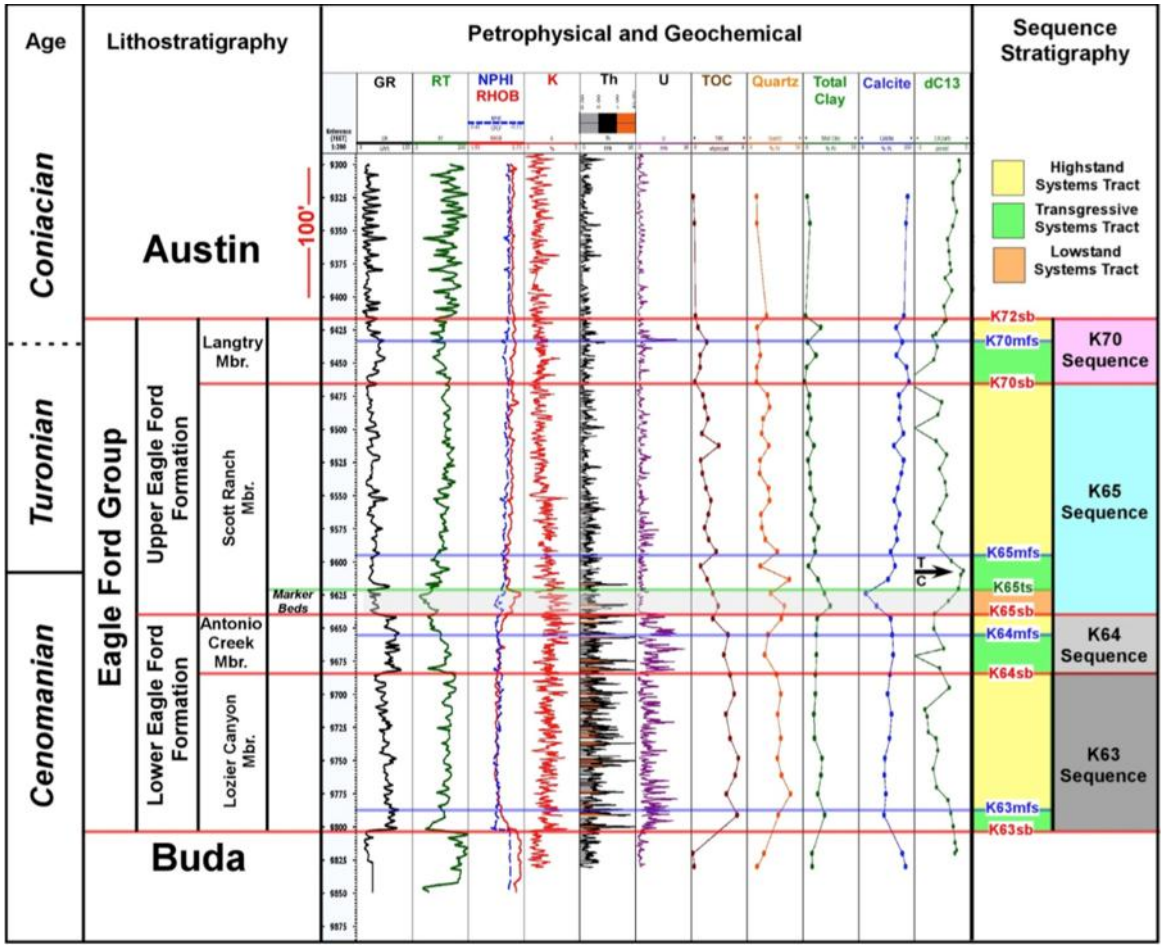


**Figure 6. Sequence stratigraphic framework for the Eagle Ford Shale Group at the Fasken "A" #1 well in Webb County, South Texas based on petrophysical and geochemical data (modified from Donovan et al., 2013a)**

### 1.1.3 Central Texas Eagle Ford Shale Geology

Fairbanks (2012) performed a facies analysis of the Eagle Ford Shale in Central Texas including samples from the Bouldin Creek outcrop, and the ACC#1 core. Harbor (2011) did a similar study in the Central Texas subsurface using samples from the W. Brechtel #1, and C.J. Hendershot #1, among other wells. The ACC#1 core is considered as a type section core for the Eagle Ford Group in the Austin area (Figure 7; Fairbanks, 2012). In this core, Fairbanks (2012) performed a detailed description of the Eagle Ford Shale and described the contacts with the underlying Buda Limestone and the overlying Austin Chalk. The author subdivided the Eagle Ford Group into four different units similar to studies previously done in the same area. From base to top these intervals correspond to the Pepper Shale, Lake Waco Formation (Waller and Bouldin Members), and South Bosque Formation (Figure 7). The facies described by Fairbanks (2012) in this area include massive argillaceous mudrocks; massive argillaceous foraminiferal mudrocks; laminated argillaceous foraminiferal mudrocks; laminated foraminiferal wackestone; cross-laminated foraminiferal packstones and grainstones massive bentonitic claystones; and nodular foraminiferal packstones and grainstones.

According to Harbor (2011) and Fairbanks (2012), the contact between the Buda and the Eagle Ford is sharp, marking a lithologic change from a light gray, highly-bioturbated, massive skeletal wackestone/packstone, which characterizes the Buda Limestone, to a dark gray, massive argillaceous mudstone that corresponds to the Eagle Ford Shale. The Pepper Shale of the Eagle Ford Group is a relatively thin (4 to 6 ft; ~1 to 2 m), recessive, dark gray, argillaceous claystone (massive argillaceous mudrock facies) interval with moderate TOC (ave. 3.2%; Fairbanks, 2012). This unit is overlain

by the Waller Member, which is mainly composed of massive and laminated argillaceous foraminiferal mudrock. The Waller Member has high TOC (ave. 3.7%) and higher carbonate content compared to the Pepper Shale and also contains smaller amounts of massive argillaceous mudrock, cross-laminated foraminiferal packstone/grainstone and nodular foraminiferal packstone/grainstone. In outcrop it is poorly exposed and its thickness in core is about 10 ft (~3 m). A sharp contact separates the Waller Member from the overlying Bouldin Member. According to Fairbanks (2012) the Bouldin Member is about 10 to 12 ft (~3 m) thick, contains the lowest clay and TOC content (ave. 2.1%), and is mainly composed of interbedded calcite-rich limestones and mudrock (laminated foraminiferal wackestone and cross-laminated and nodular foraminiferal packstones/grainstones facies). In this interval Fairbanks (2012) identified significant amounts of bentonitic claystones and enrichment in Mo, U, Mn, and V/Cr, which the author described as indication of maximum basin restriction during deposition of this member. Overlying the Bouldin Member is the South Bosque Formation. This unit is about 16 ft (~5 m) thick and is composed of the massive and laminated argillaceous foraminiferal mudrock facies, occasional amounts of bentonitic claystones, and moderate organic content (ave. 2.5%; Fairbanks, 2012). Fairbanks (2012) describes a gradational contact of about 3 ft (~91 cm) as the transition towards the overlying Austin Chalk Formation. The author describes this formation as a light gray, heavily bioturbated mudstone/wackestone.

Fairbanks (2012) assigns the Pepper Shale, Lake Waco Formation (Waller and Bouldin Members), and the basal part of the South Bosque Formation as the Lower Eagle Ford, and the rest of the South Bosque Formation as the Upper Eagle Ford Shale.

Harbor (2011) identified an additional upper member in the Eagle Ford interval south of the Austin area. This interval named “Harbor 2011” by Fairbanks (2012) is composed of disrupted bedded foraminiferal packstones, massive inoceramid packstones, and laminated foraminiferal peloidal packstones (Figure 8; Harbor, 2011). In general, all the Eagle Ford members described by Fairbanks (2012) show a southward thickening along the San Marcos Arch axis, possibly resulting from an increase in accommodation due to subsidence. This author observed an overall facies change to more fine-grained, low energy facies, with exception of the South Bosque Formation, which does not show a significant facies nor thickness variations (Fairbanks, 2012).

The Bouldin Creek outcrop is located on the northeastern flank of the San Marcos Arch and is the type locality for the Bouldin Member (Fairbanks, 2012). In this outcrop, separated for about 10 miles southwest from the ACC #1 only the intervals corresponding to the upper section of the Waller Member, the Bouldin Member, and the lower section of the South Bosque Formation are present (Fairbanks, 2012). A northeast-southwest cross-section from the Austin area across the San Marcos Arch (Figure 8; Fairbanks, 2012), which includes the ACC #1, W. Brechtel #1 and C.J. Hendershot #1 wells analyzed in this study show that the Pepper Shale is present across the region; however, the Waller Member pinches out towards the southwest being absent in the W. Brechtel #1 location (Fairbanks, 2012). On the contrary, the Bouldin Member thickens in the same direction.

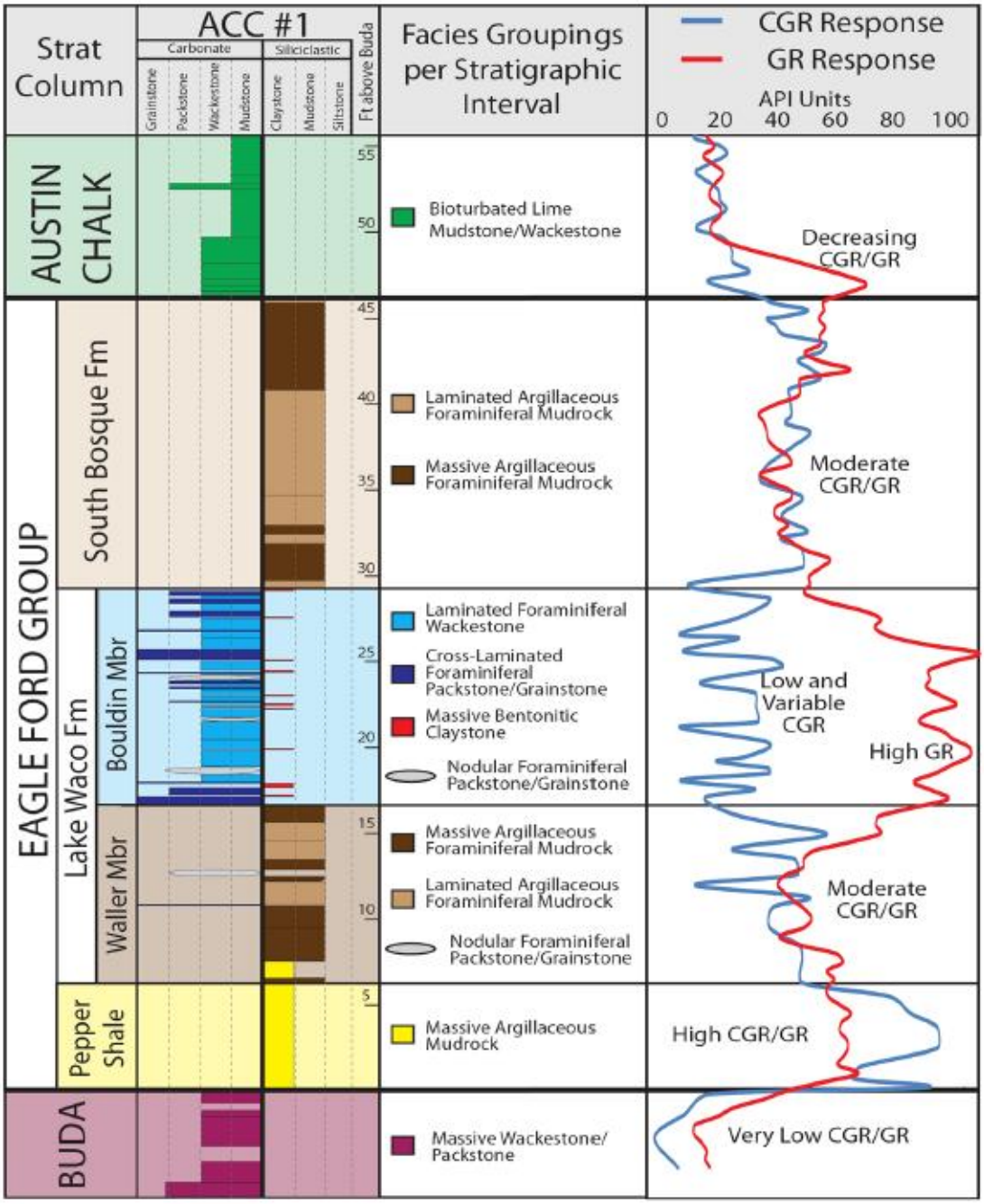


**Figure 7. Core description, facies analysis, and gamma ray logs for the ACC #1 core from Fairbanks (2012; GR = gamma ray, CGR = computed gamma ray)**

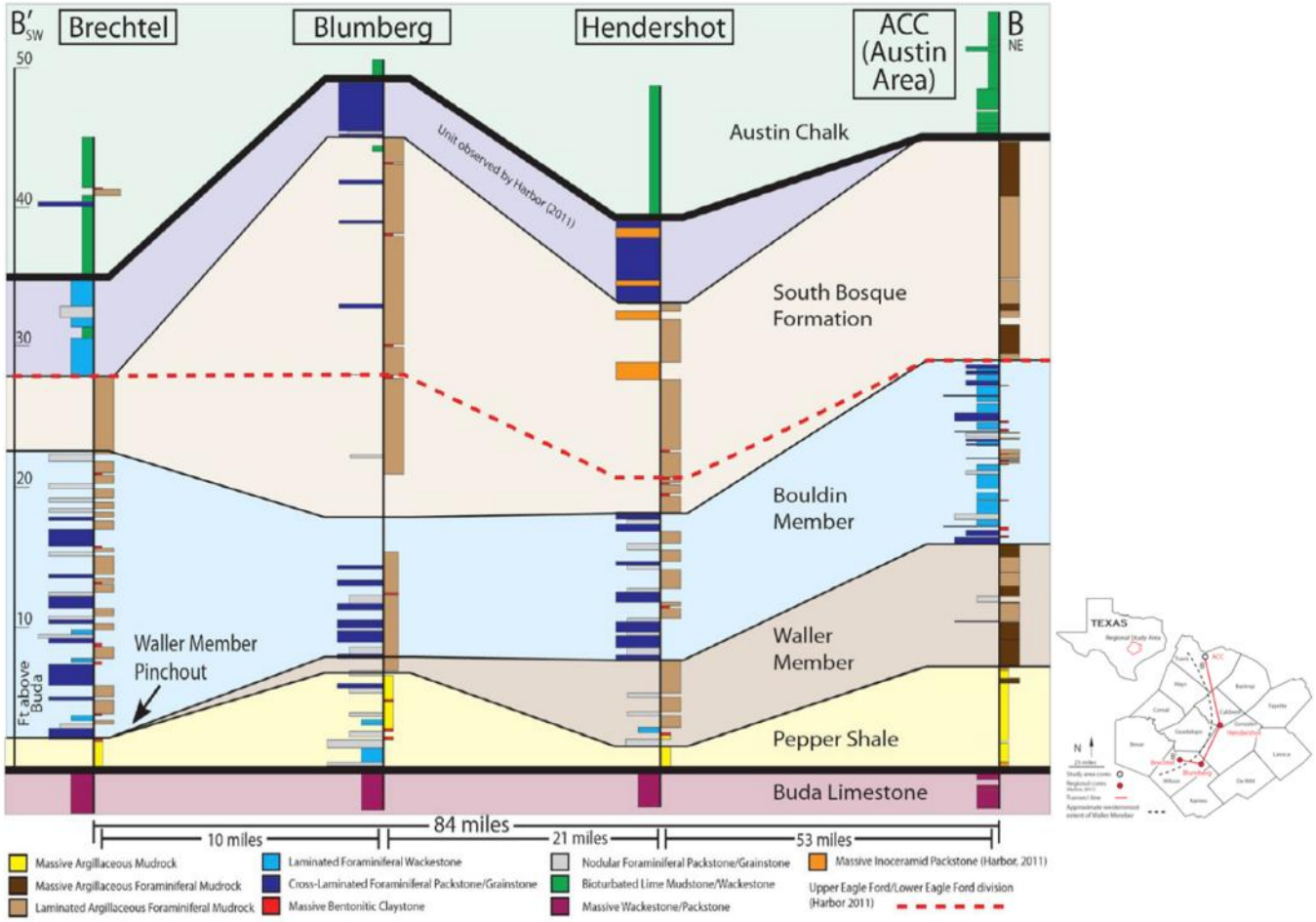


**Figure 8. Stratigraphic cross-section showing facies variation and units continuity along the San Marcos Arch (modified from Fairbanks, 2012)**

### 1.1.4 East Texas Eagle Ford Shale Geology

The Eagle Ford Shale thins towards the northwest from the Maverick Basin to the San Marcos Arch and then thickens in the same direction towards the East Texas Basin (Figure 9; Hentz and Ruppel, 2010). In East Texas, the interval between the Buda Limestone and the Austin Chalk includes from base to top the Maness Shale, Pepper Shale, and the Eagle Ford Shale. In the East Texas Basin, the siliciclastic succession of the Woodbine Group occurs between the Eagle Ford Shale and the mudrocks of the Maness Shale. The Woodbine sands pinchout southwest of the basin, and grade into the mudrocks of the Pepper Shale to the north of the San Marcos Arch (Figures 9 and 10; Hentz and Ruppel, 2010). In this area, the Eagle Ford Shale mainly consists of faintly laminated calcareous shales; organic-rich calcareous shales; laminated dolomitic shales; laminated marls, and occasional thin, reworked ash beds. These facies are interpreted as delta to prodelta deposits (Arthur and Sageman, 2004; Jennings and Antia, 2013). To the southwest, the Eagle Ford Shale contains sandstones in its uppermost part, which are referred as to the Sub-Clarksville Sand (Surles, 1987). Underlying the Eagle Ford Shale, the Maness Shale is composed of silty, slightly calcareous or dolomitic, massive, and thinly laminated shales, which are described as prodelta deposits (Arthur and Sageman, 2004; Hentz and Ruppel, 2010; Jennings and Antia, 2013).

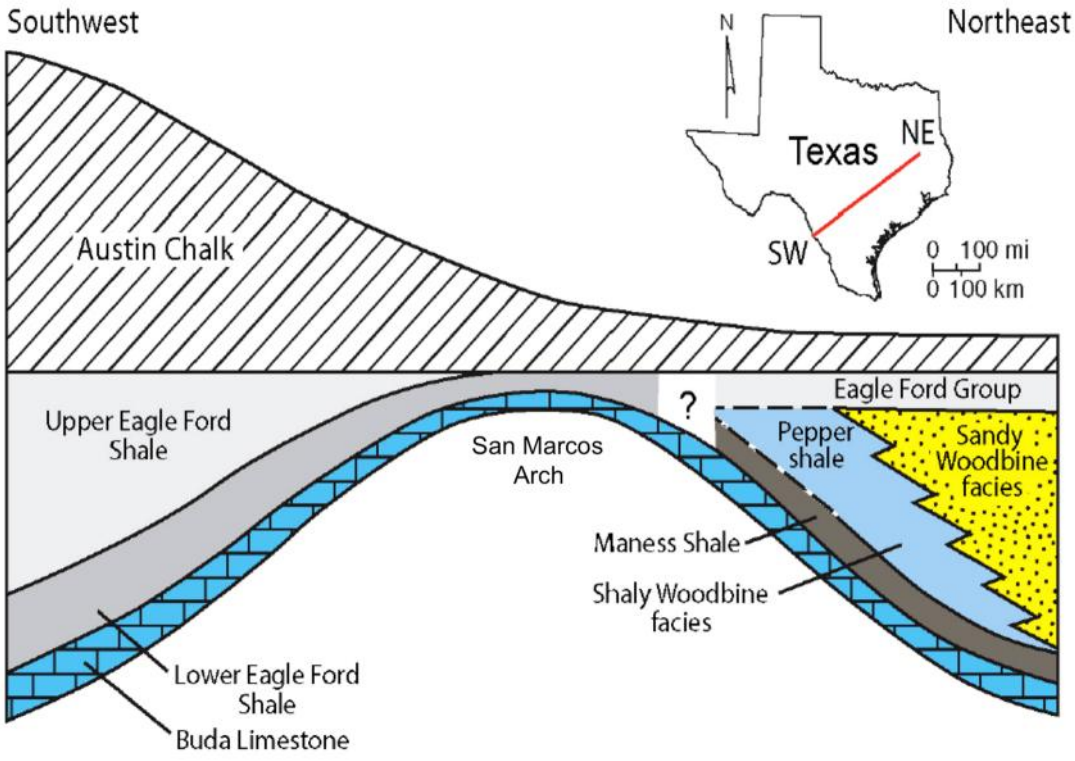


**Figure 9. Generalized SW-NE schematic strike cross section illustrating the relationships among lithostratigraphic units across the Eagle Ford Shale Play (modified from Hentz and Ruppel, 2010)**

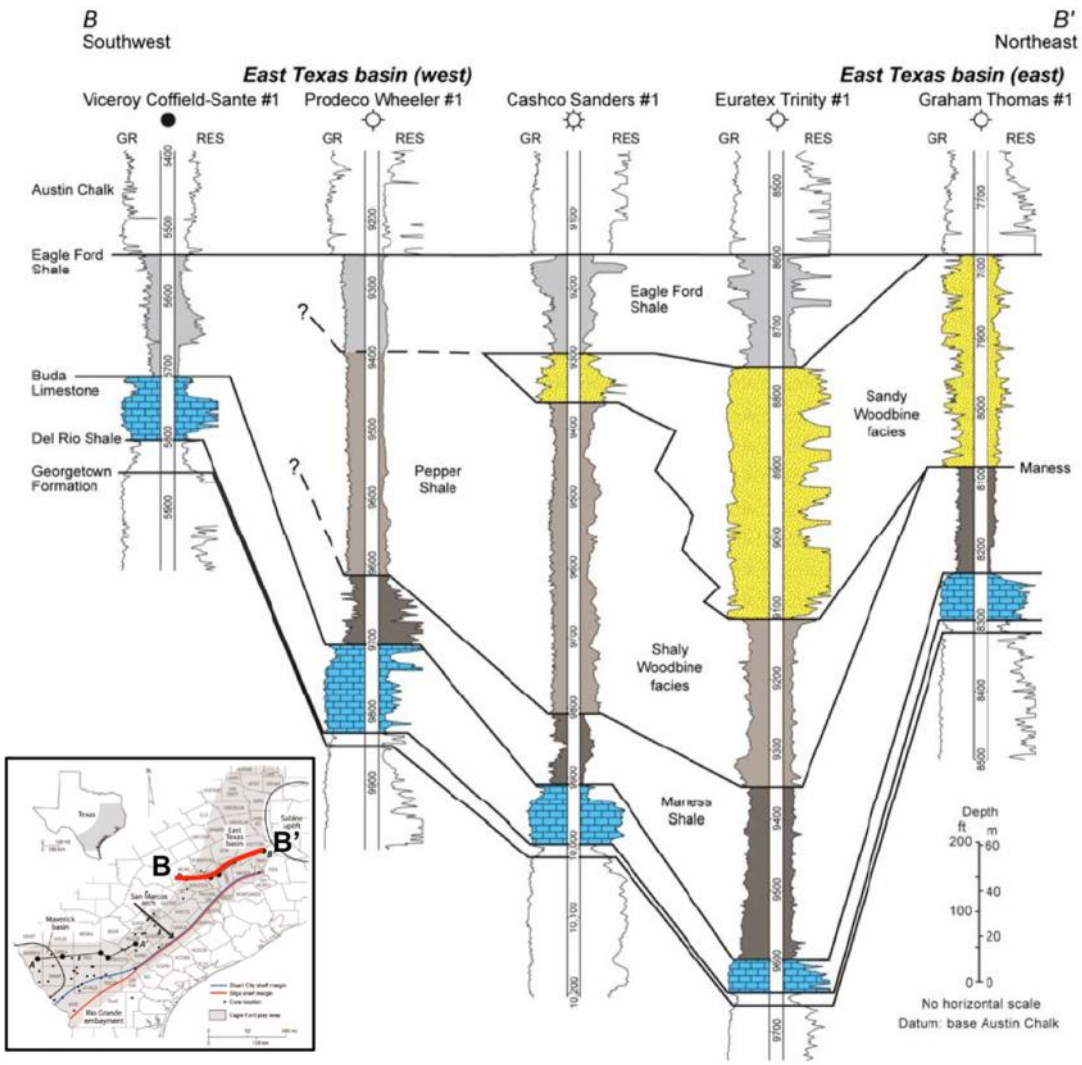


**Figure 10. SW-NE regional strike cross section of the East Texas Basin and northeast flank of the San Marcos Arch (modified from Hentz and Ruppel, 2010)**

### 1.1.5 Paleogeography and Climate

Deposition of organic rich rocks during the Cretaceous period was influenced by variations in different factors such as tectonism, volcanism, atmospheric and ocean chemistry, climate, sea-level, and sediment supply (Dean and Arthur, 1998). The impact of these phenomena produced important global eustatic sea level changes, which affected sedimentation and the extent of shelves and epicontinental seas both regionally and globally (Robinson and Kirschbaum, 1995; Dean and Arthur, 1998). In terms of plate tectonics, during the Late Cretaceous the South Atlantic Ocean started to open. North America was connected to Europe, and Australia and Antarctica were still joined. India and Madagascar began to separate, sending India on its collision course with the Eurasian plate (Scotese, 2001).

Globally, the Cretaceous climate was characterized by warm and equable temperatures, low to moderate precipitation, and a lack of ice caps, unlike today. These conditions have been attributed to a possible major “greenhouse” effect, where great amounts of $CO_2$ were released into the atmosphere due to an increase in the Earth’s volcanic activity (Robinson and Kirschbaum, 1995; Dean and Arthur, 1998).

From the middle Cretaceous, the interplay of these factors led to the development of “Oceanic Anoxic Events” (OAEs), in which mid- and deep-water oceanic masses across the Earth became highly oxygen depleted. OAEs reflect regional to global scale oceanographic and climatic changes due to a major perturbation in the ocean-atmosphere-terrestrial carbon cycle (Dean and Arthur, 1998). The Cenomainan-Turonian (C-T) boundary is marked by one of these events known as Oceanic Anoxic Event 2 (OAE2), characterized by a global sea level rise, an increase in burial of

organic carbon and consequent drop in atmospheric $CO_2$, and biotic turnover (Corbett et al., 2011). Before the beginning of the OAE2, $CO_2$ concentration ($pCO_2$) was about 4 to 18 times higher than present which contributed to the development of a greenhouse Earth (Arthur et al., 1988; Barclay et al., 2006). Increased nutrient levels resulting from higher weathering rates and upwelling produced a global increase in organic matter primary productivity, which in turn produced an important increase in organic carbon burial rates (Arthur et al., 1988; Fortwengler et al., 2003; Barclay et al., 2006; Sageman et al., 2008; Sinninghe Damsté et al., 2009). The burial of $^{13}C$-depleted organic carbon generated a rapid positive excursion ($^{13}C$ enrichment) in the stable carbon isotope composition of carbonate ($\delta^{13}C_{carb}$, 1.5-2‰), organic carbon ($\delta^{13}C_{org}$; 3.5-4‰), and phytoplankton, which can be determined at or near the C-T boundary in the sedimentary record worldwide (Arthur et al., 1988; Fortwengler et al., 2003; Sinninghe Damsté et al., 2009).

In North America, rock deposition during the Upper Cretaceous was highly influenced by the relationship between foreland basins, eustatic sea level variations, and climate. The paleogeographic location of North America during this time places the continent in a temperate to subtropical climate zone (Robinson and Kirschbaum, 1995). At the beginning of Cenomanian time, a transgression of the seas from the north and south into the North American craton began, creating the Western Interior Seaway (WIS; Figure 11) (Robinson and Kirschbaum, 1995). The WIS connected the Circum-Boreal sea with the proto-Gulf of Mexico, and during maximum transgressions it constituted a large north-south arm of the Tethys Ocean extending from the Gulf Coast to the Arctic region (Robinson and Kirschbaum, 1995; Dean and Arthur, 1998, 1998b).

WIS expansion during this time was mainly influenced by an increase in seafloor spreading rates and ice cap melting, while sediment accumulation was driven by Cordilleran tectonics, epeirogenic flexure, oceanographic variations, and climate change (Leckie et al., 1998; Scott et al., 2010). During this time, marine shale deposition was occurring in the central part of the seaway, along with extensive platform and basin carbonate buildup in southern Texas. By early Turonian the WIS had reached its maximum transgression, and extensive, highly calcareous muds were produced and deposited (e.g. upper Greenhorn Limestone, Eagle Ford Shale). It is thought that during this time climate was predominantly warm and an influx of terrigenous organic matter was minimal. The presence of volcanic ash as bentonite beds in some sequences from early to middle Turonian suggest that during this time moderate to intense volcanism was occuring (Robinson and Kirschbaum, 1995).

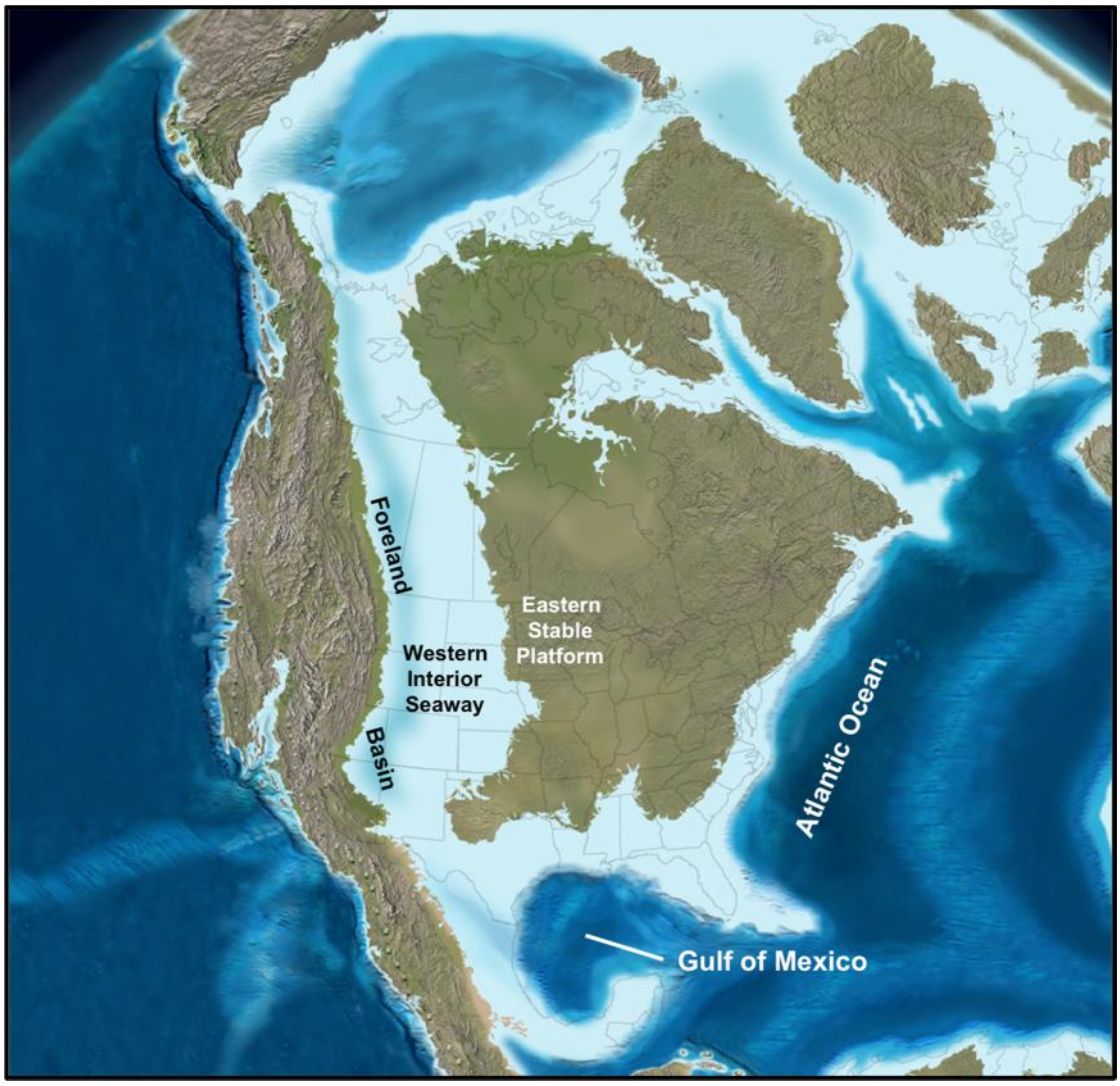


**Figure 11. Map showing the extent of Western Interior Seaway, locations of the Foreland Basin, and the Eastern Stable Platform during the Late Cretaceous (~85 Ma) (modified from Robinson and Kirschbaum, 1995 and Blakey, 2011)**

## 1.2 Objectives

The main objective of the present study is to geochemically characterize the Eagle Ford Shale in West, Southwest, Central and East Texas and demonstrate the usefulness of organic geochemistry as a tool for complementing and refining sequence stratigraphic frameworks, especially in unconventional shale gas plays. For this, an assessment of possible variations in different organic geochemical parameters in the Eagle Ford Shale from outcrop to subsurface in a local and regional context is intended. In order to accomplish these goals, the following specific objectives were defined:

- Determination of the organic richness and type of organic matter present in the Eagle Ford Shale.
- Evaluation of the source rock generation potential for hydrocarbons and thermal maturity.
- Assessment of variations in organic matter source and depositional environment conditions.
- Integration and correlation of the organic geochemistry data obtained from this research with available sequence stratigraphy data for the study area.
- Characterization of oils and condensates produced from Upper Cretaceous reservoirs and correlation with Eagle Ford Shale geochemical parameters in order to increase the understanding of the petroleum systems in the study area.

## 1.3 Methodology

### 1.3.1 Study area and sample locations

A total of 178 samples were collected for this study from outcrops and wells located throughout West, South-central, and East Texas (Figure 12, Table 1). In West Texas, the BP-leased Lozier Canyon outcrop provides an excellent exposure to evaluate organic facies variations that may be present within the Eagle Ford Shale. Results from a multidisciplinary study of this outcrop have been published in several field guidebooks and in Donovan and Staerker (2010) and Donovan et al. (2012, 2013a; 2013b). In South Texas, core samples obtained from the Newfield F. McKnight #526-1H and Swift Fasken "A" #1H wells were used to understand organic geochemical variations in the subsurface and in areas where the Eagle Ford Shale is highly mature. The West Bouldin Creek outcrop in Austin, Texas includes a thinner section of the Eagle Ford Shale and corresponds to the type locality of the Bouldin Member (Figure 12). Close to this area, core samples from the ACC#1 well, the type section for the Eagle Ford Group in Central Texas were also collected for comparison with the Bouldin Creek outcrop. Further south, two additional cores were sampled, the C.J. Hendershot #1 and W. Brechtel #1, which have been described by Harbor (2011). Finally, in East Texas, a core obtained from the Lily Hoppess #1 well containing sections corresponding to the Lower Eagle Ford and Maness Shale was used to geochemically characterize what is thought to be the most prolific interval for hydrocarbons in the Eagle Ford Shale and to evaluate regional variations that may be present between west, central, and east Texas. Additionally, oil and condensate samples from five wells

(Figure 12) located in southwest and central Texas were analyzed for and source rock/oil correlations.

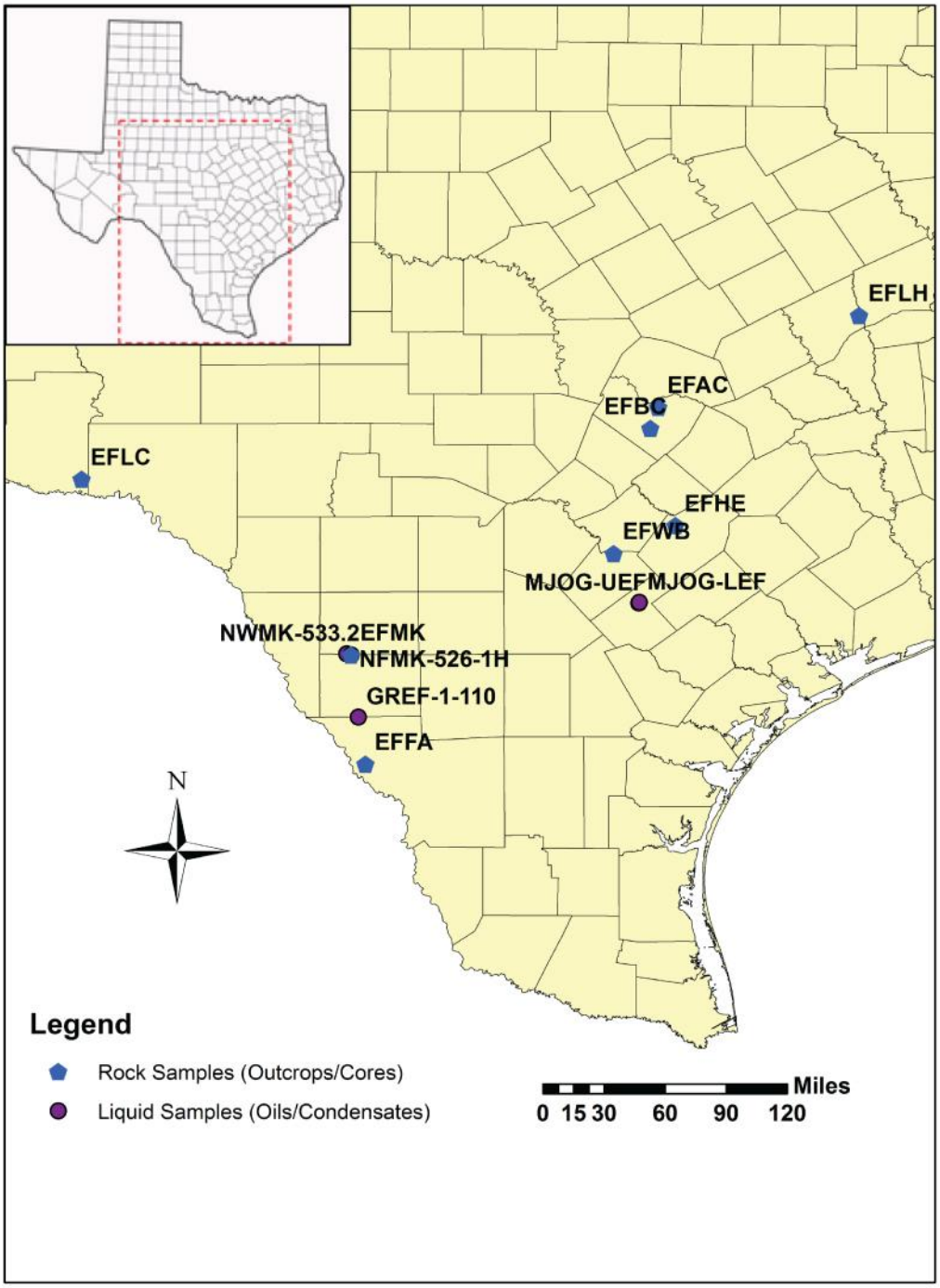


**Figure 12. Texas map showing location of the samples analyzed in this study**

### 1.3.2 Experimental

Total Organic Carbon (TOC) determination and Rock Eval pyrolysis were performed on all rock samples available for this study (Table 1). A TOC value of 1% was established as a cutoff for selecting samples for bitumen extraction. Crushed rock extracts were separated into maltenes and asphaltenes by addition of excess *n*-pentane. The maltene fraction was further fractionated into saturates, aromatics, and NSO compounds by high performance liquid chromatography (HPLC). Screening analyses of saturates and aromatics were performed by gas chromatography (GC). Selected samples were analyzed by gas chromatography-mass spectrometry (GCMS) for biomarker analyses, and gas chromatography isotope-ratio mass spectrometry (GC-IRMS) for compound-specific isotope analysis. Oils and condensates were analyzed using GC and GCMS. Rock samples from Lozier Canyon, Bouldin Creek, Fasken A #1-H, and Lily Hoppess #1 were chosen for vitrinite reflectance measurements. Rock Eval pyrolysis and TOC analyses were performed at GeoMark Research, Inc. in Humble, Texas and Core Laboratories in Houston, Texas. The remaining geochemical analyses were performed at the University of Oklahoma Organic Geochemistry Laboratories located in Norman, Oklahoma. A summary of the laboratory workflow used in this project is depicted in Figure 13.

**Table 1. List of samples for organic geochemical analyses**

| Well/Outcrop name | Abbreviation | Sample type | # of samples | Location |
|---|---|---|---|---|
| Lozier Canyon | EFLC | Outcrop | 43 | Terrell Co. |
| Newfield Ferguson McKnight #526-1H | EFMK | Core | 16 | Dimmit Co. |
| Swift Fasken “A” #1-H | EFFA | Core | 40 | Webb Co. |
| Bouldin Creek | EFBC | Outcrop | 34 | Travis Co. |
| ACC#1 | EFAC | Core | 10 | Travis Co. |
| W. Brechtel #1 | EFWB | Core | 9 | Wilson Co. |
| C.J. Hendershot #1 | EFHE | Core | 10 | Caldwell Co |
| Encana Lily Hoppess #1 | EFLH | Core | 11 | Robertson Co. |
| Newfield W. McKnight #533.2 | NWMK-533.2 | Oil | 1 | Zavala Co. |
| Newfield F. McKnight #526-1H | NFMK-526-1H | Oil | 1 | Dimmit Co. |
| Murphy Oil Murphy JOG #1-H | MJOG-UEF | Oil | 1 | Karnes Co. |
| Murphy Oil Murphy JOG #E 1-H | MJOG-LEF | Oil | 1 | Karnes Co. |
| Lewis Gates Ranch #1-110 | GREF-1-110 | Condensate | 1 | Dimmit Co. |

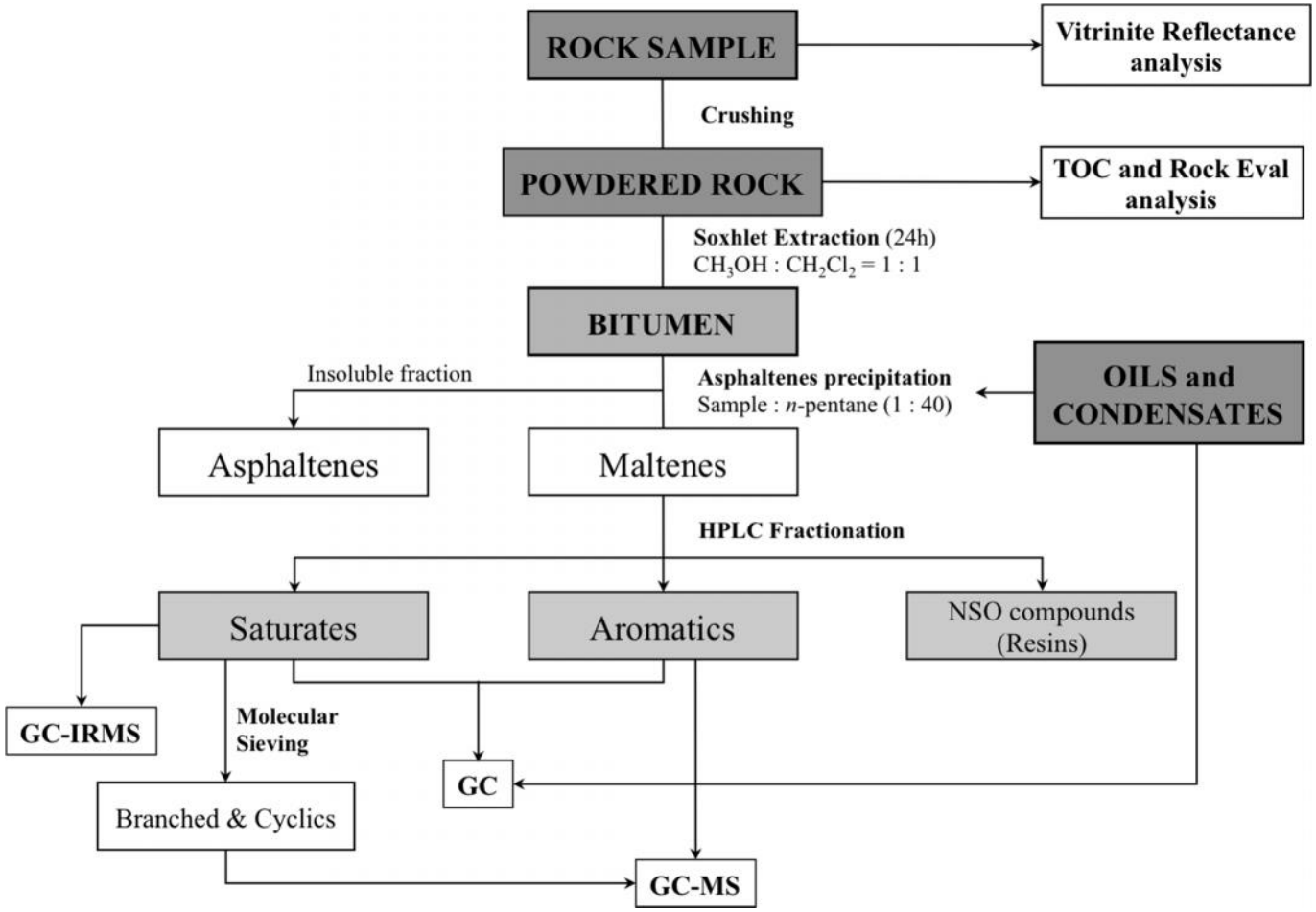


**Figure 13. Schematic workflow used for laboratory analyses of the Eagle Ford Shale rock, whole oil and condensate samples (modified from Miceli Romero and Philp, 2012)**

#### *1.3.2.1 Preliminary rock sample treatment*

Individual rock samples were washed with hot water, distilled water and a 1:1 mixture of dichloromethane ($CH_2Cl_2$) and methanol ($CH_3OH$) in order to remove any possible contaminants (e.g. drilling mud, plastic wrap, and handling). After the samples were completely dried, they were crushed using a combination of a small shatterbox and an alumina mortar and pestle until a fine powder was obtained for screening analysis (TOC and Rock Eval) and soxhlet extraction.

#### *1.3.2.2 Total Organic Carbon (TOC) and Rock Eval Pyrolysis*

Total Organic Carbon (TOC) analysis and Rock Eval pyrolysis were performed on 173 rock samples at GeoMark Research, Inc. in Humble, Texas and Core Laboratories in Houston, Texas. Approximately 1-2 grams of crushed rock were used for determination of TOC and Rock Eval parameters. From the results of these analyses samples were chosen for further bitumen extraction and maltenes fractionation.

#### *1.3.2.3 Petrographic analysis*

Measured vitrinite reflectance (Measured $\%R_o$) values were obtained from pellets prepared at the Oklahoma Geological Survey Organic Petrography Laboratories in Norman, Oklahoma and measured at the University of Oklahoma Organic Geochemistry Laboratories under the guidance of Mr. Brian Cardott. Preparation of dispersed organic pellets involved grinding about 10 grams of whole rock samples to 18 mesh and placing them in plastic ring forms. A mixture of epoxide epoxy resin and hardener (5:1) was centrifuged for 3 minutes to remove air bubbles from it and then poured into the ring forms until half full. Each crushed rock sample was sprinkled into

its designated ring form and mixed with the epoxy until all the grains were covered with the epoxy mixture and evenly spread across the bottom of the ring form. Additional bubble-free epoxy was poured into the ring forms up to the rim. The pellets were left to harden at room temperature for about 12 hours.

Dispersed organic pellets were polished using a Buehler Ecomet III Griding and Polishing Apparatus in order to remove any scratches and obtain a relief-free surface for visual analysis. Pellets were polished with 320, 400, and 600 grit paper for 3 minutes using tap water as lubricant. Each sample was subsequently rinsed off using distilled water and placed in an ultrasonic bath with distilled water and few drops of Kodak Photo-Flo 200 solution for 1 to 2 minutes. Sample pellets were further polished using a Buehler Texmet polishing cloth with Wendt Dunnington 0.3μm alumina slurry and distilled water as lubricant for 4 minutes. Pellets were then washed with distilled water and placed in the ultrasonic bath for 2 minutes. After this step, the pellets were rinsed with distilled water and blow-dried using filtered air. Finally, the pellets were polished with Wendt Dunnington 0.05μm alumina slurry following the same workflow indicated above, and placed in a desiccator to dry.

Mean random vitrinite reflectance measurements were performed using a Leitz Ortholux 2 Microscope under oil immersion and reflected white light following the methodology from ASTM (2011).

#### *1.3.2.4 Extraction and Fractionation*

A soxhlet extraction device was pre-extracted for 24 hours using a 1:1 mixture of dichloromethane ($CH_2Cl_2$) and methanol ($CH_3OH$) in order to remove contaminants. Selected samples (50g approximately) were extracted with the same solvent mixture for

24 hours. Excess solvent from the extract was evaporated using a rotary evaporator and the bitumen transferred to a glass centrifuge tube. The bitumen was separated into maltenes and asphaltenes by adding an excess (40:1) of *n*-pentane ($C_5H_{12}$). The centrifuge tubes were placed in a freezer overnight to ensure complete asphaltene precipitation.

Maltene fractions were transferred to 250mL round bottom flasks to evaporate the solvent excess and then placed in glass vials. This fraction was then diluted in a ratio of 20mg sample per 50uL *n*-hexane ($C_6H_{14}$) for compound class fractionation by HPLC using an HPLC Agilent 1260 Infinity. Saturates, aromatics and NSO (nitrogen, sulfur, and oxygen) compounds (or resins) were separated using different flow rates and solvent mixtures of *n*-hexane ($C_6H_{14}$) and dichloromethane, dichloromethane and ethyl acetate ($C_4H_8O_2$), and ethyl acetate and methanol respectively.

Saturate and aromatic fractions were diluted using 1mL of dichloromethane per 3mg of sample for GC and GC-MS analyses. The same dilution rate was used on the saturates for GC-IRMS analyses.

#### *1.3.2.5 Molecular sieving*

*n*-Alkanes were isolated from the saturate fraction using molecular sieves following the methodology described by West et al. (1990). A glass wool-plugged Pasteur pipette was packed with approximately 2g of silicalite powder that was previously activated by heating overnight at 500°C and washed with three bed volumes of *n*-pentane in order to remove impurities. The sample was added to the column and allowed to stand for 2 minutes. Then three additional bed volumes of *n*-pentane were used to elute the sample. The *n*-alkanes were retained in the sieve while the branched

and cyclic (B&C) compounds eluted from the column. This fraction was also diluted with 1mL of dichloromethane per 3mg of sample for biomarker analyses.

#### *1.3.2.6 Gas Chromatography (GC)*

GC analyses were performed using an Agilent 6890 series gas chromatograph equipped with a 30m x 0.32mm Agilent/J&W Scientific HP-5 fused silica capillary column coated with a 0.25µm liquid film and a flame ionization detector (FID). The volume injected in the GC instrument was 1uL per sample. The temperature program started with an initial temperature of 40ºC with 10 minutes hold time. The temperature was increased to 300ºC at a rate of 4ºC per minute followed by an isothermal period of 24 minutes for a total run of 99 minutes. The injector and flame ionization detector (FID) temperatures were set at 300ºC and 310ºC respectively. Samples were analyzed in splitless mode using helium (He) as the carrier gas at a flow rate of 1.4mL per minute. *n*-alkanes and isoprenoids were identified in each chromatogram using relative retention times.

#### *1.3.2.7 Gas Chromatography-Mass Spectrometry (GC-MS)*

Biomarker analyses of the branched and cyclic alkanes (B&C) and aromatic fractions were carried out using an Agilent 7890 gas chromatograph coupled with a 5975 mass selective detector (MSD) using single ion monitoring (SIM, Table 2). The GC used a 60m x 0.25mm Agilent/J&W Scientific DB-5 fused silica capillary column coated with a 0.25µm film thickness. The injected volume of branched and cyclic and aromatic fractions was 1uL per run. The GC program started at 40ºC with 1.5 minutes hold time and was later increased to 300ºC at a rate of 4ºC per minute and then held

constant for 34 minutes for a total run time of 100.5 minutes. Samples were run in splitless mode and Helium was used as the carrier gas with a flow rate of 1.4mL per minute. Biomarkers were identified from fragmentograms corresponding to each ion using relative retention times and by comparison with published data.

**Table 2. List of ions selected for GC-MS analysis of branched and cyclic and aromatic fractions from Eagle Ford Shale samples**

| Fraction | m/z | Biomarker |
|---|---|---|
| **Branched & Cyclics** | **66.0** | Deuterated *n*-Tetracosane (internal standard) |
| | **191.3** | Tri/tetra/pentacyclic Hopanes |
| | **217.3** | Regular steranes, Diasteranes, Pregnanes |
| | **133.1** | Aryl Isoprenoids |
| | **253.3** | Monoaromatic Steroids |
| **Aromatics** | **188.2** | Deuterated Phenanthrene (internal standard) |
| | **178.3** | Phenanthrene |
| | **192.3** | Methylphenanthrenes |
| | **206.3** | Dimethylphenanthrenes |
| | **231.3** | Triaromatic Steranes |

*1.3.2.8 Quantitative Biomarker Analysis*

Quantitation of biomarkers present in the branched and cyclics, and aromatic fractions of source rock extracts, condensates, and oils was done by adding a known aliquot of internal standard (ISTD) to each sample before GCMS analysis. The branched and cyclics, and aromatic samples were quantitatively spiked with deuterated *n*-tetracosane ($C_{24}D_{50}$) and deuterated phenanthrene ($C_{14}D_{10}$) respectively. The resulting solution was injected into the GCMS. The relative concentration of biomarkers in ppm or µg/g SAT (saturates) or ARO (aromatics) reported here was calculated from peak areas of each biomarker compared to that of the ISTD using a response factor.

In particular, the response factor of the ISTD ($RF_{ISTD}$) for each sample was calculated using the peak area of the ISTD ($A_{ISTD}$) as follows:

$$RF_{ISTD} = \frac{C_{ISTD\ inj}}{A_{ISTD}} \qquad [1]$$

The concentration of the ISTD in the solution prepared for GCMS injection ($C_{ISTD\ inj}$) was calculated using the formula:

$$C_{ISTD\ inj} = \frac{C_{ISTD} \times V_{ISTD}}{V_{B\&C\ or\ ARO} + V_{ISTD}} \qquad [2]$$

where,

$C_{ISTD}$ = Concentration of ISTD in the internal standard solution

$V_{ISTD}$ = Total volume of internal standard added to the B&C or Aromatics solution

$V_{B\&C\ or\ ARO}$ = Total volume of B&C or Aromatics solution prepared for injection

In our experiments, $V_{B\&C\ \text{or}\ ARO} >> V_{ISTD}$ (e.g. $V_{B\&C\ or\ ARO}$ = 100μL and $V_{ISTD}$ = 2μL), therefore equation [2] can be approximately calculated as:

$$C_{ISTD\ inj} \approx \frac{C_{ISTD} \times V_{ISTD}}{V_{B\&C\ or\ ARO}} \qquad [3]$$

The concentration of the biomarker ($C_a$) in the solution prepared for GCMS injection was calculated using the formula:

$$C_a = RF_{ISTD} \times A_{bio}$$

$$C_a \approx \frac{C_{ISTD} \times \left[\frac{V_{ISTD}}{V_{B\&C\ or\ ARO}}\right]}{A_{ISTD}} \times A_{bio} \qquad [4]$$

where,

$A_{bio}$ = Peak area of the biomarker

The concentration of the solution prepared for GCMS injection ($C_b$) was calculated as follows:

$$C_b = \frac{C_{B\&C\ or\ ARO} \times V_{B\&C\ or\ ARO}}{V_{B\&C\ or\ ARO} + V_{ISTD}} \qquad [5]$$

and $C_b \approx C_{B\&C}$

where,

$C_{B\&C\ or\ ARO}$ = Concentration of the B&C or Aromatics solution

Hence, the concentration of biomarkers in the saturate or aromatic fraction ($C_{bio\ X}$) is:

$$C_{bio\ X} = \frac{C_a}{C_b} \times F_X \times (1 \times 10^6) \qquad [6]$$

or

$$C_{bio\ X} \approx \frac{C_{ISTD} \times V_{ISTD}}{A_{ISTD} \times V_{B\&C\ or\ ARO}} \times \frac{1}{C_{B\&C\ or\ ARO}} \times A_{bio} \times F_X \times 1 \times 10^6 \qquad [7]$$

where,

Subscript $X$ = Saturate or aromatic fraction

If $X$ = Saturate, $F_{Sat} = \frac{m_{B\&C}}{m_{Sat}}$

IF $X$ = Aromatic $F_{Aro} = 1$

$m_{B\&C}$ = Amount of B&C obtained from molecular sieving

$m_{Sat}$ = Amount of saturate fraction used for molecular sieving

$1x10^6$ = Conversion factor to µg biomarker/g Saturates or Aromatics

In case of source rocks extracts, it is recommended to express the concentrations in µg biomarker/g TOC, whereas crude oil concentrations should be reported in µg biomarker/g whole oil. Therefore, after obtaining the biomarker concentrations relative to the saturate or aromatic fractions, another factor needs to be added to the calculations in order to normalize the biomarker concentrations relative to TOC and whole oil, respectively.

For source rock extracts:

$$C_{bio\,x} = \frac{\mu g\ biomarker}{g\ Saturates} \times \frac{m_{Sat}}{m_{TOC}}$$

and

$$\frac{m_{Sat}}{m_{TOC}} = \frac{\frac{m_{Sat}}{m_{Maltenes}} \times \frac{m_{Maltenes}}{m_{Extract}} \times \frac{m_{Extract}}{m_{Rock}}}{\frac{m_{TOC}}{m_{Rock}}}$$

where

$\frac{m_{Sat}}{m_{TOC}}$ = Amount of saturate fraction, $m_{Sat}$ (g) within one gram (1g) of total organic carbon (TOC)

$\frac{m_{Sat}}{m_{Maltenes}}$ = Amount of saturate fraction, $m_{Sat}$ (g) recovered from the maltenes fraction, $m_{Maltenes}$ (g) by HPLC

$\frac{m_{Maltenes}}{m_{Extract}}$ = Amount of maltenes, $m_{Maltenes}$ (g) recovered from the source rock extract, $m_{Extract}$ (g) by *n*-$C_5$ precipitation

$\frac{m_{Extract}}{m_{Rock}}$ = Amount of extract, $m_{Extract}$ (g) recovered from the source rock, $m_{Rock}$ (g) by Soxhlet extraction

$\frac{m_{TOC}}{m_{Rock}}$ = Amount of TOC $m_{TOC}$ (g) determined in the source rock $m_{Rock}$ (g) by LECO TOC

TOC is generally reported as weight percent (%wt.), which corresponds to the amount of TOC (g) in 100g of rock.

For oil samples:

$$C_{bio\,X} = \frac{\mu g\ biomarker}{g\ Saturates} \times \frac{m_{Sat}}{m_{WO}}$$

and

$$\frac{m_{Sat}}{m_{WO}} = \frac{m_{Sat}}{m_{Maltenes}} \times \frac{m_{Maltenes}}{m_{WO}}$$

$\frac{m_{Sat}}{m_{WO}}$ or g Sat/g oil is the number of grams saturate fraction recovered from one gram oil.

$\frac{m_{Sat}}{m_{Maltenes}}$ is the amount of saturate fraction $m_{sat}$ (g) recovered from $m_{Maltene}$(g) maltene by liquid chromatography.

$\frac{m_{Maltenes}}{m_{WO}}$ is the amount of Maltene $m_{Maltene}$ (g) recovered from $m_{oil}$(g) oil by *n*-$C_5$ precipitation.

Regarding the biomarker concentrations in the aromatic fraction, the term $m_{Sat}$ was substituted for the term $m_{Aro}$, which corresponds to the amount of aromatic fraction recovered from the maltenes fraction by HPLC.

### *1.3.2.9 Gas Chromatography Isotope-Ratio Mass Spectrometry (GC-IRMS)*

Individual compounds of the saturate fractions were analyzed for compound specific isotopes using an Agilent 7890 gas chromatograph with a Isolink and Carbon combustion reactor interfaced to an Conflo IV and a Thermo MAT 253 isotope-ratio mass spectrometer. The GC used a 60m x 0.25mm x 0.25µm film Agilent/J&W Scientific DB-1MS capillary column. The injection volume of sample was 1uL. The temperature program was initially set at 40ºC and held isothermal for 1.5 minutes. Then it was increased at a rate of 4ºC per minute to 300ºC and held constant for 24 minutes for a total run time of 90 minutes. Samples were analyzed in splitless mode injection using He as the carrier gas. This method pulses $CO_2$ standard according to the time events set up. The samples are run with deuterated *n*-nonane ($C_9D_{20}$), *n*-decane ($C_{10}D_{22}$), *n*-hexadecane ($C_{16}D_{34}$), *n*-nonadecane ($C_{19}D_{40}$), *n*-tetracosane ($C_{24}D_{50}$), and *n*-dotriacontane ($C_{32}D_{66}$) as external standards.

# CHAPTER II

# 2. RESULTS AND DISCUSSION

Data presented in the following chapters uses the Formations, Members, and Facies subdivision proposed by Donovan et al. (2012, 2013a and b, 2014) for the Eagle Ford Group at the Lozier Canyon outcrop (EFLC), Fasken "A" #1 core (EFFA), Bouldin Creek outcrop (EFBC), and ACC #1 core (EFAC). Harbor (2011) and Fairbanks (2012) also defined a facies subdivision for the Bouldin Creek outcrop (EFBC) and ACC #1 (EFAC) cores. These data overlap allowed the assignment of the same nomenclature from Donovan et al. (2012, 2013a and b) to these cores and to extend it to the W. Brechtel #1 (EFWB) and C.J. Hendershot #1 (EFHE) cores. This nomenclature was adopted to standardize the different geologic units and facilitate the interpretations and correlations of geochemical data. In the case of the Ferguson McKnight #526-1H (EFMK) and Lily Hoppess #1 (EFLH) wells, the available data was not sufficient to assign Donovan et al.'s (2012, 2013a and b) terminology and the original Formation assignment will be used.

## 2.1 Geochemical Screening

Outcrop and subsurface rock samples analyzed in this study were initially screened using Rock Eval pyrolysis and TOC. From these data, sets of subsamples were selected for biomarker and isotope analyses. Table 3 shows the definitions of Rock Eval pyrolysis terms used in the discussion and presented in subsequent Figures and Tables. Appendix B shows detailed Rock Eval pyrolysis and TOC data obtained from the outcrop and core samples analyzed.

**Table 3. Parameters, terms, and definitions derived from Rock Eval pyrolysis analyses (modified from Peters, 1986 and Jarvie et al., 2007)**

| | | |
|---|---|---|
| **TOC** | Total Organic Carbon | wt.% |
| **$S_1$** | Free volatile hydrocarbons thermally flushed from a rock sample at 300°C (free oil content) | mg HC/g rock |
| **$S_2$** | Products that crack during standard Rock Eval pyrolysis temperatures (remaining potential) | mg HC/g rock |
| **$S_3$** | Organic carbon dioxide released from rock samples | mg $CO_2$/g rock |
| **$T_{max}$** | Temperature at peak evolution of $S_2$ hydrocarbons | °C |
| **HI** | Hydrogen Index = $S_2$ x 100/TOC | mg HC/g TOC |
| **OI** | Oxygen Index = $S_3$ x 100/TOC | mg $CO_2$/g TOC |
| **$S_1$/TOC** | Normalized Oil Content = $S_1$ x 100/TOC | |
| **$S_2/S_3$** | Describes type of hydrocarbons generated | Values from 0.00 to >5.00 |
| **PI** | Production Index = $S_1/(S_1+S_2)$ (or transformation ratio) | Values from 0.00 to 1.00 |

### 2.1.1 Organic Richness

Throughout Texas, the Eagle Ford Shale proves to be an excellent potential source rock based on its TOC, HI, and thermal maturity. Table 4 shows average TOC for the outcrop and subsurface rock samples analyzed in this study. In general, the Eagle Ford Shale shows good to excellent source rock potential based on the guidelines of Peters and Cassa (1994). Several EFLC and EFBC samples may have higher "pre-weathering" TOC and HI values, since some of these outcrop samples were affected by weathering, which tends to decrease the amount of organic carbon. In particular, the upper section from the Lozier Canyon outcrop is highly weathered, and when

recalculating TOC for the EFLC samples including only Facies A through C, the average TOC values increase to 2.44% (Figure 14).

**Table 4. Average TOC values for the Eagle Ford Shale outcrop and subsurface rock samples analyzed in this study**

| Well name | # of samples | Average TOC (wt.%) |
|---|---|---|
| EFLC | 40 | 1.8 |
| EFMK | 26 | 2.1 |
| EFFA | 40 | 4.0 |
| EFBC | 34 | 3.0 |
| EFAC | 10 | 3.8 |
| EFWB | 9 | 4.6 |
| EFHE | 10 | 4.7 |
| EFLH | 22 | 4.2 |

Figure 14 shows the TOC geochemical logs for the outcrops and wells analyzed. The logs show a fair variability in terms of organic richness, which may be a result of variations in organic facies. In general, the outcrops and wells analyzed contain greater amounts of organic carbon in the Lower Eagle Ford Shale, particularly in the Lozier Canyon Member. In the case of the EFFA samples, it is possible that the TOC values have been affected by the high maturity of the Eagle Ford Shale in this area.

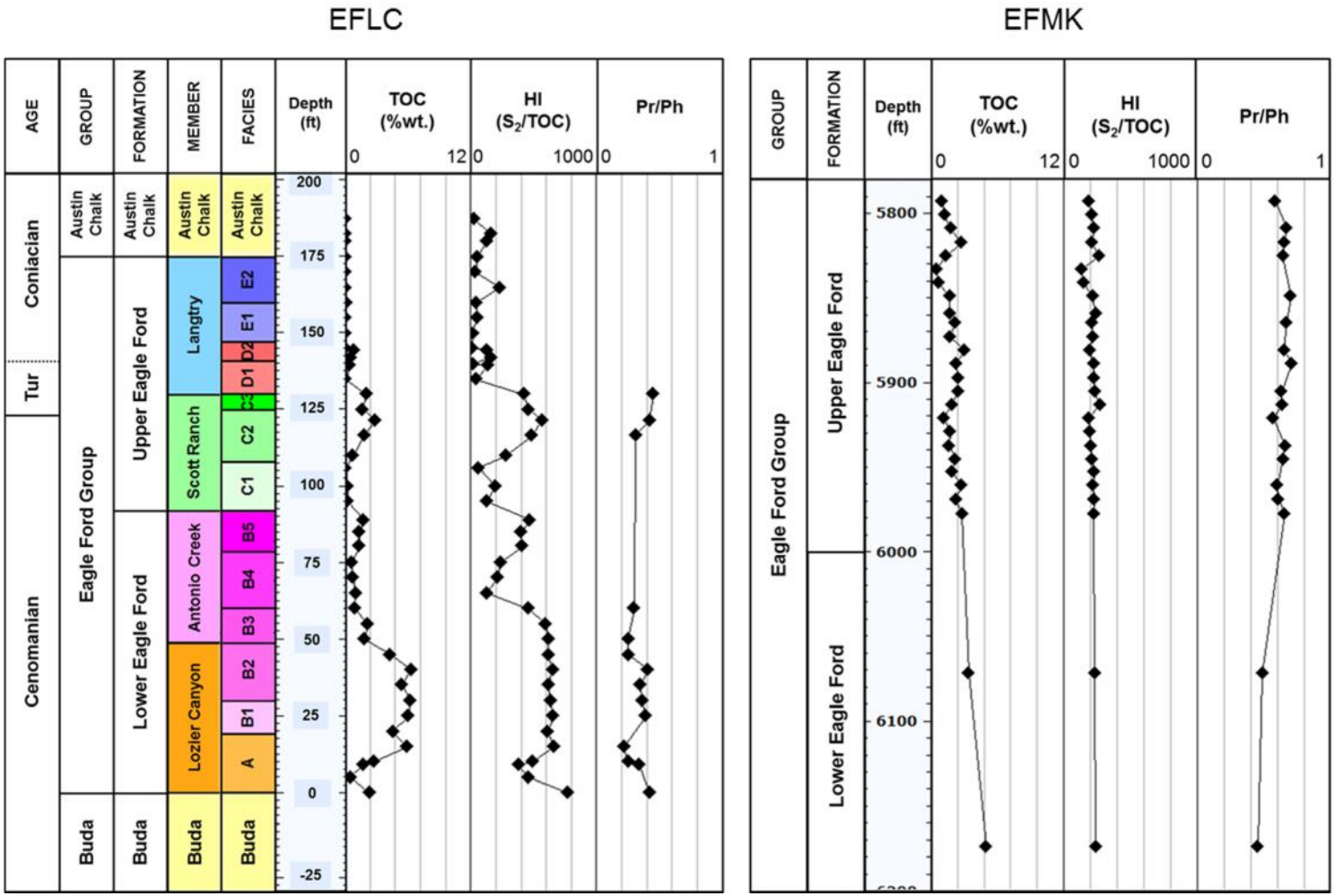


**Figure 14. TOC, HI, and Pr/Ph geochemical logs for the Eagle Ford Shale outcrop and subsurface samples analyzed in this study (Pr = pristane; Ph = phytane)**

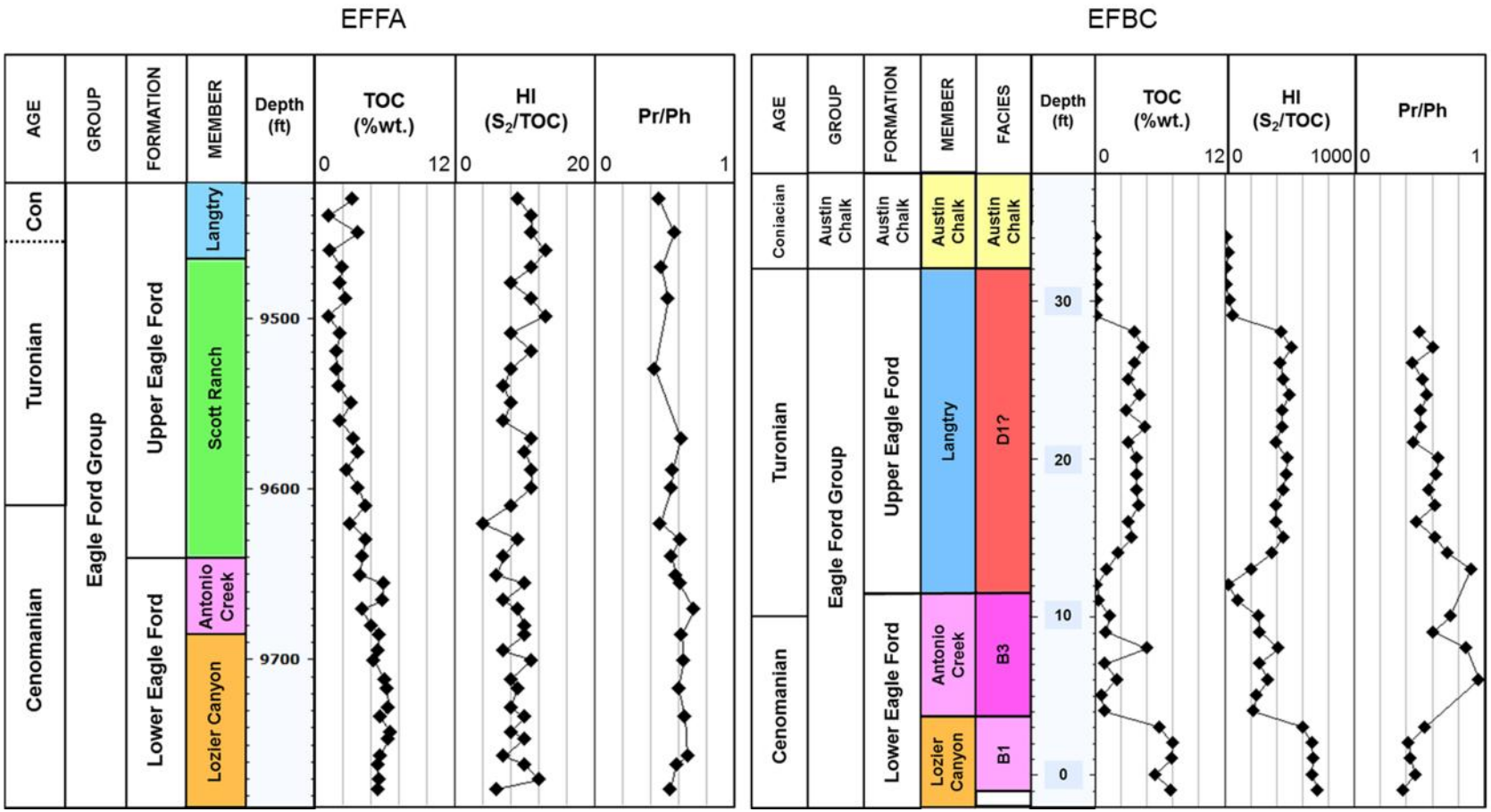


**Figure 14. TOC, HI, and Pr/Ph geochemical logs for the Eagle Ford Shale outcrop and subsurface samples analyzed in this study (Pr = pristane; Ph = phytane; cont.)**

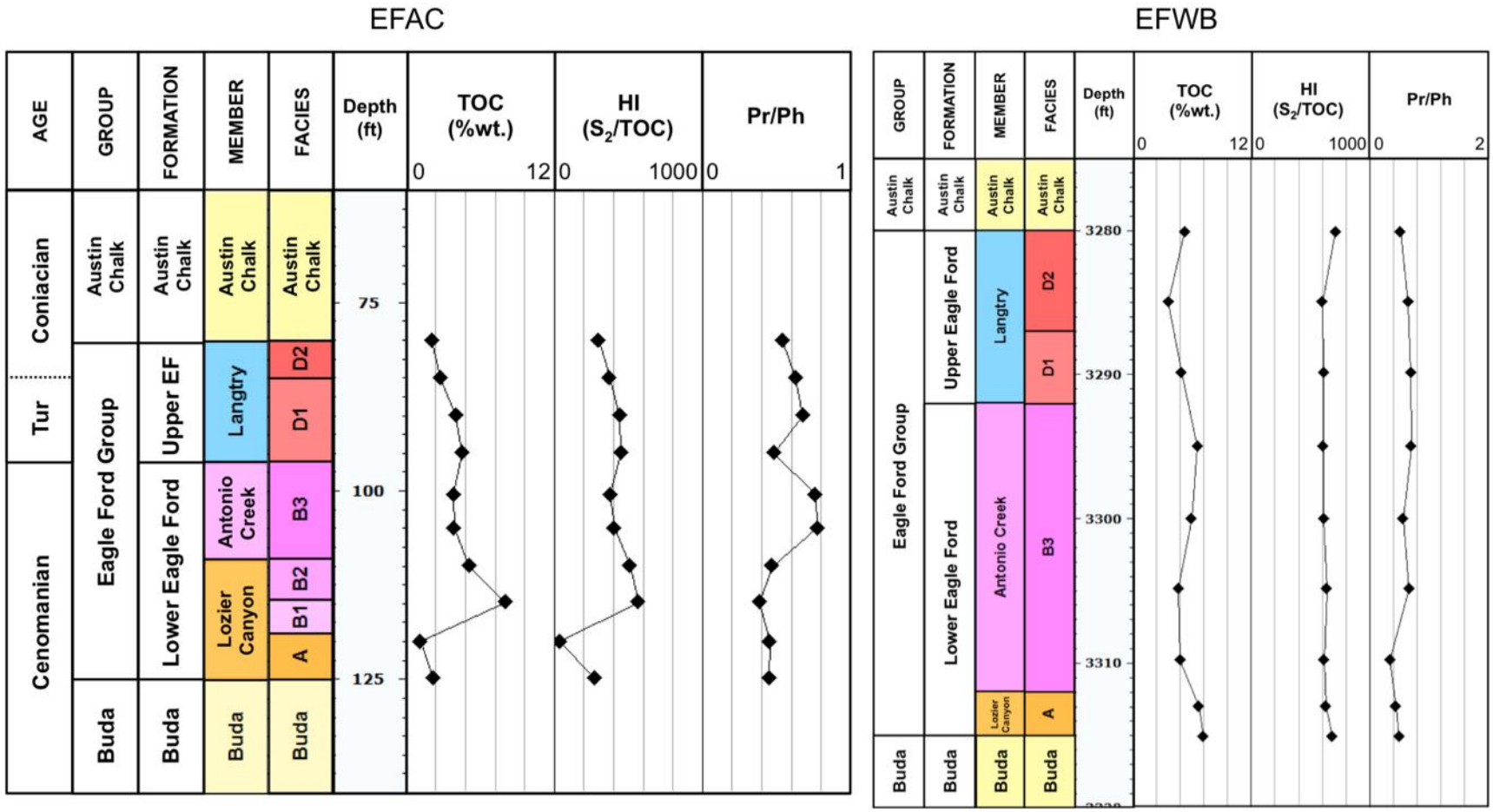


**Figure 14. TOC, HI, and Pr/Ph geochemical logs for the Eagle Ford Shale outcrop and subsurface samples analyzed in this study (Pr = pristane; Ph = phytane; cont.)**

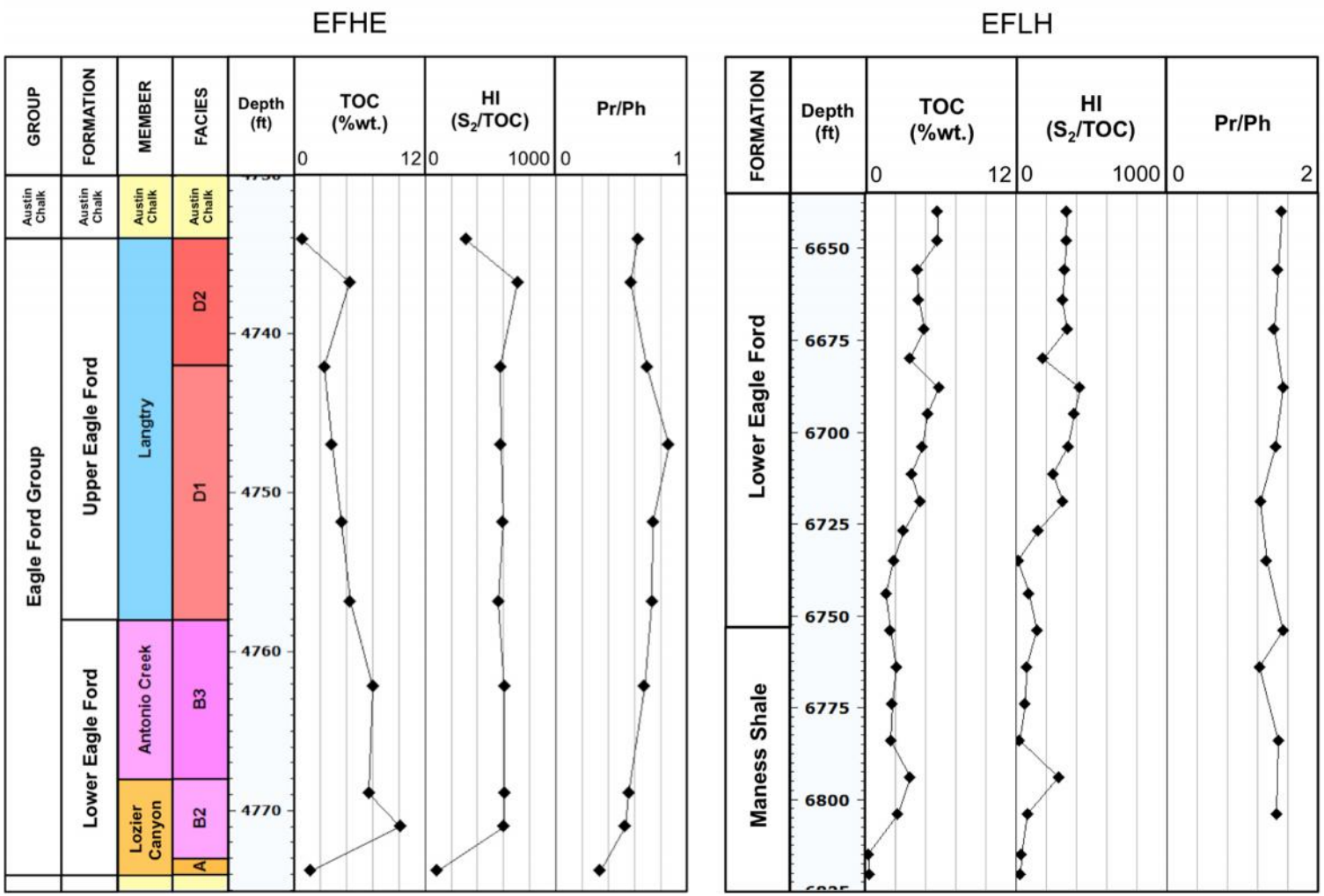


**Figure 14. TOC, HI, and Pr/Ph geochemical logs for the Eagle Ford Shale outcrop and subsurface samples analyzed in this study (Pr = pristane; Ph = phytane; cont.)**

### 2.1.2 Organic Matter Type

Rock Eval parameters were used for an initial evaluation of the kerogen type in the Eagle Ford Shale. A plot of Hydrogen Index (HI) versus Oxygen Index (OI), also known as a Van Krevelen-type diagram (Figure 15; Tissot et al., 1974; Tissot and Welte, 1984; Hunt, 1979) shows great variations of HI between the samples. Rock samples from EFAC, EFWB, EFHE, EFBC and some from EFLC show a predominance of Type II kerogen, which is mainly of marine origin. In addition, the high HI values for these samples may be a result of their low maturity. The few EFLC samples plotted towards the Type III field of the Van Krevelen-type diagram correspond to samples from the upper section of the outcrop, which are affected by weathering. In this case, their low HI values may be a result of organic matter alteration and not due to a terrigenous source. Very low HI values from the EFFA samples are the result of its high thermal maturity. Consequently, these samples show a Type III, gas-prone kerogen signature, which in this case is not related to organic matter source. In general, the EFLH samples are dominated by Type II-III kerogen. Interestingly, the samples with HI values lower than 200 correspond to Maness Shale samples. Deposition of Maness Shale sediments in the East Texas region was influenced by the Dexter fluvial system, which distributed siliciclastic sediments sourced from the Ouachita Highlands south into Texas and Louisiana (Adams and Carr, 2010). This sedimentary process may have possibly produced dilution of the organic matter due to a clastic input into the Maness Shale sediments. From the current sample distribution on the Van Krevelen-type diagram, one would be cautious to establish a definite organic matter type. Nevertheless, source rocks have mixes of different types of kerogen due to

variations in environmental conditions throughout the depositional history of the rock, and in some cases, due to their maturation history. Maturity influences the amounts and composition of kerogen and bitumen in the source rock, which in turn affects the HI and OI values calculated to construct this diagram.

Geochemical logs of HI (Figure 14) show a similar trend to that of TOC, indicating that in general, the Eagle Ford Shale has good oil and gas potential, particularly in the interval corresponding to the Lozier Canyon Member.

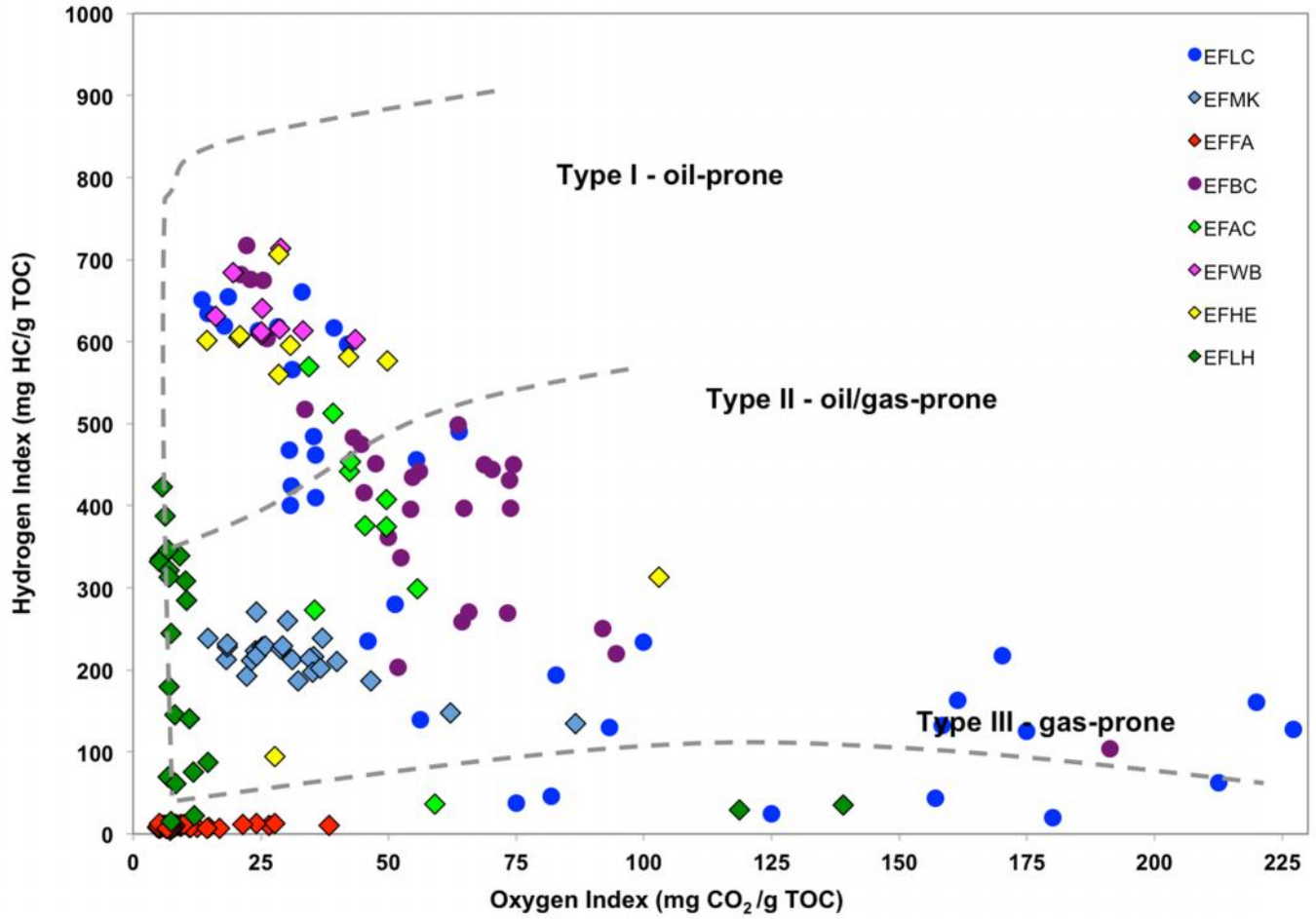


**Figure 15. Modified Van Krevelen diagram for the Eagle Ford Shale samples. HI values for EFFA samples are unreliable due to their low remaining hydrocarbon potential**

An alternative approach to assess the kerogen quality in potential source rock samples, especially in those rocks with high carbonate content is by using a diagram of $S_2$ versus TOC (Cornford et al., 1998; Figure 16). This diagram confirms the predominance of Type-II oil-prone kerogen for most of the Eagle Ford Shale samples and shows the low remaining hydrocarbon potential of the EFFA samples as a result of their high maturity. Initially, it was thought that the mix of Type II-III kerogen that characterizes the EFMK samples was related to an organic matter mix or variations in thermal maturity. However, when diagrams of $S_1$ versus TOC (Figure 17) and $T_{max}$ versus PI (Figure 18) were generated, it was observed that these samples might be contaminated or stained with non-indigenous hydrocarbons or migrated oil. According to Hunt (1979), sidewall cores, cores, and cuttings can be contaminated by drilling mud and handling during the drilling process, affecting the source rock extracts. Therefore, these samples needed to be carefully evaluated on subsequent analyses.

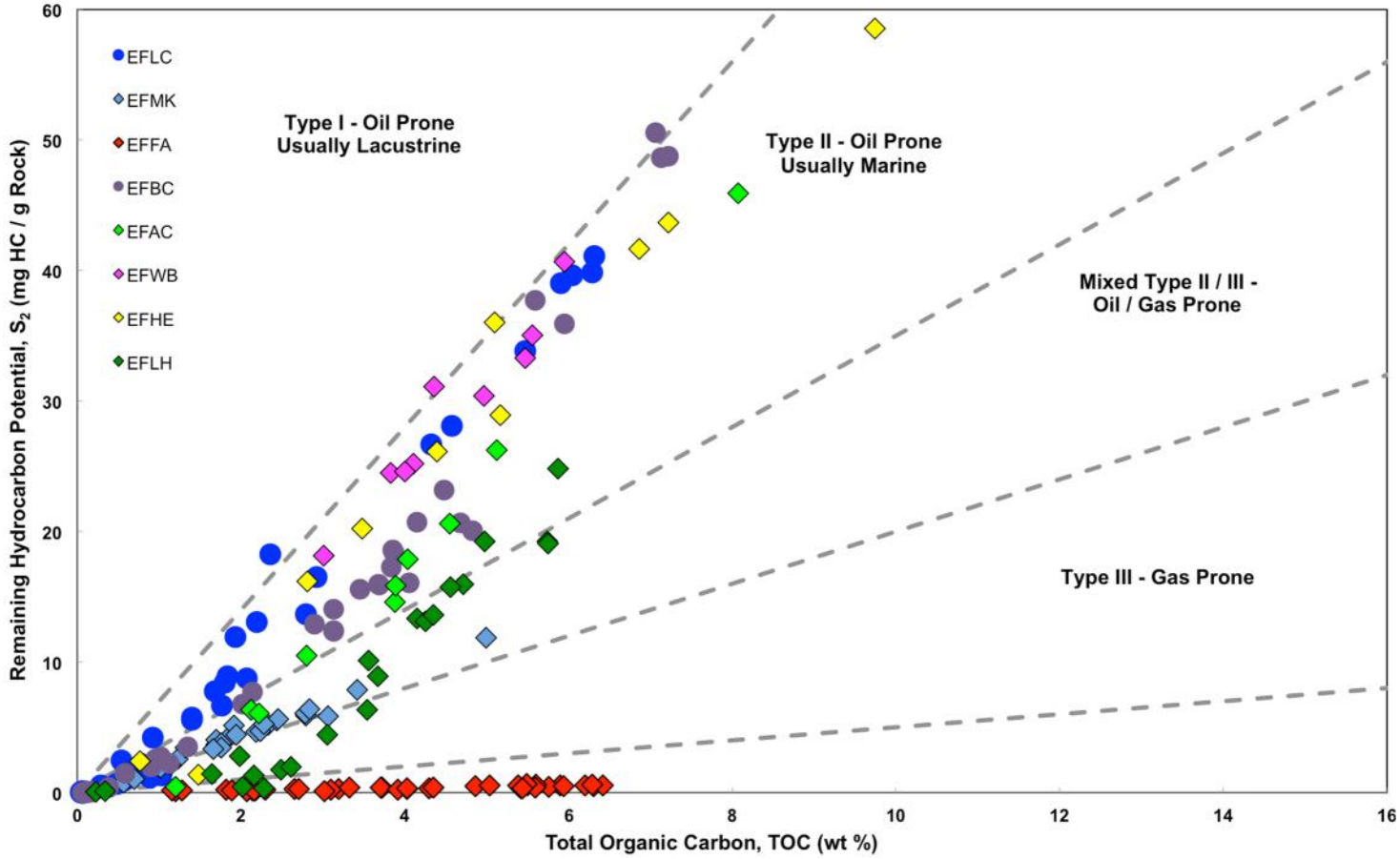


**Figure 16. Rock Eval Remaining Hydrocarbon Potential ($S_2$) vs. TOC plot for determination of kerogen type and maturity of Eagle Ford Shale samples (plot template modified from GeoMark Research Ltd.)**

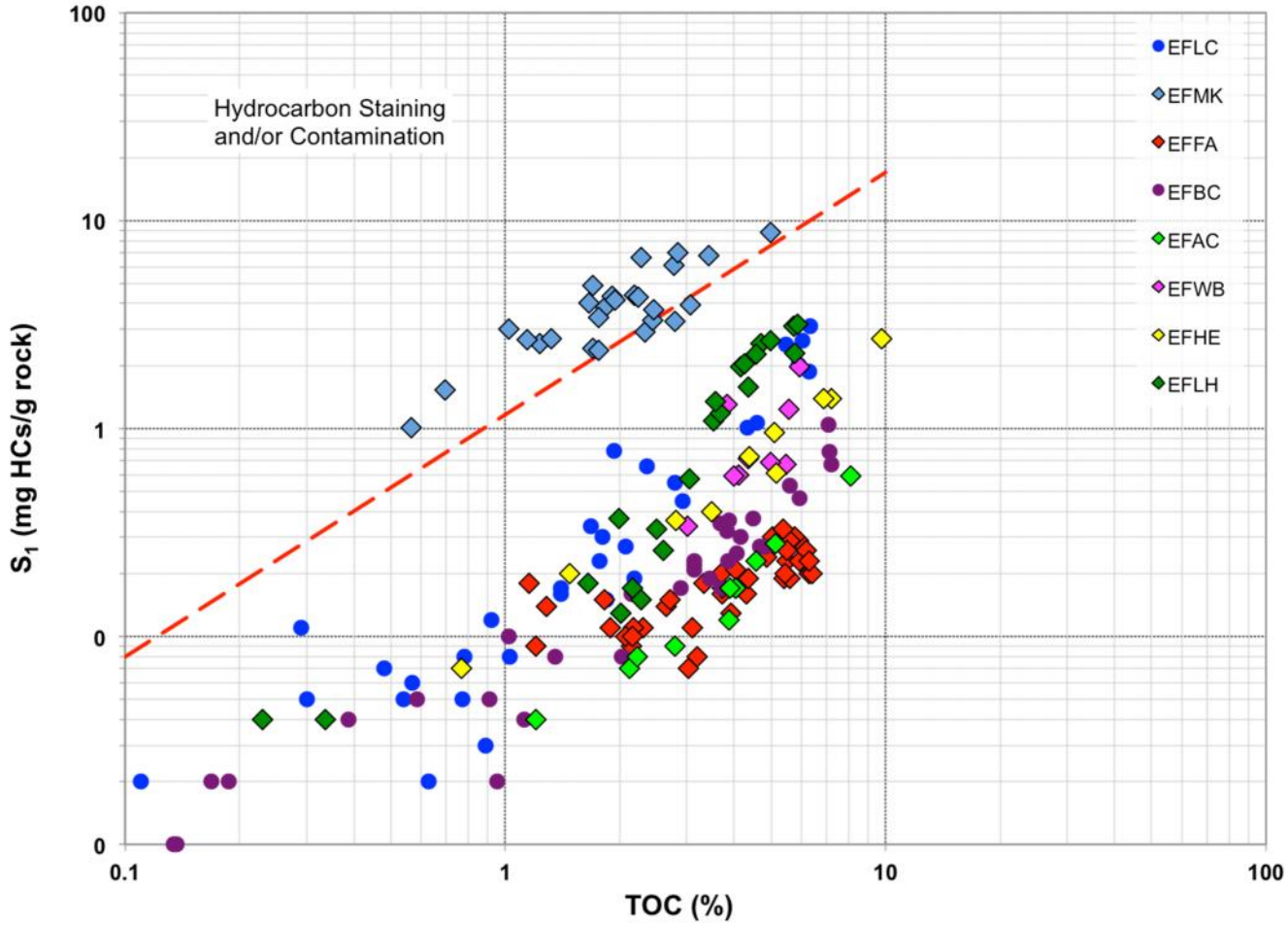


**Figure 17. $S_1$ vs. TOC plot for the Eagle Ford Shale samples showing possible hydrocarbon contamination of the EFMK samples (plot template modified from GeoMark Research Ltd.)**

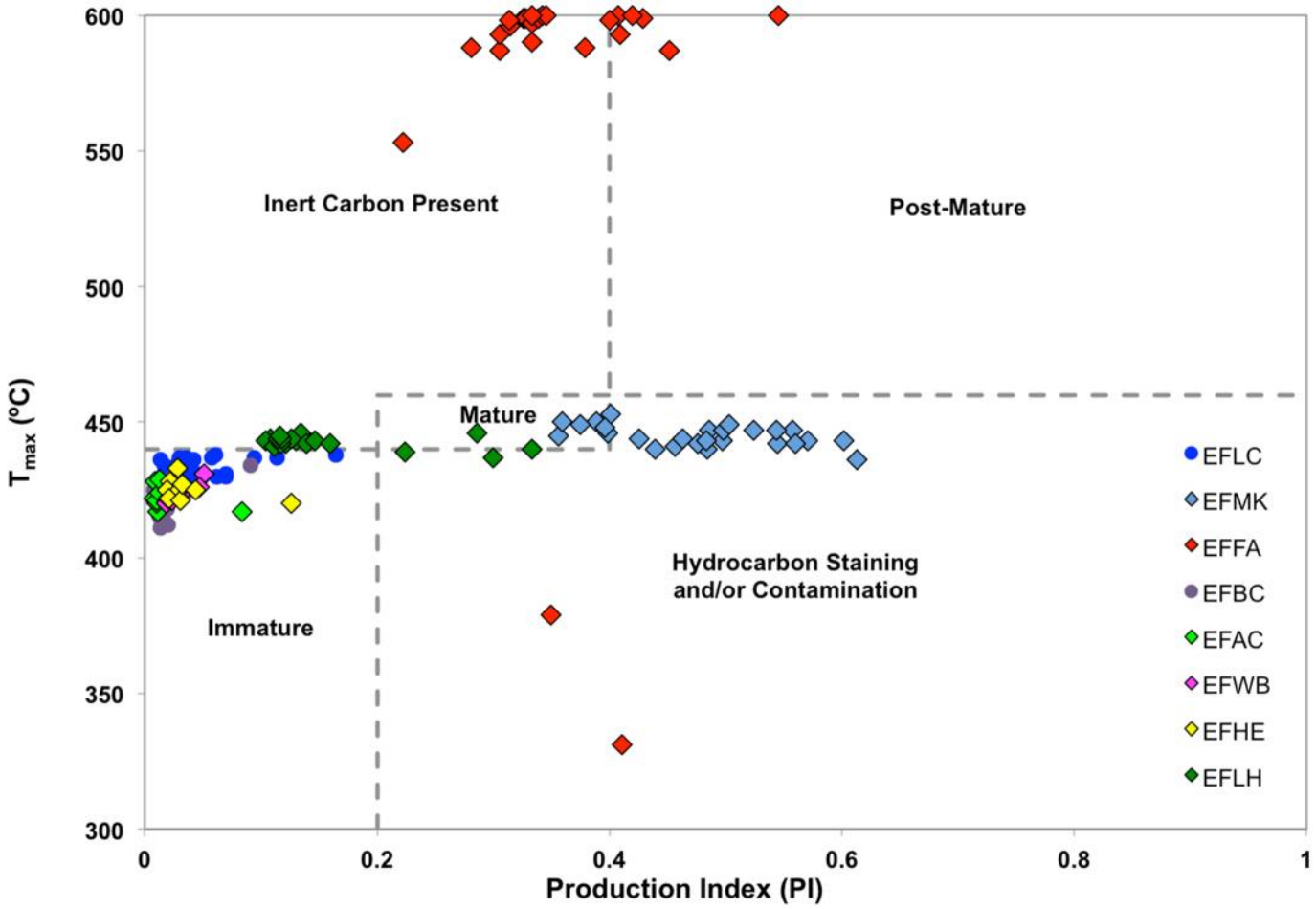


**Figure 18. $T_{max}$ vs. Production Index (PI) plot for determination of thermal maturity and sample contamination of Eagle Ford Shale samples (plot template modified from GeoMark Research Ltd.)**

### 2.1.3 Thermal Maturity from Rock Eval and Vitrinite Reflectance Analysis

Based on Rock Eval $T_{max}$ values (Figures 18 and 19), most of the Eagle Ford Shale samples analyzed from East and West Texas are thermally immature to marginally mature (early oil window; $T_{max} < 445°C$). The EFFA samples have very low $S_2$ values (Appendix B) indicating the low remaining hydrocarbon potential for these rocks. As a result, HI and $T_{max}$ parameters, which are calculated from $S_2$ are unreliable for these samples. The $T_{max}$ versus PI plot (Figure 18) shows that the EFFA samples may contain dead or inert carbon and some samples from the EFMK core may be contaminated with hydrocarbons as previously mentioned.

Vitrinte reflectance ($\%R_o$) measurements were attempted on four Eagle Ford Shale samples from four different locations: EFLH-9, EFLC-10, EFBC-8, and EFFA-3. Overall, vitrinite identification of these samples was challenging. In the Eagle Ford Shale samples selected for $R_o$ analysis the vitrinite is scarce. This fact was rather expected since vitrinite is mainly derived from land-plant material (ASTM, 2011). Because the Eagle Ford Shale was deposited in a carbonate environment there is very low (if any) terrigenous organic matter contribution. Most of the vitrinite fragments identified were isolated and pitted. Isolated grains are generally unreliable for measuring vitrinite reflectance, since these may be unrelated to the sample and correspond to contamination acquired during sample preparation. Pitted vitrinite usually shows lower reflectance values. In addition, some vitrinite clasts were smaller than the measuring spot of the microscope used for the analyses, which also lead to unreliable measurements. In the East Texas EFLH-9 sample, ten (10) vitrinite clasts were identified and measured, ranging from 0.91 to 1.22%$R_o$ with a mean random $R_o$

measurement of 1.04%, indicating that in this area the Eagle Ford Shale is in the oil window. Figure 20 shows a photomicrograph of a vitrinite clast (1.06%$R_o$), bitumen (0.62%$R_o$), and lignite contamination (0.29%$R_o$) from sample EFLH-9 (Brian Cardott, 2013, personal communication). This figure illustrates the variability of macerals and bitumen content observed in the Eagle Ford Shale samples that could potentially lead to errors in the identification and measurement of vitrinite reflectance. The amount of vitrinite observed in this sample compared to the Central and West Texas samples might indicate an input of terrigenous organic matter for the East Texas area. Rock pellets EFLC-10 and EFBC-8 corresponding to outcrop samples were too weathered for obtaining a statistically representative sample, and sample EFFA-3 was too mature to observe any type of maceral. However, Liro et al. (1994) were able to measure vitrinite reflectance in samples from the Bouldin Creek outcrop (samples EFBC in this study), obtaining values of 0.45%$R_o$, which indicates that in this area the Eagle Ford Shale is thermally immature. Slatt et al. (2012) characterized samples from the Comstock West outcrop (US Highway 90, Val Verde County, Texas), and determined that in this location the Eagle Ford Shale is immature, with $T_{max}$ values between 423 and 429°C and a mean random vitrinite reflectance value of 0.53%. The interval analyzed in their study corresponds to Facies B of Donovan and Staerker (2010) and Donovan et al. (2012; 2013a and b) at the Lozier Canyon site. Since the Lozier Canyon outcrop is located about 40 miles northwest from the Comstock West outcrop, it is inferred that the thermal maturity at Lozier Canyon would be similar. Edman (2012) analyzed the thermal maturity of several Eagle Ford Shale rocks, bitumens, and oils from the First Shot oil field (Wilson, Gonzales, and Karnes Counties, Texas) using a combination of

vitrinite reflectance measurements and various maturity geochemical parameters. The author determined that the thermal maturity of the Eagle Ford Shale at the oil field location ranged from early to late oil window (0.50 to 1.21%$R_o$; Edman, 2012). The First Shot oil field is located about 20 miles south from the EFWB and EFHE wells analyzed in this study; hence, the maturity in the Austin area should be similar to that observed by Edman (2012).

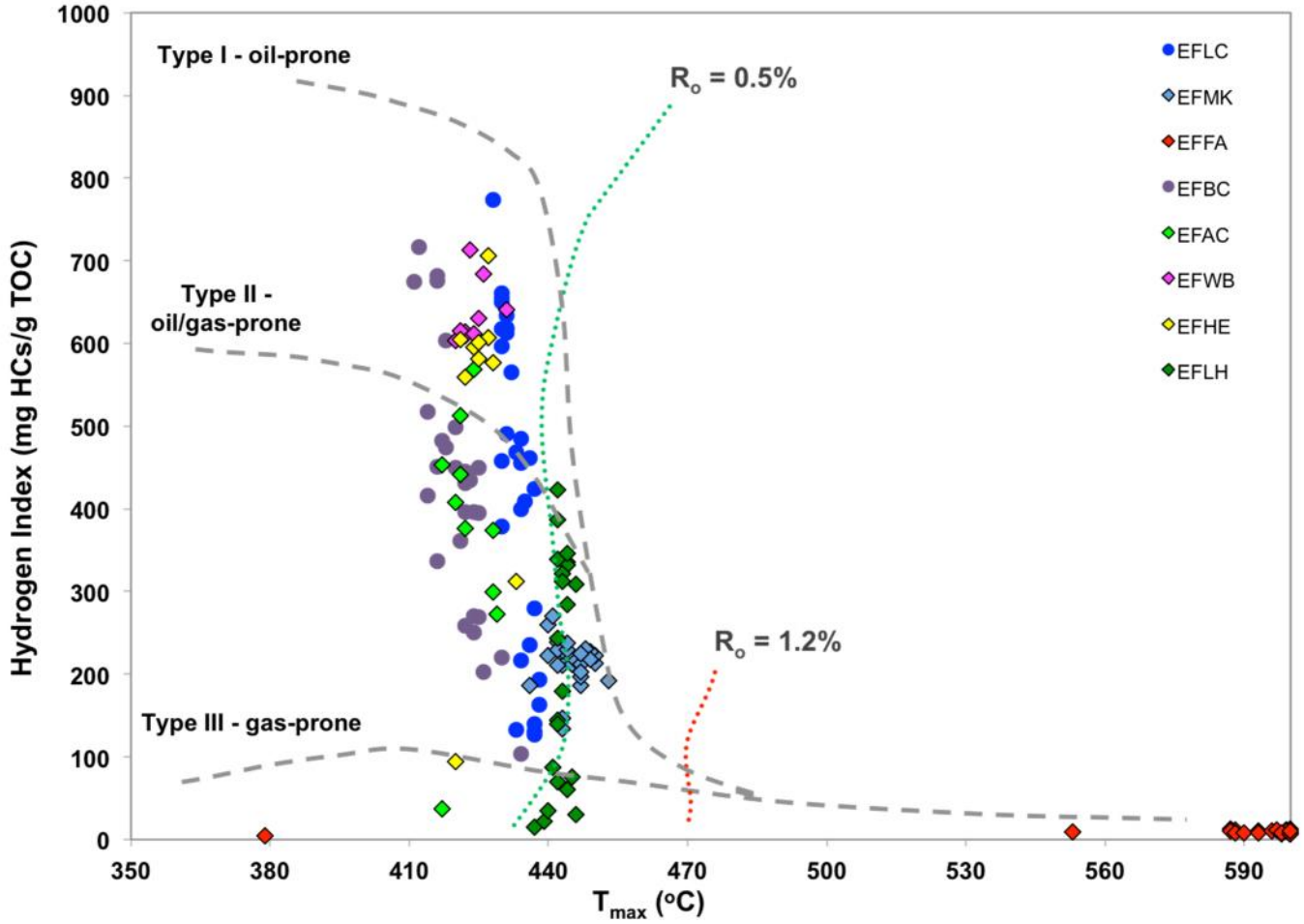


**Figure 19. $T_{max}$ vs. HI plot showing maturity and kerogen type of the Eagle Ford Shale samples. HI values for EFFA samples are unreliable due to their low remaining hydrocarbon potential**

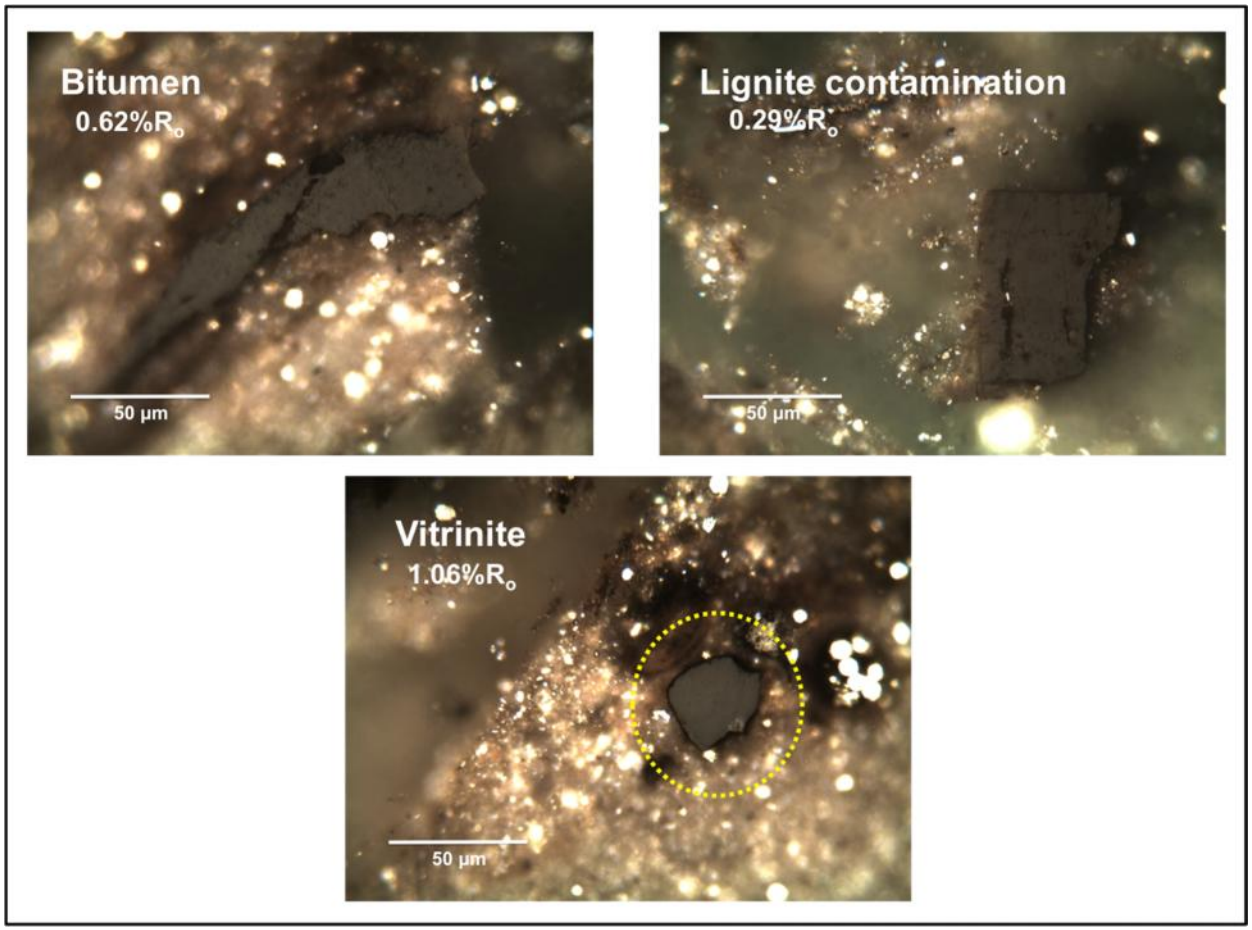


**Figure 20. Photomicrographs from the EFLH-9 Eagle Ford Shale sample (Photomicrographs courtesy of Brian Cardott, 2013)**

### 2.1.4 Gas Chromatography

#### *2.1.4.1 n-Alkanes distribution*

Gas chromatograms from the saturate fraction of bitumen extracted from Eagle Ford Shale samples show minimal compositional variations between the different members (Figure 21). Detailed results of these analyses including formulas, selected chromatograms, and ratios calculated are presented in Appendices A, C, and D respectively. Table 5 summarizes some of the geochemical parameters calculated from the *n*-alkanes fingerprints for each sample set. The terrigenous to aquatic ratio (TAR), is a parameter calculated to evaluate the type of organic matter input that compares the high-odd-carbon-numbered *n*-alkanes (terrigenous organic matter) with the low-odd-carbon-numbered *n*-alkanes (marine organic matter; Peters et al., 2005). The carbon preference index (CPI; Bray and Evans, 1961) compares the odd-carbon-numbered *n*-alkanes ($n$-$C_{25}$-$n$-$C_{33}$) against the even-carbon-numbered *n*-alkanes ($n$-$C_{24}$-$n$-$C_{34}$). In general, *n*-alkanes originated from marine organic matter do not show carbon-number preference, whereas *n*-alkanes derived from terrigenous organic matter tend to show odd-carbon-number predominance. Low maturity hypersaline and carbonate source rocks usually show low CPI values due to a predominance of even-numbered *n*-alkanes (Peters et al., 2005). In some cases, CPI can be used to roughly assess thermal maturity. According to Peters et al. (2005), oils and bitumens with CPI values significantly above 1.0 (odd predominance) are indicative of low thermal maturity. The TAR and CPI ratios are therefore influenced by source and thermal maturity (Peters et al., 2005), and additional geochemical parameters need to be correlated with these ratios when characterizing oils and source rocks.

In case of the Eagle Ford Shale samples analyzed, the majority shows a unimodal distribution towards the low-carbon-number members, and a slight preference of even-carbon-numbered *n*-alkanes (Figure 21). The bitumen samples show a maximum around *n*-$C_{17}$, whereas the oil and condensate samples have *n*-alkanes maxima around *n*-$C_{14}$ and *n*-$C_{15}$. The discrepancy between *n*-alkanes maxima between extracts and oils is mainly due to the loss of low carbon number *n*-alkanes during source rock extraction. Based on their *n*-alkane distributions and low TAR and CPI ratios (~0.2 and ~1.0 respectively), it is inferred that these samples are genetically related. These observations point towards a marine origin and the existence of reducing (anoxic) conditions during source rock deposition. In some samples, peak identification beyond *n*-$C_{26}$ was problematic due to the low intensity of the *n*-alkanes and coelution with steranes and hopanes. This case was particularly true for EFBC, EFAC, EFWB, EFHE, and EFFA samples, for which the TAR ratio could not be calculated. The *n*-alkanes distribution for the EFFA samples is also affected by its high thermal maturity, as indicated by its high CPI values (>1.2). Relatively high CPI and TAR values (>0.25 and >1.0 respectively) for the EFLH samples could be a result of high thermal maturity, although it may also suggest a contribution of terrigenous organic matter. A number of chromatograms from EFLC and EFBC show low *n*-alkanes intensities, which could be related to weathering. According to Hunt (1979), outcrops are commonly exposed to complex weathering processes that significantly decrease the amount of hydrocarbon and organic carbon content in the rocks. Therefore, the chromatographic signature can show similar characteristics to those of biodegraded oil (Philp et al., 1992). The degree of weathering that may affect outcrops is dependent on its porosity, permeability,

fracturing, microbiological activity, and climate (Hunt, 1979). However, Hunt (1979) also points out that the presence of pyrite may indicate low weathering degree, and in turn, a small decrease in the hydrocarbon and organic carbon content. Both, the Lozier Canyon and Bouldin Creek outcrops contain dispersed and framboidal pyrite (Aris Pramudito 2014, personal communication). Consequently, it is considered here that the data derived from these samples can be used with confidence.

**Table 5. Summary table of *n*-alkanes analyses from the saturate fraction of Eagle Ford Shale bitumens and oils (ND = not determined)**

| Samples | Range | n-alkane distribution | n-alkane maximum | Pr/Ph range | TAR range | CPI range |
|---|---|---|---|---|---|---|
| EFLC | *n*-$C_{14}$-*n*-$C_{29}$ | unimodal | *n*-$C_{22}$ | 0.22-0.45 | 0.20-3.70 | 0.41-1.48 |
| EFMK | *n*-$C_{13}$-*n*-$C_{36}$ | unimodal | *n*-$C_{16}$ | 0.91-1.42 | 0.10-0.18 | 0.95-1.01 |
| EFFA | *n*-$C_{13}$-*n*-$C_{27}$ | unimodal | *n*-$C_{17}$ | 0.86-1.42 | ND | 1.21-1.69 |
| EFBC | *n*-$C_{15}$-*n*-$C_{25}$ | unimodal | *n*-$C_{17}$ | 0.75-1.92 | ND | 0.56-0.61 |
| EFAC | *n*-$C_{14}$-*n*-$C_{26}$ | bimodal | *n*-$C_{17}$ and *n*-$C_{22}$ | 0.77-1.55 | ND | 0.80-1.29 |
| EFWB | *n*-$C_{14}$-*n*-$C_{26}$ | bimodal | *n*-$C_{17}$ and *n*-$C_{22}$ | 0.35-0.71 | ND | 0.61-0.83 |
| EFHE | *n*-$C_{14}$-*n*-$C_{26}$ | unimodal | *n*-$C_{17}$ | 0.67-1.72 | ND | 0.49-0.67 |
| EFLH | *n*-$C_{13}$-*n*-$C_{37}$ | unimodal | *n*-$C_{17}$ | 1.23-1.54 | 0.25-0.58 | 1.05-1.13 |
| NWMK-533.2 | *n*-$C_{11}$-*n*-$C_{35}$ | unimodal | *n*-$C_{15}$ | 1.07 | 0.23 | 0.99 |
| NFMK-526-1H | *n*-$C_{11}$-*n*-$C_{35}$ | unimodal | *n*-$C_{15}$ | 0.80 | 0.21 | 0.98 |
| MJOG-UEF | *n*-$C_{11}$-*n*-$C_{36}$ | unimodal | *n*-$C_{14}$ | 0.80 | 0.23 | 0.97 |
| MJOG-LEF | *n*-$C_{11}$-*n*-$C_{36}$ | unimodal | *n*-$C_{14}$ | 1.14 | 0.21 | 1.00 |
| GREF-1-110 | *n*-$C_{11}$-*n*-$C_{36}$ | unimodal | *n*-$C_{13}$ | 1.25 | 0.18 | 1.04 |

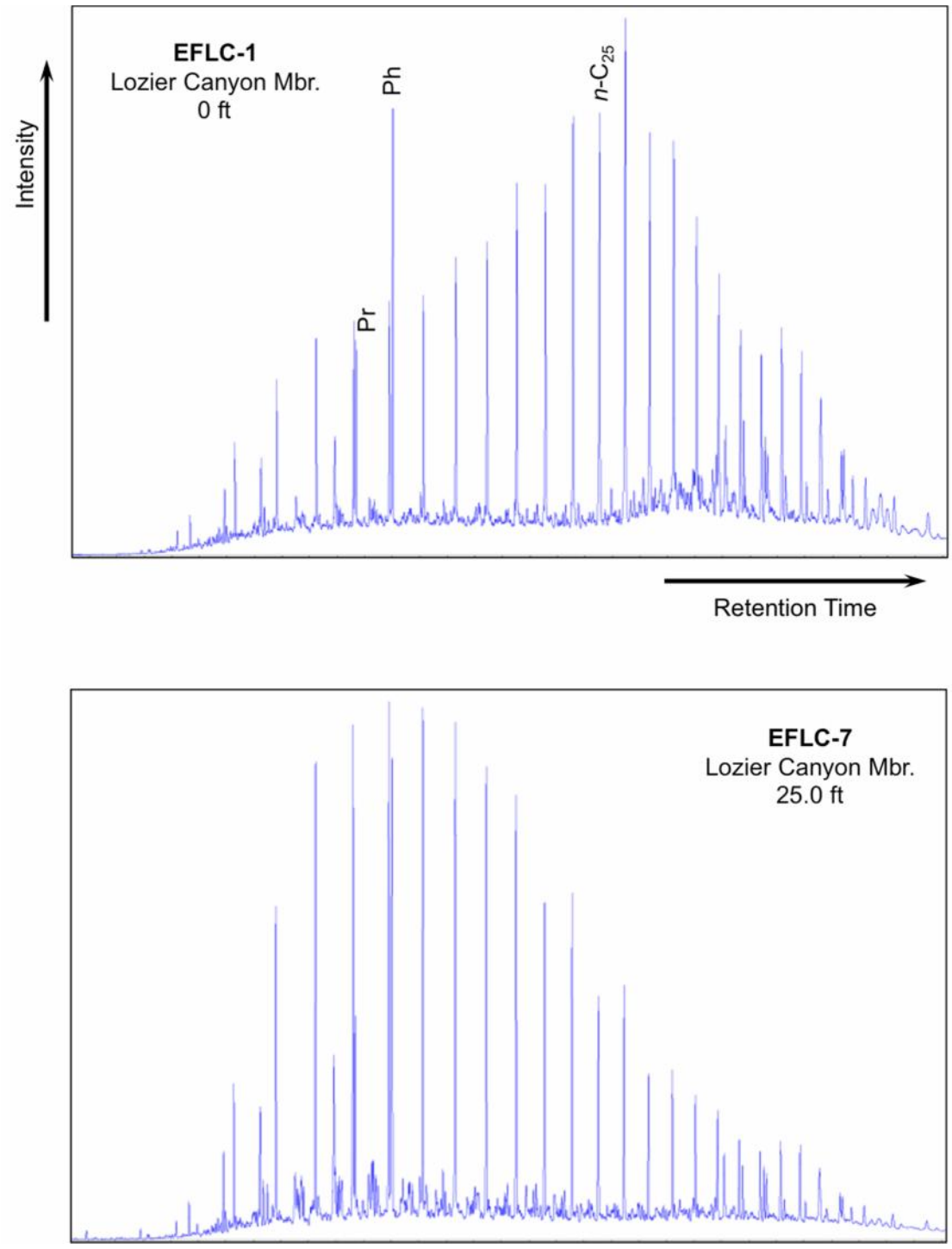


**Figure 21. Gas chromatograms of the saturate fractions from bitumen extracts of the EFLC outcrop (Pr = pristane; Ph = phytane, *n*-$C_{25}$ = $C_{25}$ normal alkane)**

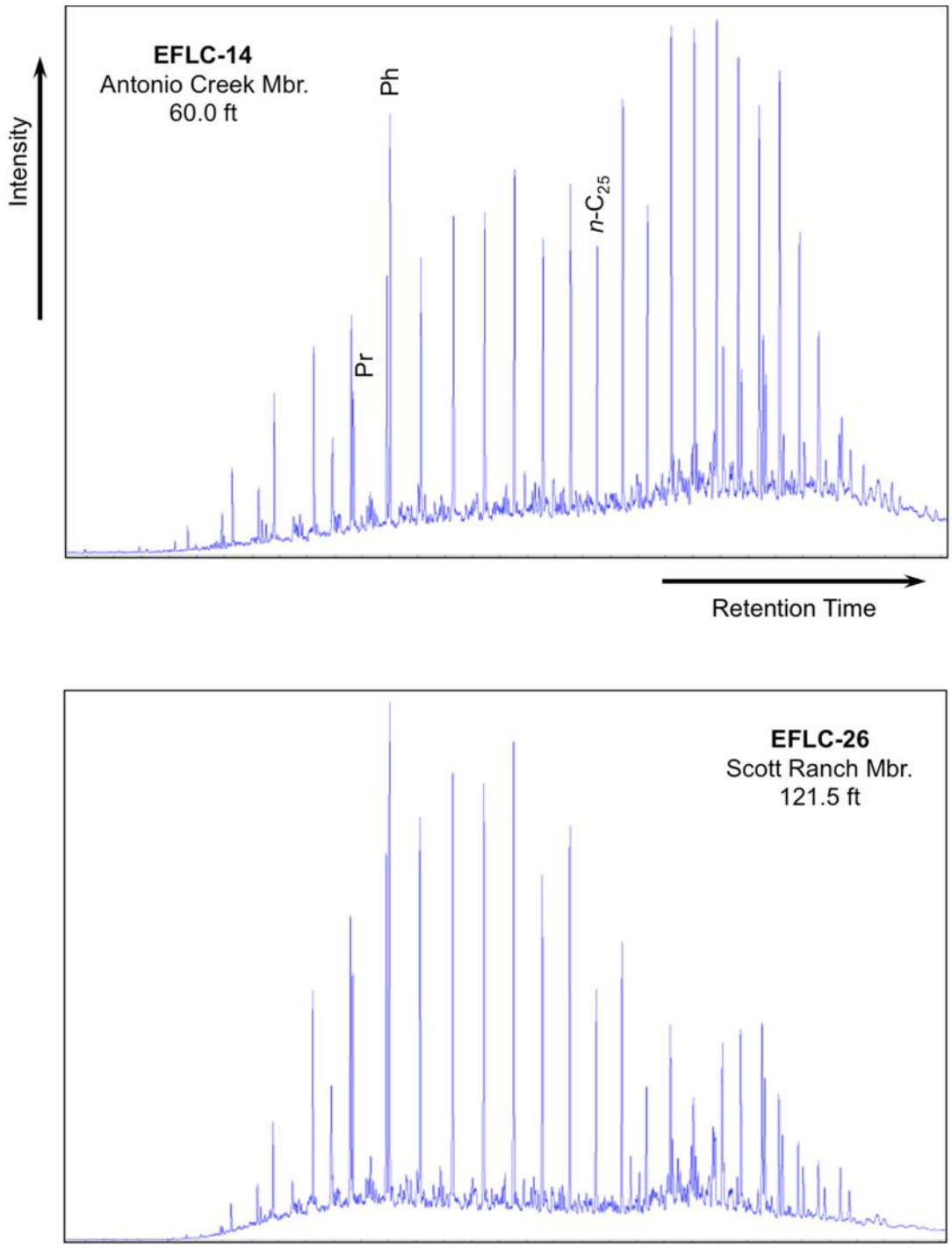


**Figure 21. Gas chromatograms of the saturate fractions from bitumen extracts of the EFLC outcrop (Pr = pristane; Ph = phytane, *n*-$C_{25}$ = $C_{25}$ normal alkane; cont.)**

### *2.1.4.2 Pristane and Phytane*

Pristane (Pr) and phytane (Ph) were determined in the *n*-alkanes fingerprints from the saturate fractions of the bitumens and oils (Figure 21, Appendix D). These acyclic isoprenoids have been widely used for evaluating redox conditions during source rock deposition, since their origin is dependent on oxygen availability (Didyk et al., 1978; Waples, 1985; Peters et al., 2005). Pr and Ph are primarily derived from the phytyl side chain of the chlorophyll-a during diagenesis. However, other sources, such as unsaturated isoprenoids in zooplankton and higher animals, tocopherols, and archaea, have been proposed as precursors of Pr and Ph (Blumer et al., 1963; Blumer and Thomas, 1965; Goosens et al., 1984; Rowland, 1990; Bechtel et al., 2007), and Pr can also be derived from isoprenoids bound to kerogen during catagenesis (Larter et al., 1979).

Several chemical pathways generate Pr and Ph from the phytyl chain of chlorophyll. Under reducing conditions, phytol undergoes hydrogenation and reduction to generate phytane. Conversely, under oxic conditions, oxidation and decarboxylation of the phytol chain produces pristane (Tissot and Welte, 1984; Peters et al., 2005). Consequently, the Pr/Ph ratio assists in evaluating the redox potential of the depositional environment of the source rock (Didyk et al., 1978; Shanmugam, 1985; Peters et al., 2005). Pr/Ph ratios lower than 1 are associated with anoxic conditions, whereas Pr/Ph greater than 1 suggest oxic conditions during source rock deposition. In addition, for rocks and oils within the oil window Peters et al. (2005) pointed out that Pr/Ph values greater than 3 are related to terrigenous organic matter input under oxic-

suboxic conditions, while Pr/Ph values lower than 0.8 indicate anoxic, hypersaline or carbonate depositional environments (ten Haven et al., 1987; Peters et al., 2005).

Overall, the majority of the bitumen and oil samples show low Pr/Ph ratios indicating the presence of reducing conditions (anoxia) during source rock deposition (Table 5; Appendix E). Geochemical logs of Pr/Ph ratios for outcrop and core samples show variations in redox potential that inversely correlates with TOC and HI values (Figure 14). In general, Pr/Ph ratios of samples from EFLC, EFBC, EFAC, EFWB, EFHE, EFMK, and EFFA, suggest that the Lozier Canyon Member experienced stronger reducing conditions compared to the upper members of the Eagle Ford Group. This may have contributed to organic matter preservation, which resulted in its high TOC values. Additionally, a progressive increase in Pr/Ph ratios towards the upper members is observed, suggesting an increase in oxygen content in the water column during deposition of these units. Similarly, Pr/Ph ratios for the EFMK core suggest occurrence of stronger reducing conditions during deposition of the Lower Eagle Ford (Figure 14). On the other hand, the Lower Eagle Ford and underlying Maness Shale analyzed in the East Texas EFLH core do not indicate marked changes in redox conditions during deposition.

Another set of parameters useful for evaluating variations in redox conditions, organic matter source, maturity, and alteration in source rock extracts and oils involves the relationship between Pr and Ph and *n*-alkanes $C_{17,}$ and *n*-$C_{18}$ (Shanmugam, 1985). Figure 22 shows a crossplot of Pr/*n*-$C_{17}$ versus Ph/*n*-$C_{18}$ for the bitumens and oils analyzed in this study. This diagram indicates that these samples are mainly composed of marine organic matter. However, few samples corresponding to EFLH, EFHE, and

EFBC also plot in the mixed organic matter field of the diagram, suggesting a marine and terrigenous organic matter input. Liro et al. (1994) found a similar result between Pr/*n*-$C_{17}$ and Ph/*n*-$C_{18}$ for samples in the upper section of the Bouldin Creek outcrop (EFBC samples in the present study). These authors attributed the variations in organic matter source to a change to more proximal environmental conditions during deposition of the younger section of the Eagle Ford Shale at this locality. The EFBC samples plotted in the mixed organic matter field of the diagram (Figure 22) correspond to samples from the Langtry Member, suggesting a similar interpretation to that of Liro et al. (1994) for the Upper Eagle Ford Shale at the Austin area. Rock samples from EFFA, EFMK, EFLH, and oils show the highest maturity level according to the lower proportion of isoprenoids relative to *n*-alkanes.

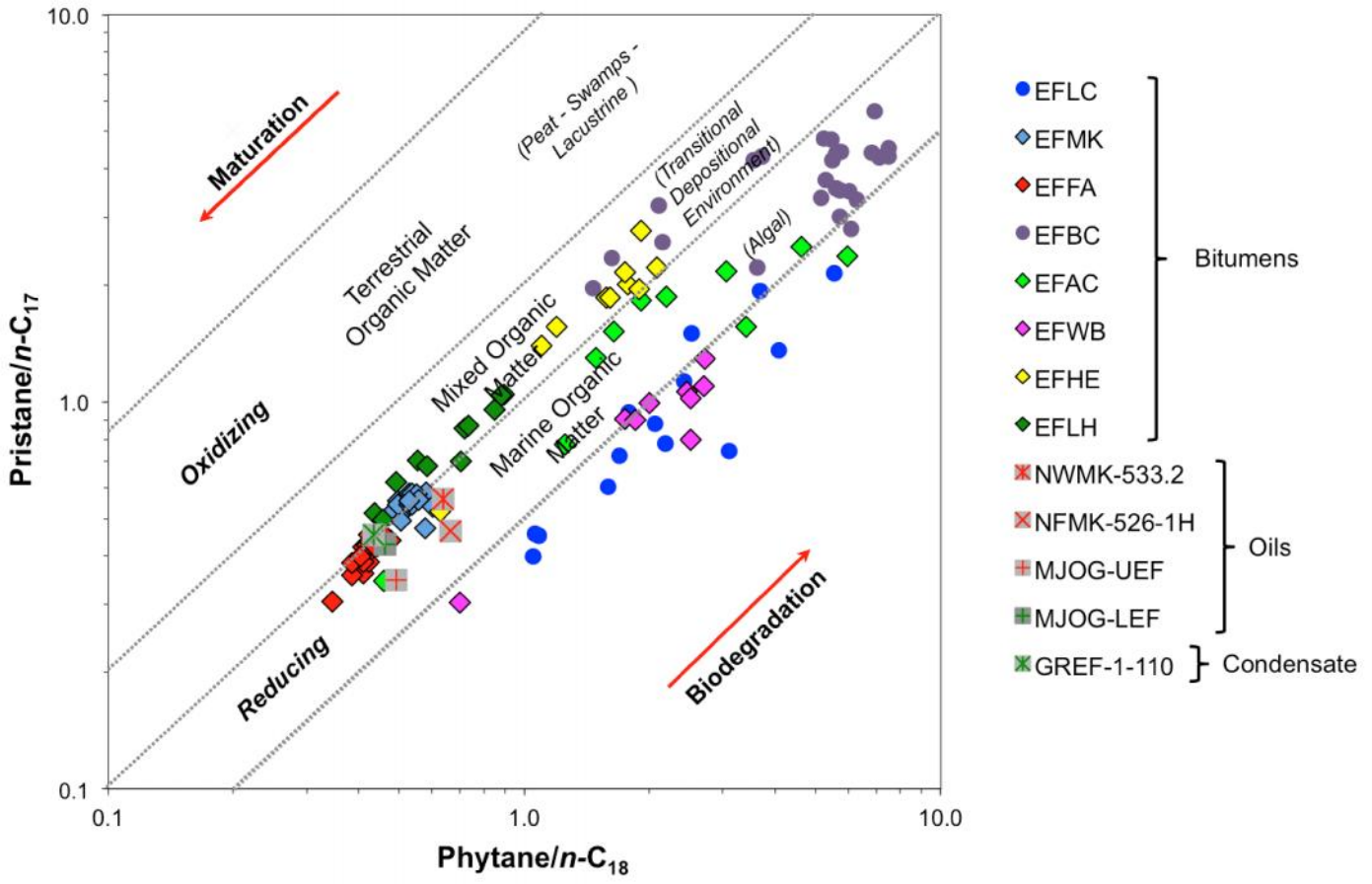


**Figure 22. Isoprenoids plot of Pristane/*n*-$C_{17}$ versus Phytane/*n*-$C_{18}$ showing redox conditions, maturity, and depositional environments for samples of the Eagle Ford Shale (*n*-$C_{17}$ = $C_{17}$ normal alkane; *n*-$C_{18}$ = $C_{18}$ normal alkane)**

## 2.2 Biomarker and geochemical parameters for evaluation of organic matter source

### 2.2.1 Steranes

This group of biomarkers is commonly used for evaluation of organic matter source, maturity, and correlation studies. Steroids are derived from sterols, which are compounds present in eukaryotic organisms, mainly algae and higher plants (Tissot and Welte, 1984; Peters et al., 2005). Distributions of steranes, diasteranes, and pregnanes were determined in the B&C fractions of bitumens and oils by SIM/GC-MS through analysis of the m/z 217.3 ion. Fragmentograms of steranes distributions for the EFLC samples are presented in Figure 23. Peak identification is presented in Table 6. Formulas for calculation of geochemical ratios are in Appendix A. Numerical values of the geochemical ratios calculated are in Appendix H. Biomarkers quantitation results are in Appendix L.

#### *2.2.1.1 Regular steranes*

Most of the Eagle Ford Shale analyzed samples show a higher proportion of $C_{27}$ steranes compared to that of the $C_{28}$ and $C_{29}$ homologs, suggesting a marine organic matter source for these samples. The distribution of regular steranes for samples EFLC, EFMK, and EFLH also shows a higher proportion of the $C_{27}\beta\beta$, $C_{28}\beta\beta$, and $C_{29}\beta\beta$ isomers compared to their $\alpha\alpha$ counterparts (Figure 23). This feature has been attributed to hypersaline environments (ten Haven et al., 1988), suggesting that deposition of the Eagle Ford Shale in West and East Texas was restricted enough to allow development of water-density stratification and hypersaline conditions.

Samples EFBC and EFAC feature a steranes distribution typical of immature source rocks (Figure 23). These samples are characterized by a predominance of the αα-20R steranes (biological configuration) and higher amounts of the $C_{28}$ relative to the $C_{29}$ steranes, which are consistent with Waples and Machihara (1991) descriptions of steranes distribution of low maturity oils and extracts.

A ternary diagram of the distribution of $C_{27}$, $C_{28}$ and $C_{29}$ regular steranes (Figure 24) was used to assess possible variations in depositional environment of the Eagle Ford Shale samples following a similar approach to that of Huang and Meinschein (1979) and Moldowan et al. (1985). $C_{27}$ steranes (cholestane) originate from precursors found in plankton and marine invertebrates. $C_{28}$ steranes (ergostane) are also derived from similar precursors, although they can also be generated from terrigenous organisms. (Huang and Meinschein, 1979; Moldowan et al., 1985). Similarly, $C_{29}$ steranes (stigmastane) are derived from terrigenous sources and marine algae (Volkman, 1986). The regular steranes ternary plot for the Eagle Ford Shale samples (Figure 24) shows that the analyzed bitumens and oils are grouped together in a single area of the plot, indicating a common genetic relationship. Moreover, these samples cluster in the “open marine” and “marine shale/carbonate” fields of the Huang and Meinschein (1979) and Moldowan et al. (1985) ternary plots, respectively.

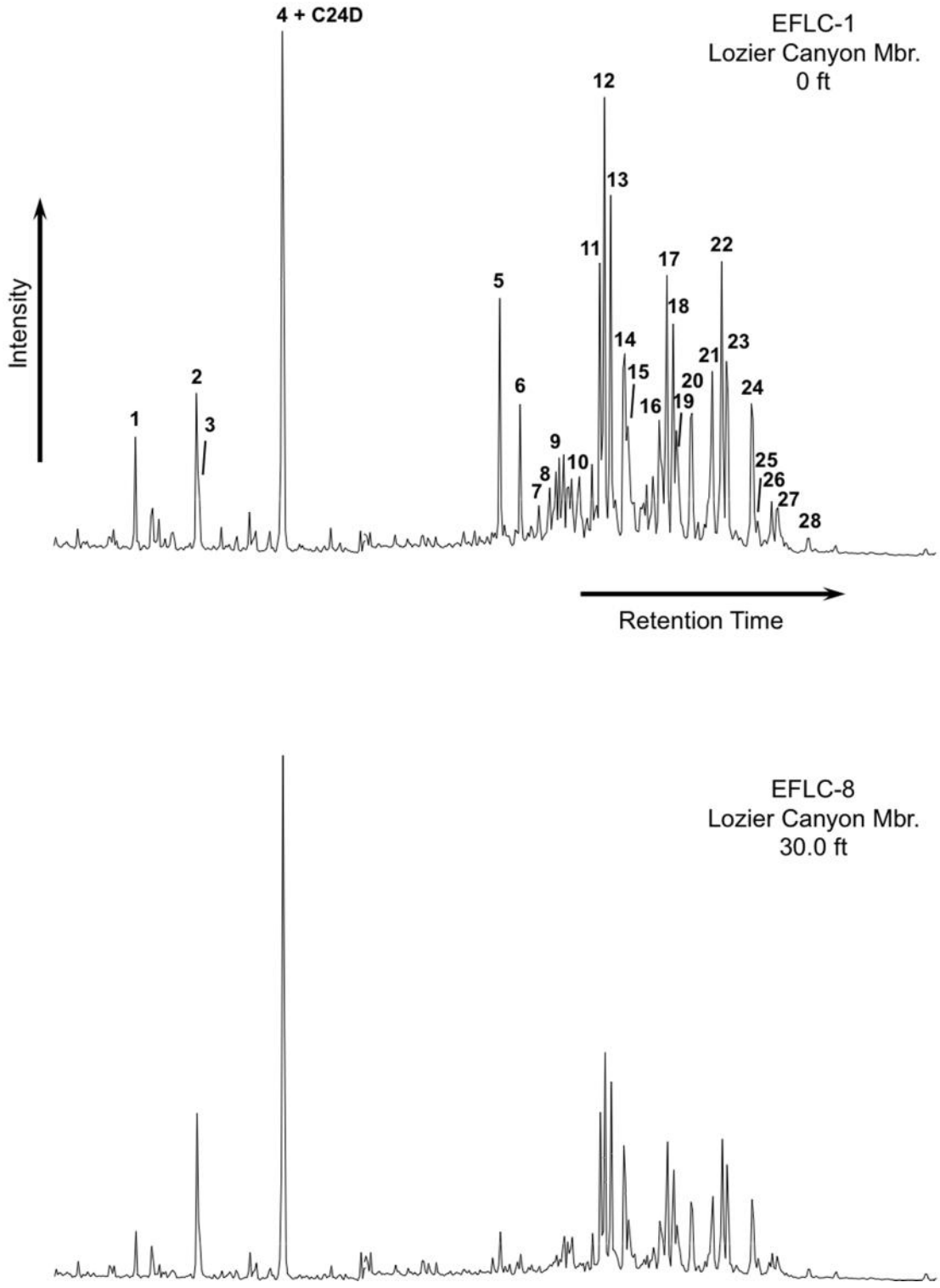


**Figure 23. Partial fragmentograms of the m/z 217.3 ion showing distribution of steranes in the B&C fractions of the EFLC samples. Peak identification is presented in Table 6**

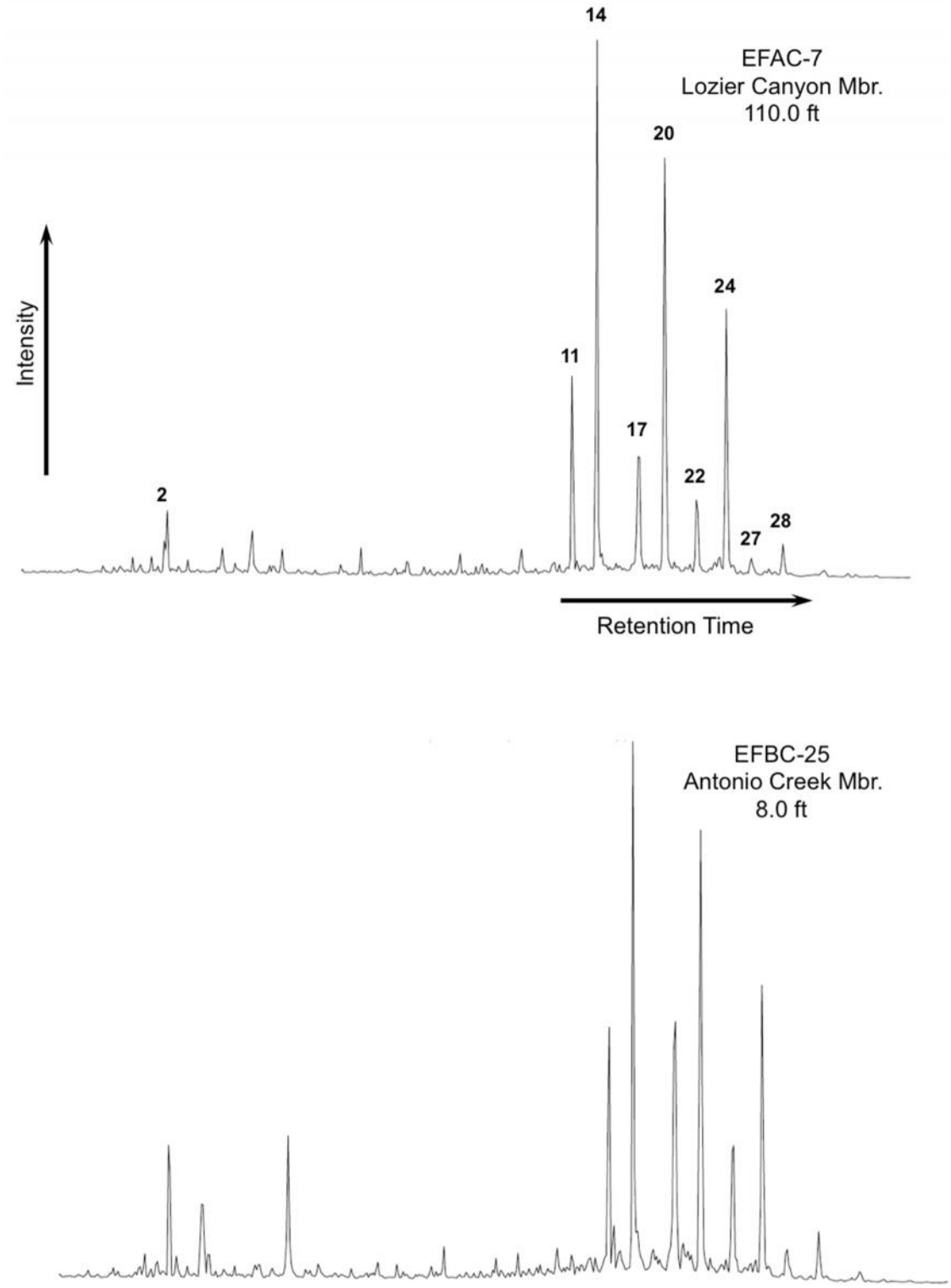


**Figure 23. Partial fragmentograms of the m/z 217.3 ion showing distribution of steranes in the B&C fractions of the EFBC and EFAC samples. Peak identification is presented in Table 6 (cont.)**

**Table 6. Identification of steranes in the partial m/z 217.3 fragmentogram of the B&C fractions**

| Peak # | Compound |
|---|---|
| **C24D** | Deuterated *n*-tetracosane (ISTD) |
| **1** | **$C_{21}$αα** Diapregnane |
| **2** | **$C_{21}$ββ** 14β(H),17β(H)-Pregnane |
| **3** | **$C_{22}$αα** Diahomopregnane |
| **4** | **$C_{22}$ββ** 14β(H),17β(H)-Homopregnane |
| **5** | **$C_{27}$** 13β(H),17α(H)-Diacholestane (20S) |
| **6** | **$C_{27}$** 13β(H),17α(H)-Diacholestane (20R) |
| **7** | **$C_{27}$** 13α(H),17β(H)-Diacholestane (20S) |
| **8** | **$C_{27}$** 13α(H),17β(H)-Diacholestane (20R) |
| **9** | **$C_{28}$** 24-Methyl-13β(H),17α(H)-Diacholestane (20S) |
| **10** | **$C_{28}$** 24-Methyl-13β(H),17α(H)-Diacholestane (20R) |
| **11** | **$C_{28}$** 24-Methyl-13α(H),17β(H)-Diacholestane (20S) + **$C_{27}$** 14α(H),17α(H)-Cholestane (20S) |
| **12** | **$C_{29}$** 24-Ethyl-13β(H),17α(H)-Diacholestane (20S) + **$C_{27}$** 14β(H),17β(H)-Cholestane (20R) |
| **13** | **$C_{27}$** 14β(H),17β(H)-Cholestane (20S) + **$C_{28}$** 24-Methyl-13α(H),17β(H)-Diacholestane (20R) |
| **14** | **$C_{27}$** 14α(H),17α(H)-Cholestane (20R) |
| **15** | **$C_{29}$** 24-Ethyl-13β(H),17α(H)-Diacholestane (20R) |
| **16** | **$C_{29}$** 24-Ethyl-13α(H),17β(H)-Diacholestane (20S) |
| **17** | **$C_{28}$** 24-Methyl-14α(H),17α(H)-Cholestane (20S) |
| **18** | **$C_{28}$** 24-Methyl-14β(H),17β(H)-Cholestane (20R) + **$C_{29}$** 24-Ethyl-13α(H),17β(H)-Diacholestane (20R) |
| **19** | **$C_{28}$** 24-Methyl-14β(H),17β(H)-Cholestane (20S) |
| **20** | **$C_{28}$** 24-Methyl-14α(H),17α(H)-Cholestane (20R) |
| **21** | **$C_{29}$** 24-Ethyl-14α(H),17α(H)-Cholestane (20S) |
| **22** | **$C_{29}$** 24-Ethyl-14β(H),17β(H)-Cholestane (20R) |
| **23** | **$C_{29}$** 24-Ethyl-14β(H),17β(H)-Cholestane (20S) |
| **24** | **$C_{29}$** 24-Ethyl-14α(H),17α(H)-Cholestane (20R) |
| **25** | **$C_{30}$** 24-Propyl-14α(H),17α(H) -Cholestane (20S) |
| **26** | **$C_{30}$** 24-Propyl-14β(H),17β(H) -Cholestane (20R) |
| **27** | **$C_{30}$** 24-Propyl-14β(H),17β(H) -Cholestane (20S) |
| **28** | **$C_{30}$** 24-Propyl-14α(H),17α(H) -Cholestane (20R) |

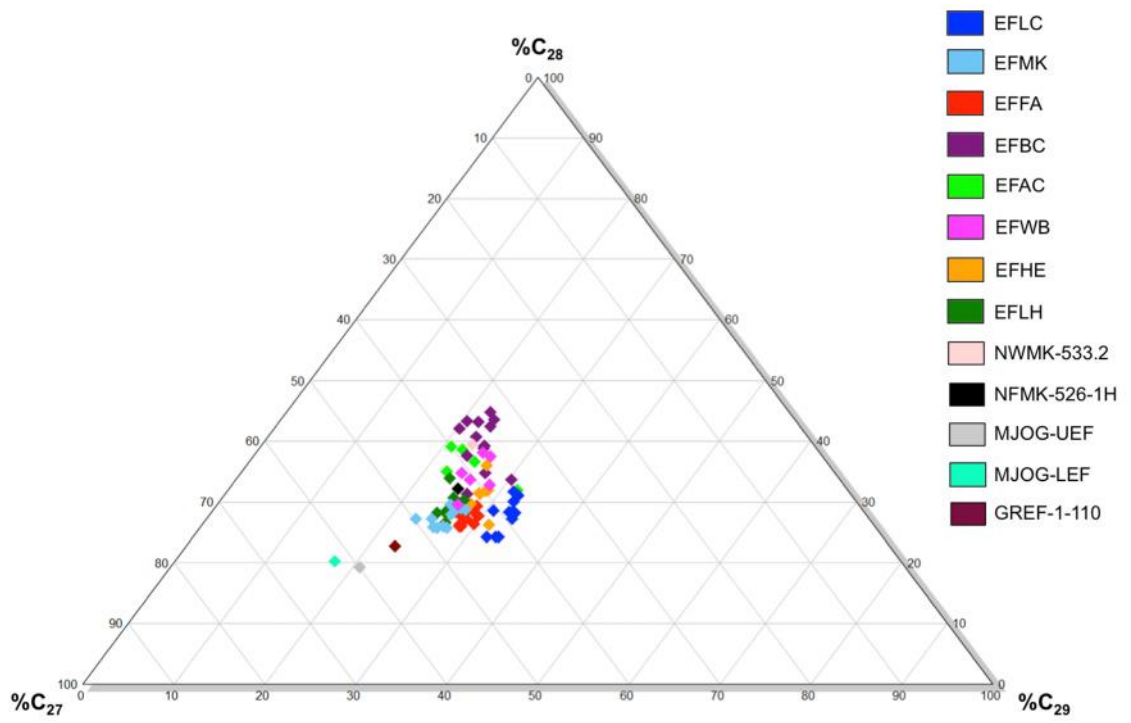


**Figure 24. Ternary diagram of $C_{27}$, $C_{28}$, and $C_{29}$ regular steranes for the Eagle Ford Shale samples**

Another group of steranes that are used for determining organic matter type are the $C_{30}$ 4-desmethylsteranes (also named 24-*n*-propylcholestanes or $C_{30}$ steranes). These compounds are derived from Chrysophyte, a marine algae of the order *Sarcinochrysidales*, which makes them specific biomarkers for marine organic matter (Moldowan et al., 1985; Peters et al., 2005). $C_{30}$ steranes were detected in all the samples analyzed. The steranes index, which combines the proportions of the $C_{30}$ sterane versus the $C_{27}$ to $C_{30}$ steranes (Appendix H) can be used to evaluate marine organic input (Peters et al., 2005). Geochemical logs of this ratio for the bitumen samples show small variations in source input within the different Eagle Ford members (Figure 25, Appendix F), suggesting a greater marine input in the lower Lozier Canyon Member and Antonio Creek Member.

#### *2.2.1.2 Diasteranes (rearranged steranes)*

Diasteranes are generated by the reduction of diasterenes, which are derived from sterols during diagenesis. This conversion reaction is catalyzed by acidic sites on clays, and promoted by low pH and oxic conditions (Moldowan et al., 1986; Peters, et al., 2005). Therefore, these biomarkers can be used as lithology and redox conditions indicators. The $C_{27}$ diasteranes/$C_{27}$ steranes ratio can help differentiate between carbonate and siliciclastic source rocks in unaltered samples of similar thermal maturity (Mello et al., 1988; Peters et al., 2005). Low $C_{27}$ diasteranes/$C_{27}$ steranes ratios are associated with anoxic carbonate sediments; whereas high ratios usually indicate clay-rich source rocks. Nevertheless, this evidence needs to be correlated with other geochemical parameters, since significant amounts of diasteranes have also been found in some clay-poor carbonate environments (Clark and Philp, 1989; Peters et al., 2005).

Geochemical logs of $C_{27}$ diasteranes/$C_{27}$ steranes for the Eagle Ford Shale samples show lower values of this ratio in the Lozier Canyon Member, suggesting that this interval has lower clay content relative to the other members (Figure 25, Appendix F). These observations are supported by the descriptions of Donovan et al. (2013b) for the different Eagle Ford Shale members at Lozier Canyon, which characterize the Scott Ranch, Antonio Creek and Langtry members as clay-rich and containing significant amounts of bentonite beds. It is possible that these clays promoted steranes rearrangement to diasteranes. Diasteranes in samples EFAC and EFBC were present in very low concentrations or not detected at all possibly due to their low maturity.

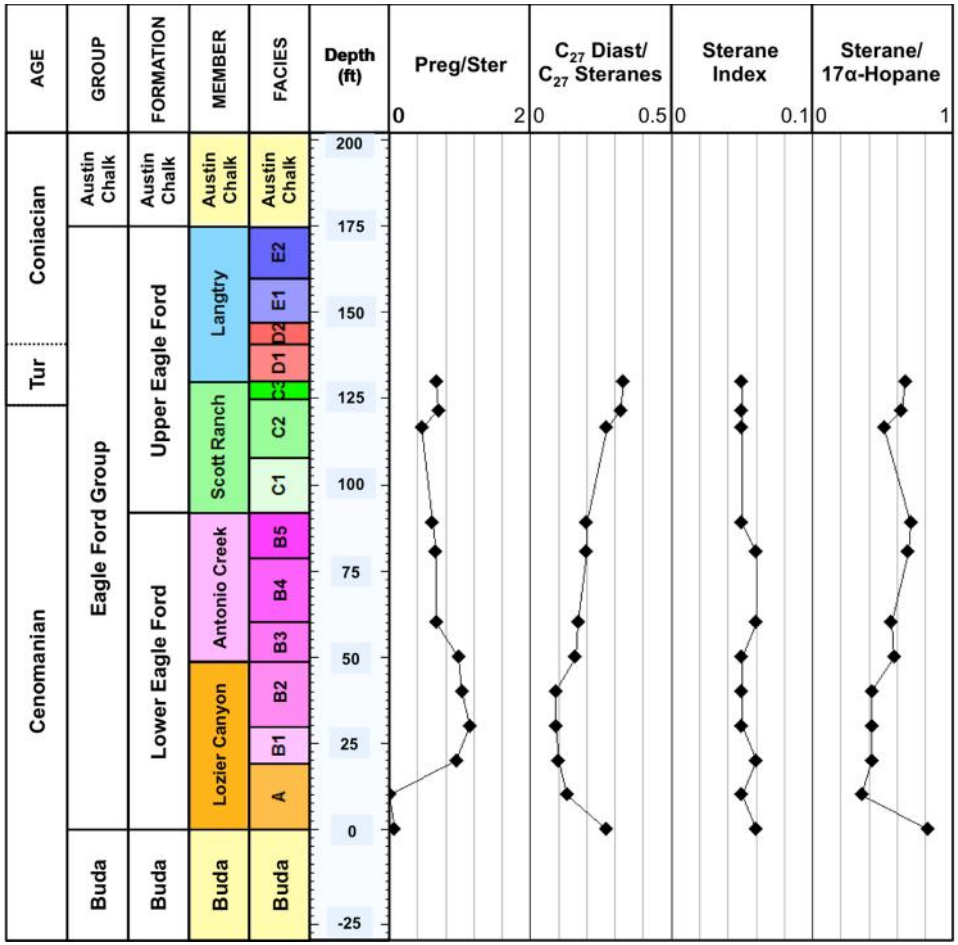


**Figure 25. Geochemical logs of steranes ratios for the EFLC samples. Formulas for calculation of ratios are in Appendix A. Geochemical logs from other locations analyzed are in Appendix F. Numerical values of biomarker ratios are in Appendix H**

#### *2.2.1.3 Pregnanes*

The origin of pregnane ($C_{20}$ sterane) and homopregnane ($C_{21}$ sterane) is not well understood (ten Haven et al., 1985, 1988). However, these compounds have been determined in high concentrations in bitumen extracted from source rocks associated with hypersaline depositional conditions. Wang (1993) analyzed extracts from the Springer Formation and found that pregnanes were more resistant to weathering compared to regular steranes and diasteranes. Pregnanes are also produced from degradation of the higher-carbon-numbered steranes at high maturity levels (R. Paul Philp, personal communication, 2014).

Geochemical logs of the pregnanes/steranes ratio for the Eagle Ford Shale samples show higher values in the Lower member, indicating the possibility of hypersaline, anoxic conditions present in the water column during deposition of this unit (Figure 25, Appendix F). In contrast, overall concentrations of pregnanes are much higher than those of dia- and regular steranes in samples from the EFMK and EFFA wells (Appendix L). These high maturity samples do not show any evidence of alteration, suggesting an enrichment of pregnanes relative to regular and rearranged steranes. Zhang et al. (2014) found that high pregnane/sterane and low 30-Norhopane/$C_{30}$ hopane in oil and bitumens from the Tazhong Uplift suggested enrichment of pregnane due to thermal maturation. A similar relation between these two geochemical parameters was observed for the EFMK, EFFA, and EFLH samples (Appendices H and I).

### 2.2.2 Terpanes

Terpanes constitute a group of compounds derived from prokaryotic organisms (eubacteria and blue-green algae), and plants. (Ourisson et al., 1982; Tissot and Welte, 1984; Peters et al. 2005). Terpane compounds include acyclic, bicyclic, tricyclic, tetracyclic, and pentacyclic homologous series (Peters et al., 2005). Tri-, tetra-, and pentacyclic terpanes were identified in the Eagle Ford Shale bitumens and oils by analysis of their B&C fractions through SIM/GC-MS of the m/z 191.3 ion. Fragmentograms of these compounds are presented in Figure 26. Peak identifications are in Table 7. Formulas for calculation of geochemical ratios are in Appendix A. Biomarkers quantitation results are in Appendix M. Geochemical ratios of terpanes (Appendix I) and their relationships with other biomarker groups helped assessing variations in organic matter, redox conditions, and thermal maturity for the Eagle Ford Shale bitumens and oils.

The regular steranes/17α-Hopanes ratio is frequently used to evaluate eukaryote (plankton and/or benthic algae) versus prokaryote (bacteria) organic matter input in sediments. High values of this ratio are indicative of marine depositional environments, whereas low, near zero values are associated with terrigenous and/or reworked organic matter (Peters et al., 2005). In general, high steranes/17α-Hopanes ratios are identified throughout the Eagle Ford Shale Group, indicating a greater marine organic matter input during deposition of these units (Figure 25, Appendix I). In the EFLH well, steranes/17α-hopanes does not show much variation except for a decrease in this ratio near the boundary between the Maness and Eagle Ford Shale. This change might be

related to variations in depositional conditions that favored an increase in prokaryotic input at the end of Maness Shale deposition.

#### *2.2.2.1 Tricyclic terpanes*

Tricyclic terpanes (cheilanthanes) are thought to be derived from algae and bacterial precursors (Ourisson et al., 1982; Aquino Neto et al., 1981; Peters et al., 2005). Volkman et al. (1989) found significant amounts of tricyclic terpanes in bitumen from rocks containing *Tasmanites*, suggesting an origin from these organisms. Philp and Gilbert (1986) determined that tricyclic terpanes are abundant in marine oils. These compounds are highly resistant to thermal maturation and biodegradation compared to the hopanes. For that reason, tricyclic terpanes are commonly used in source rock characterization, evaluation of thermal maturity, biodegradation, and in oil-source rock correlations (Zumberge, 1987; Peters et al., 2005). Ratios of tricyclics/17α-hopanes and $C_{23}$ tricyclic/$C_{30}$ hopane help determining organic matter source by comparing bacterial and/or algal input versus prokaryotic contribution in source rock extracts and oils (Peters et al., 2005). Mello et al. (1988) observed high amounts of tricyclic terpanes associated with lacustrine saline and marine carbonate environments. Overall, the analyzed samples show higher tricyclics/17α-hopanes and $C_{23}$ tricyclic/$C_{30}$ hopane ratios in Lower Eagle Ford Shale (Figure 27, Appendix I), indicating a greater marine input during deposition of this member, as previously suggested.

Tricyclic terpane ratios are also helpful to differentiate depositional environments and identify source rock lithology (Peters et al., 2005). Particularly, the $C_{22}/C_{21}$ and the $C_{24}/C_{23}$ tricyclic terpane ratios assist in the identification of bitumens and oils derived from carbonate rocks. Extracts and oils derived from these source rocks

typically show high $C_{22}/C_{21}$ and low $C_{24}/C_{23}$ tricyclic terpane ratios, while marine source rocks show low $C_{22}/C_{21}$ (0.20-0.50) and high $C_{24}/C_{23}$ (0.50-1.00) tricyclic terpanes (Peters et al., 2005). Figure 28 shows a plot of $C_{22}/C_{21}$ versus $C_{24}/C_{23}$ tricyclic terpane ratios for bitumens and oils samples from the Eagle Ford Shale. From this graph it is suggested that most of these samples are derived from marine shales, with exception of few EFLC bitumens, which point to be derived from carbonate source rocks. Another geochemical parameter useful for determining source type is the $C_{26}/C_{25}$ tricyclic terpane ratio (Figure 29), which helps distinguishing marine (0.50-1.30) from lacustrine source rocks (>1.0; Peters et al., 2005). Combination of this ratio with the $C_{31}R/C_{30}$ hopane ratio also assists in determining source rock type. Figure 29 shows the relation between these two parameters and indicate that the Eagle Ford Shale samples analyzed have a marine origin.

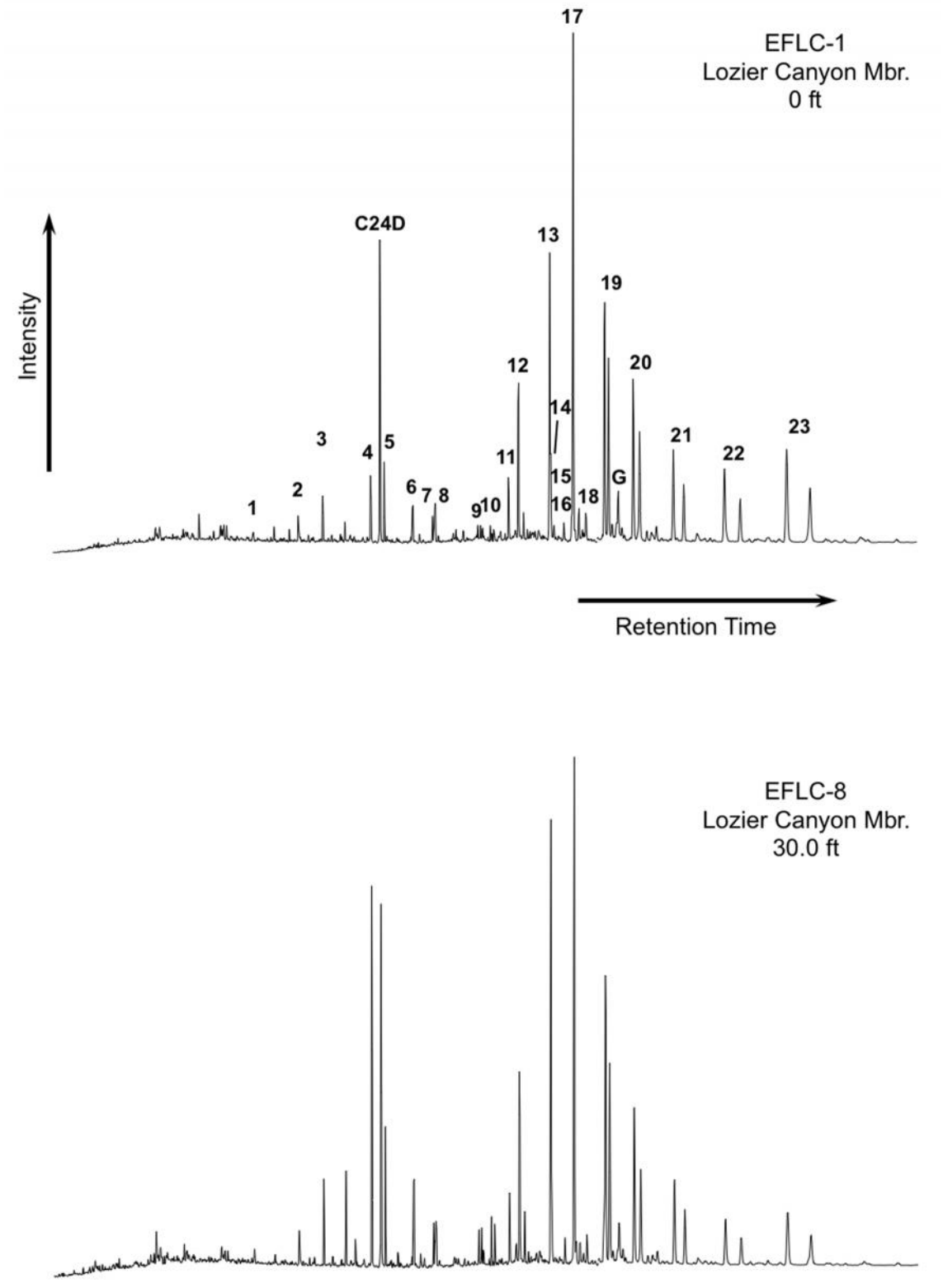


**Figure 26. Partial fragmentograms of the m/z 191.3 ion showing distribution of terpanes in the B&C fractions of the EFLC samples. Peak identification is presented in Table 7**

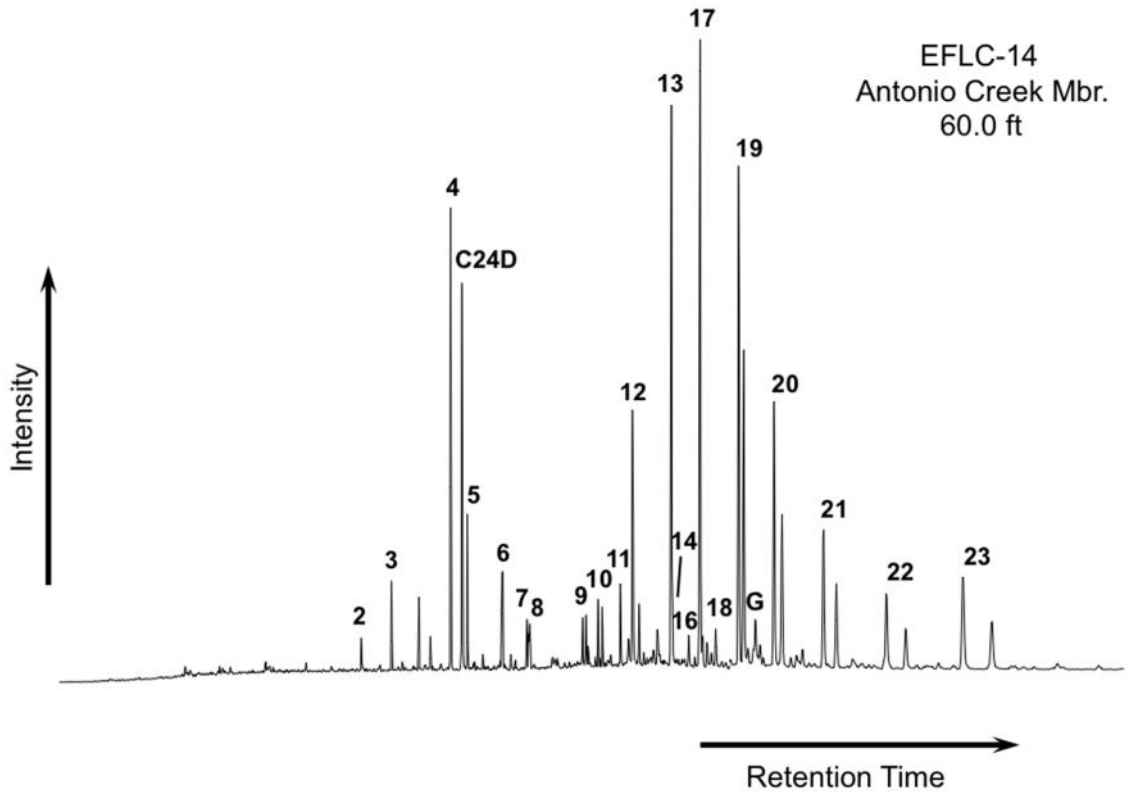


**Figure 26. Partial fragmentograms of the m/z 191.3 ion showing distribution of terpanes in the B&C fractions of the EFLC samples. Peak identification is presented in Table 7 (cont.)**

**Table 7. Identification of terpanes in the partial m/z 191.3 fragmentogram of the B&C fractions**

| Peak # | Compound |
|---|---|
| **C24D** | Deuterated *n*-tetracosane (ISTD) |
| **1** | **$C_{20}$** Tricyclic terpane (Cheilanthane) |
| **2** | **$C_{21}$** Tricyclic terpane (Cheilanthane) |
| **3** | **$C_{22}$** Tricyclic terpane (Cheilanthane) |
| **4** | **$C_{23}$** Tricyclic terpane (Cheilanthane) |
| **5** | **$C_{24}$** Tricyclic terpane (Cheilanthane) |
| **6** | **$C_{25}$** Tricyclic terpanes (Cheilanthanes 22S and 22R) |
| **7** | **$C_{24}$** Tetracyclic terpane |
| **8** | **$C_{26}$** Tricyclic terpanes (Cheilanthanes 22S and 22R) |
| **9** | **$C_{28}$** Tricyclic terpanes (Cheilanthanes 22S and 22R) |
| **10** | **$C_{29}$** Tricyclic terpanes (Cheilanthanes 22S and 22R) |
| **11** | **$C_{27}$** 18α(H)-22,29,30-Trisnorneohopane (Ts) |
| **12** | **$C_{27}$** 17α(H)-22,29,30-Trisnorhopane (Tm) |
| **13** | **$C_{29}$** 17α(H),21β(H)-30-Norhopane |
| **14** | **$C_{29}$Ts** 18α(H)-30-Norneohopane |
| **15** | **$C_{30}$D** 15α-methyl-17α(H)-27-Norhopane (Diahopane) |
| **16** | **$C_{29}$** 17β(H),21α(H)-30-Normoretane |
| **17** | **$C_{30}$** 17α(H),21β(H)-Hopane |
| **18** | **$C_{30}$** 17β(H),21α(H)-Moretane |
| **19** | **$C_{31}$** 17α(H),21β(H)-Homohopanes (22S & 22R) |
| **21** | **$C_{32}$** 17α(H),21β(H)-Bishomohopane (22S & 22R) |
| **22** | **$C_{33}$** 17α(H),21β(H)-Trishomohopane (22S & 22R) |
| **23** | **$C_{34}$** 17α(H),21β(H)-Tetrakishomohopane (22S & 22R) |
| **24** | **$C_{35}$** 17α(H),21β(H)-Pentakishomohopane (22S & 22R) |
| **G** | Gammacerane |

#### *2.2.2.2 Tetracyclic terpanes*

Tetracyclic terpanes can be synthesized from bacteria or derived from hopanoid precursors. Similarly to the tricyclic terpanes, these compounds are more resistant to thermal maturity and biodegradation (Peters et al., 2005). Tetracyclic terpanes range from $C_{24}$ to $C_{27}$, where the $C_{24}$ homolog has a widespread occurrence (Aquino Neto et al., 1981; Peters et al., 2005). The $C_{24}$ tetracyclic terpane is frequently used as an indicator of carbonate and evaporite depositional environments (Palacas et al., 1984; Clark and Philp, 1989; Peters et al., 2005). The $C_{24}$ tetracyclic terpane was identified in all the analyzed bitumens and oils, and the $C_{24}$ tetracyclic terpane/$C_{30}$ hopane ratio show small variations within the different Eagle Ford Shale members (Figure 27, Appendix I). Because of the carbonate platform depositional environment of the Eagle Ford Shale it is unlikely that the presence of the $C_{24}$ tetracyclic terpane be related to a significant higher plant input. It is possible that these variations are more dependent on lithology than in organic facies variations. Rangel et al. (2000) observed significant amounts of $C_{24}$ tetracyclic terpane in the siliciclastic facies of La Luna Formation. A correlation between $C_{24}$ tetracyclic terpane/ $C_{30}$ hopane ratio and $C_{27}$ diasteranes/$C_{27}$ steranes was observed in the Antonio Creek and the upper interval of the Scott Ranch Member, suggesting that in this case, the presence of $C_{24}$ tetracyclic terpane may be dependent on clastic input.

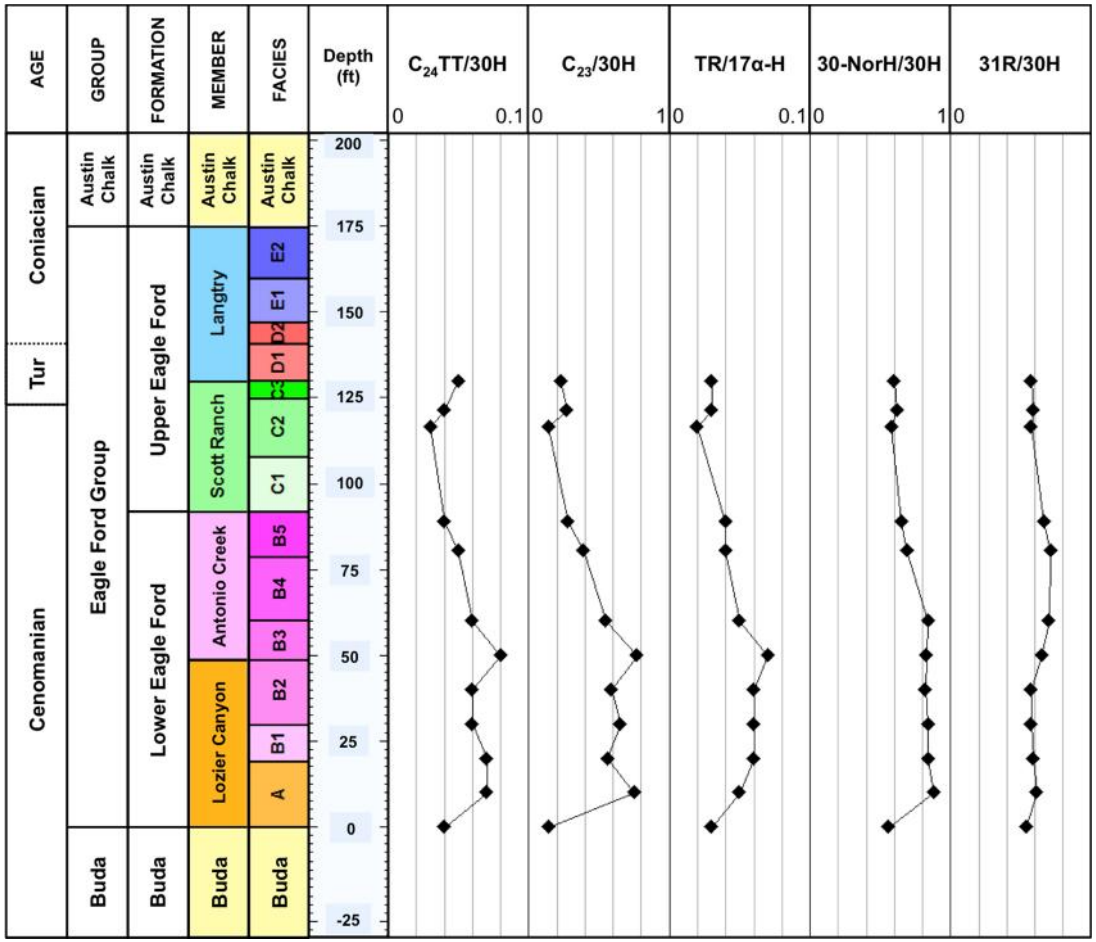


**Figure 27. Geochemical logs of biomarker ratios of terpanes for the EFLC samples. Formulas for calculation of ratios are in Appendix A. Geochemical logs from other locations analyzed are in Appendix G. Numerical values of biomarker ratios are in Appendix I**

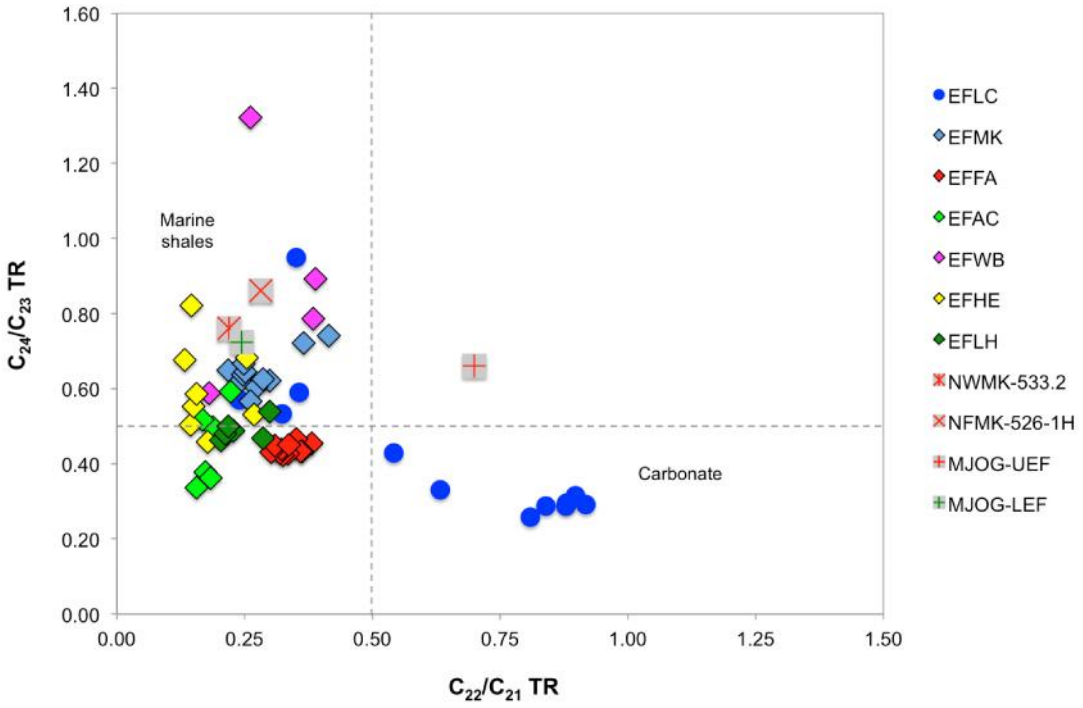


**Figure 28. Plot of $C_{22}/C_{21}$ versus $C_{24}/C_{23}$ tricyclic terpanes shows source rock depositional environments for Eagle Ford Shale bitumens and oils (Dotted lines are used as a guide and do not represent fixed fields on the diagram. Plot modified from Peters et al., 2005)**

### *2.2.2.3 Hopanes*

Hopanes or pentacyclic terpanes are biomarkers derived from hopanoid compounds present in cell membranes of prokaryotes (bacteria and cyanobacteria). Because of their origin, hopanes are ubiquitous in bitumens and oils (Peters and Moldowan, 1991). The $C_{29}$ 17α(H)-norhopane (30-Norhopane) and the $C_{30}$ 17α(H)-hopane are usually the major peaks in the m/z 191 fragmentograms and these biomarkers may be used as environmental indicators (Waples and Machihara, 1991; Peters et al., 2005). The 30-NorH/30H hopane ratio increases with increasing thermal maturity due to the higher stability of the $C_{29}$ hopane compared to the $C_{30}$ homolog (Peters et al., 2005). Most of the Eagle Ford Shale samples analyzed have 30-NorH/30H

values lower than 1.0; however, higher concentrations of 30-Norhopane were observed in the Lozier Canyon Member, probably due to higher amounts of carbonates in this interval (Figure 27, Appendix I). Immature samples EFBC and EFAC have 30-NorH/30H ratios greater than 1.0, which point towards a marine carbonate origin for the Eagle Ford Shale. The higher 30-NorH/30H ratios in the EFFA samples and oils are possibly the result of their high thermal maturity. When compared to the $C_{35}S/C_{34}S$ hopanes ratio, the 30-NorH/30H can help identify source facies of oils and extracts (Figure 30). According to Peters et al. (2005), the majority of oils and bitumens generated from marine carbonates have high $C_{35}S/C_{34}S$ and 30-NorH/30H ratios (>0.8 and >0.6 respectively). This relationship is observed in samples EFLC, EFMK, and EFHE (Figure 30). On the contrary, samples from EFWB, EFLH, and the NWMK-533.2 oil suggest to be derived from a siliciclastic source. In addition, the low values of the $C_{35}S/C_{34}S$ ratio for the EFLH samples suggest dysoxic to oxic source rock deposition. The relationship between $C_{35}S/C_{34}S$ as redox indicators will be explained in the next section. Geochemical logs of the 30-NorH/30H for the bitumens (Figure 27, Appendix G) show higher values of this ratio in the Lozier Canyon Member, possibly suggesting a higher carbonate input during deposition of this interval. In addition, it is inferred that the 30-NorH/30H values greater than 1.0 for the EFFA bitumens are not indicative of source type, but the result of the high thermal maturity of these samples. Correlation of this parameter with other geochemical ratios, such as tricyclics/17α-hopanes, $C_{23}$ tricyclic/$C_{30}$ hopane, and $C_{24}$ tetracyclic terpane/$C_{30}$ hopane ratios point towards a marine source rock for these Eagle Ford Shale bitumens and oils.

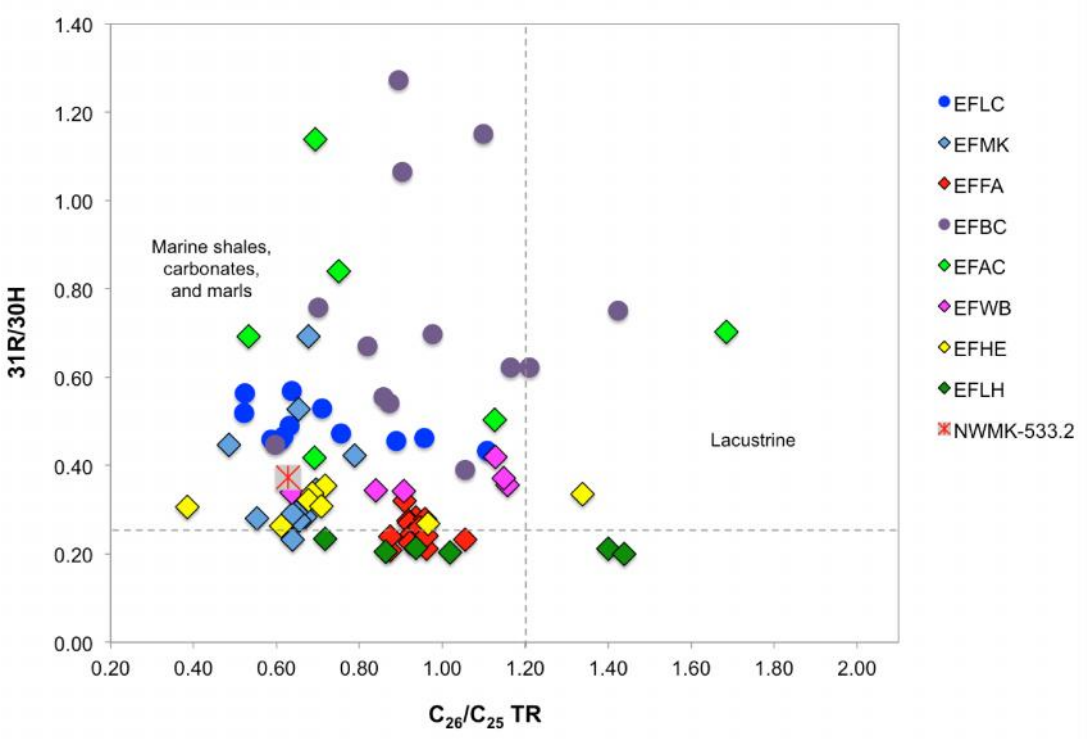


**Figure 29. Plot of $C_{26}/C_{25}$ versus $C_{31}R/C_{30}$ Hopane shows that the Eagle Ford Shale bitumens and oils are mainly of marine origin (Dotted lines are used as a guide and do not represent fixed fields on the diagram. Plot modified from Peters et al., 2005)**

The $C_{31}$ 22R/$C_{30}$ hopane ratio (31R/30H) is applied to differentiate source rocks of marine versus lacustrine origin. $C_{31}$ 22R/$C_{30}$ hopane ratios greater than 0.25 are associated with marine shale, carbonate, and marl source rocks (Peters et al., 2005). Geochemical logs of this ratio for the Eagle Ford Shale extracts (Figure 27, Appendix G) do not show much variation between the different members, and the majority of samples have values of 31R/30H indicative of a marine origin (Figure 29).

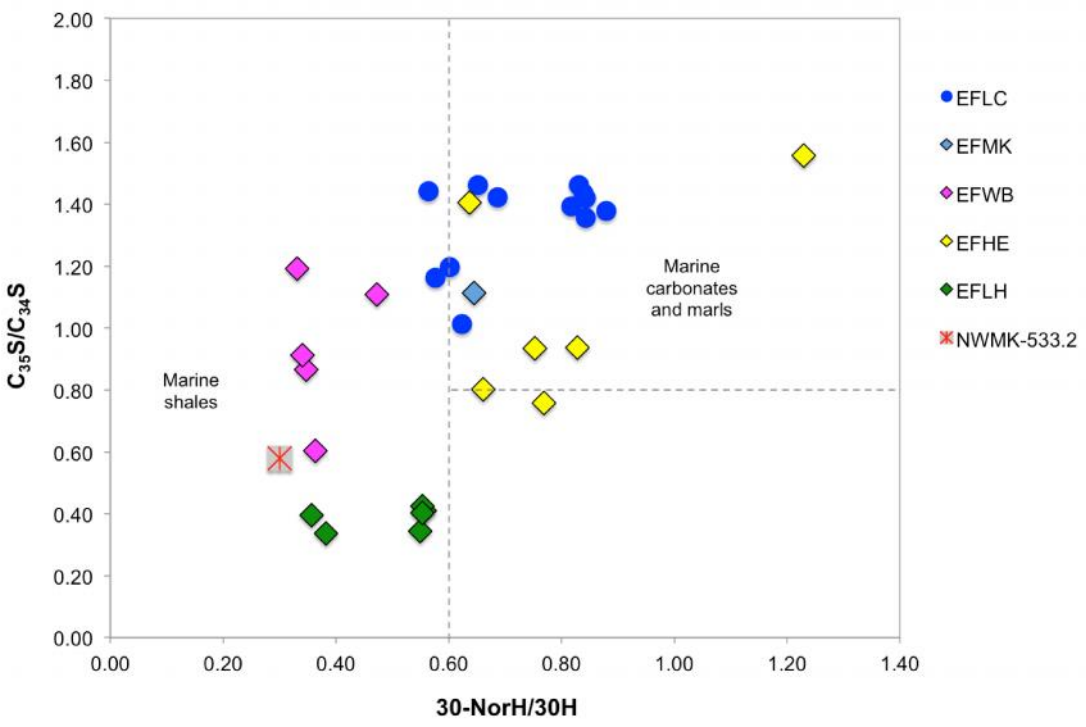


**Figure 30. Plot of 30-Nor/$C_{30}$ hopane versus $C_{35}S/C_{34}S$ homohopanes suggest most of the Eagle Ford Shale rock samples are of marine origin (Dotted lines are used as a guide and do not represent fixed fields on the diagram. Plot modified from Peters et al. 2005)**

The relative distribution of the extended hopanes or homohopanes ($C_{31}$-$C_{35}$) has been widely used to assess redox potential during marine source rock deposition. These compounds originated from bacteriohopanetetrol and other $C_{35}$ hopanoids (Peters and Moldowan, 1991; Waples and Machihara, 1991). Particularly, higher proportions of the $C_{35}$ homohopane with respect to its $C_{34}$ homolog are associated with anoxic marine depositional environments due to preferential preservation of the $C_{35}$ homolog (Peters and Moldowan, 1991; Moldowan et al., 1992; Peters et al., 2005). The $C_{35}S/C_{34}S$ ratio is one of the geochemical parameters used for evaluation of redox variations at the time of source rock deposition. Values of this ratio greater than 0.8 are frequently related to

marine carbonate source rocks (Figure 30; Peters et al., 2005). Moreover, the homohopane index ($C_{35}/C_{31}$-$C_{35}$) is commonly calculated in extracts and oils to evaluate redox conditions, identifying variations in organic facies in the same source rock, and for oils and source rocks correlation studies (Clark and Philp, 1989; Peters and Moldowan, 1991; Peters et al., 2005).

Plots of homohopane distributions for the Eagle Ford Shale bitumens and oils analyzed (Figure 31) indicate that in general, these source rocks were deposited under anoxic conditions, which promoted preservation of the $C_{35}$ homohopane. Samples from the East Texas EFLH core, and the NWMK-533.2 oil do not show this predominance of the $C_{35}$ homohopane, suggesting source rock deposition under suboxic-oxic conditions. $C_{34}$ and $C_{35}$ homohopanes were not detected in most of the EFMK and EFFA extracts, and the rest of the analyzed oils. This could be attributed to the high maturity of these samples, since it has been observed that thermal maturation can increase the proportion of the lower molecular weight homohopanes (Moldowan et al., 1992). Another observation is the difference in homohopane distributions within each Eagle Ford Shale member for all outcrops and cores analyzed, which could indicate organic facies variations between the different units (Figure 31). For example, samples EFLH-15 and -20 from the EFLH core, which correspond to the Maness Shale, show different homohopane distributions from samples EFLH-1 to -13, which are from the Lower Eagle Ford Shale. In the case of the EFLC outcrop, samples EFLC-25, -26, and -28 corresponding to the Scott Ranch Member (lower Upper Eagle Ford Shale) do not show a strong predominance of $C_{35}$ over $C_{34}$ homohopanes, possibly indicating deposition of this member under suboxic-oxic conditions. Variations in homohopane distributions in

samples from the EFHE core, suggest organic facies changes between samples EFHE-1 and -2 (Langtry Member); EFHE-3 to -7 (Langtry and Antonio Creek members); and EFHE-9 and -10 (Lozier Canyon Member).

Gammacerane was tentatively identified in all the Eagle Ford Shale samples analyzed with exception of the MJOG oils, where terpanes in general show very low concentrations (Figure 26). This compound is a $C_{30}$ triterpane originated during diagenesis by reduction of tetrahymanol, whose precursor corresponds to *Tetrahymena*, a fresh water ciliated protozoan (ten Haven et al., 1989; Peters et al., 2005). Gammacerane is a specific biomarker for water-column stratification and hypersaline conditions in marine and non-marine environments (Sinninghe Damsté et al., 1995; Peters et al., 2005).

The occurrence of gammacerane in the Eagle Ford Shale samples suggests that regional hypersaline conditions and water stratification may have developed during deposition of these sediments. This observation positively correlated with the low Pr/Ph ratios and the predominance of the ββ steranes over the αα steranes, both parameters also related to hypersalinity (ten Haven et al., 1988). Nevertheless, the presence of gammacerane in these samples needs to be further confirmed by fullscan GCMS analysis in order to analyze variations in the concentration if this biomarker in the Eagle Ford Shale.

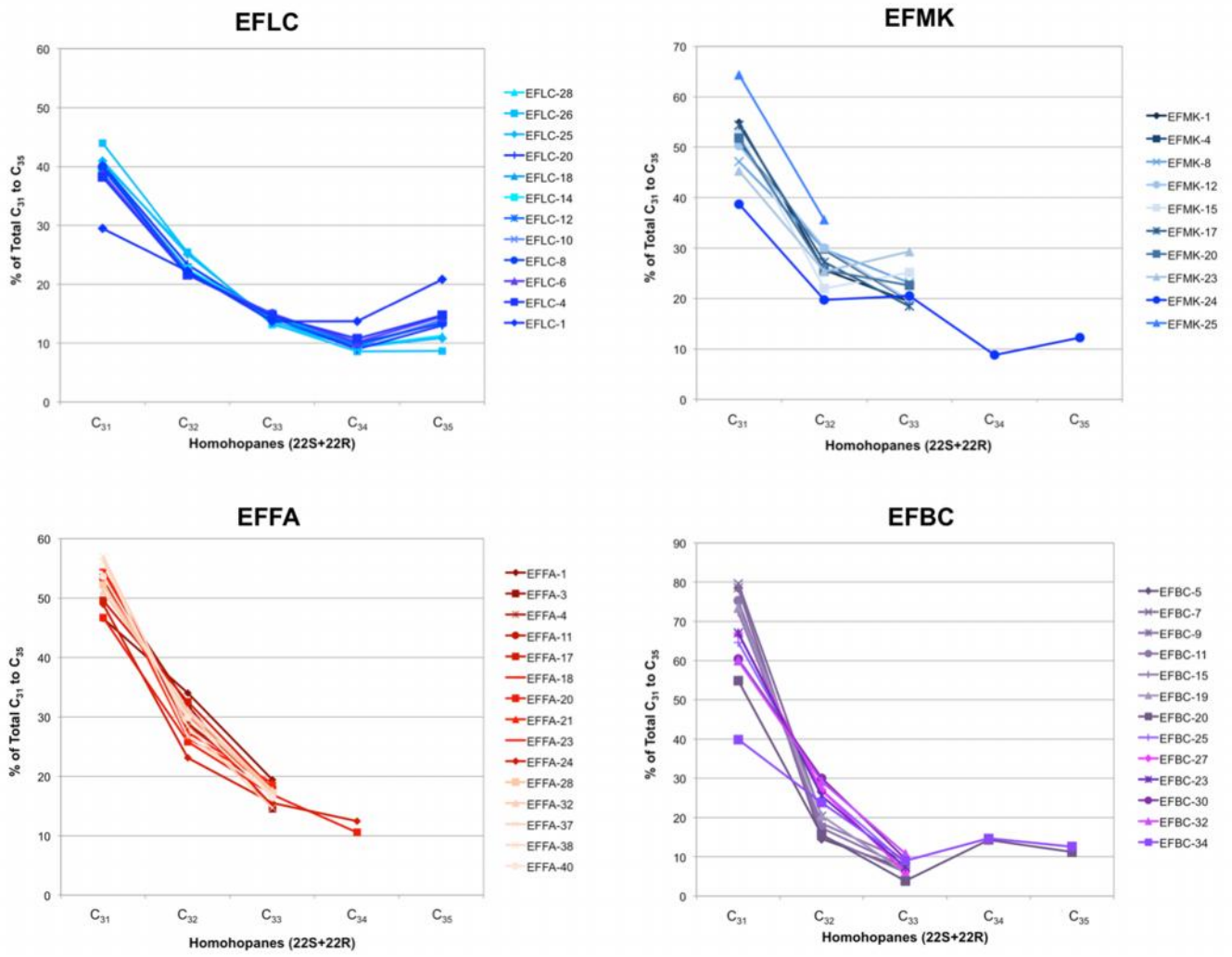


**Figure 31. Homohopanes distribution for bitumens and oils from the Eagle Ford Shale**

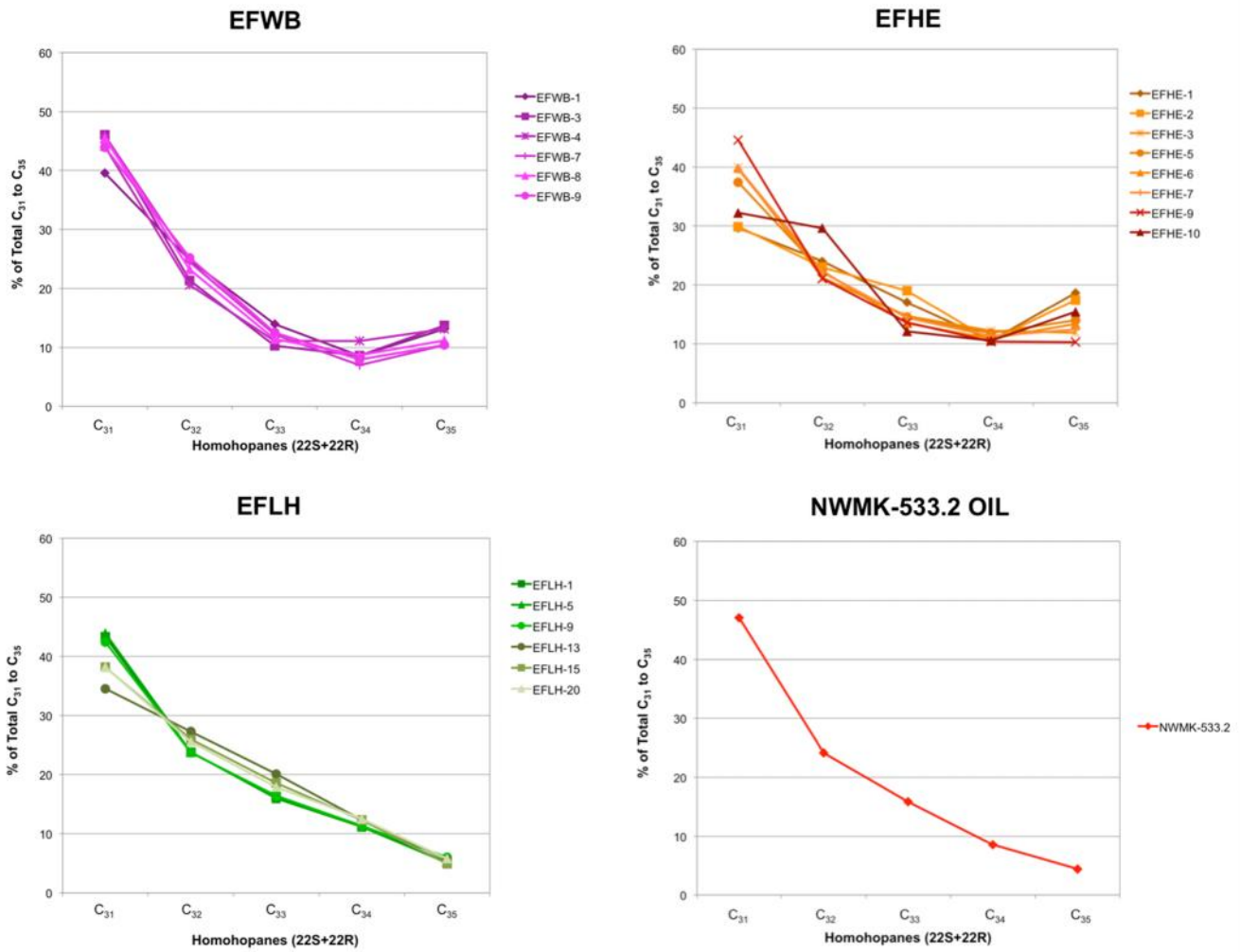


**Figure 31. Homohopanes distribution for bitumens and oils from the Eagle Ford Shale (cont.)**

### 2.2.3 Aryl Isoprenoids

Aryl isoprenoids, or trimethylbenzenes, are compounds derived from isorenieratene, a $C_{40}$ diaromatic carotenoid pigment produced by the green sulfur bacteria *Chlorobiaceae* (Brown and Kenig, 2004; Schwark and Frimmel, 2004). *Chlorobiaceae* performs photosynthesis under light-penetrated, $H_2S$-saturated, anoxic waters; thus, compounds derived from these bacteria can be specific indicators of photic zone anoxia (PZA; Schwark and Frimmel, 2004).

Analysis of aryl isoprenoids was performed in the B&C fractions of bitumens and oils by SIM/GC-MS using ions m/z 133.1 and 134.1. Results from aryl isoprenoids quantitation are in Appendix N. In all the analyzed samples, only the 1-alkyl-2,3,6-trimethylbenzenes (m/z = 133.1) were identified. The 1-alkyl-3,4,5-trimethylbenzenes (m/z = 134.1) were absent or in very low concentrations hampering detection of these compounds. The identified aryl isoprenoids were a series of $C_{13}$-$C_{22}$ homologs, and detection beyond the $C_{26}$ homolog was problematic (Figure 32). Evaluation of these compounds to understand possible variability of PZA in the Eagle Ford Shale was performed through the calculation of the aryl isoprenoid ratio (AIR; Appendix A). Schwark and Frimmel (2004) introduced this ratio by analyzing the proportions of the short-chain ($C_{13}$-$C_{17}$) and intermediate-chain ($C_{18}$-$C_{22}$) aryl isoprenoids. High AIR (3.0) are associated with episodic PZA, which leads to alteration of the long- and intermediate-chain aryl isoprenoids. On the contrary, low AIR (0.5) indicates persistent PZA, which contributes to preservation of the long-chain aryl isoprenoids (Schwark and Frimmel, 2004).

Most of the analyzed samples show AIR greater than 1 (Appendix J) suggesting that the Eagle Ford Shale experienced episodic periods of PZA, where shifts of the chemocline occurred periodically. Koopmans et al. (1996) determined that β-isorenieratane and β-carotane are also precursors for the 2,3,6 trimethyl-substituted aryl isoprenoids. When derived from these compounds, the 2,3,6 trimethyl-substituted aryl isoprenoids are depleted in $\delta^{13}C$ and cannot be used as specific biomarkers for PZA. In the present study, the $\delta^{13}C$ values for the aryl isoprenoids were not determined. Nevertheless, geochemical logs of AIR for the Eagle Ford Shale samples show a positive correlation with Pr/Ph (Figure 33; Appendix C), and aryl isoprenoids were used to tentatively evaluate variations and degree of PZA. A graph of AIR versus Pr/Ph (Figure 34) helps to better assess redox conditions and PZA during sediments deposition (Schwark and Frimmel, 2004). From this diagram it can be observed that samples from EFLC and EFBC outcrops, and the EFAC core were possibly deposited under anoxic-suboxic conditions and persistent PZA. Samples EFWB and EFHE seem to have experienced episodic PZA. High AIR in samples EFMK, EFFA, and oils could be consequence of their high thermal maturity, which tend to generate short-chain aryl isoprenoids from the long-chain homologs.

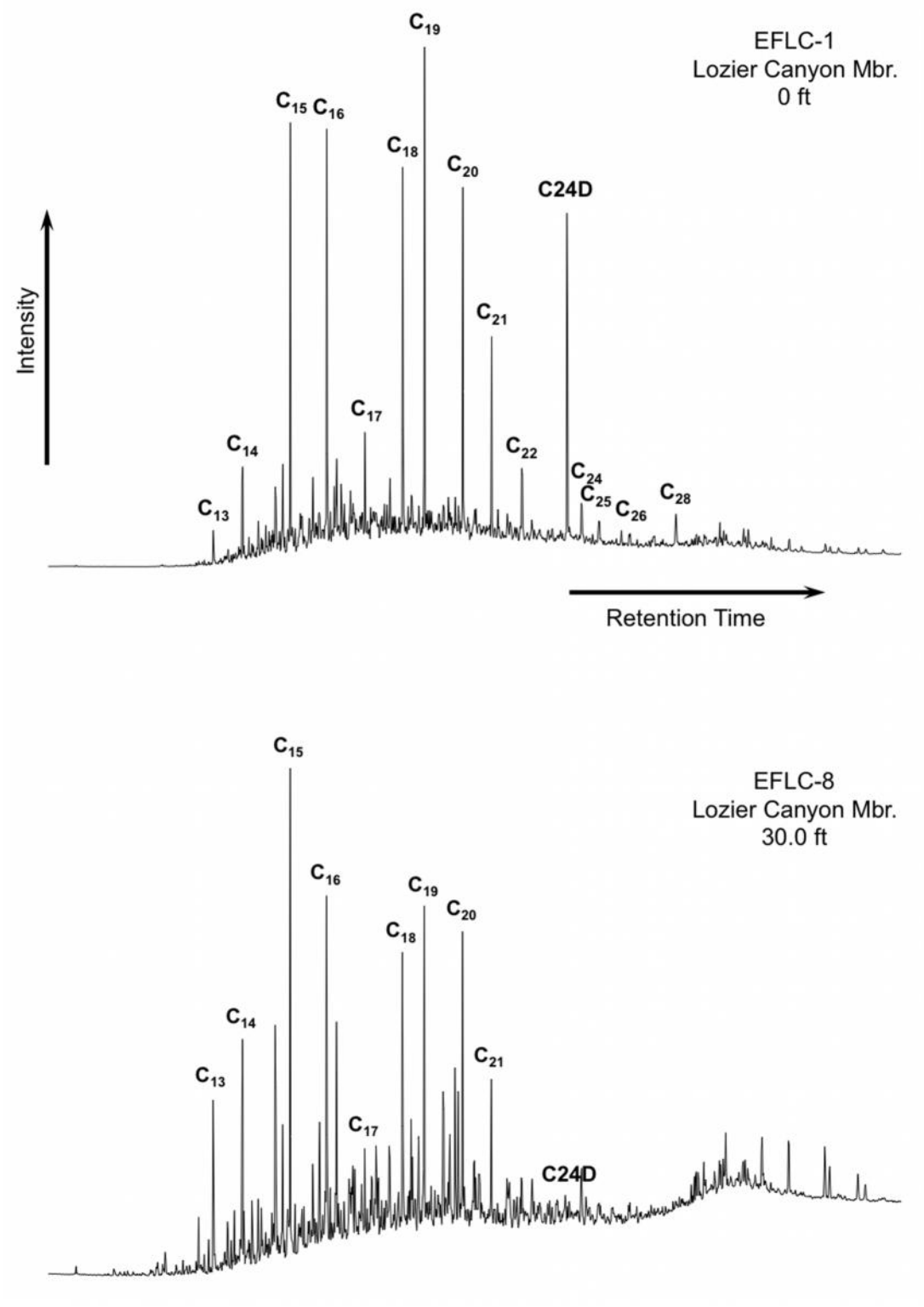


**Figure 32. Partial fragmentograms of the m/z 133.1 ion showing the aryl isoprenoids distribution in the B&C fractions of the EFLC samples. Number of carbon atoms for the 2,3,6-trimethyl substituted aryl isoprenoids is indicated above each peak (C24D = internal standard)**

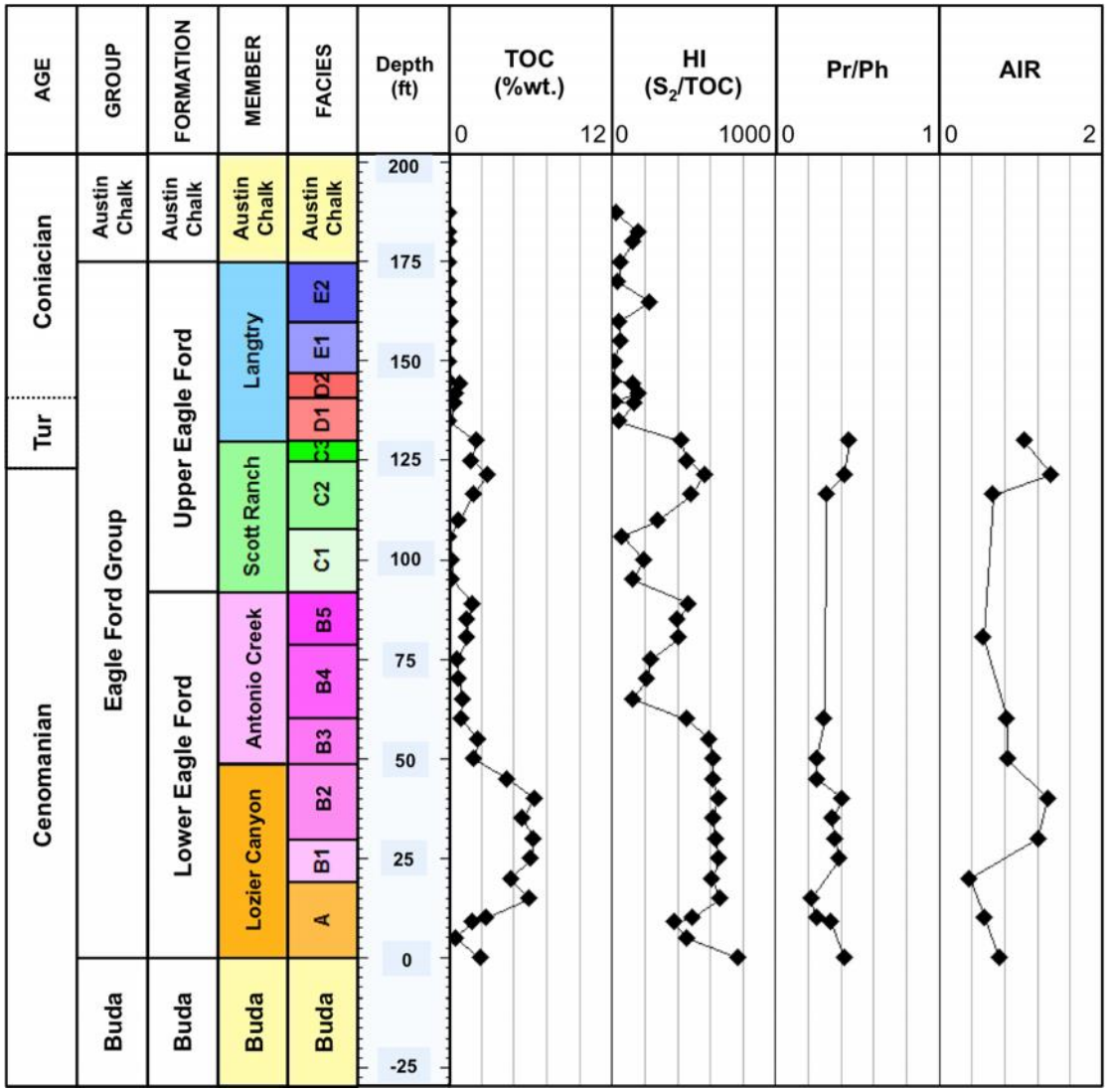


**Figure 33. Geochemical logs of biomarker ratios of aryl isoprenoids for Eagle Ford Shale samples at Lozier Canyon. Formulas for calculation of ratios are in Appendix A. Geochemical logs from other locations analyzed are in Appendix C. Numerical values of AIR are in Appendix J**

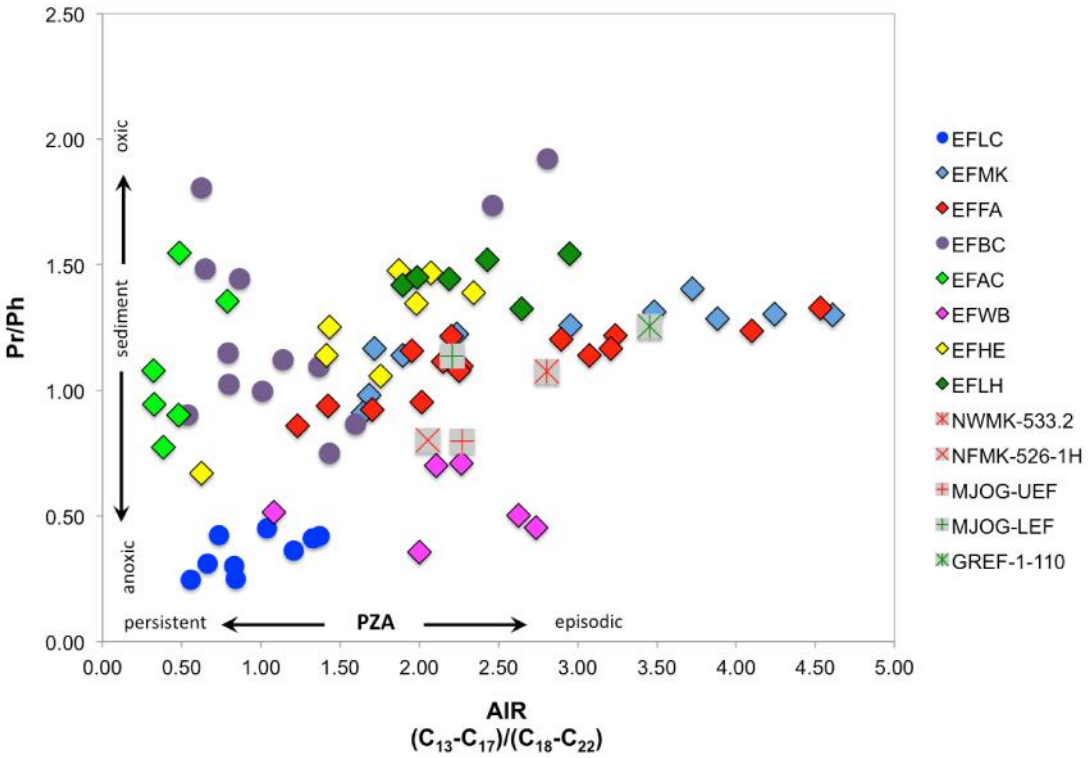


**Figure 34. AIR versus Pr/Ph plot for the Eagle Ford Shale samples (Dotted line is used as a guide and does not represent fixed fields on the diagram. Plot template from Schwark and Frimmel, 2004)**

### 2.2.4 Monoaromatic Steroids

Monoaromatic steroids (MAS) are a group of biomarkers derived from sterols containing more than one double bond (Peters et al., 2005). These biomarkers were determined in the B&C fraction of Eagle Ford Shale bitumens and oils through SIM/GC-MS by analysis of the m/z 253.3 ion (Figure 35, Table 8). Compared to the regular steranes ternary plot, the proportions of the $C_{27}$, $C_{28}$, and $C_{29}$ MAS plotted in a ternary diagram provide a better characterization of the variations in depositional environments, and are particularly useful for distinguishing marine from non-marine oils (Moldowan et al., 1985). These authors indicated that oils and bitumens derived from marine organic matter contain greater amounts of $C_{28}$ MAS than those of non-marine origin. In addition, Moldowan et al. (1985) observed that some oils derived from marine carbonate source rocks contain higher amounts of $C_{29}$ MAS than oils derived from marine shales. The bitumens and oils from the Eagle Ford Shale have a greater concentration of $C_{28}$ MAS, followed by $C_{27}$ and $C_{29}$ MAS (Appendix O) and their distribution is similar to that of the regular steranes (Figure 36), indicating a marine source for these samples.

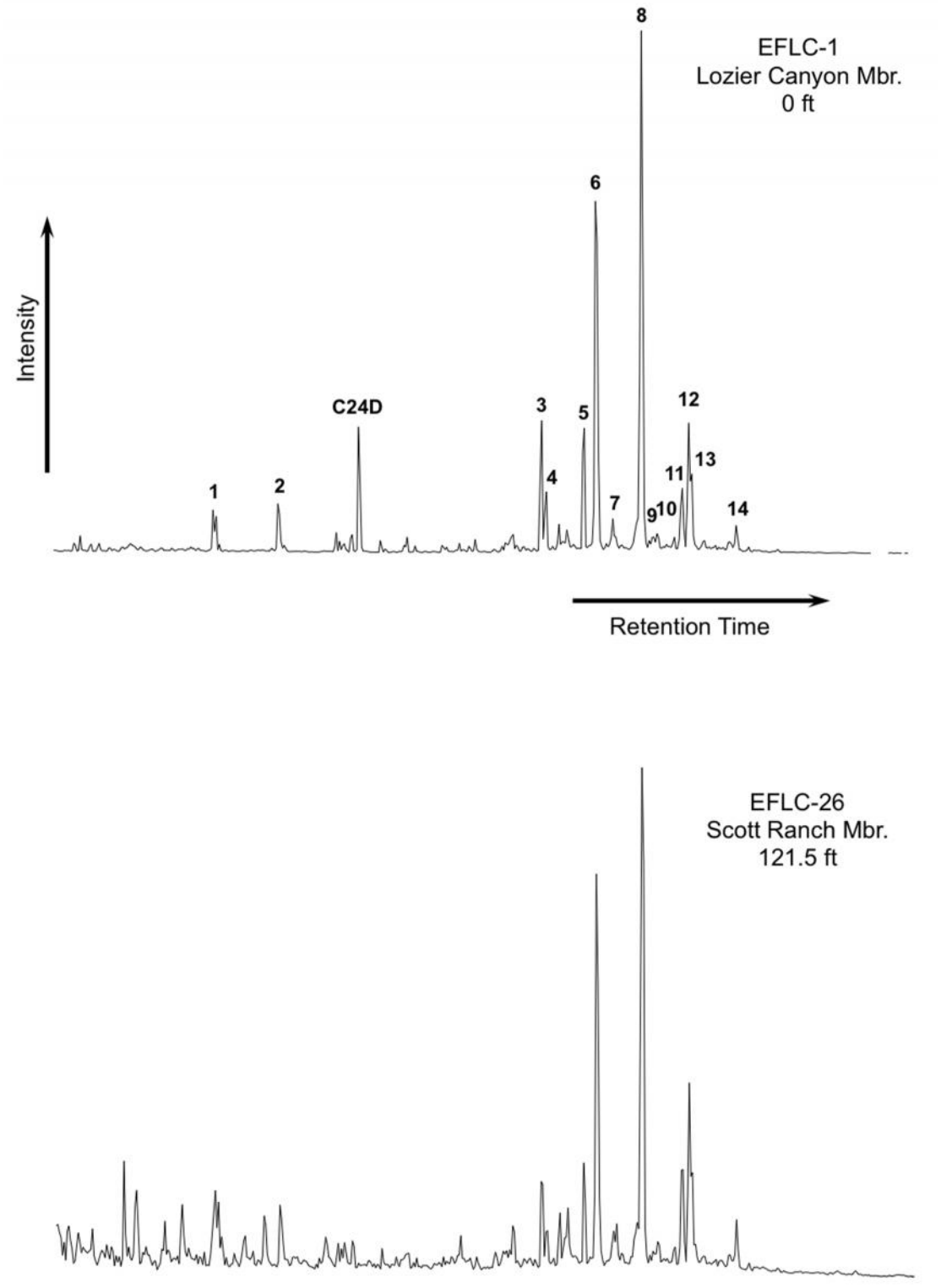


**Figure 35. Partial fragmentograms of the m/z 253.3 ion showing distribution of the monoaromatic steroids (MAS) in the B&C fractions of the EFLC samples. Peak identification is presented in Table 8**

**Table 8. Identification of monoaromatic steroids (MAS) in the partial m/z 253.3 fragmentogram of the B&C fractions**

| Peak # | Compound |
|---|---|
| **C24D** | Deuterated *n*-tetracosane (ISTD) |
| **1** | **$C_{21}$** Pregnane |
| **2** | **$C_{22}$** 20-Methylpregnane |
| **3** | **$C_{27}$** 5β-Cholestane 20S |
| **4** | **$C_{27}$** Diacholestane 20S |
| **5** | **$C_{27}$** Monoaromatic steroid |
| **6** | **$C_{28}$** 5β-Ergostane 20S + **$C_{28}$** Diaergostane 20S |
| **7** | **$C_{27}$** 5α-Cholestane 20R |
| **8** | **$C_{28}$** 5α-Ergostane 20S |
| **9** | **$C_{28}$** 5β-Ergostane 20R + **$C_{28}$** Diaergostane 20R |
| **10** | **$C_{29}$** 5β-Stigmastane 20S + **$C_{29}$** Diastigmastane 20S |
| **11** | **$C_{29}$** 5α-Stigmastane 20S |
| **12** | **$C_{28}$** 5α-Ergostane 20R |
| **13** | **$C_{29}$** 5β-Stigmastane 20R + **$C_{29}$** Diastigmastane 20R |
| **14** | **$C_{29}$** 5α-Stigmastane 20R |

Peak 5 could be $C_{27}$ 5β-Cholestane 20R + $C_{27}$ Diacholestane 20R or $C_{27}$ 5α-Cholestane 20S

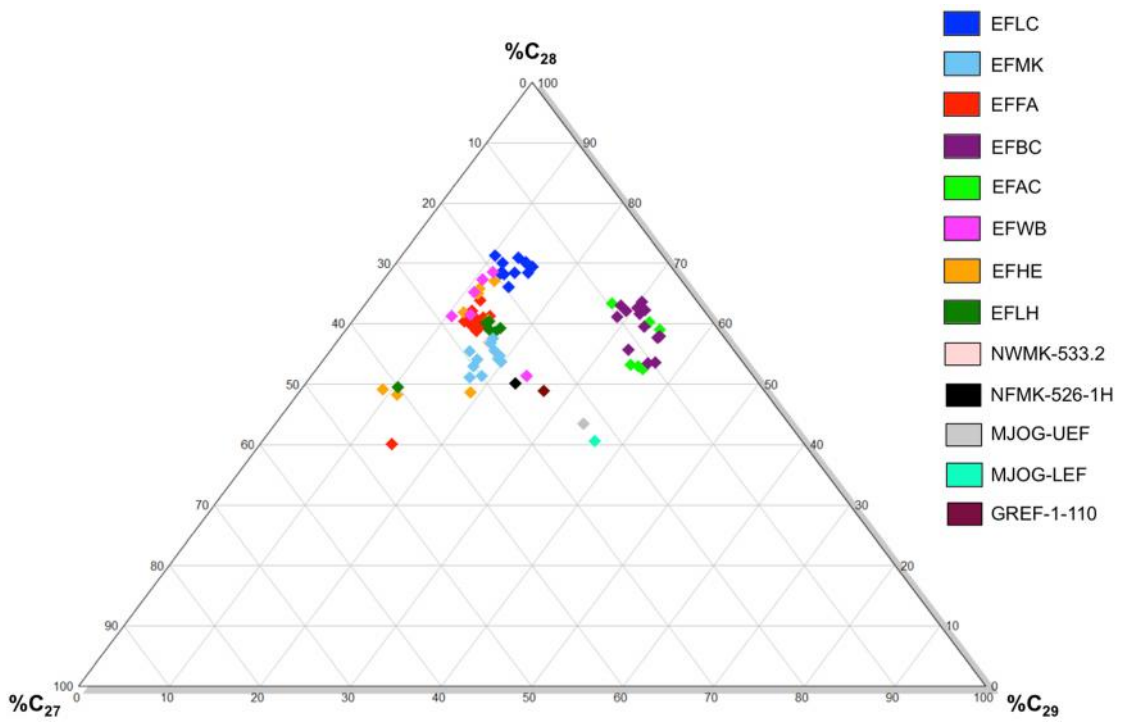


**Figure 36. Ternary diagram of $C_{27}$, $C_{28}$, and $C_{29}$ monoaromatic steroids for Eagle Ford Shale bitumens and oils (Plot modified from Moldowan et al., 1985)**

## 2.3 Biomarkers and geochemical parameters for evaluation of thermal maturity

### 2.3.1 Steranes

Steroid precursors in nature have only an R configuration at C-20, that with increasing maturation are progressively converted to mixture of R (biological) and S (thermal) isomers (Peters et al., 2005). As a result, geochemical ratios of biomarker isomers provide a useful tool for thermal maturity assessment. For example, the $C_{29}$ 20S/(20S+20R) steranes ratio increases with thermal maturity from 0 to about 0.5, reaching equilibrium at 0.52 to 0.55 (Seifert and Moldowan, 1986; Peters et al., 2005). Organic facies changes, weathering, and biodegradation may affect this maturity

parameter (Peters et al., 2005). The $C_{29}$ ββ/(ββ+αα) steranes ratio is not influenced by organic matter source, and its racemic mixture is reached at higher maturity levels compared to the $C_{29}$ 20S/(20S+20R) steranes. With increasing thermal maturation isomerization at C-14 and C-17 in the $C_{29}$ 20S and 20R regular steranes increases the ββ/(ββ+αα) ratio from near-zero values to about 0.7. Equilibrium reaction for this conversion is reached at about 0.67 to 0.71 (Peters et al., 2005). Comparison of the $C_{29}$ ββ/(ββ+αα) versus $C_{29}$ 20S/(20S+20R) sterane ratios are commonly used to evaluate thermal maturation of oils and bitumens and to perform quality control of these geochemical parameters (Figure 37; Seifert and Moldowan, 1986; Peters et al., 2005). Calculation of these maturity ratios for the Eagle Ford Shale (Appendix A) indicates that all samples are thermally mature, with the exception of samples EFBC and EFAC, which are immature (Table 9; Appendix H).

It is possible that the high $C_{29}$ 20S/(20S+20R) sterane ratios for the EFLC samples are attributed to weathering. Clayton and King (1987) found that weathering in shale outcrops produce preferential loss of the $C_{29}$ αα 20S sterane diasteromer. In addition, it has been suggested that this ratio also decreases in high maturity samples (Peters et al., 1990), which could explain why the EFFA samples appear to have low maturity, even though other thermal maturity parameters describe them as high maturity source rocks.

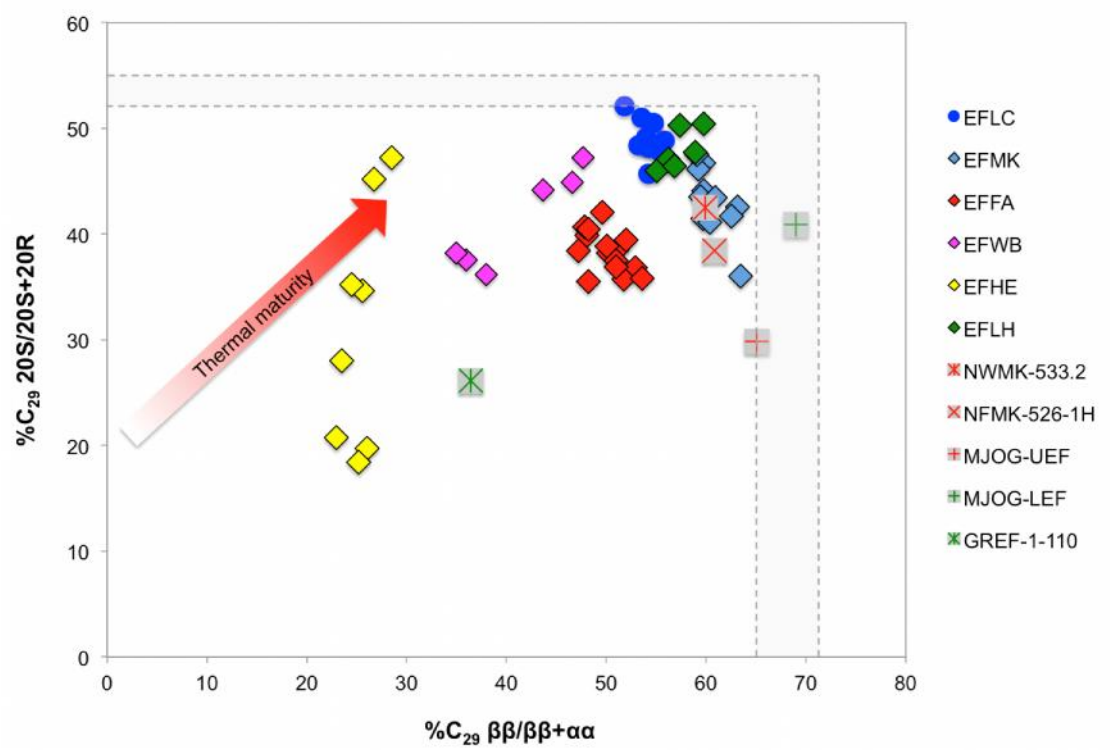


**Figure 37. Plot of $C_{29}$ ββ/(ββ+αα) steranes versus $C_{29}$ 20S/(20S+20R) steranes showing variations in thermal maturity for the Eagle Ford Shale source rocks and liquids (Gray area represents end points of isomerization reactions. Plot modified from Peters, 1999)**

**Table 9. Average steranes isomerization ratios for the Eagle Ford Shale bitumens and liquids (ND = not determined; *not averaged)**

| Sample | # of samples | $C_{29}$ 20S/(20S+20R) | $C_{29}$ ββ/(ββ+αα) |
|---|---|---|---|
| EFLC | 12 | 0.49 | 0.54 |
| EFMK | 11 | 0.43 | 0.61 |
| EFFA | 15 | 0.38 | 0.50 |
| EFBC | 13 | 0.01 | 0.34 |
| EFAC | 6 | ND | 0.26 |
| EFWB | 6 | 0.41 | 0.41 |
| EFHE | 8 | 0.31 | 0.25 |
| EFLH | 6 | 0.48 | 0.57 |
| NWMK-533.2 OIL | * | 0.42 | 0.60 |
| NFMK-526-1H OIL | * | 0.38 | 0.61 |
| MJOG-UEF OIL | * | 0.30 | 0.65 |
| MJOG-LEF OIL | * | 0.41 | 0.69 |
| GREF-1-110 COND. | * | 0.26 | 0.36 |

### 2.3.2 Terpanes

#### *2.3.2.1 Hopanes*

A maturity parameter based on epimer ratios of 17α-homohopanes is the $C_{31}$ 22S/(22S+22R) ratio. The biological configuration of the homohopanes is the 22R, and during the early stages of organic matter maturation, isomerization at the C-22 position occurs, gradually converting homohopanes to a mixture of 22R and 22S configurations (Peters and Moldowan, 1991; Peters et al., 2005). The 22S/(22S+22R) ratio increases from 0 to ~0.6 reaching equilibrium at ratios of 0.57 to 0.62 (early oil window) after which no additional thermal maturity information can be obtained (Peters et al., 2005). Samples from the EFBC outcrop and the EFAC core have greater concentrations of the

22R diasteromer and 22S/(22S+22R) ratios of ~0.2 and ~0.3 respectively, pointing towards the low maturity of these samples (Appendices I and M). The bitumens and liquids analyzed from the other outcrops and cores have average 22S/(22S+22R) ratios greater than 0.50, indicating that these samples have reached the main stage of oil generation (Table 10).

**Table 10. Average $C_{31}$ 22S/(22S+22R) hopane ratios for Eagle Ford Shale bitumens and oils (*not averaged)**

| Sample | # of samples | $C_{31}$ 22S/(22S+22R) |
|---|---|---|
| EFLC | 12 | 0.61 |
| EFMK | 11 | 0.53 |
| EFFA | 15 | 0.56 |
| EFBC | 13 | 0.23 |
| EFAC | 6 | 0.32 |
| EFWB | 6 | 0.59 |
| EFHE | 8 | 0.58 |
| EFLH | 6 | 0.58 |
| NWMK-533.2 OIL | * | 0.50 |

*2.3.2.2 Moretanes*

Hopanoids in organisms have a 17β(H),21(β)H-configuration (ββ), which becomes unstable during organic matter burial and easily converts to βα-moretanes and αβ-hopanes. However, $C_{29}$ and $C_{30}$ moretanes are less stable than hopanes and their concentrations decrease relative to hopanes with increasing maturity. As a result, the ratio moretanes/hopanes is used to evaluate thermal maturity for immature to early oil window samples (Peters et al., 2005). This ratio decreases from approximately 0.8 (immature) to <0.15 (minimum 0.05) with increasing maturation (Peters et al., 2005).

High moretanes/hopanes ratios have been associated with hypersaline source rocks (Rullkötter and Marzi, 1988), and in transgressive to highstand systems tracts, with significant terrigenous organic matter input (Isaken and Bohacs, 1995), which suggests that this ratio may also be influenced by depositional environment (Peters et al., 2005). Ratios of $C_{30}$ moretanes/hopanes calculated for Eagle Ford Shale samples have average values lower than 0.19 (Table 11, Appendix I) indicating that all samples with exception of EFBC and EFAC are thermally mature.

**Table 11. Average $C_{30}$ Moretane/Hopane ratios for Eagle Ford Shale bitumens and oils (*not averaged)**

| Sample | # of samples | $C_{30}$ Moretanes/Hopanes |
|---|---|---|
| EFLC | 12 | 0.06 |
| EFMK | 11 | 0.16 |
| EFFA | 15 | 0.19 |
| EFBC | 13 | 1.57 |
| EFAC | 6 | 1.57 |
| EFWB | 6 | 0.13 |
| EFHE | 8 | 0.14 |
| EFLH | 6 | 0.12 |
| NWMK-533.2 OIL | * | 0.07 |

*2.3.2.3 Ts and Tm*

$C_{27}$ 17α-22,29,30-trisnorhopane (Tm) and $C_{27}$ 18α-22,29,30-trisnorneohopane (Ts) are terpanes frequently used to assess maturation from immature to postmature stage (Peters et al., 2005). Tm becomes less stable than Ts with increasing thermal maturity; therefore, the Ts/(Ts+Tm) ratio can be used as a maturity indicator,

particularly for samples of similar lithology and organic facies (Moldowan et al., 1994; Peters et al., 2005).

Ts and Tm can be correlated with other parameters to evaluate thermal maturity and depositional environment. For example, the relationship between the Ts/(Ts+Tm) ratio and the diasteranes/(diasteranes+regular) $C_{27}$ steranes ratio for the Eagle Ford Shale samples reveals three different groups (Figure 38). The first group clusters samples from EFLH, EFMK, EFFA and oils, which are affected by high thermal maturity, indicated by the high Ts/(Ts+Tm) ratios. In the second group, correlation of these ratios gathers samples EFWB, EFHE, and EFLC, suggesting that these bitumens were derived from low maturity, anoxic carbonate source rocks. The third group encompasses four EFLC samples. Ts/(Ts+Tm) ratios for these samples indicate low maturity; however, the diasteranes/(diasteranes+regular) $C_{27}$ steranes ratios are slightly higher for these samples compared to the second group, suggesting that the rocks that sourced these bitumens are more clay-rich. In fact, three of these samples correspond to the Scott Ranch Member, in which Donovan et al. (2013) identified several bentonite beds. In case of the EFBC samples, the low diasteranes/(diasteranes+regular) $C_{27}$ steranes ratios could be a result of their low maturity, instead of their lithology. Moreover, in samples from the immature EFAC core, which is closely located to the EFBC outcrop, no $C_{27}$ diasteranes could be identified.

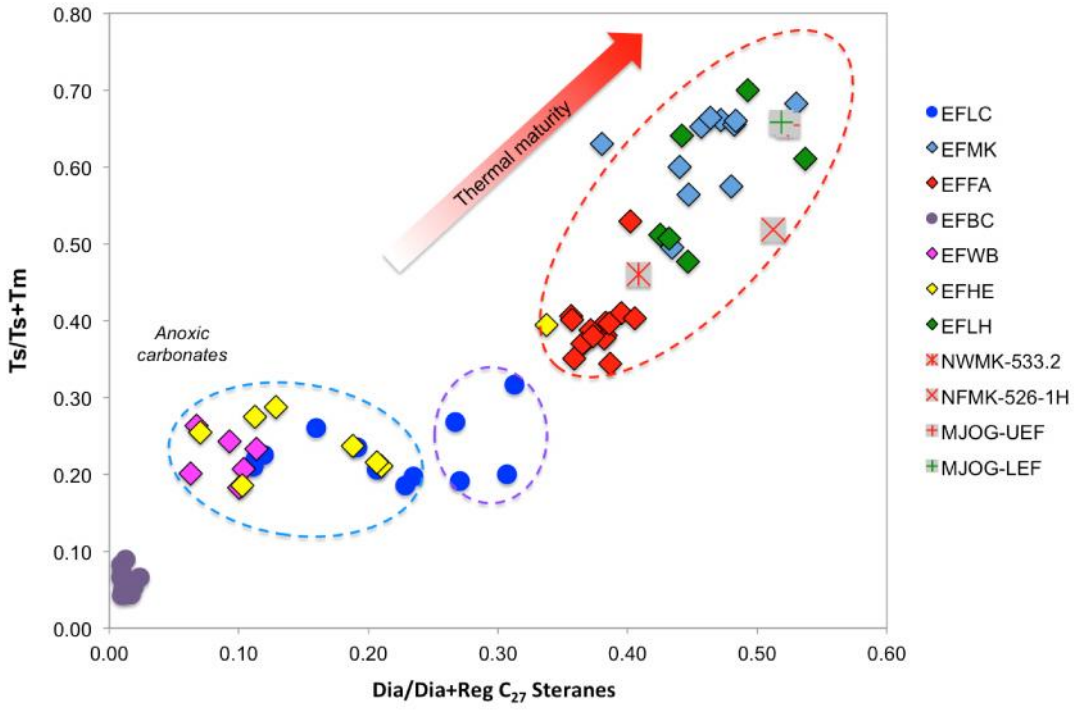


**Figure 38. Plot of diasteranes/(diasteranes+regular) $C_{27}$ Steranes versus Ts/(Ts+Tm) ratios shows differences in thermal maturity, source, and redox potential for Eagle Ford Shale samples (Plot modified from Moldowan et al., 1994).**

### 2.3.3 Monoaromatic and Triaromatic Steroids

Monoaromatic and triaromatic steroids were determined in the B&C and aromatic fractions of Eagle Ford source rock extracts and oil samples, respectively. Identification was carried out by analysis of ions m/z 231.3 and 253.3 through SIM/GC-MS. Selected fragmentograms of MAS and TAS are presented in Figures 35 and 39. Peak identifications are in Table 12. Generation of ABC-ring triaromatic steroids (TA) from A-ring monoaromatic (MA) steroids occurs during maturation by aromatization of B and C rings and the loss of both, a methyl group at the A/B junction and the stereocenter at C-5 (Mackenzie, 1984). The ratio TA28/(MA29+TA28) increases from 0

to 100% during maturation and provides thermal maturity information from immature to early oil window ($R_o$~0.8%; Mackenzie, 1984; Peters et al., 2005). The ratios MA(I)/MA(I+II) and TA(I)/TA(I+II) are additional geochemical parameters used to evaluate thermal maturity from immature to late oil generation window ($R_o$~1.4%; Peters et al., 2005). These ratios increase from 0 to 100% with increase in thermal maturity. This increase may occur due to conversion of long- to short-chain aromatic steroids, preferential thermal degradation of the long- versus short-chain compounds, or both. However, the since the TAS are derived from the MAS, the TA(I)/TA(I+II) ratio is more sensitive at high levels of thermal maturity compared to the MAS ratio (Peters et al., 2005).

MAS and TAS ratios (Appendix K) obtained for the Eagle Ford Shale samples indicate that the EFLC, EFBC and EFAC samples are thermally immature as suggested by the other maturity parameters previously described. In addition, these aromatic steroids ratios indicate that samples EFWB and EFHE are marginally mature, while samples EFLH, EFMK, EFFA, and oils are mature, possibly peak oil to late oil window.

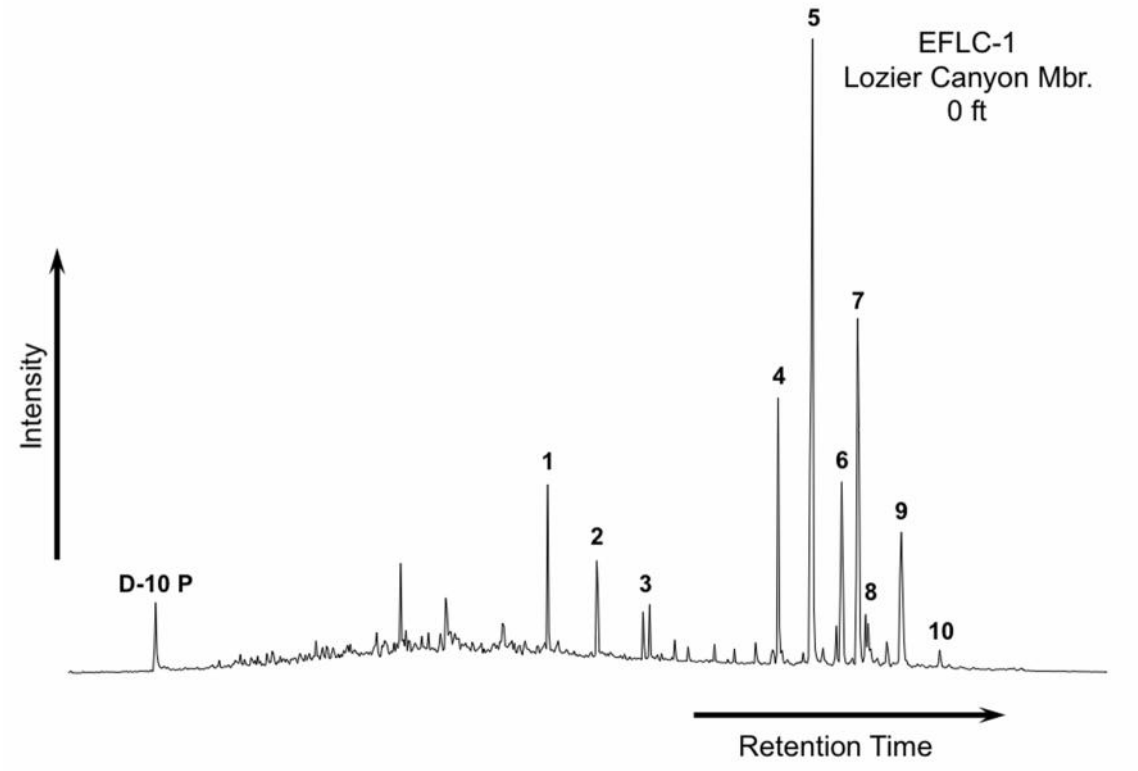


**Figure 39. Partial fragmentograms of the m/z 231.3 ion showing distribution of the triaromatic steroids (TAS) in the aromatic fractions of sample EFLC-1. Peak identification is presented in Table 12**

**Table 12. Identification of triaromatic steroids (TAS) in the partial m/z 231.3 fragmentogram of the aromatic fractions**

| Peak # | Compound |
|---|---|
| **D-10 P** | Deuterated Phenanthrene (ISTD) |
| **1** | **$C_{20}$** Pregnane |
| **2** | **$C_{21}$** 20-Methylpregnane |
| **3** | **$C_{22}$** 20-Ethylpregnanes (a and b are epimeric at $C_{20}$) |
| **4** | **$C_{26}$** Cholestane (20S) |
| **5** | **$C_{26}$** Cholestane (20R) + **$C_{27}$** Ergostane (20S) |
| **6** | **$C_{28}$** Stigmastane (20S) (24-Ethylcholestane 20S) |
| **7** | **$C_{27}$** Ergostane (20R) (24-Methylcholestane 20R) |
| **8** | **$C_{29}$** 24-*n*-Propylcholestane (20S) (a and b are epimeric at |
| **9** | **$C_{28}$** Stigmastane (20R) |
| **10** | **$C_{29}$** 24-*n*-Propylcholestane (20R) |

### 2.3.4 Phenanthrenes

Phenanthrenes, methylphenanthrenes, and dimethylphenanthrenes were identified in the aromatic fraction of bitumens and oils by SIM/GC-MS through the analysis of ions m/z 178.3, 192.3, and 206.3 (Figure 40, Table 13). Results from quantitation of phenanthrenes compounds are in Appendix P. A number of ratios derived from the distribution of these compounds have been used as geochemical maturity parameters (Radke and Welte, 1981; Radke et al., 1984; 1986). In particular, the Methylphenanthrene Indices (MPI-1 and MPI-2) are the most commonly applied. With increasing temperature and burial, an increase of the 2- and 3-methylphenanthrenes relative to the 1- and 9-methylphenanthrenes occurs (Radke et al., 1982). Radke and Welte (1981) recognized a positive correlation between MPI-1 and vitrinite reflectance for samples within the oil window (0.65-1.35%$R_o$), and a negative correlation for samples of high thermal maturity (1.35-2.00%$R_o$). From these

observations, the authors derived two equations for $R_o$ calculation, which can be used to estimate thermal maturity for bitumens and oils (Radke and Welte, 1981; Appendix A).

Values of MPI-1 and MPI-2 ratios were obtained for the Eagle Ford Shale samples (Appendix K), and from the MPI-1 parameter, vitrinite reflectance was calculated (Table 14). The equation from Radke and Welte (1981) corresponding to low maturity levels was used for calculating vitrinite reflectance from all samples. Overall, the results are in agreement with the maturity parameters previously described which indicate that most of the Eagle Ford Shale samples analyzed are immature to peak oil window ($R_c$ ~0.58-0.93).

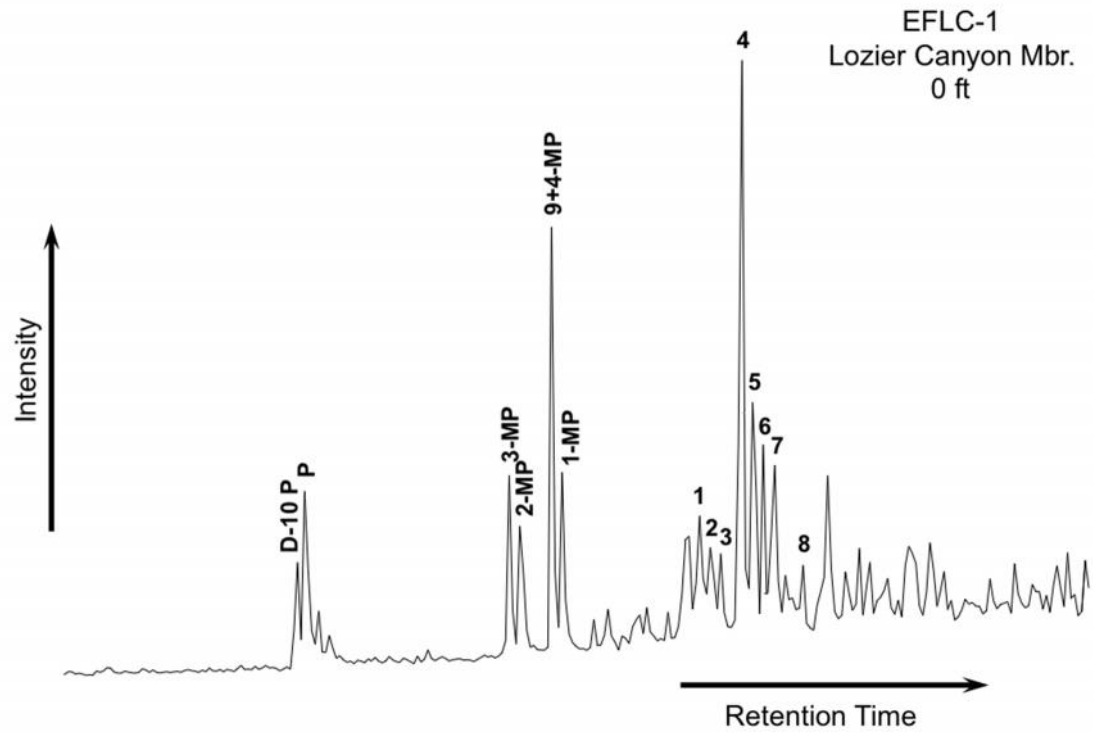


**Figure 40. Summed mass chromatograms of m/z 106.3, 192.3, 206.3 ions showing distribution of phenanthrenes compounds in the aromatic fractions of sample EFLC-1. Peak identification is presented in Table 13**

**Table 13. Identification of phenanthrenes in the partial mass chromatograms of m/z 178.3, 192.3, 206.3 of the aromatic fractions**

| Peak # | Compound |
|---|---|
| **D-10 P** | Deuterated Phenanthrene (ISTD) |
| **P** | Phenanthrene |
| **3-MP** | 3-Methylphenanthrene |
| **2-MP** | 2-Methylphenanthrene |
| **9+4-MP** | 9+4-Methylphenanthrene |
| **1-MP** | 1-Methylphenanthrene |
| **1** | Dimethylphenanthrene |
| **2** | Dimethylphenanthrene |
| **3** | Dimethylphenanthrene |
| **4** | Dimethylphenanthrene |
| **5** | Dimethylphenanthrene |
| **6** | Dimethylphenanthrene |
| **7** | Dimethylphenanthrene |
| **8** | Dimethylphenanthrene |

**Table 14. Calculated vitrinite reflectance ($R_c$) for Eagle Ford Shale bitumens and oils from MPI-1 values**

| Sample | $R_c$ |
|---|---|
| EFLC | 0.58 |
| EFMK | 0.83 |
| EFFA | 0.93 |
| EFBC | 0.66 |
| EFAC | 0.63 |
| EFWB | 0.77 |
| EFHE | 0.74 |
| EFLH | 0.72 |
| NWMK-533.2 | 0.78 |
| NFMK-526-1H | 0.79 |
| MJOG-UEF | 0.84 |
| MJOG-LEF | 0.89 |
| GREF-1-110 | 0.92 |

## 2.4 Isotope Analysis

Compound specific isotope analysis (CSIA) was performed on the saturate fractions of bitumens and oil samples. At least one sample from each Eagle Ford Shale member per well was selected for CSIA in order to address possible source and maturity variations. Carbon isotope values ($\delta^{13}C$) for individual *n*-alkanes are reported in per mil (‰) relative to the Vienna Pee Dee Belemnite (VPDB) standard (Appendix Q). Figures 41 to 46 show the *n*-alkane isotope profiles for Eagle Ford Shale samples of different maturity. The carbon isotopic composition of all the samples, including oils and condensates varies from -32.6 to -29.9‰, and in general there is no significant variability on the isotope values for the *n*-alkanes in the range analyzed.

Considering that all the analyzed samples essentially come from the same self-sourced unconventional reservoir, factors such as source rock age, hydrocarbon mixing, and reservoir alteration processes do not have an influence on the isotopic values of the bitumens and liquids analyzed. Therefore, any observed changes in the isotopic composition of the samples would be expected to result from source and thermal maturity variations. Overall, the isotopic profiles for the Eagle Ford Shale samples do not show marked changes in the $\delta^{13}C$ values. The range of $\delta^{13}C$ values and the apparently flat and uniform isotopic profiles are in agreement with a marine origin for the samples analyzed (Murray et al., 1994). Even though biomarker data suggest a terrigenous organic matter input for the EFLH well, the *n*-alkanes isotope profiles do not reflect these variations in source. Enrichment in the overall $\delta^{13}C$ values of *n*-alkanes along with a $^{13}C$ depletion in the long-chain *n*-alkanes range is commonly observed in samples with terrigenous organic matter contribution (Murray et al., 1994; Dowling et

al., 1995), a characteristic that is not detected in the Eagle Ford Shale samples analyzed from the EFLH core. These observations suggest there are no significant variations in organic facies or depositional environments among the different Eagle Ford Shale members. Likewise, despite the fact that the samples analyzed have different thermal maturity levels, the isotopic data do not reflect variations regarding this effect. This is an interesting observation since usually hydrocarbons become enriched in $\delta^{13}C$ values with increasing maturity (Clayton, 1991). The similarity in the $\delta^{13}C$ values between the bitumens and the analyzed liquids indicate that the oils and condensates were generated from the Eagle Ford Shale.

Unfortunately, the lack of published literature regarding CSIA for marine shales using an unconventional reservoir analysis approach prevents making comparisons and correlations of the isotopic data obtained in this research with analog settings.

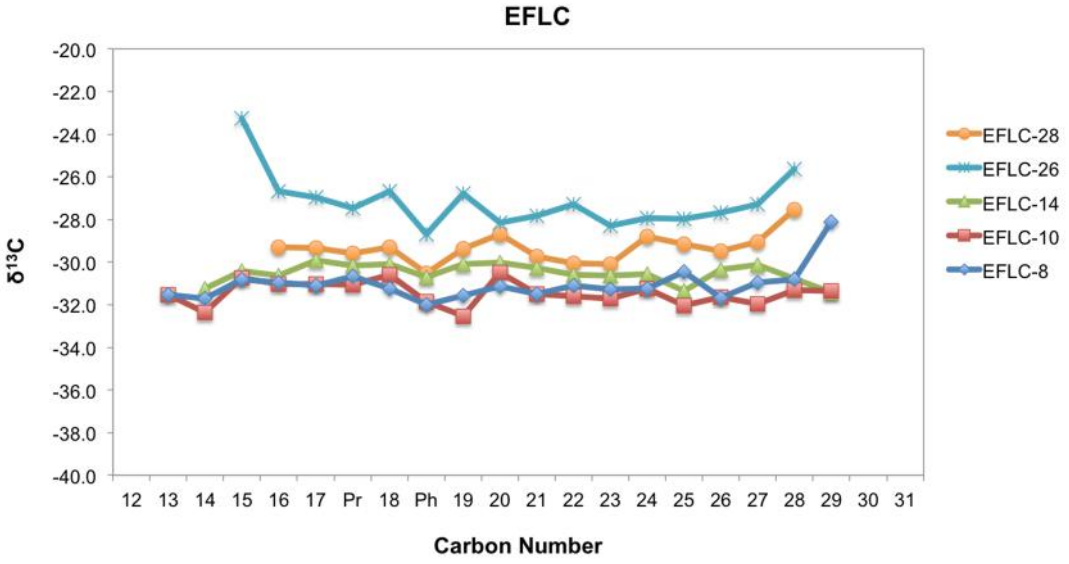


**Figure 41. *n*-Alkane isotope profile from the EFLC extracts (immature)**

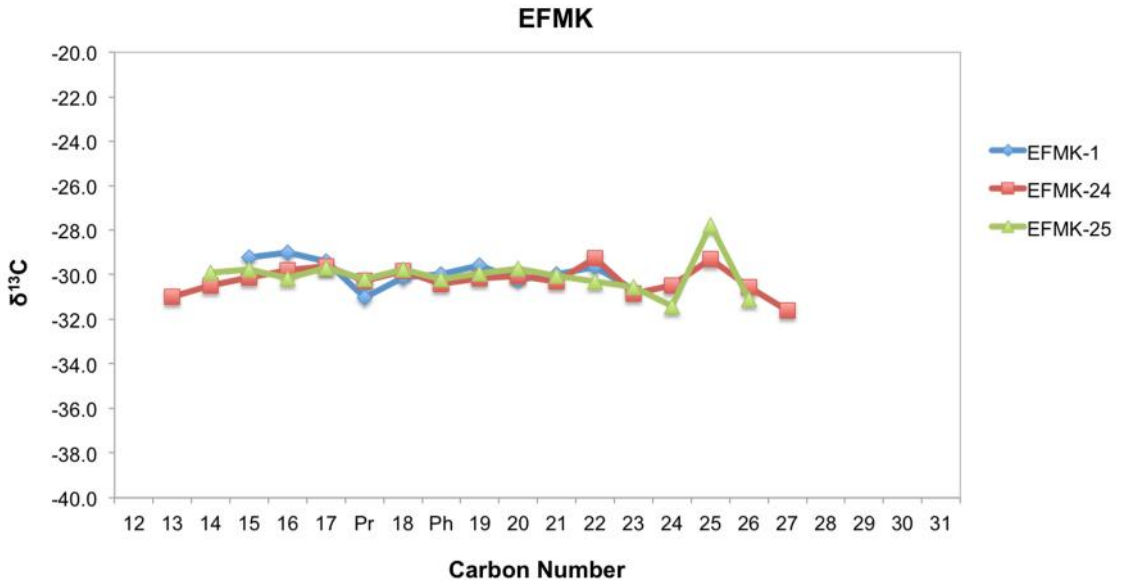


**Figure 42. *n*-Alkane isotope profile from the EFMK extracts (oil window)**

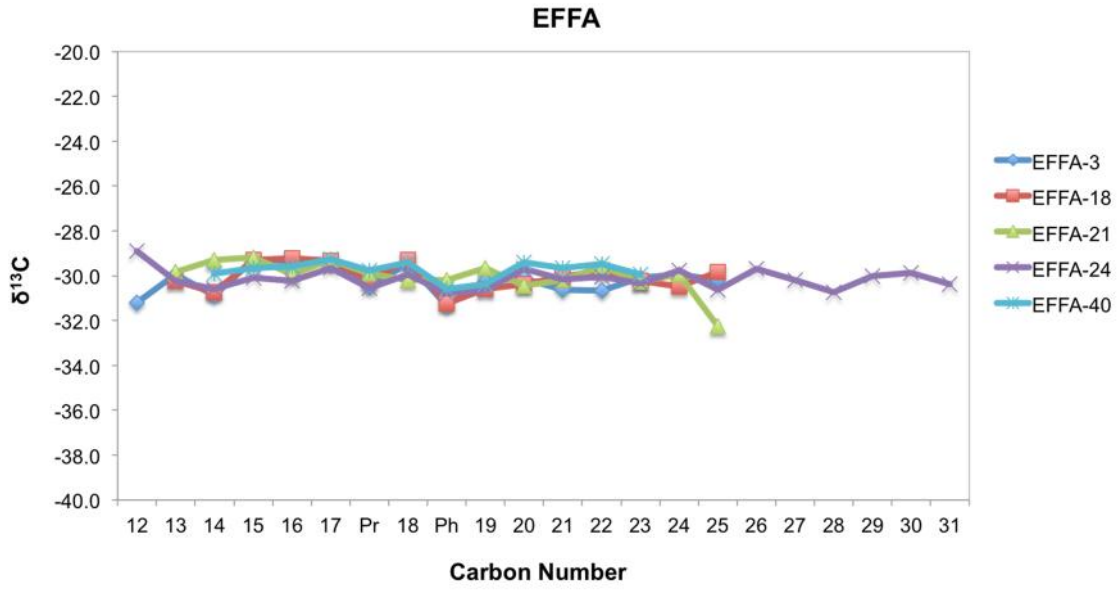


**Figure 43. *n*-Alkane isotope profile from the EFFA extracts (peak oil window)**

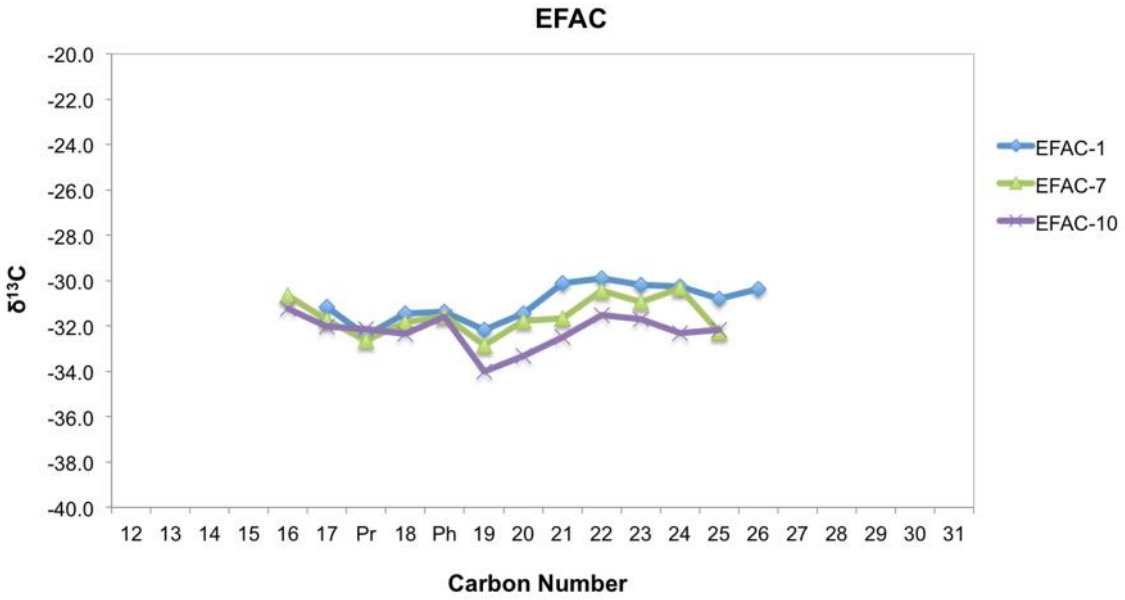


**Figure 44. *n*-Alkane isotope profile from the EFAC extracts (immature)**

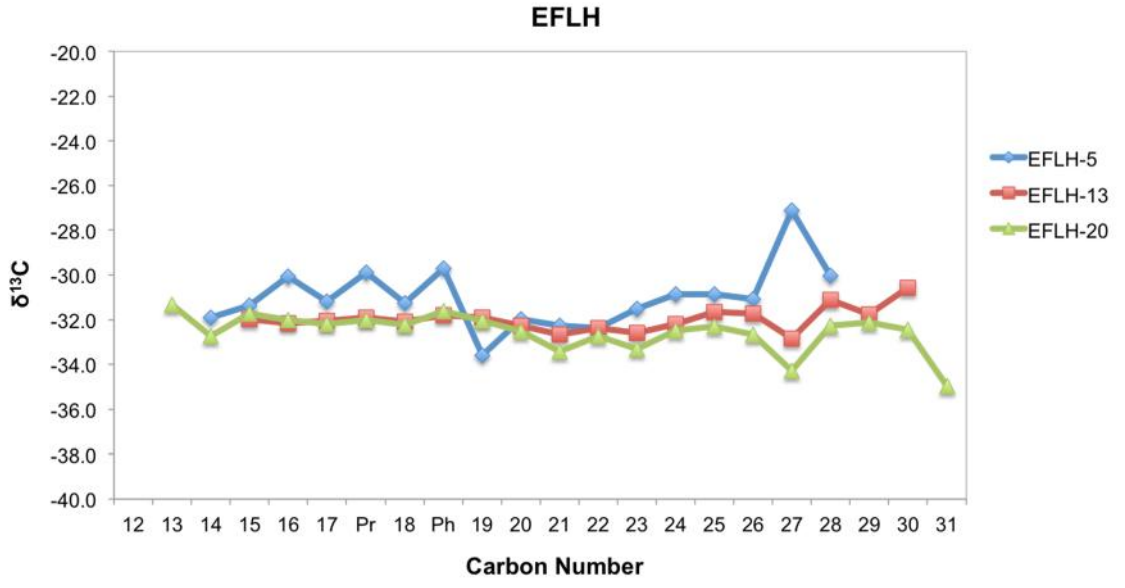


**Figure 45. *n*-Alkane isotope profile from the EFLH extracts (oil window)**

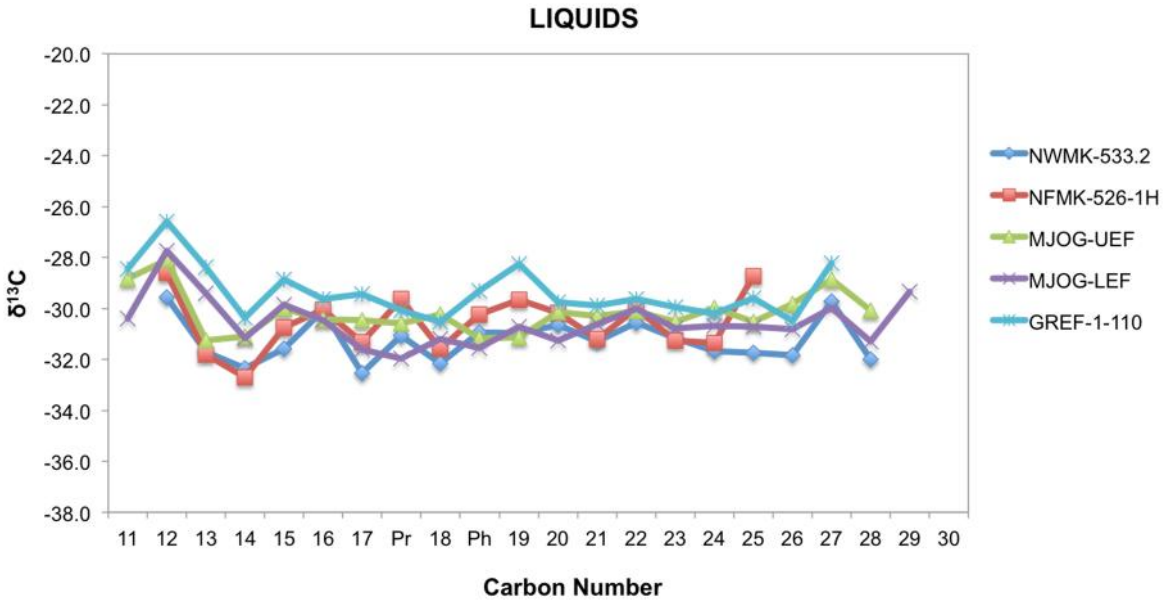


**Figure 46. *n*-Alkane isotope profile from oils and condensate samples (condensate/wet gas window)**

# 3. CHAPTER III

## 3.1 Regional and local organic geochemistry of the Eagle Ford Shale

Geochemical analyses of the Eagle Ford Shale from outcrop and core samples reveal minimal variations in the organic matter type and environmental conditions during deposition of the different Eagle Ford Shale Group members. Detailed geochemical logs of the biomarker ratios calculated for each outcrop, core, and region analyzed in this study are presented in Appendices F through H. Numerical values of these ratios are presented in Appendices I through K. Preliminary analyses of the Eagle Ford Shale samples indicate a similar genetic relationship and generally do not show significant changes in source and depositional settings. Despite the fact that these samples occur in areas separated by important geological structures, they share similar organic geochemical characteristics that point out their common origin. Based on TOC and Rock Eval parameters, the Eagle Ford Shale samples show organic matter quality and good source rock potential. These source rocks are dominated by Type II kerogen and were deposited under marine carbonate anoxic conditions with minimal terrigenous organic matter input, as indicated by low TAR and CPI values. The exception to the latter occurs in the EFLH core (East Texas) where various geochemical parameters, such as high TAR and CPI ratios, Pr/*n*-$C_{17}$ and Ph/*n*-$C_{18}$ values, low $C_{31}$R/30H, and low 30-NorH/30H ratios indicate these sediments were possibly influenced by terrigenous material and deposited under suboxic-oxic conditions. This organic matter source variation in East Texas, with respect to the other locations, may be result of the presence of the deltaic depositional system that influenced sedimentation of the Woodbine-Eagle Ford Shale units. Biomarker parameters reflecting the marine organic

matter source for the Eagle Ford Shale sediments include the steroids distributions, and high steranes/17α-hopanes, $C_{23}$ tricyclic terpane/$C_{30}$ hopane, and $C_{31}$R/30H ratios.

Generally, the Eagle Ford Shale was deposited under anoxic conditions as indicated by their low Pr/Ph values, and the high concentrations of $C_{35}$ homohopanes relative to their $C_{34}$ homologs. The presence of aryl isoprenoids suggests the occurrence of PZA conditions during source rock deposition, although AIR values indicate that these conditions were intermittent, pointing towards periodic shifts of the chemocline. The predominance of even numbered *n*-alkanes and ββ steranes, high pregnane/sterane ratios, and tentative identification of gammacerane reveal that the Eagle Ford Shale probably experienced hypersaline conditions and water-column stratification, particularly in West and East Texas. This observation suggests that these regions were possibly more restricted compared to Central Texas.

The Eagle Ford Shale is immature to marginally mature in the EFLC, EFBC, and EFAC wells (West and Central Texas), as determined by $T_{max}$ values, Ts and Tm ratios, and steranes and hopanes isomer ratios. These same thermal maturity parameters indicate that in the EFMK and EFFA wells (Southwest Texas) the Eagle Ford Shale is in the oil window. Based on these maturity parameters and measured $R_o$, the Eagle Ford Shale is in the main stage of oil generation at the EFLH well (East Texas).

Organic facies variations within the Eagle Ford Shale were determined through correlation of bulk geochemical parameters and biomarker ratios calculated for each member. Tables 15 and 16 show average values of these parameters for each Eagle Ford Shale member for every geographic location considered. Limited data availability for the East Texas EFLH core prevented identification of the different Eagle Ford Shale

members. However, a general characterization of the Lower Eagle Ford Shale based on the same geochemical parameters was carried out on this location. Geochemical data obtained from the EFLC outcrop was the only one considered for the evaluation of vertical variations in West Texas due to the low maturity of these samples compared to the EFMK and EFFA cores.

Across the three regions considered, the Lower Eagle Ford Shale has the highest TOC and HI values. In particular, the Lozier Canyon Member is the most organic-rich (TOC>4.0%; HI>270) followed by the Antonio Creek Member (Table 15). In Central Texas, all the Eagle Ford Shale members show high HI values, suggesting their good source rock potential. Depositional conditions of the different Eagle Ford Shale members seem to have been fairly constant in the West Texas area. Low Pr/Ph ratios suggest the prevalence of anoxic conditions throughout the entire deposition of the Eagle Ford Shale in this area. In addition, variations in Pr/Ph ratios show a positive correlation with AIR. This relationship indicates that variations in PZA occurred during deposition of these units, particularly in the upper interval of the Lozier Canyon Member. Relatively high Pr/Ph ratios and AIR suggest deposition of this member under episodic PZA. This interval contains the greatest amount of organic carbon throughout the analyzed section, indicating the possibility of significant organic matter production during this time. This observation may be supported by a marked increase in phosphorous concentration within the Lozier Canyon Member (at the contact between Donovan et al.'s, 2013 A and B facies; Aris Pramudito, 2014 personal communication), which suggests an increase in nutrient availability that could have promoted production. In Central Texas, Pr/Ph ratios suggest stronger anoxic depositional conditions for the

Lozier Canyon Member compared to the Antonio Creek and Langtry members, whereas deposition of the Lower Eagle Ford Shale in East Texas possibly took place under oxic-suboxic conditions. These observations are supported by the $C_{35}S/C_{34}S$ ratios, which are also consistent with a marine carbonate depositional environment for the Eagle Ford Shale. The presence of pregnanes suggests the establishment of hypersaline conditions during deposition of the Lower Eagle Ford Shale, particularly in the East and West Texas areas, although an enrichment of these biomarkers in the EFMK, EFFA, and EFLH samples might be related to their higher thermal maturity.

Despite the observed variations in depositional conditions, changes in organic matter source were minimal. The $C_{23}$ tricyclic terpane/$C_{30}$ hopane and $C_{24}/C_{23}$ tricyclic terpane ratios suggest that the Lower Eagle Ford Shale Formation was deposited in a marine carbonate environment, whereas the Upper Eagle Ford Shale Formation might have received some terrigenous input. This observation correlates with the diasteranes/(diasteranes+regular) $C_{27}$ steranes ratio, which indicates a progressive increase in siliciclastic contribution during deposition of the Antonio Creek and the Upper Eagle Ford Shale members. This ratio shows a relationship with the facies description of Donovan et al. (2012, 2013), which refers to significant bentonite beds in the Antonio Creek, Scott Ranch, and Langtry members. These minimal variations in organic matter source are further confirmed by isotopic data. Isotopic profiles are consistent with a marine organic input for the Eagle Ford Shale; however, $\delta^{13}C$ values do not show significant differences that could be related to organic facies or depositional environment changes. Furthermore, the isotope data analyzed do not reflect the variations in thermal maturity among the different samples.

Donovan et al., (2012, 2013) developed a sequence stratigraphic framework for the Eagle Ford Shale Group at the Lozier Canyon outcrop (EFLC) and the Fasken "A" #1 well (EFFA). The frameworks at these locations were used to determine possible correlations between organic geochemical parameters and the different stratigraphic sequences proposed by these authors. It was observed that low Pr/Ph, AIR, $C_{24}$ tricyclic terpanes and $C_{31}$R/30H ratios; and high TOC, HI, and $C_{23}$ tricyclic terpanes occurred during the highstand systems tract (HST), whereas the contrary was observed at the transgressive systems tract (TST). However, these interpretations need to be further refined by a high-resolution study in order to determine if these variations are consistent within a sequence stratigraphic context for shale gas systems.

**Table 15. Average of bulk and *n*-alkanes geochemical parameters for the Eagle Ford Shale members across West, Southwest, Central and East Texas (ND = not determined)**

| | WEST TEXAS | | | | CENTRAL TEXAS | | | | EAST TEXAS |
|---|---|---|---|---|---|---|---|---|---|
| **Eagle Ford Formation** | **Lower Eagle Ford Shale** | | **Upper Eagle Ford Shale** | | **Lower Eagle Ford Shale** | | **Upper Eagle Ford Shale** | | **Lower Eagle Ford Shale** |
| **Eagle Ford Shale Member** | **Lozier Canyon** | **Antonio Creek** | **Scott Ranch** | **Langtry** | **Lozier Canyon** | **Antonio Creek** | **Scott Ranch** | **Langtry** | |
| **TOC** | 4.22 | 1.34 | 1.25 | 0.21 | 5.34 | 3.17 | | 3.02 | 4.18 |
| **$T_{max}$** | 524 | 434 | 381 | 109 | 421 | 423 | | 360 | 443 |
| **HI** | 278 | 255 | 106 | 62 | 505 | 412 | | 407 | 270 |
| **OI** | 19 | 51 | 31 | 166 | 32 | 57 | NOT PRESENT | 102 | 8 |
| **Pr/Ph** | 0.33 | 0.28 | 0.39 | | 0.84 | 1.19 | | 1.16 | 1.44 |
| **TAR** | 2.44 | 2.37 | 0.59 | ND | 0.41 | ND | | ND | 0.36 |
| **CPI** | 1.07 | 0.96 | 0.74 | | 0.85 | 0.73 | | 0.74 | 1.07 |

**Table 16. Average biomarker ratios for the Eagle Ford Shale members across West, Southwest, Central and East Texas (ND = not determined)**

| | WEST TEXAS | | | | CENTRAL TEXAS | | | | EAST TEXAS |
|---|---|---|---|---|---|---|---|---|---|
| **Eagle Ford Formation** | **Lower Eagle Ford Shale** | | **Upper Eagle Ford Shale** | | **Lower Eagle Ford Shale** | | **Upper Eagle Ford Shale** | | **Lower Eagle Ford Shale** |
| **Eagle Ford Shale Member** | **Lozier Canyon** | **Antonio Creek** | **Scott Ranch** | **Langtry** | **Lozier Canyon** | **Antonio Creek** | **Scott Ranch** | **Langtry** | |
| **$C_{27}$% reg. steranes** | 39.17 | 37.59 | 42.78 | | 39.13 | 37.56 | | 39.32 | 44.74 |
| **$C_{28}$% reg. steranes** | 28.00 | 30.22 | 24.21 | | 34.74 | 37.72 | | 35.27 | 29.89 |
| **$C_{29}$% reg. steranes** | 32.83 | 32.19 | 33.01 | | 26.13 | 24.72 | | 25.41 | 25.37 |
| **$C_{29}$ 20S/(20S + 20R) steranes** | 0.50 | 0.49 | 0.48 | ND | 0.19 | 0.18 | | 0.12 | 0.47 |
| **$C_{29}$ ββ/(ββ + αα) steranes** | 0.54 | 0.55 | 0.54 | | 0.32 | 0.35 | | 0.30 | 0.57 |
| **Pregnane/Steranes** | 0.64 | 0.73 | 0.61 | | 0.21 | 0.26 | | 0.16 | 1.18 |
| **$C_{27}$ Steranes (Dia/(Dia + Reg)** | 0.15 | 0.22 | 0.30 | | 0.07 | 0.06 | | 0.06 | 0.47 |
| **Sterane Index** | 0.05 | 0.06 | 0.05 | | 0.05 | 0.05 | | 0.06 | 0.07 |
| **Steranes/17α-Hopanes** | 0.49 | 0.63 | 0.60 | | 1.02 | 1.86 | NOT | 2.05 | 0.60 |
| **Tricyclics/17α-Hopanes** | 0.05 | 0.05 | 0.03 | | 0.04 | 0.04 | PRESENT | 0.04 | 0.09 |
| **$C_{24}$ T/$C_{23}$ T** | 0.42 | 0.33 | 0.56 | | 0.55 | 0.46 | | 0.60 | 0.49 |
| **$C_{24}$ Tetra/$C_{30}$ Hopane** | 0.06 | 0.06 | 0.04 | | 0.06 | 0.14 | | 0.05 | 0.06 |
| **$C_{23}$ T/$C_{30}$ Hopane** | 0.54 | 0.50 | 0.21 | | 0.20 | 0.50 | | 0.19 | 0.26 |
| **$C_{31}$ 22S/(22S+22R)** | 0.61 | 0.61 | 0.62 | ND | 0.38 | 0.35 | | 0.43 | 0.58 |
| **Moretane/$C_{30}$ Hopane** | 0.07 | 0.06 | 0.06 | | 0.97 | 0.90 | | 0.98 | 0.12 |
| **Ts/Ts+Tm** | 0.24 | 0.21 | 0.24 | | 0.14 | 0.14 | | 0.14 | 0.57 |
| **$C_{31}$R/$C_{30}$ Hopane** | 0.46 | 0.54 | 0.46 | | 0.52 | 0.81 | | 0.48 | 0.21 |
| **$C_{35}$S/$C_{34}$S** | 1.40 | 1.45 | 1.12 | | 0.86 | 0.92 | | 0.96 | 0.39 |
| **$C_{29}$/$C_{30}$ Hopane** | 0.79 | 0.75 | 0.60 | | 1.04 | 0.89 | | 0.90 | 0.49 |

# 4. CONCLUSIONS

The Eagle Ford Shale Group is a source rock with excellent potential as demonstrated by TOC and Rock Eval parameters. It is dominated by Type II kerogen indicating a marine organic matter input. Biomarker distributions of regular steranes and monoaromatic steroids (MAS), high steranes/17α-hopanes, $C_{23}$ tricyclic terpane/$C_{30}$ hopane, $C_{24}/C_{23}$ tricyclic terpane, and $C_{31}R/C_{30}$ hopane ratios are consistent with a marine carbonate depositional environment for the Eagle Ford Shale sediments. However, high terrigenous-to-aquatic (TAR) and carbon preference index (CPI) ratios, low $C_{31}R$/30H, and low 30-NorH/30H ratios suggest that in East Texas, the Eagle Ford Shale was possibly sourced by terrigenous material, reflecting the influence of the Harris Delta during deposition of these sediments. Low Pr/Ph values, and high $C_{35}S/C_{34}S$ homohopanes suggest that these source rocks were deposited under anoxic conditions. The presence of aryl isoprenoids and the aryl isoprenoids ratio (AIR) suggest the occurrence of intermittent photic zone anoxia (PZA). The predominance of even numbered *n*-alkanes and ββ steranes, high pregnanes/steranes ratios, and the tentative identification of gammacerane suggest the establishment of hypersaline conditions during Eagle Ford Shale deposition particularly in West and East Texas.

Thermal maturity parameters such as $T_{max}$, Ts and Tm ratios, and steranes and hopanes isomer ratios indicate that in West and Central Texas the Eagle Ford Shale is immature to marginally mature. These parameters show a progressive increase in thermal maturity towards the southeast, from the Lozier Canyon site in Terrell County (early oil window) to the Fasken “A” #1 well in Webb County (dry gas window). Based

on measured $R_o$ values it was determined that in East Texas, the Eagle Ford Shale is in the main stage of oil generation.

Analysis of geochemical logs suggests a narrow range of vertical variation within the Eagle Ford Shale Group. The Lower Eagle Ford Shale Formation has the highest TOC and HI values and in particular, the Lozier Canyon Member is the most organic-rich. Low Pr/Ph ratios suggest the prevalence of stronger anoxic conditions during deposition of the Lower Eagle Ford Shale compared to the Upper Eagle Ford Shale Formation, where the latter may have received an additional siliciclastic and terrigenous organic matter input. Isotope data also points to a marine organic input for the Eagle Ford Shale, but $\delta^{13}C$ values do not show significant differences that could be related to organic facies, depositional environment, or thermal maturity changes.

Correlation of geochemical data with an already established sequence stratigraphic framework for the Eagle Ford Shale Group in West and Central Texas allowed observation of organic geochemical trends and stratigraphic sequences. Low Pr/Ph, AIR, $C_{24}$ tricyclic terpanes and $C_{31}R/30H$ ratios; and high TOC, HI, and $C_{23}$ tricyclic terpanes intervals were associated with the highstand systems tract (HST), whereas opposite trends were observed within the transgressive systems tract (TST). These observations result in a general interpretation and it is recommended that a high-resolution organic geochemistry study be performed preferably at the same locations. Higher sampling density from fresh outcrops and/or cores may help enhance lower-order variations in biomarker concentrations, geochemical ratios, and isotopic compositions that could improve the use of organic geochemistry in sequence stratigraphic studies.

# 5. REFERENCES


Adams, R.L. and Carr, J.P. (2010) Regional depositional systems of the Woodbine, Eagle Ford, and Tuscaloosa of the U.S. Gulf Coast. *GCAGS Transactions* **60,** 3-27.

American Society for Testing and Materials (2011) Standard test method for microscopical determination of the reflectance of vitrinite dispersed in sedimentary rocks: West Conshohocken, PA, ASTM International, Annual book of ASTM standards: Petroleum products, lubricants, and fossil fuels; Gaseous fuels; coal and coke, Sec. 5, v. 5.06, D7708-11, 823-830.

Aquino Neto, F.R., Trendel, J.M., Restle, A., Connan, J. and Albrecht, P.A. (1981) Occurrence and formation of tricyclic and tetracyclic terpanes in sediments and petroleums. In Bjorøy M. et al. (1983) *Advances in organic geochemistry 1981*, 659-667.

Arthur, M.A., Dean, W.E. and Pratt, L.M. (1998) Geochemical and climatic effects of increased marine organic carbon burial at the Cenomanian/Turonian boundary. *Nature* **335,** 714-717.

Arthur, M.A. and Sageman, B.B. (2004) Sea-level control on source-rock development: Perspectived from the Holocene Black Sea, the Mid-Cretaceous Western Interior Basin of North America, and the Late Devonian Appalachian Basin. *SEPM Special Publication* **82,** 35-59.

Barclay, R., McElwain, J. and Sageman, B. (2006) Ecological change across the Cenomanian-Turonian boundary. *Geological Society of America Abstracts with Programs* **38**(7), pp.339.

Bechtel, A., Hamor-Vido, M., Sachsenhofer, R.F., Reischenbacher, D., Gratzer, R. and Puttmann, W. (2007) The middle Eocene Markushegy sub-bituminous coal (Hungary): paleoenvironmental implications from petrographic and geochemical studies. *International Journal of Coal Geology* **72,** 33-52.

Blakey, R. (2011) Colorado Plateau Geosystems, Inc., http://cpgeosystems.com/index.html, accessed March 3rd, 2014.

Blumer, M., Mullin, M.M., and Thomas, D.W. (1963) Pristane in zooplankton. *Science* **140,** 974.

Blumer, M. and Thomas, D.W. (1965) "Zamene", isomeric $C_{19}$ monoolefins from marine zooplankton, fishes, and mammals. *Science* **148,** 370-371.

Bray, E.E. and Evans, E.D. (1961) Distribution of n-paraffins as a clue to recognition of source beds. Geochimica et Cosmochimica Acta 22, 2-15.

Brown, T.C. and Kenig, F. (2004) Water column structure during deposition of Middle Devonian-Lower Mississippian black and green/gray shales of the Illinois and Michigan Basins: a biomarker approach. *Palaeogeography, Palaeoclimatology, Palaeoecology* **215,** 59-85.

Clark, J.P. and Philp, R.P. (1989) Geochemical characterization of evaporite and carbonate depositional environments and correlation of associated crude oils in the Black Creek Basin, Alberta. *Canadian Geologists Bulletin* **37,** 401-416.

Clayton, J.L. and King, J.D. (1987) Effects of weathering on biological marker and aromatic hydrocarbon composition of organic matter in Phosphoria Shale outcrop. *Geochimica et Cosmochimica Acta* **51,** 2153-2157.

Clayton, C.J. (1991) Effect of maturity on carbon isotope ratios of oils and condensates. *Organic Geochemistry* **17,** 887-899.

Corbett, M.J., Lowery, C., Miceli Romero, A., Watkins, D.K., Leckie, R.M., Li, W., Pramudito, A., Donovan, A., Staerker, S. (2011) A bio-chemostratigraphic framework of Oceanic Anoxic Event 2 at Lozier Canyon, TX: correlations to the Western Interior Seaway and comparison to sequence stratigraphic surfaces. *GSA Annual Meeting Abstracts with Programs* **43**(5), p. 611.

Cornford, C., Gardner, P. and Burgess, C. (1998) Geochemical truths in large data sets. I: Geochemical screening data. *Organic Geochemistry* **29**(1-3), 519-530.

Dean, W.E. and Arthur, M.A. (1998a) Cretaceous Western Interior Seaway drilling project: An overview. In Dean, W.E. and Arthur, M.A. (eds.) Stratigraphy and Paleoenvironments of the Cretaceous Western Interior Seaway, USA. *SEPM Concepts in Sedimentology and Paleontology* **6,** 1-10.

Dean, W.E. and Arthur, M.A. (1998b) Geochemical expressions of cyclicity in Cretaceous pelagic limestone sequences: Niobrara Formation, Western Interior Seaway. In Dean, W.E. and Arthur, M.A. (eds.) Stratigraphy and Paleoenvironments of the Cretaceous Western Interior Seaway, USA. SEPM *Concepts in Sedimentology and Paleontology* **6,** 227-255.

Didyk, B.M., Simoneit, B.R.T., Brassell, S.C., Eglinton, G. (1978) Organic geochemical indicators of palaeoenvironmental conditions of sedimentation. *Nature* **272,** 216-222.

Donovan, A.D. and Staerker, T.S. (2010) Sequence stratigraphy of the Eagle Ford (Boquillas) Formation in the subsurface of South Texas and outcrops of West Texas. *GCAGS Transactions* **60,** 861-899.

Donovan, A.D., Staerker, T.S., Pramudito, A., Li, W., Corbett, M.J., Lowery, C.M., Miceli Romero, A. and Gardner, R.D. (2012) The Eagle Ford outcrops of West Texas: A laboratory for understanding heterogeneities within unconventional mudstone reservoirs. *GCAGS Journal* **1,** 162-185.

Donovan, A.D., Staerker, T.S., Gardner, R.D., Pramudito, A., Pope, M., Wehner, M., Corbett, M.J., Miceli Romero, A., Lowery, C.M., and Xu, C. (2013a) *The Eagle Ford outcrops of West Texas: A laboratory for understanding heterogeneities, as well as sequence stratigraphic controls, on unconventional mudstone reservoirs.* AAPG/BP Field Trip Handbook, pp.53.

Donovan, A.D., Staerker, S.T., Pramudito, A., Gardner, R., Pope, M.C., Corbett, M., Lowery, C. and Miceli Romero, A. (2013b) *A 3-D outcrop perspective of an unconventional carbonate mudstone reservoir*. Unconventional Resources Technology Conference, URTeC Control ID #158094. Denver, Colorado, 12-14 August 2013.

Donovan, A.D., Gardner, R.D., Staerker, T.S., Pramudito, A., Corbett, M.J., Wehner, M., Xu, G. and Pope, M. (2014) *Field guide to the Eagle Ford Group: West Texas.* Spring 2014 SEPM/AAPG Unconventional Reservoirs Field Seminar.

Dowling, L.M., Boreham, C.J., Hope, J.M., Murray, A.P. and Summons, R.E. (1995) Carbon isotopic composition of hydrocarbons in ocean-transported bitumens from the coastline of Australia. *Organic Geochemistry* **23**(8), 729-737.

Durham, L.S. (2013) Finding production trends, parameters Eagle Ford data base provides a sweet spot. *AAPG Explorer* **34**(3), 16, 18.

Dzou, L.I.P., Noble, R.A. and Senftle, J.T. (1995) Maturation effects on absolute biomarker concentration in a suite of coals and associated vitrinite concentrates. *Organic Geochemistry* **23**(7), 681-697.

Edman, J.D. (2012) *How local variations in thermal maturity affect shale oil economics and producibility.* http://www.worldoil.com/March-2012-How-local-variations-in-thermal-maturity-affect-shale-oil-economics-and-producibility.html, accessed March 12th, 2014.

Edman, J. D., and J. K. Pitman (2010) Geochemistry of Eagle Ford Group source rocks and oils from the First Shot Field area, Texas. *GCAGS Transactions* **60,** 217–234.

Energy Information Administration (EIA) (2010) Shale gas plays maps. http://www.eia.doe.gov/oil_gas/rpd/shale_gas.pdf, accessed October 10th, 2013.

Fairbanks, M.D. (2012) *High resolution stratigraphy and facies architecture of the Upper Cretaceous (Cenomanian – Turonian) Eagle Ford Group, Central Texas.* Master of Science Thesis, University of Texas at Austin, pp.132.

Fortwengler, M., Sageman, B., McElwain, J. and Kenig, F. (2003) Integrated paleobiological and geochemical assessment of carbon cycle perturbations and climate change during Cenomanian-Turonian OAE II, North America. *Geological Society of America Abstracts with Programs* **35**(6), pp.289.

Gardner, R.D., Pope, M.C., Wehner, M.P. and Donovan, A.D. (2013) Comparative stratigraphy of the Eagle Ford Group strata in Lozier Canyon and Antonio

Creek, Terrell County, Texas. *Gulf Coast Association of Geological Societies Journal* **2,** 42-52.

Goossens, H., de Leeuw, J. W., Schenck, P. A. and Brassell, S. C. (1984) Tocopherols as likely precursors of pristane in ancient sediments and crude oils. *Nature* **312,** 440-442.

Harbor, R.L. (2011) *Facies characterization and stratigraphic architecture of organic-rich mudrocks, Upper Cretaceous Eagle Ford Formation, South Texas*. Master of Science Thesis, University of Texas at Austin, pp.195.

Hentz, T.F. and Ruppel, S.C. (2010) Regional lithostratigraphy of the Eagle Ford Shale: Maverick Basin to East Texas Basin. *Gulf Coast Association of Geological Societies Transactions* **60,** 325-337.

Hill, R.T. (1887) The Texas section of the American Cretaceous. *American Journal of Science* **34,** 287-309.

Huang, W.Y. and Meinschein, W.G. (1979) Sterols as ecological indicators. *Geochimica et Cosmochimica Acta* **43,** 739-745.

Hunt, J.H. (1979) *Petroleum geochemistry and geology*. p.617. W.H. Freeman and Company. USA.

Isaksen, G.H. and Bohacs, K.M. (1995) Geological controls on source rock geochemistry through relative sea level; Triassic, Barents Sea. In Katz, B.J. (ed.) *Petroleum Source Rocks.* Springer-Verlag, New York, pp. 25-50.

Jarvie D. M., Hill R. J., Ruble T. E. and Pollastro R. M. (2007) Unconventional shale-gas systems: The Mississippian Barnett Shale of north-central Texas as one

model for thermogenic shale-gas assessment. *American Association of Petroleum Geologists Bulletin* **91**(4), 475-499.

Jennings, D.S. and Antia, J. (2013) Petrographic characterization of the Eagle Ford Shale, South Texas: Mineralogy, common constituents, and distribution of nanometer-scale pore types. In Camp, W., Diaz, E., and Wawak, B. (eds.) Electron microscopy of shale hydrocarbon reservoirs. *AAPG Memoir* **102,** p. 101-113.

Larter, S.R., Solli, H., Douglas, A.G., de Lange, F., and de Leeuw, J.W. (1979) Occurrence and significance of prist-1-ene in kerogene pyrolysates. *Nature* **279,** 405-407.

Leckie, R.M., Yuretich, R.F., West, O.O, Finkelstein, D. and Schmidt, M. (1998) Paleoceanography of the spithwestern Western Interior Sea during the time of the Cenomanian-Turonian boundary (Late Cretaceous). Dean, W.E. and Arthur, M.A. (eds.) Stratigraphy and Paleoenvironments of the Cretaceous Western Interior Seaway, USA. SEPM *Concepts in Sedimentology and Paleontology* **6,** 101-126.

Lewan, M.D., Little, J., Formolo, M.J.; Anonymous (2012) Expulsion efficiencies and timing of oil generation from different source-rock facies in the Eagle Ford Group and Boquillas Formation as determined by hydrous pyrolysis. *AAPG Search and Discovery Article #90142*, accessed on February 13th, 2014.

Liro, L.M., Dawson, W.C., Katz, B.J. and Robison, V.D. (1994) Sequence stratigraphic elements and geochemical variability within a “condensed section”: Eagle Ford

Group, East-Central Texas. *Gulf Coast Association of Geological Societies Transactions* **44,** 393-402.

Mackenzie, A.S. (1984) Application of biological markers in petroleum geochemistry. In Brooks, J. and Welte, D.H. (eds.) *Advances in Petroleum Geochemistry*, Volume 1. Academic Press, London, pp.115-214.

Mello, M.R., Telnaes, N., Gaglianone, P.C., Chicarelli, M.I., Brassell, S.C., and Maxwell, J.R. (1988) Organic geochemical characterisation of depositional paleoenvironments of source rocks and oils in Brazilian marginal basins. *Organic Geochemistry* **13,** 31-45.

Miceli Romero, A. and Philp, R.P. (2012) Organic geochemistry of the Woodford Shale, southeasten Oklahoma: How variable can shales be? *AAPG Bulletin* **96**(3), 493-517.

Moldowan, J.M., Seifert, W.K. and Gallegos, E.J. (1985) Relationship between petroleum composition and depositional environment of petroleum source rocks. *AAPG Bulletin* **69**(8), 1255-1268.

Moldowan, J.M., Sundararaman, P. and Schoell, M. (1986) Sensitivity of biomarker properties to depositional environment and/or source input in the Lower Toarcian of S.W. Germany. *Organic Geochemistry* **10,** 915-926.

Moldowan, J.M., Lee, C.Y., Sundararaman, P., Salvatori, T., Alajbeg, A., Gjukić, B., Demaison, G.J., Slougui, N. and Watt, D. (1992) Source correlation and maturity assessment of selected oils and rocks from the Central Adriatic Basin (Italy and Yugoslavia). In Moldowan, J.M., Albrecht, P. and Philp R.P. (eds.) *Biological Markers in Sediments and Petroleum*, 370-401.

Moldowan, J.M., Peters, K.E., Carlson, R.M.K., Schoell, M., and Abu-Ali, M.A. (1994) Diverse applications of petroleum biomarker maturity parameters. *The Arabian Journal for Science and Engineering* **19** (2B), 273-298.

Murray, A.P., Summons, R.E., Boreham, C.J. and Dowling, L.M. (1994) Biomarker and *n*-alkane isotope profiles for Tertiary oils: relationship to source rock depositional setting. *Organic Geochemistry* **22**(3-5), 521-542.

Ourisson, G., Albrecht, P. and Rohmer, M. (1982) Predictive microbial biochemistry – from molecular fossils to prokaryotic membranes. *Trends in biochemical sciences* **7**(7), 236-239.

Palacas, J.G., Anders, D.E. and King, J.D. (1984) South Florida Basin – a prime example of carbonate source rocks in petroleum. In Palacas, J.G. (ed.) Petroleum geochemistry and source rock potential of carbonate rocks. *AAPG Special Publication* **18,** 71-96.

Peters, K.E. (1986) Guidelines for evaluating petroleum source rock using programmed pyrolysis. *American Association of Petroleum Geologists Bulletin* **70**(3), 318-329.

Peters, K.E., Moldowan, J.M. and Sundararaman, P. (1990) Effects of hydrous pyrolysis on biomarker thermal maturity parameters: Monterey phosphatic and siliceous members. *Organic Geochemistry* **15,** 249-265.

Peters, K.E. and Moldowan, J.M. (1991) Effects of source, thermal maturity, and biodegradation on the distribution and isomerization of homohopanes in petroleum. *Organic Geochemistry* **17**(1), 47-61.

Peters, K.E. and Cassa, M.R. (1994) Applied source rock geochemistry. In Magoon L. B. and Dow W. G. (eds.) The petroleum system – from source to trap. *AAPG Memoir* **60,** 93-120.

Peters, K.E., Walters, C.C., and Moldowan, J.M. (2005) *The biomarker guide, Volumes 1 and 2: biomarkers and isotopes in petroleum exploration and earth history.* Second Edition, p. 1155. Cambridge University Press. USA.

Philp, R.P., Chen, J.H., Galvez-Sinibaldi, A., Wang, H.D., and Allen, J.D. (1992) Effects of weathering and maturity on the geochemical characteristics of the Woodford Shale. In Johnson, K.S. and Cardott. B.J. (eds.) Source rocks in the Southern Midcontinent. *Oklahoma Geological Survey Circular* **93,** 106-121.

Philp, R.P. and Gilbert, T.D. (1986) Biomarker distributions in oils and predominantly derived from terrigenous source material. In Leythaeuser, D. and Rullkötter, J. (eds.) *Advances in Organic Geochemistry,* 73-84.

Rangel, A., Parra, P. and Niño, C. (2000) The La Luna Formation: chemostratigraphy and organic facies in the Middle Magdalena Basin. *Organic Geochemistry* **31,** 1267-1284.

Radke, M. and Welte, D.H. (1981) The Methylphenanthrene Index (MPI): A maturity parameter based on aromatic hydrocarbons. *Advances in Organic Geochemistry*, 504-512.

Radke, M., Leythaeuser, D. and Teichmüller, M. (1984) Relationship between rank and composition of aromatic hydrocarbons for coal of different origins. *Organic Geochemistry* **6,** 423-430.

Radke, M., Welte, D.H. and Willsch, H. (1986) Maturity parameters based on aromatic hydrocarbons: influence of the organic matter type. *Organic Geochemistry* **10,** 51-63.

Railroad Commission of Tevas (RRC) (2013) Eagle Ford Information. http://www.rrc.state.tx.us/eagleford/, accessed November 14th, 2013.

Robinson, L.N. and Kirschbaum, M.A. (1995) Paleogeography of the Late Cretaceous of the Western Interior of middle North America – coal distribution and sediment accumulation. *USGS Professional Paper* **1561,** 1-115.

Robison, C.R. (1997) Hydrocarbon source rock variability within the Austin Chalk and Eagle Ford Shale (Upper Cretaceous), East Texas, USA. *International Journal of Coal Geology* **34,** 287-305.

Rowland, S.J. (1990) Production of acyclic isoprenoids hydrocarbons by laboratory maturation of methanogenic bacteria. *Organic Geochemistry* **15,** 9-16.

Rullkötter, J. and Marzi, R. (1988) Natural and artificial maturation of biological markers in a Toarcian shale from northern Germany. *Organic Geochemistry* **13,** 639-645.

Sageman, B., Barclay, R. and McElwain, J. (2008) Recent advances in the study of Cretaceous OAEs. In 33rd International Geological Congress, Oslo, Norway.

Schwark, L. and Frimmel, A. (2004) Chemostratigraphy of the Posidonia Black Shale, SW Germany II. Assessment of extent and persistence of photic-zone anoxia using aryl isoprenoids distributions. *Chemical Geology* **206,** 231-248.

Scotese, C. R. (2001) Atlas of Earth History, Volume 1, Paleogeography. PALEOMAP Project, Arlington, Texas, 52 pp. http://www.scotese.com/earth.htm. Accessed on December 12th, 2013.

Scott, R.W., Anderson, J., Shang, F. and Tapp, L. (2010) Albian-Turonian flooding processes, timing and rates in the U.S. Western Interior Cretaceous Seaway. *Geological Society of America Abstracts with Programs* **42**(5), pp.547.

Seifert, W.K. and Moldowan, J.M. (1986) Use of biological markers in petroleum exploration. In Johns, R.B. (ed.) *Methods in geochemistry and geophysics 24*, pp. 261-290.

Shanmugam, G. (1985) Significance of coniferous rain forests and related organic matter in generating commercial quantities of oil, Gippsland Basin, Australia. *AAPG Bulletin* **69**(8), 1241-1254.

Sinninghe Damsté, J.S., Kenig, F., Koopmans, M.P., Koster, J.; Schouten, S., Hayes, J.M. and de Leeuw, J.W. (1995) Evidence for gammacerane as an indicator of water column stratification. *Geochimica et Cosmochimica Acta* **59**(9), 1895-1900.

Sinninghe Damsté J.S., Mueller, A., van Bentum, E., Reichart, G.J. and Schouten, S. (2009) Oceanic anoxia, organic carbon burial and climate change during OAE-2. *Goldschmit Conference Abstracts 2009*, pp. A1230.

Slatt, R.M., O'Brien, N.R., Miceli Romero, A., and Rodriguez, H. (2012) Eagle Ford Condensed Section and Its Oil and Gas Storage and Flow Potential. In AAPG Annual Convention and Exhibition, Long Beach, CA. *Search and Discovery Article # 90142;* accessed February 10, 2014.

Surles, M.A. (1987) Stratigraphy of the Eagle Ford Group (Upper Cretaceous) and its source-rock potential in the East Texas Basin. *Baylor Geological Studies Bulletin* **45,** pp. 57.

ten Haven, H.L., de Leeuw, J.W., and Schenck, P.A. (1985) Organic geochemical studies of a Messinian evaporitic basin, northern Apennines (Italy) I: Hydrocarbon biological markers for a hypersaline environment. *Geochimica et Cosmochimica Acta* **49,** 2181-2191.

ten Haven, H.L., de Leeuw, J.W., Rullkötter, J., and Sinninghe Damsté, J.S. (1987) Restricted utility of the pristane/phytane ratio as a paleoenvironmental indicator. *Nature* **330,** 641-643.

ten Haven, H.L., de Leeuw, J.W., Sinninghe Damsté, J.S., Schenck, P.A., Palmer, S.E., and Zumberge, J.E. (1988) Application of biological markers in the recognition of palaeohypersaline environments. *Geological Society of London Special Publications* **40,** 123-130.

ten Haven, H.L., Rohmer, M., Rullkötter, J. and Bisseret, P. (1989) Tetrahymanol, the most likely precursor of gammacerane, occurs ubiquitously in marine sediments. *Geochimica et Cosmochimica Acta* **53,** 3073-3079.

Tissot, B., Durand, B., Espitalié, J. and Combaz, A. (1974) Influence of nature and diagenesis of organic matter in formation of petroleum. *American Association of Petroleum Geologists Bulletin* **58**(3), 499-506.

Tissot, B.P. and Welte, D.H. (1984) *Petroleum formation and occurrence.* Springer-Verlag Berlin Heidelberg, Germany, pp. 699.

Volkman, J.K. (1986) A review of sterol markers for marine and terrigenous organic matter. *Organic Geochemistry* **9**(2), 83-99.

Volkman, J.K., Banks, M.R., Denwer, K. and Aquino Neto, F.R. (1989) Biomarker composition and depositional setting of *Tasmanite* oil shale from northern Tasmania, Australia. 14th International Meeting of Organic Geochemistry, Paris, France.

Wang, H.D. (1993) *A geochemical study of potential source rocks and crude oils in the Anadarko Basin, Oklahoma.* PhD. Dissertation, University of Oklahoma, pp.326.

Waples, D.W. (1985) *Geochemistry in petroleum exploration.* International Human Resources Development Corporation. USA.

Waples, D.W. and Machihara T. (1991) Biomarkers for geologists – A practical guide to the application of steranes and triterpanes in petroleum geology. *AAPG Methods in Exploration* **9,** pp. 85.

West, N., Alexander, R. and Kagi, R. (1990) The use of silicalite for rapid isolation of branched and cyclic alkane fractions of petroleum. *Organic Geochemistry* **15** (5), 499-501.

Wingert, W.S. (1992) GCMS analysis of diamondoid hydrocarbons in Smackover petroleums. *Fuel* **71,** 37-43.

Zhang, S., Huang, H., Su, J., Zhu, G., Wang, X. and Larter, S. (2014) Geochemistry of Paleozoic marine oils from the Tarim Basin, NW China. Part 4: Paleobiodegradation and oil charge mixing. *Organic Geochemistry* **67,** 41-57.

Zumberge, J.E. (1987) Prediction of source rocks characteristics based on terpane biomarkers in crude oils: a multivariate statistical approach. *Geochimica et Cosmochimica Acta* **51,** 1625-1637.

# 6. APPENDIX

## A. Abbreviations and formulas used for calculation of geochemical biomarker ratios

*n-Alkanes*

**Carbon Preference Index (CPI)**

$$CPI = \frac{1}{2}\left[\frac{C_{25}+C_{27}+C_{29}+C_{31}+C_{33}}{C_{26}+C_{28}+C_{30}+C_{32}+C_{34}} + \frac{C_{25}+C_{27}+C_{29}+C_{31}+C_{33}}{C_{24}+C_{26}+C_{28}+C_{30}+C_{32}}\right]$$

**Terrigenous/Aquatic Ratio (TAR):**

$$TAR = \left[\frac{C_{27}+C_{29}+C_{31}}{C_{15}+C_{17}+C_{19}}\right]$$

**Long- versus Short-chain *n*-alkanes:**

$$\text{long-/short-chain n-alkanes} = \frac{\sum(C_{21}-C_{31})}{\sum(C_{15}-C_{21})}$$

*Steranes*

**$C_{27}$%, $C_{28}$%, $C_{29}$%** = $C_{27}$, $C_{28}$, $C_{29}$ [14α(H),17α(H)- + 14β (H),17β (H)-Cholestane (20S+ 20R)]

**$C_{29}$ 20S/(20S + 20R)** = $C_{29}$ [14α(H),17α(H)-Cholestane (20S)]/[14α(H),17α(H)-Cholestane (20S+20R)]

**$C_{29}$ ββ/(ββ + αα)** = $C_{29}$ [14β(H),17β(H)-Cholestane (20S+20R)]/[14β(H),17β(H)- + 14α(H),17α(H)-Cholestane (20S+20R)]

**Preg/Ster** = $C_{21}$ 14β(H),17β(H)-Pregnane/$C_{27}$ 14α(H),17α(H)-Cholestane (20R)

**$C_{27}$ Dia/$C_{27}$ Sterane =** [$C_{27}$ 13β(H),17α(H)-Diacholestane (20S+20R)]/[$C_{27}$ 14α(H),17α(H)- + 14β(H),17β(H)-Cholestane (20S+20R)]

**$C_{27}$ Dia/(Dia+Reg) =** [$C_{27}$ 13β(H),17α(H)- + 13α(H),17β(H)-Diacholestane (20S+20R)]/ [$C_{27}$ 13β(H),17α(H)- + 13α(H),17β(H)-Diacholestane (20S+20R) + $C_{27}$ 14α(H),17α(H)- + 14β(H),17β(H)-Cholestane (20S+20R)]

**Sterane Index =** $C_{30}$/($C_{27}$-$C_{30}$) = [$C_{30}$ 14α(H),17α(H)- + 14β(H),17β(H)-Cholestane (20S+20R)]/ $C_{27}$, $C_{28}$, $C_{29}$, $C_{30}$ [14α(H),17α(H)- + 14β(H),17β(H)-Cholestane (20S+20R)]

*Hopanes*

**Sterane/17α-Hopanes =** [$C_{27}$, $C_{28}$, $C_{29}$, $C_{30}$ 14α(H),17α(H)- + 14β(H),17β(H)-Cholestane (20S+20R)]/[$C_{29}$ 17α(H),21β(H)-30-Norhopane + $C_{30}$ 17α(H),21β(H)-Hopane + $C_{31}$+$C_{32}$+$C_{33}$ 17α(H),21β(H)-Homohopanes (22S+22R)]

**TR/17α-H** = $C_{28}$ + $C_{29}$ Tricyclic terpanes (20S+20R)/17α-Hopanes

**C22/C21TR =** $C_{22}$/$C_{21}$ Tricyclic terpanes

**C24/C23TR =** $C_{24}$/$C_{23}$ Tricyclic terpanes

**C26/C25TR =** $C_{26}$/$C_{25}$ Tricyclic terpanes

**C23TR/30H =** $C_{23}$ Tricyclic terpanes/$C_{30}$ 17α(H),21β(H)-Hopane

**C24TT/30H =** $C_{24}$ Tetracyclic terpane/$C_{30}$ 17α(H),21β(H)-Hopane

**30-NorH/30H =** $C_{29}$ 17α(H),21β(H)-30-Norhopane/$C_{30}$ 17α(H),21β(H)-Hopane

**Mor/30H =** $C_{30}$ 17β(H),21α(H)-Moretane/$C_{30}$ 17α(H),21β(H)-Hopane

**31R/30H =** $C_{31}$ 17α(H),21β(H)-Homohopane (22R)/$C_{30}$ 17α(H),21β(H)-Hopane

**35S/34S =** $C_{35}$ 17α(H),21β(H)-Pentakishomohopane (22S)/$C_{34}$ 17α(H),21β(H)-Tetrakishomohopane (22S)

**HH Index =** $C_{35}/(C_{31} - C_{35})$ = $C_{35}$ 17α(H),21β(H)-Pentakishomohopane (22S+22R)/[$C_{31}$+$C_{32}$+$C_{33}$+$C_{34}$+$C_{35}$ 17α(H),21β(H)-Homohopanes (22S+22R)]

**C31 22S/22S+22R =** $C_{31}$ [17α(H),21β(H)-Homohopanes (22S)/17α(H),21β(H)-Homohopanes (22S+22R)]

*Aryl Isoprenoids*

**Aryl Isoprenoid ratio (AIR):**

AIR = ($C_{13}$-$C_{17}$)/($C_{18}$-$C_{22}$) 2,3,6-trimethyl substituted aryl isoprenoids

*Aromatics*

**MPI-1:**

$$MPI\ 1 = 1.5 \times \frac{[2 - MP + 3 - MP]}{[P + 1 - MP + 9 - MP]}$$

**Calculated vitrinite reflectance:**

For 0.65 to 1.35%$R_o$: $R_c$ = 0.60 MPI-1 + 0.40

For 1.35 to 2.00%$R_o$: $R_c$ = -0.60 MPI-1 + 2.30

**MPI-2:**

$$MPI\ 2 = 3 \times \frac{[2 - MP]}{P + 1 - MP + 9 - MP}$$

**MA(I):**

$$MA(I) = \sum C_{27} - C_{29}\ MAS$$

**MA(II):**

$$MA\ (II) = \sum C_{21} - C_{22}\ MAS$$

**TA(I):**

$$TA(I) = \sum C_{26} - C_{28}\ (20S + 20R)\ TAS$$

**TA(II):**

$$TA(II) = \sum C_{20} - C_{21}\ TAS$$

**C26TA 20S/20S+20R =** $C_{26}$ Cholestane 20S/20S+20R (Triaromatic steroids)

**TA28 =** $C_{28}$ Stigmastane (20S+20R) (Triaromatic steroids)

**MA29 =** $C_{29}$ [5α- + 5β-Stigmastane (20S+20R)]

**C27R/C28R TAS =** $C_{27}$ Ergostane (20R)/$C_{28}$ Stigmastane (20R)

**C26S/C28S TAS =** $C_{26}$ Cholestane (20S)/$C_{28}$ Stigmastane (20S)

**%$C_{27}$, %$C_{28}$, %$C_{29}$ MAS =** Σ$C_{27}$, Σ$C_{28}$, Σ$C_{29}$ MAS

## B. Total Organic Carbon (TOC) and Rock Eval (RE) parameters for the Eagle Ford Shale samples

*Lozier Canyon outcrop*

| Sample | Depth (ft) | TOC | $S_1$ | $S_2$ | $S_3$ | $T_{max}$ | HI | OI | $S_2/S_3$ | $S_1$/TOC | PI | $S_1 + S_2$ |
|---|---|---|---|---|---|---|---|---|---|---|---|---|
| EFLC-43 | 187.5 | 0.04 | 0.02 | 0.01 | 0.05 | 0 | 25 | 125 | 0 | 50 | 0.67 | 0.03 |
| EFLC-42 | 182.5 | 0.05 | 0.02 | 0.08 | 0.11 | 0 | 160 | 220 | 1 | 40 | 0.20 | 0.10 |
| EFLC-41 | 180.0 | 0.04 | 0.03 | 0.05 | 0.07 | 0 | 125 | 175 | 1 | 75 | 0.38 | 0.08 |
| EFLC-40 | 175.0 | 0.07 | 0.04 | 0.04 | 0.37 | 0 | 57 | 529 | 0 | 57 | 0.50 | 0.08 |
| EFLC-39 | 170.0 | 0.08 | 0.02 | 0.03 | 0.06 | 0 | 38 | 75 | 1 | 25 | 0.40 | 0.05 |
| EFLC-38 | 165.0 | 0.06 | 0.03 | 0.14 | 0.06 | 0 | 233 | 100 | 2 | 50 | 0.18 | 0.17 |
| EFLC-37 | 160.0 | 0.11 | 0.02 | 0.05 | 0.09 | 0 | 45 | 82 | 1 | 18 | 0.29 | 0.07 |
| EFLC-36 | 155.0 | 0.06 | 0.04 | 0.03 | 0.25 | 0 | 50 | 417 | 0 | 67 | 0.57 | 0.07 |
| EFLC-35 | 150.0 | 0.06 | 0.01 | 0.01 | 0.21 | 0 | 17 | 350 | 0 | 17 | 0.50 | 0.02 |
| EFLC-34 | 145.0 | 0.07 | 0.04 | 0.01 | 0.23 | 0 | 14 | 329 | 0 | 57 | 0.80 | 0.05 |
| EFLC-33 | 144.5 | 0.89 | 0.03 | 1.18 | 1.41 | 433 | 133 | 158 | 1 | 3 | 0.02 | 1.21 |
| EFLC-32 | 142.0 | 0.57 | 0.06 | 0.93 | 0.92 | 438 | 163 | 161 | 1 | 11 | 0.06 | 0.99 |
| EFLC-31 | 140.0 | 0.05 | 0.02 | 0.01 | 0.09 | 0 | 20 | 180 | 0 | 40 | 0.67 | 0.03 |
| EFLC-30 | 139.5 | 0.48 | 0.07 | 0.67 | 0.27 | 437 | 140 | 56 | 2 | 15 | 0.09 | 0.74 |
| EFLC-29 | 135.0 | 0.07 | 0.03 | 0.03 | 0.11 | 0 | 43 | 157 | 0 | 43 | 0.50 | 0.06 |
| EFLC-28 | 130.0 | 2.07 | 0.27 | 8.77 | 0.64 | 437 | 423 | 31 | 14 | 13 | 0.03 | 9.04 |
| EFLC-27 | 125.0 | 1.68 | 0.34 | 7.76 | 0.60 | 436 | 462 | 36 | 13 | 20 | 0.04 | 8.10 |
| EFLC-26 | 121.5 | 2.92 | 0.45 | 16.52 | 0.91 | 432 | 566 | 31 | 18 | 15 | 0.03 | 16.97 |
| EFLC-25 | 116.5 | 1.84 | 0.15 | 8.92 | 0.65 | 434 | 485 | 35 | 14 | 8 | 0.02 | 9.07 |
| EFLC-24 | 110.0 | 0.78 | 0.08 | 2.18 | 0.40 | 437 | 279 | 51 | 5 | 10 | 0.04 | 2.26 |
| EFLC-23 | 106.0 | 0.08 | 0.08 | 0.05 | 0.17 | 0 | 63 | 213 | 0 | 100 | 0.62 | 0.13 |
| EFLC-22 | 100.0 | 0.29 | 0.11 | 0.56 | 0.24 | 438 | 193 | 83 | 2 | 38 | 0.16 | 0.67 |

*Lozier Canyon outcrop (cont.)*

| Sample | Depth (ft) | TOC | $S_1$ | $S_2$ | $S_3$ | $T_{max}$ | HI | OI | $S_2/S_3$ | $S_1$/TOC | PI | $S_1 + S_2$ |
|---|---|---|---|---|---|---|---|---|---|---|---|---|
| EFLC-21 | 95.0 | 0.30 | 0.05 | 0.39 | 0.28 | 437 | 130 | 93 | 1 | 17 | 0.11 | 0.44 |
| EFLC-20 | 89.0 | 1.80 | 0.30 | 8.43 | 0.55 | 433 | 468 | 31 | 15 | 17 | 0.03 | 8.73 |
| EFLC-19 | 85.0 | 1.40 | 0.16 | 5.60 | 0.43 | 434 | 400 | 31 | 13 | 11 | 0.03 | 5.76 |
| EFLC-18 | 80.5 | 1.40 | 0.17 | 5.73 | 0.50 | 435 | 409 | 36 | 11 | 12 | 0.03 | 5.90 |
| EFLC-17 | 75.0 | 0.63 | 0.02 | 1.48 | 0.29 | 436 | 235 | 46 | 5 | 3 | 0.01 | 1.50 |
| EFLC-16 | 70.0 | 0.77 | 0.05 | 1.67 | 1.31 | 434 | 217 | 170 | 1 | 6 | 0.03 | 1.72 |
| EFLC-15 | 65.0 | 1.03 | 0.08 | 1.31 | 2.34 | 437 | 127 | 227 | 1 | 8 | 0.06 | 1.39 |
| EFLC-14 | 60.0 | 0.92 | 0.12 | 4.19 | 0.51 | 434 | 455 | 55 | 8 | 13 | 0.03 | 4.31 |
| EFLC-13 | 55.0 | 2.19 | 0.19 | 13.07 | 0.92 | 430 | 597 | 42 | 14 | 9 | 0.01 | 13.26 |
| EFLC-12 | 50.0 | 1.93 | 0.78 | 11.91 | 0.76 | 430 | 617 | 39 | 16 | 40 | 0.06 | 12.69 |
| EFLC-11 | 45.0 | 4.32 | 1.01 | 26.69 | 1.22 | 431 | 618 | 28 | 22 | 23 | 0.04 | 27.70 |
| EFLC-10 | 40.0 | 6.32 | 3.10 | 41.11 | 0.85 | 430 | 650 | 13 | 48 | 49 | 0.07 | 44.21 |
| EFLC-9 | 35.0 | 5.47 | 2.54 | 33.86 | 0.98 | 431 | 619 | 18 | 35 | 46 | 0.07 | 36.40 |
| EFLC-8 | 30.0 | 6.29 | 1.87 | 39.88 | 0.92 | 431 | 634 | 15 | 43 | 30 | 0.04 | 41.75 |
| EFLC-7 | 25.0 | 6.05 | 2.64 | 39.61 | 1.13 | 430 | 655 | 19 | 35 | 44 | 0.06 | 42.25 |
| EFLC-6 | 20.0 | 4.58 | 1.07 | 28.08 | 1.12 | 431 | 613 | 24 | 25 | 23 | 0.04 | 29.15 |
| EFLC-5 | 15.0 | 5.91 | 2.03 | 39.05 | 1.95 | 430 | 661 | 33 | 20 | 34 | 0.05 | 41.08 |
| EFLC-4 | 10.0 | 2.79 | 0.55 | 13.68 | 1.78 | 431 | 490 | 64 | 8 | 20 | 0.04 | 14.23 |
| EFLC-3 | 9.0 | 1.77 | 0.23 | 6.70 | 1.44 | 430 | 379 | 81 | 5 | 13 | 0.03 | 6.93 |
| EFLC-2 | 5.0 | 0.54 | 0.05 | 2.47 | 0.32 | 430 | 457 | 59 | 8 | 9 | 0.02 | 2.52 |
| EFLC-1 | 0.0 | 2.36 | 0.66 | 18.27 | 0.52 | 428 | 774 | 22 | 35 | 28 | 0.03 | 18.93 |

*Ferguson McKnight #526-1H core*

| Sample | Depth (ft) | TOC | $S_1$ | $S_2$ | $S_3$ | $T_{max}$ | HI | OI | $S_2/S_3$ | $S_1$/TOC | PI | $S_1 + S_2$ |
|---|---|---|---|---|---|---|---|---|---|---|---|---|
| EFMK-1 | 5793.0 | 1.02 | 3.01 | 1.90 | 0.33 | 436 | 186 | 32 | 6 | 295 | 0.61 | 4.91 |
| EFMK-2 | 5801.0 | 1.23 | 2.56 | 2.59 | 0.49 | 443 | 211 | 40 | 5 | 208 | 0.50 | 5.15 |
| EFMK-3 | 5809.0 | 1.83 | 3.83 | 4.08 | 0.45 | 440 | 223 | 25 | 9 | 209 | 0.48 | 7.91 |
| EFMK-4 | 5817.5 | 2.79 | 3.28 | 5.93 | 0.51 | 445 | 213 | 18 | 12 | 118 | 0.36 | 9.21 |
| EFMK-5 | 5825.5 | 1.32 | 2.69 | 3.43 | 0.40 | 440 | 260 | 30 | 9 | 204 | 0.44 | 6.12 |
| EFMK-6 | 5833.0 | 0.57 | 1.01 | 0.76 | 0.49 | 443 | 134 | 87 | 2 | 178 | 0.57 | 1.77 |
| EFMK-7 | 5841.0 | 0.69 | 1.54 | 1.02 | 0.43 | 443 | 147 | 62 | 2 | 222 | 0.60 | 2.56 |
| EFMK-8 | 5849.0 | 1.70 | 2.44 | 3.68 | 0.60 | 446 | 216 | 35 | 6 | 144 | 0.40 | 6.12 |
| EFMK-9 | 5859.0 | 1.70 | 4.86 | 4.06 | 0.63 | 442 | 239 | 37 | 6 | 286 | 0.54 | 8.92 |
| EFMK-10 | 5864.5 | 2.18 | 4.37 | 4.63 | 0.68 | 447 | 212 | 31 | 7 | 200 | 0.49 | 9.00 |
| EFMK-11 | 5873.5 | 1.76 | 2.39 | 3.76 | 0.61 | 450 | 214 | 35 | 6 | 136 | 0.39 | 6.15 |
| EFMK-12 | 5881.0 | 3.06 | 3.93 | 5.88 | 0.68 | 453 | 192 | 22 | 9 | 128 | 0.40 | 9.81 |
| EFMK-13 | 5889.0 | 2.33 | 2.91 | 5.19 | 0.56 | 450 | 223 | 24 | 9 | 125 | 0.36 | 8.10 |
| EFMK-14 | 5897.5 | 2.44 | 3.33 | 5.55 | 0.45 | 449 | 227 | 18 | 12 | 136 | 0.38 | 8.88 |
| EFMK-15 | 5905.5 | 2.45 | 3.71 | 5.66 | 0.45 | 448 | 231 | 18 | 13 | 151 | 0.40 | 9.37 |
| EFMK-16 | 5913.5 | 1.91 | 4.33 | 5.16 | 0.46 | 441 | 270 | 24 | 11 | 227 | 0.46 | 9.49 |
| EFMK-17 | 5921.0 | 1.14 | 2.67 | 2.12 | 0.53 | 447 | 186 | 46 | 4 | 234 | 0.56 | 4.79 |
| EFMK-18 | 5929.0 | 1.76 | 3.44 | 3.47 | 0.62 | 447 | 197 | 35 | 6 | 195 | 0.50 | 6.91 |
| EFMK-19 | 5937.5 | 1.66 | 4.01 | 3.36 | 0.61 | 447 | 202 | 37 | 6 | 242 | 0.54 | 7.37 |
| EFMK-20 | 5945.5 | 2.24 | 4.30 | 4.73 | 0.52 | 442 | 211 | 23 | 9 | 192 | 0.48 | 9.03 |
| EFMK-21 | 5953.0 | 1.94 | 4.13 | 4.42 | 0.49 | 443 | 228 | 25 | 9 | 213 | 0.48 | 8.55 |
| EFMK-22 | 5961.0 | 2.78 | 6.12 | 6.05 | 0.67 | 449 | 218 | 24 | 9 | 220 | 0.50 | 12.17 |
| EFMK-23 | 5969.0 | 2.28 | 6.66 | 5.23 | 0.59 | 442 | 229 | 26 | 9 | 292 | 0.56 | 11.89 |
| EFMK-24 | 5977.5 | 2.84 | 7.04 | 6.40 | 0.82 | 447 | 225 | 29 | 8 | 248 | 0.52 | 13.44 |
| EFMK-25 | 6072.0 | 3.42 | 6.76 | 7.85 | 1.00 | 444 | 230 | 29 | 8 | 198 | 0.46 | 14.61 |
| EFMK-26 | 6174.0 | 4.99 | 8.78 | 11.87 | 0.73 | 444 | 238 | 15 | 16 | 176 | 0.43 | 20.65 |

*Fasken "A" #1 core*

| Sample | Depth (ft) | TOC | $S_1$ | $S_2$ | $S_3$ | $T_{max}$ | HI | OI | $S_2/S_3$ | $S_1$/TOC | PI | $S_1 + S_2$ |
|---|---|---|---|---|---|---|---|---|---|---|---|---|
| EFFA-1 | 9430.5 | 3.20 | 0.08 | 0.28 | 0.30 | 553 | 9 | 9 | 1 | 3 | 0.22 | 0.36 |
| EFFA-2 | 9440.0 | 1.20 | 0.09 | 0.13 | 0.32 | 593 | 11 | 27 | 0 | 7 | 0.41 | 0.22 |
| EFFA-3 | 9450.0 | 3.72 | 0.16 | 0.41 | 0.31 | 588 | 11 | 8 | 1 | 4 | 0.28 | 0.57 |
| EFFA-4 | 9460.5 | 1.28 | 0.14 | 0.17 | 0.31 | 587 | 13 | 24 | 1 | 11 | 0.45 | 0.31 |
| EFFA-5 | 9470.5 | 2.30 | 0.11 | 0.25 | 0.88 | 587 | 11 | 38 | 0 | 5 | 0.31 | 0.36 |
| EFFA-6 | 9479.5 | 2.18 | 0.11 | 0.18 | 0.24 | 588 | 8 | 11 | 1 | 5 | 0.38 | 0.29 |
| EFFA-7 | 9489.0 | 2.66 | 0.14 | 0.29 | 0.23 | 599 | 11 | 9 | 1 | 5 | 0.33 | 0.43 |
| EFFA-8 | 9499.0 | 1.16 | 0.18 | 0.15 | 0.32 | 600 | 13 | 28 | 0 | 16 | 0.55 | 0.33 |
| EFFA-9 | 9509.0 | 2.14 | 0.09 | 0.18 | 0.27 | 590 | 8 | 13 | 1 | 4 | 0.33 | 0.27 |
| EFFA-10 | 9519.5 | 1.82 | 0.15 | 0.20 | 0.39 | 599 | 11 | 21 | 1 | 8 | 0.43 | 0.35 |
| EFFA-11 | 9530.0 | 1.89 | 0.11 | 0.16 | 0.28 | 600 | 8 | 15 | 1 | 6 | 0.41 | 0.27 |
| EFFA-12 | 9540.0 | 2.07 | 0.10 | 0.14 | 0.35 | 601 | 7 | 17 | 0 | 5 | 0.42 | 0.24 |
| EFFA-13 | 9550.0 | 3.09 | 0.11 | 0.25 | 0.35 | 593 | 8 | 11 | 1 | 4 | 0.31 | 0.36 |
| EFFA-14 | 9560.5 | 2.16 | 0.10 | 0.15 | 0.31 | 598 | 7 | 14 | 0 | 5 | 0.40 | 0.25 |
| EFFA-15 | 9570.5 | 3.32 | 0.18 | 0.37 | 0.31 | 599 | 11 | 9 | 1 | 5 | 0.33 | 0.55 |
| EFFA-16 | 9578.5 | 3.71 | 0.17 | 0.37 | 0.31 | 596 | 10 | 8 | 1 | 5 | 0.31 | 0.54 |
| EFFA-17 | 9589.0 | 2.70 | 0.15 | 0.30 | 0.27 | 597 | 11 | 10 | 1 | 6 | 0.33 | 0.45 |
| EFFA-18 | 9599.5 | 3.70 | 0.20 | 0.39 | 0.30 | 599 | 11 | 8 | 1 | 5 | 0.34 | 0.59 |
| EFFA-19 | 9610.0 | 4.30 | 0.16 | 0.35 | 0.34 | 598 | 8 | 8 | 1 | 4 | 0.31 | 0.51 |

*Fasken "A" #1 core (cont.)*

| Sample | Depth (ft) | TOC | $S_1$ | $S_2$ | $S_3$ | $T_{max}$ | HI | OI | $S_2/S_3$ | $S_1$/TOC | PI | $S_1 + S_2$ |
|---|---|---|---|---|---|---|---|---|---|---|---|---|
| EFFA-21 | 9629.5 | 4.35 | 0.19 | 0.38 | 0.29 | 602 | 9 | 7 | 1 | 4 | 0.33 | 0.57 |
| EFFA-22 | 9639.5 | 4.03 | 0.21 | 0.29 | 0.31 | 600 | 7 | 8 | 1 | 5 | 0.42 | 0.50 |
| EFFA-23 | 9650.5 | 3.91 | 0.13 | 0.25 | 0.29 | 600 | 6 | 7 | 1 | 3 | 0.34 | 0.38 |
| EFFA-24 | 9655.5 | 5.90 | 0.29 | 0.57 | 0.35 | 604 | 10 | 6 | 2 | 5 | 0.34 | 0.86 |
| EFFA-25 | 9665.5 | 5.76 | 0.30 | 0.43 | 0.31 | 331 | 7 | 5 | 1 | 5 | 0.41 | 0.73 |
| EFFA-26 | 9670.5 | 4.03 | 0.17 | 0.35 | 0.29 | 603 | 9 | 7 | 1 | 4 | 0.33 | 0.52 |
| EFFA-27 | 9680.5 | 4.86 | 0.24 | 0.48 | 0.30 | 604 | 10 | 6 | 2 | 5 | 0.33 | 0.72 |
| EFFA-28 | 9685.5 | 5.49 | 0.23 | 0.56 | 0.28 | 605 | 10 | 5 | 2 | 4 | 0.29 | 0.79 |
| EFFA-29 | 9695.0 | 5.42 | 0.19 | 0.36 | 0.28 | 600 | 7 | 5 | 1 | 4 | 0.35 | 0.55 |
| EFFA-30 | 9700.5 | 5.04 | 0.30 | 0.54 | 0.36 | 604 | 11 | 7 | 2 | 6 | 0.36 | 0.84 |
| EFFA-31 | 9711.5 | 5.95 | 0.23 | 0.48 | 0.31 | 604 | 8 | 5 | 2 | 4 | 0.32 | 0.71 |
| EFFA-32 | 9717.0 | 6.20 | 0.26 | 0.54 | 0.41 | 604 | 9 | 7 | 1 | 4 | 0.33 | 0.80 |
| EFFA-33 | 9728.5 | 6.31 | 0.20 | 0.51 | 0.35 | 603 | 8 | 6 | 1 | 3 | 0.28 | 0.71 |
| EFFA-34 | 9733.5 | 5.60 | 0.29 | 0.58 | 0.32 | 600 | 10 | 6 | 2 | 5 | 0.33 | 0.87 |
| EFFA-35 | 9742.5 | 6.42 | 0.20 | 0.54 | 0.30 | 602 | 8 | 5 | 2 | 3 | 0.27 | 0.74 |
| EFFA-36 | 9746.5 | 6.29 | 0.23 | 0.60 | 0.31 | 602 | 10 | 5 | 2 | 4 | 0.28 | 0.83 |
| EFFA-37 | 9756.5 | 5.59 | 0.19 | 0.39 | 0.36 | 601 | 7 | 6 | 1 | 3 | 0.33 | 0.58 |
| EFFA-38 | 9761.5 | 5.39 | 0.33 | 0.54 | 0.35 | 604 | 10 | 6 | 2 | 6 | 0.38 | 0.87 |
| EFFA-39 | 9770.5 | 5.49 | 0.26 | 0.67 | 0.28 | 604 | 12 | 5 | 2 | 5 | 0.28 | 0.93 |
| EFFA-40 | 9776.0 | 5.44 | 0.20 | 0.34 | 0.36 | 603 | 6 | 7 | 1 | 4 | 0.37 | 0.54 |

*Bouldin Creek outcrop*

| Sample | Depth (ft) | TOC | $S_1$ | $S_2$ | $S_3$ | $T_{max}$ | HI | OI | $S_2/S_3$ | $S_1$/TOC | PI | $S_1 + S_2$ |
|---|---|---|---|---|---|---|---|---|---|---|---|---|
| EFBC_Aus2 | 34.0 | 0.06 | 0.01 | 0.01 | 0.47 | 0 | 17 | 783 | 0 | 17 | 0.50 | 0.02 |
| EFBC-Aus | 33.0 | 0.07 | 0.01 | 0.02 | 0.52 | 0 | 28 | 716 | 0 | 14 | 0.33 | 0.03 |
| EFBC-1 | 32.0 | 0.07 | 0.01 | 0.01 | 0.42 | 0 | 15 | 615 | 0 | 15 | 0.50 | 0.02 |
| EFBC-2 | 31.0 | 0.14 | 0.01 | 0.02 | 0.50 | 0 | 15 | 365 | 0 | 7 | 0.33 | 0.03 |
| EFBC-3 | 30.0 | 0.19 | 0.02 | 0.07 | 0.59 | 0 | 37 | 316 | 0 | 11 | 0.22 | 0.09 |
| EFBC-4 | 29.0 | 0.13 | 0.01 | 0.09 | 0.42 | 0 | 67 | 313 | 0 | 7 | 0.10 | 0.10 |
| EFBC-5 | 28.0 | 3.68 | 0.35 | 15.99 | 2.01 | 423 | 435 | 55 | 8 | 10 | 0.02 | 16.34 |
| EFBC-6 | 27.0 | 4.48 | 0.37 | 23.18 | 1.51 | 414 | 517 | 34 | 15 | 8 | 0.02 | 23.55 |
| EFBC-7 | 26.0 | 3.69 | 0.17 | 15.92 | 2.72 | 422 | 431 | 74 | 6 | 5 | 0.01 | 16.09 |
| EFBC-8 | 25.0 | 3.13 | 0.22 | 14.08 | 2.33 | 425 | 450 | 74 | 6 | 7 | 0.02 | 14.30 |
| EFBC-9 | 24.0 | 4.15 | 0.30 | 20.70 | 2.64 | 420 | 499 | 64 | 8 | 7 | 0.01 | 21.00 |
| EFBC-10 | 23.0 | 2.90 | 0.17 | 12.89 | 2.04 | 422 | 444 | 70 | 6 | 6 | 0.01 | 13.06 |
| EFBC-11 | 22.0 | 4.68 | 0.27 | 20.67 | 2.62 | 422 | 442 | 56 | 8 | 6 | 0.01 | 20.94 |
| EFBC-12 | 21.0 | 3.13 | 0.23 | 12.37 | 1.70 | 425 | 395 | 54 | 7 | 7 | 0.02 | 12.60 |
| EFBC-13 | 20.0 | 3.85 | 0.23 | 18.58 | 1.66 | 417 | 483 | 43 | 11 | 6 | 0.01 | 18.81 |
| EFBC-14 | 19.0 | 3.87 | 0.36 | 18.37 | 1.73 | 418 | 475 | 45 | 11 | 9 | 0.02 | 18.73 |
| EFBC-15 | 18.0 | 3.84 | 0.32 | 17.29 | 2.64 | 420 | 450 | 69 | 7 | 8 | 0.02 | 17.61 |
| EFBC-16 | 17.0 | 4.05 | 0.25 | 16.05 | 2.62 | 422 | 396 | 65 | 6 | 6 | 0.02 | 16.30 |
| EFBC-17 | 16.0 | 3.13 | 0.21 | 12.41 | 2.31 | 424 | 396 | 74 | 5 | 7 | 0.02 | 12.62 |

*Bouldin Creek outcrop (cont.)*

| Sample | Depth (ft) | TOC | $S_1$ | $S_2$ | $S_3$ | $T_{max}$ | HI | OI | $S_2/S_3$ | $S_1$/TOC | PI | $S_1 + S_2$ |
|---|---|---|---|---|---|---|---|---|---|---|---|---|
| EFBC-18 | 15.0 | 3.45 | 0.19 | 15.57 | 1.64 | 416 | 451 | 48 | 9 | 6 | 0.01 | 15.76 |
| EFBC-19 | 14.0 | 2.14 | 0.16 | 7.74 | 1.07 | 421 | 362 | 50 | 7 | 7 | 0.02 | 7.90 |
| EFBC-20 | 13.0 | 1.12 | 0.04 | 2.27 | 0.58 | 426 | 203 | 52 | 4 | 4 | 0.02 | 2.31 |
| EFBC-21 | 12.0 | 0.17 | 0.02 | 0.05 | 0.60 | 0 | 30 | 355 | 0 | 12 | 0.29 | 0.07 |
| EFBC-22 | 11.0 | 0.39 | 0.04 | 0.40 | 0.74 | 434 | 103 | 191 | 1 | 10 | 0.09 | 0.44 |
| EFBC-23 | 10.0 | 1.35 | 0.08 | 3.49 | 0.87 | 422 | 259 | 64 | 4 | 6 | 0.02 | 3.57 |
| EFBC-24 | 9.0 | 1.02 | 0.10 | 2.76 | 0.67 | 424 | 271 | 66 | 4 | 10 | 0.03 | 2.86 |
| EFBC-25 | 8.0 | 4.83 | 0.27 | 20.09 | 2.18 | 414 | 416 | 45 | 9 | 6 | 0.01 | 20.36 |
| EFBC-26 | 7.0 | 0.95 | 0.02 | 2.57 | 0.70 | 425 | 269 | 73 | 4 | 2 | 0.01 | 2.59 |
| EFBC-27 | 6.0 | 2.02 | 0.08 | 6.79 | 1.06 | 416 | 336 | 52 | 6 | 4 | 0.01 | 6.87 |
| EFBC-28 | 5.0 | 0.59 | 0.05 | 1.47 | 0.54 | 424 | 250 | 92 | 3 | 9 | 0.03 | 1.52 |
| EFBC-29 | 4.0 | 0.91 | 0.05 | 2.00 | 0.86 | 430 | 220 | 95 | 2 | 6 | 0.02 | 2.05 |
| EFBC-30 | 3.0 | 5.95 | 0.46 | 35.91 | 1.56 | 418 | 604 | 26 | 23 | 8 | 0.01 | 36.37 |
| EFBC-31 | 2.0 | 7.22 | 0.67 | 48.76 | 1.66 | 416 | 675 | 23 | 29 | 9 | 0.01 | 49.43 |
| EFBC-32 | 1.0 | 7.13 | 0.77 | 48.63 | 1.51 | 416 | 682 | 21 | 32 | 11 | 0.02 | 49.40 |
| EFBC-33 | 0.0 | 5.59 | 0.53 | 37.70 | 1.42 | 411 | 674 | 25 | 27 | 9 | 0.01 | 38.23 |
| EFBC-34 | -1.0 | 7.06 | 1.04 | 50.59 | 1.57 | 412 | 717 | 22 | 32 | 15 | 0.02 | 51.63 |

*ACC#1 core*

| Sample | Depth (ft) | TOC | $S_1$ | $S_2$ | $S_3$ | $T_{max}$ | HI | OI | $S_2/S_3$ | $S_1$/TOC | PI | $S_1 + S_2$ |
|---|---|---|---|---|---|---|---|---|---|---|---|---|
| EFAC-1 | 80.0 | 2.12 | 0.07 | 6.34 | 1.18 | 428 | 299 | 56 | 5 | 3 | 0.01 | 6.41 |
| EFAC-2 | 85.0 | 2.80 | 0.09 | 10.48 | 1.39 | 428 | 374 | 50 | 8 | 3 | 0.01 | 10.57 |
| EFAC-3 | 90.0 | 4.04 | 0.17 | 17.86 | 1.71 | 421 | 442 | 42 | 10 | 4 | 0.01 | 18.03 |
| EFAC-4 | 95.0 | 4.55 | 0.23 | 20.63 | 1.94 | 417 | 453 | 43 | 11 | 5 | 0.01 | 20.86 |
| EFAC-5 | 100.5 | 3.88 | 0.12 | 14.58 | 1.76 | 422 | 376 | 45 | 8 | 3 | 0.01 | 14.70 |
| EFAC-6 | 105.0 | 3.89 | 0.17 | 15.84 | 1.93 | 420 | 407 | 50 | 8 | 4 | 0.01 | 16.01 |
| EFAC-7 | 110.0 | 5.12 | 0.28 | 26.27 | 2.00 | 421 | 513 | 39 | 13 | 5 | 0.01 | 26.55 |
| EFAC-8 | 114.8 | 8.07 | 0.59 | 45.91 | 2.77 | 424 | 569 | 34 | 17 | 7 | 0.01 | 46.50 |
| EFAC-9 | 120.0 | 1.20 | 0.04 | 0.44 | 0.71 | 417 | 37 | 59 | 1 | 3 | 0.08 | 0.48 |
| EFAC-10 | 124.8 | 2.22 | 0.08 | 6.06 | 0.79 | 429 | 273 | 36 | 8 | 4 | 0.01 | 6.14 |



*W. Brechtel #1 core*

| Sample | Depth (ft) | TOC | $S_1$ | $S_2$ | $S_3$ | $T_{max}$ | HI | OI | $S_2/S_3$ | $S_1$/TOC | PI | $S_1 + S_2$ |
|---|---|---|---|---|---|---|---|---|---|---|---|---|
| EFWB-1 | 3280.1 | 4.36 | 0.72 | 31.11 | 1.26 | 423 | 714 | 29 | 25 | 17 | 0.02 | 31.83 |
| EFWB-2 | 3285.0 | 3.01 | 0.34 | 18.15 | 1.31 | 420 | 603 | 44 | 14 | 11 | 0.02 | 18.49 |
| EFWB-3 | 3289.9 | 4.11 | 0.60 | 25.22 | 1.37 | 422 | 614 | 33 | 18 | 15 | 0.02 | 25.82 |
| EFWB-4 | 3295.0 | 5.47 | 0.67 | 33.31 | 1.37 | 422 | 609 | 25 | 24 | 12 | 0.02 | 33.98 |
| EFWB-5 | 3300.0 | 4.97 | 0.69 | 30.39 | 1.25 | 424 | 611 | 25 | 24 | 14 | 0.02 | 31.08 |
| EFWB-6 | 3304.9 | 3.83 | 1.31 | 24.52 | 0.97 | 431 | 640 | 25 | 25 | 34 | 0.05 | 25.83 |
| EFWB-7 | 3309.8 | 4.00 | 0.59 | 24.61 | 1.15 | 421 | 615 | 29 | 21 | 15 | 0.02 | 25.20 |
| EFWB-8 | 3313.0 | 5.56 | 1.24 | 35.07 | 0.90 | 425 | 631 | 16 | 39 | 22 | 0.03 | 36.31 |
| EFWB-9 | 3315.1 | 5.95 | 1.99 | 40.69 | 1.17 | 426 | 684 | 20 | 35 | 33 | 0.05 | 42.68 |

*C.J. Hendershot #1 core*

| Sample | Depth (ft) | TOC | $S_1$ | $S_2$ | $S_3$ | $T_{max}$ | HI | OI | $S_2/S_3$ | $S_1$/TOC | PI | $S_1 + S_2$ |
|---|---|---|---|---|---|---|---|---|---|---|---|---|
| EFHE-1 | 4734.1 | 0.77 | 0.07 | 2.40 | 0.79 | 433 | 313 | 103 | 3 | 9 | 0.03 | 2.47 |
| EFHE-2 | 4736.8 | 5.10 | 0.96 | 36.03 | 1.45 | 427 | 706 | 28 | 25 | 19 | 0.03 | 36.99 |
| EFHE-3 | 4742.1 | 2.81 | 0.36 | 16.19 | 1.40 | 428 | 576 | 50 | 12 | 13 | 0.02 | 16.55 |
| EFHE-4 | 4747.0 | 3.48 | 0.40 | 20.22 | 1.47 | 425 | 581 | 42 | 14 | 11 | 0.02 | 20.62 |
| EFHE-5 | 4751.9 | 4.39 | 0.73 | 26.14 | 1.35 | 424 | 595 | 31 | 19 | 17 | 0.03 | 26.87 |
| EFHE-6 | 4756.9 | 5.17 | 0.61 | 28.93 | 1.47 | 422 | 560 | 28 | 20 | 12 | 0.02 | 29.54 |
| EFHE-7 | 4762.2 | 7.22 | 1.40 | 43.69 | 1.50 | 421 | 605 | 21 | 29 | 19 | 0.03 | 45.09 |
| EFHE-8 | 4768.9 | 6.86 | 1.40 | 41.67 | 1.43 | 427 | 607 | 21 | 29 | 20 | 0.03 | 43.07 |
| EFHE-9 | 4771.0 | 9.74 | 2.70 | 58.56 | 1.41 | 425 | 601 | 14 | 42 | 28 | 0.04 | 61.26 |
| EFHE-10 | 4773.8 | 1.48 | 0.20 | 1.39 | 0.41 | 420 | 94 | 28 | 3 | 14 | 0.13 | 1.59 |

*Lily Hoppess #1 core*

| Sample | Depth (ft) | TOC | $S_1$ | $S_2$ | $S_3$ | $T_{max}$ | HI | OI | $S_2/S_3$ | $S_1$/TOC | PI | $S_1 + S_2$ |
|---|---|---|---|---|---|---|---|---|---|---|---|---|
| EFLH-1 | 6640.0 | 5.74 | 3.10 | 19.25 | 0.31 | 444 | 335 | 5 | 62 | 54 | 0.14 | 22.35 |
| EFLH-2 | 6648.0 | 5.75 | 2.31 | 19.08 | 0.30 | 444 | 332 | 5 | 64 | 40 | 0.11 | 21.39 |
| EFLH-3 | 6656.0 | 4.15 | 1.99 | 13.34 | 0.29 | 443 | 322 | 7 | 46 | 48 | 0.13 | 15.33 |
| EFLH-4 | 6664.0 | 4.25 | 2.04 | 13.11 | 0.44 | 446 | 308 | 10 | 30 | 48 | 0.13 | 15.15 |
| EFLH-5 | 6672.0 | 4.71 | 2.57 | 15.95 | 0.43 | 442 | 338 | 9 | 37 | 55 | 0.14 | 18.52 |
| EFLH-6 | 6680.0 | 3.54 | 1.09 | 6.35 | 0.25 | 443 | 180 | 7 | 25 | 31 | 0.15 | 7.44 |
| EFLH-7 | 6688.0 | 5.87 | 3.17 | 24.83 | 0.33 | 442 | 423 | 6 | 75 | 54 | 0.11 | 28.00 |
| EFLH-8 | 6695.0 | 4.97 | 2.66 | 19.26 | 0.31 | 442 | 387 | 6 | 62 | 53 | 0.12 | 21.92 |
| EFLH-9 | 6704.0 | 4.56 | 2.27 | 15.77 | 0.31 | 444 | 346 | 7 | 51 | 50 | 0.13 | 18.04 |
| EFLH-10 | 6711.5 | 3.67 | 1.19 | 8.94 | 0.27 | 442 | 244 | 7 | 33 | 32 | 0.12 | 10.13 |
| EFLH-11 | 6719.0 | 4.35 | 1.58 | 13.60 | 0.31 | 443 | 312 | 7 | 44 | 36 | 0.10 | 15.18 |
| EFLH-12 | 6727.0 | 3.06 | 0.57 | 4.42 | 0.25 | 442 | 145 | 8 | 18 | 19 | 0.11 | 4.99 |
| EFLH-13 | 6735.0 | 2.28 | 0.15 | 0.35 | 0.17 | 437 | 15 | 7 | 2 | 7 | 0.30 | 0.50 |
| EFLH-14 | 6744.0 | 1.65 | 0.18 | 1.43 | 0.24 | 441 | 87 | 15 | 6 | 11 | 0.11 | 1.61 |
| EFLH-15 | 6754.0 | 1.99 | 0.37 | 2.78 | 0.22 | 442 | 140 | 11 | 13 | 19 | 0.12 | 3.15 |
| EFLH-16 | 6764.0 | 2.49 | 0.33 | 1.74 | 0.17 | 442 | 70 | 7 | 10 | 13 | 0.16 | 2.07 |
| EFLH-17 | 6774.0 | 2.16 | 0.17 | 1.31 | 0.18 | 444 | 61 | 8 | 7 | 8 | 0.11 | 1.48 |
| EFLH-18 | 6784.0 | 2.02 | 0.13 | 0.45 | 0.24 | 439 | 22 | 12 | 2 | 6 | 0.22 | 0.58 |
| EFLH-19 | 6794.0 | 3.56 | 1.35 | 10.12 | 0.37 | 444 | 284 | 10 | 27 | 38 | 0.12 | 11.47 |
| EFLH-20 | 6804.0 | 2.61 | 0.26 | 1.97 | 0.31 | 445 | 75 | 12 | 6 | 10 | 0.12 | 2.23 |
| EFLH-21 | 6815.0 | 0.23 | 0.04 | 0.08 | 0.32 | 440 | 35 | 139 | 0 | 17 | 0.33 | 0.12 |
| EFLH-22 | 6820.5 | 0.34 | 0.04 | 0.10 | 0.40 | 446 | 30 | 119 | 0 | 12 | 0.29 | 0.14 |

## C. Geochemical logs of TOC, HI, Pr/Ph and AIR for the Eagle Ford Shale bitumens analyzed

*Ferguson McKnight #526-1H core*

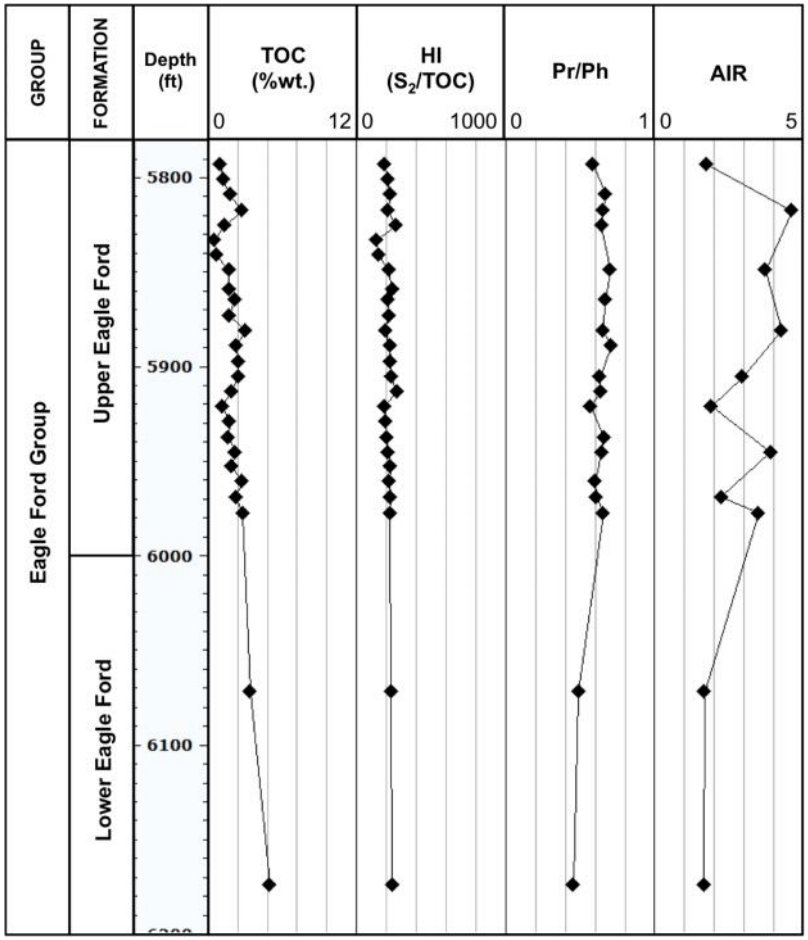

*Fasken "A" #1 core*

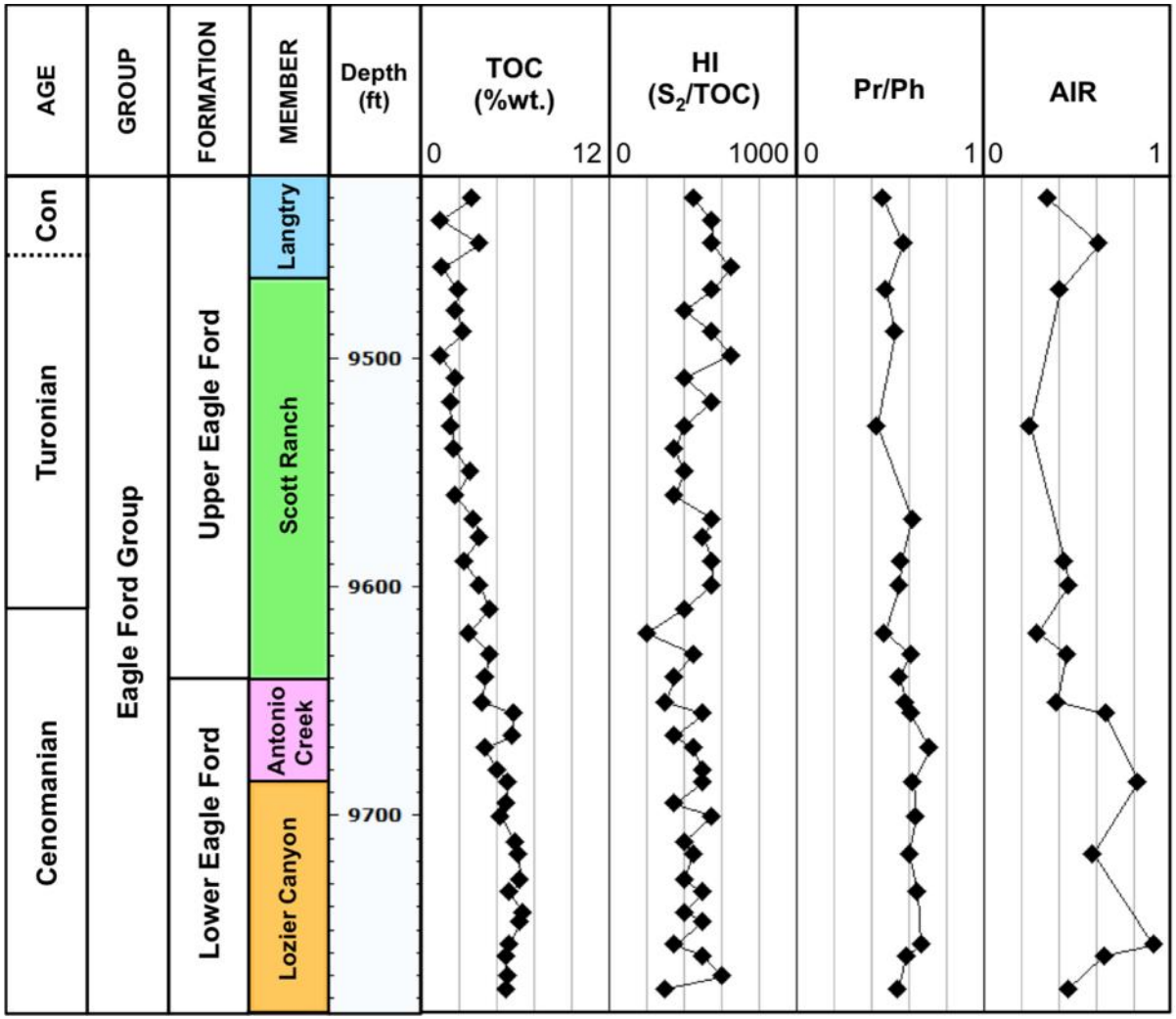

*Bouldin Creek outcrop*

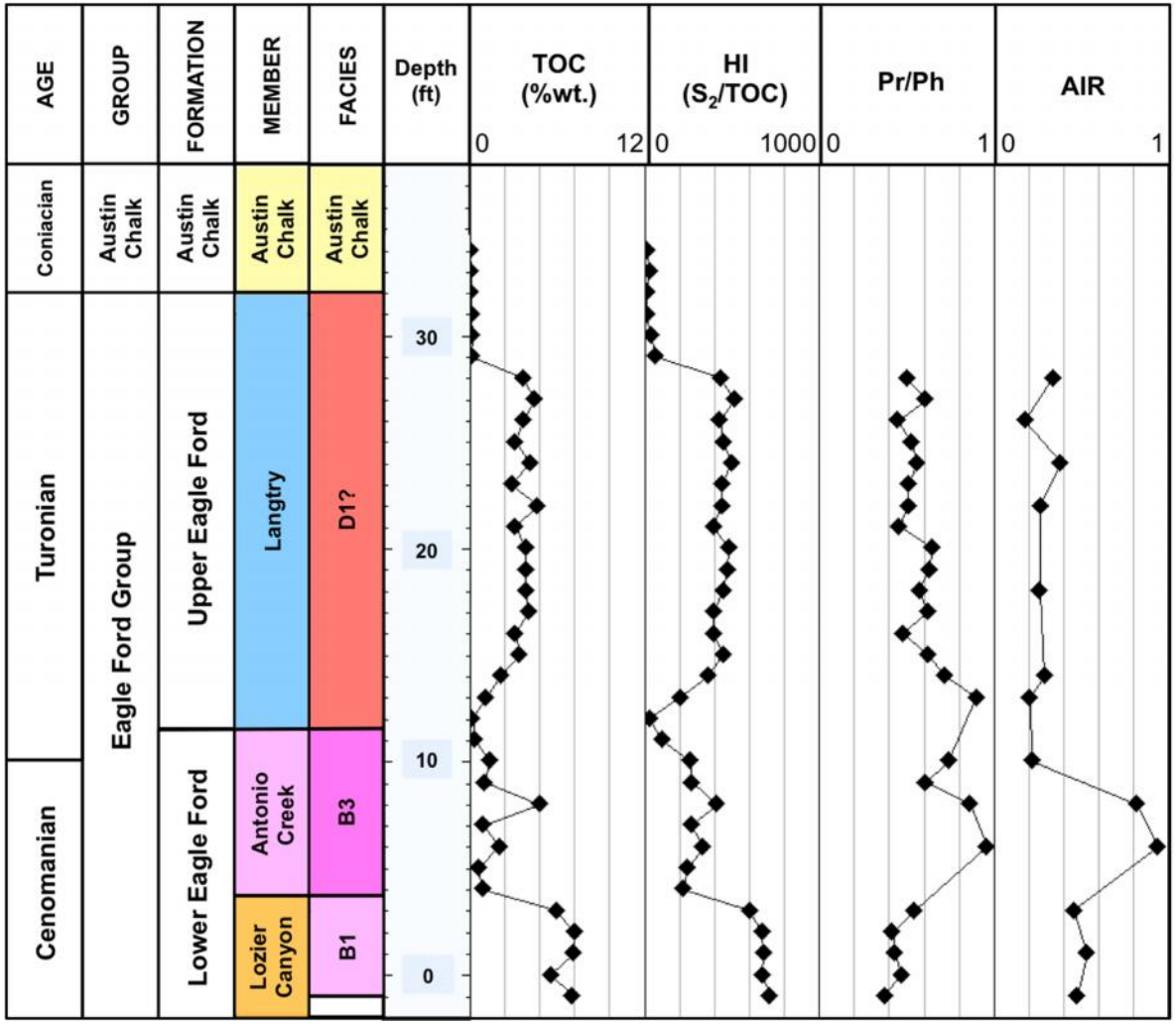

*ACC #1 core*


AGE
GROUP
FORMATION
MEMBER
FACIES
Depth (ft)
TOC (%wt.)
HI ($S_2$/TOC)
Pr/Ph
AIR
Cenomanian
Tur
Coniacian
Buda
Eagle Ford Group
Austin Chalk
Lower Eagle Ford
Upper EF
Lozier Canyon
Antonio Creek
Langtry
A
B1
B2
B3
D1
D2
0
12
1000
1
75
100
125

*W. Brechtel #1 core*

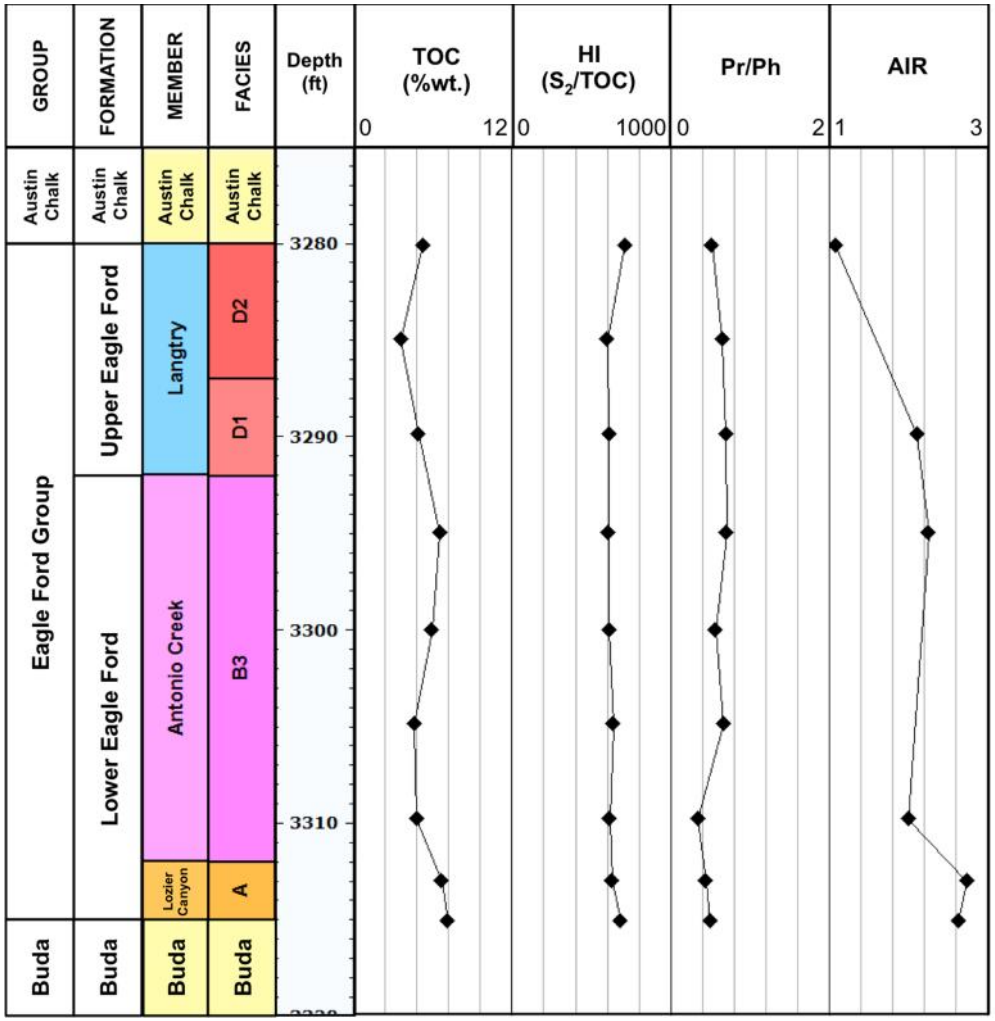

*C. J. Hendershot #1 core*

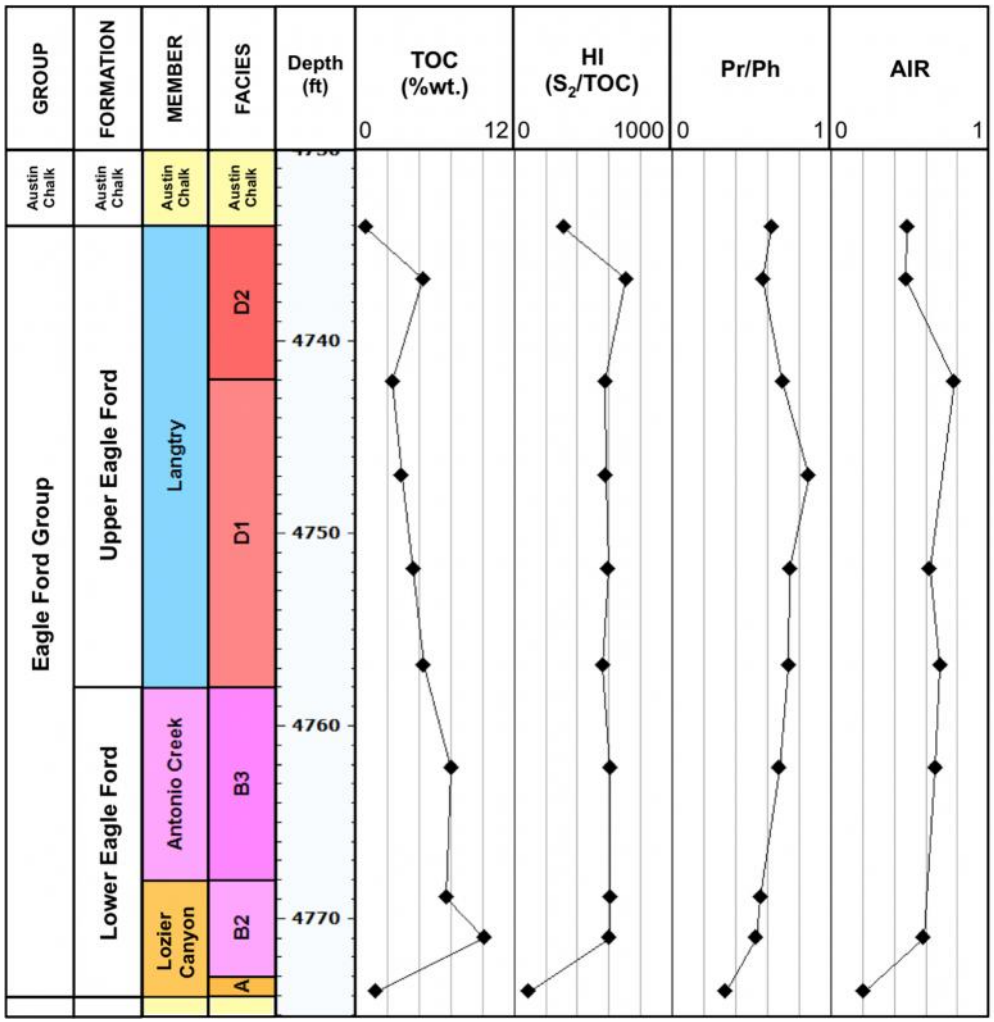

*Lily Hoppess #1 core*

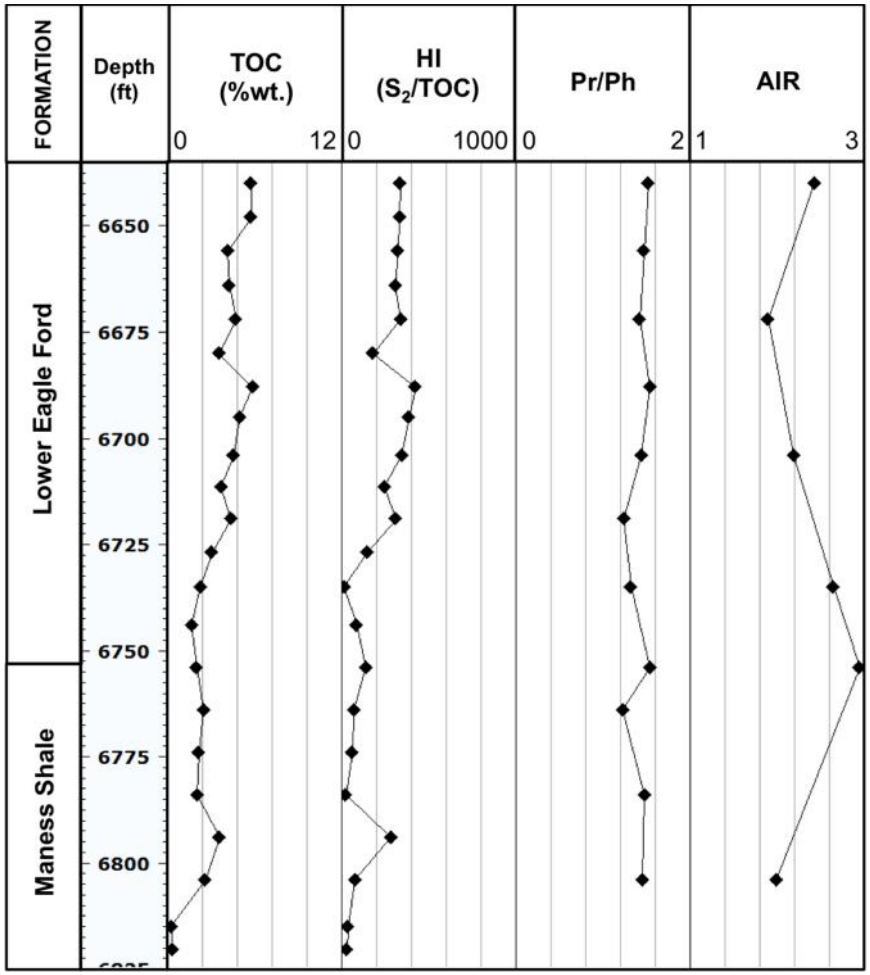

**D. Gas chromatograms of the saturate fractions for the Eagle Ford Shale samples analyzed in this study (Pr = pristane; Ph = phytane, n-$C_{25}$ = $C_{25}$ normal alkane)**

*Ferguson McKnight #526-1H core*

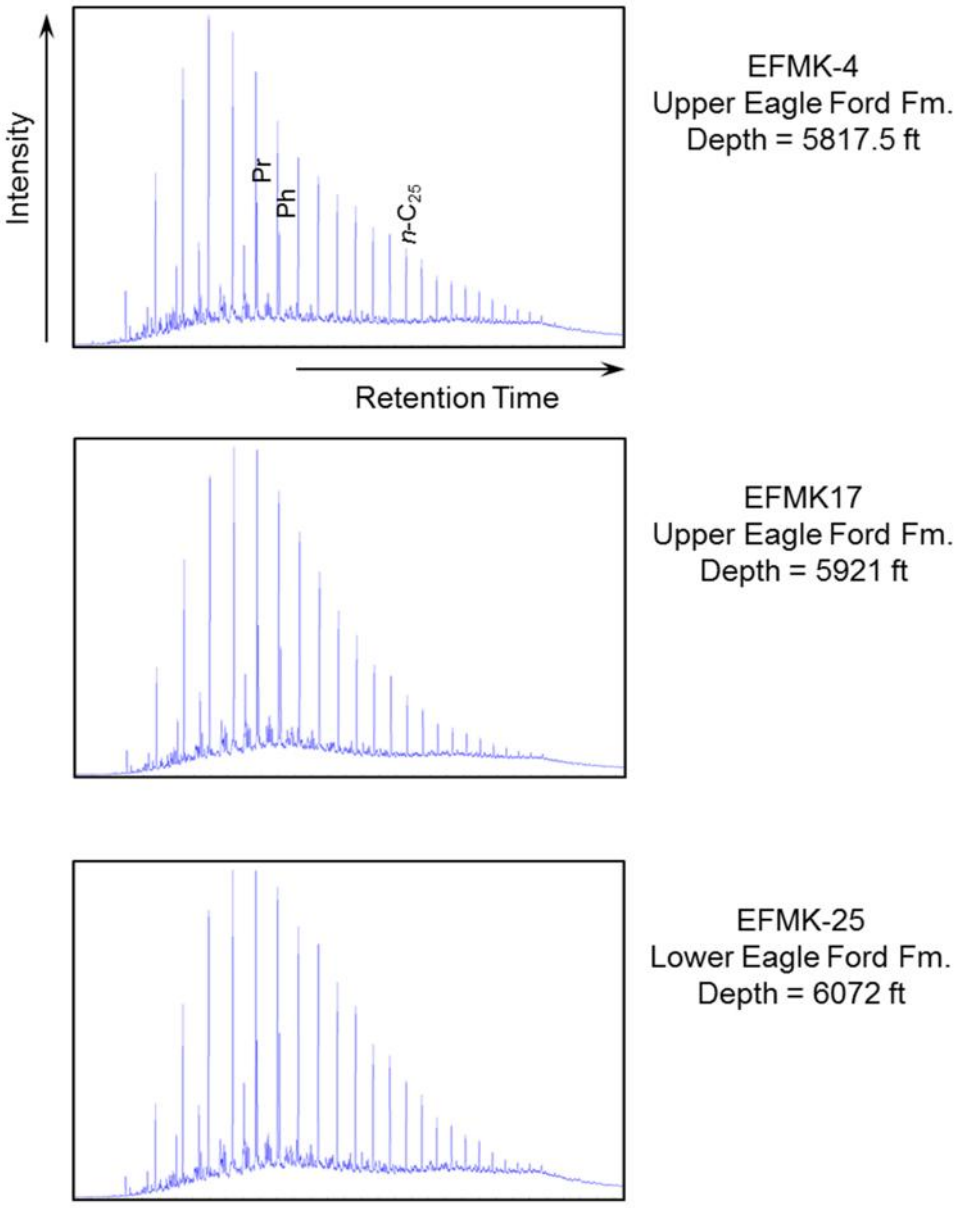

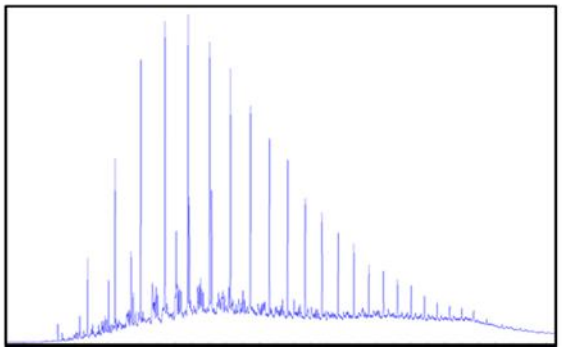

EFMK-26
Lower Eagle Ford Fm.
Depth = 6174 ft

*Fasken "A" #1 core*

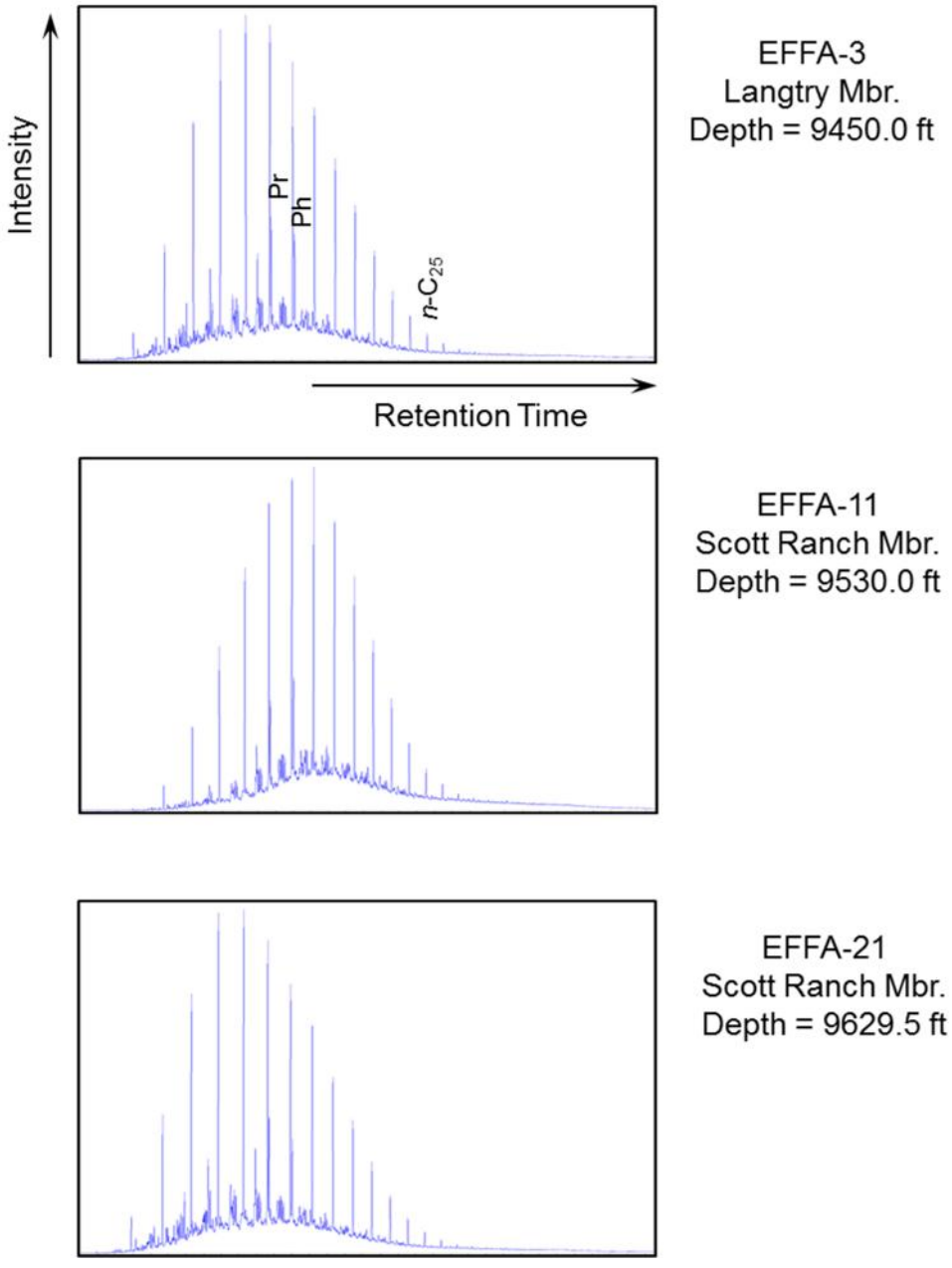

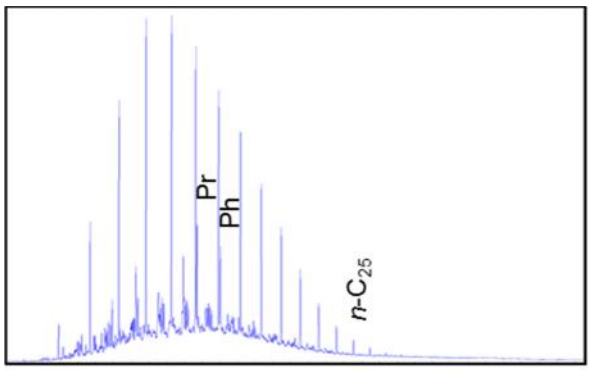


EFFA-24
Antonio Creek Mbr.
Depth = 9655.5 ft

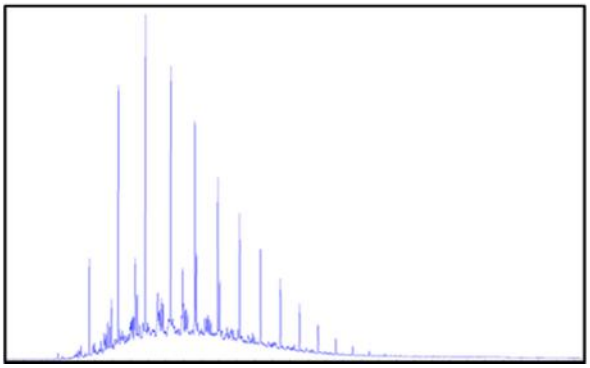

EFFA-37
Lozier Canyon Mbr.
Depth = 9756.5 ft

*Bouldin Creek outcrop*

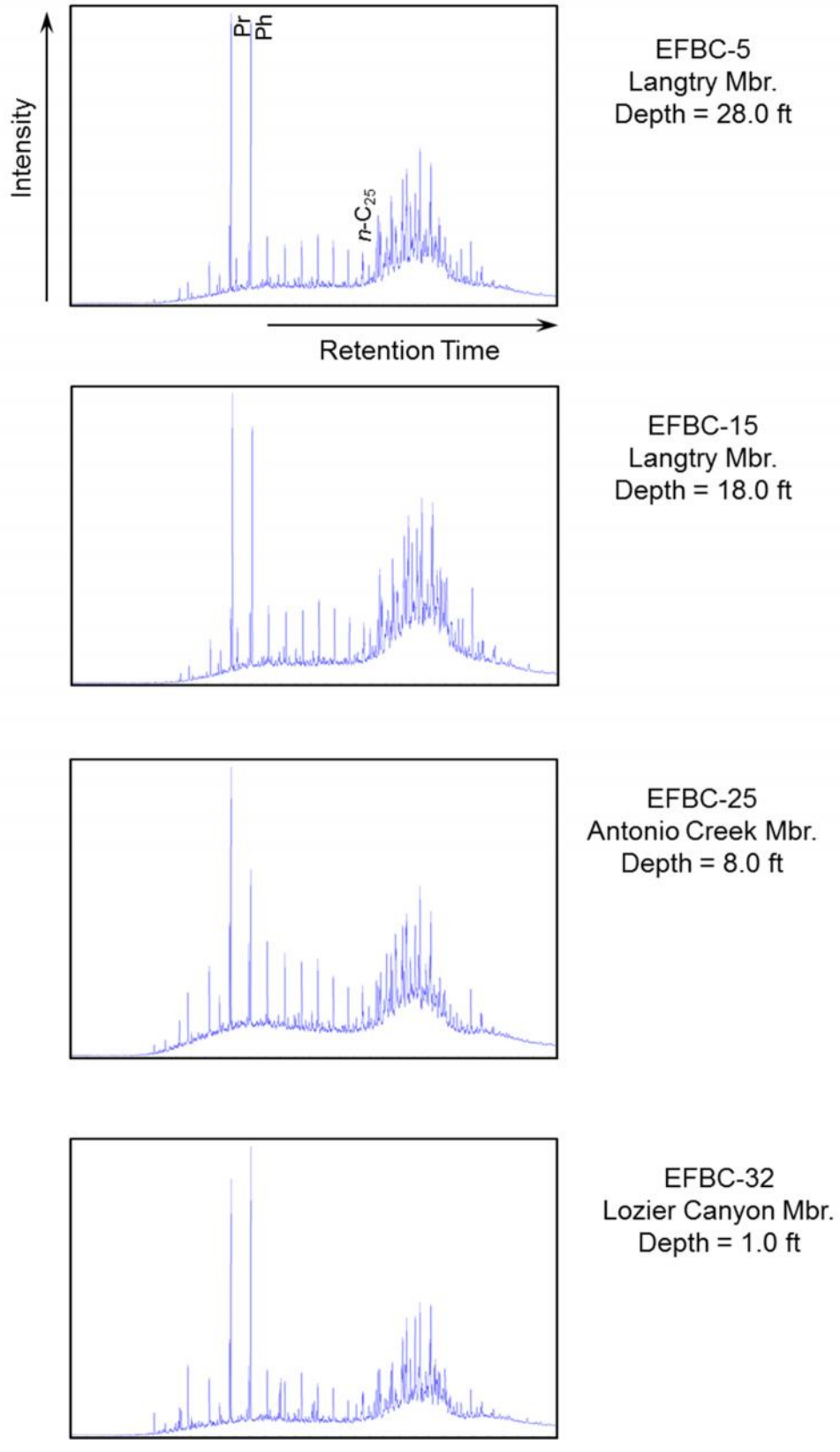

*ACC #1 core*

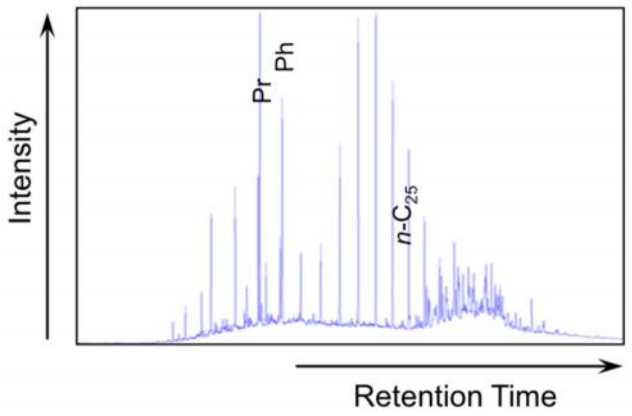


EFAC-3
Langtry Mbr.
Depth = 90.0 ft

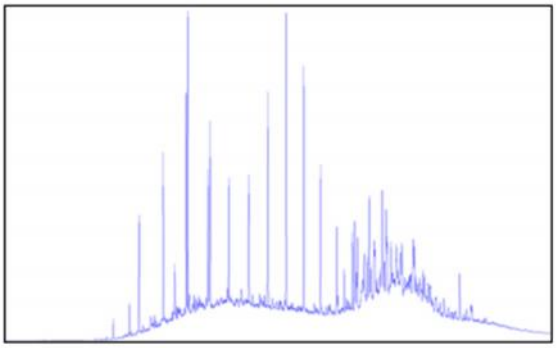

EFAC-6
Antonio Creek Mbr.
Depth = 105.0 ft

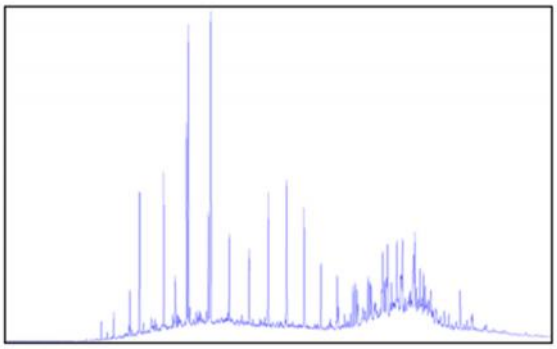

EFAC-7
Lozier Canyon Mbr.
Depth = 110.0 ft

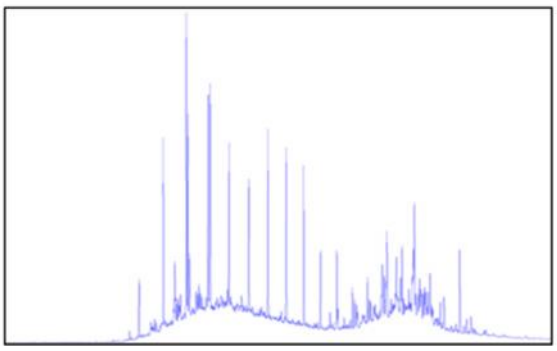

EFAC-10
Lozier Canyon Mbr.
Depth = 124.8 ft

*W. Brechtel #1 core*

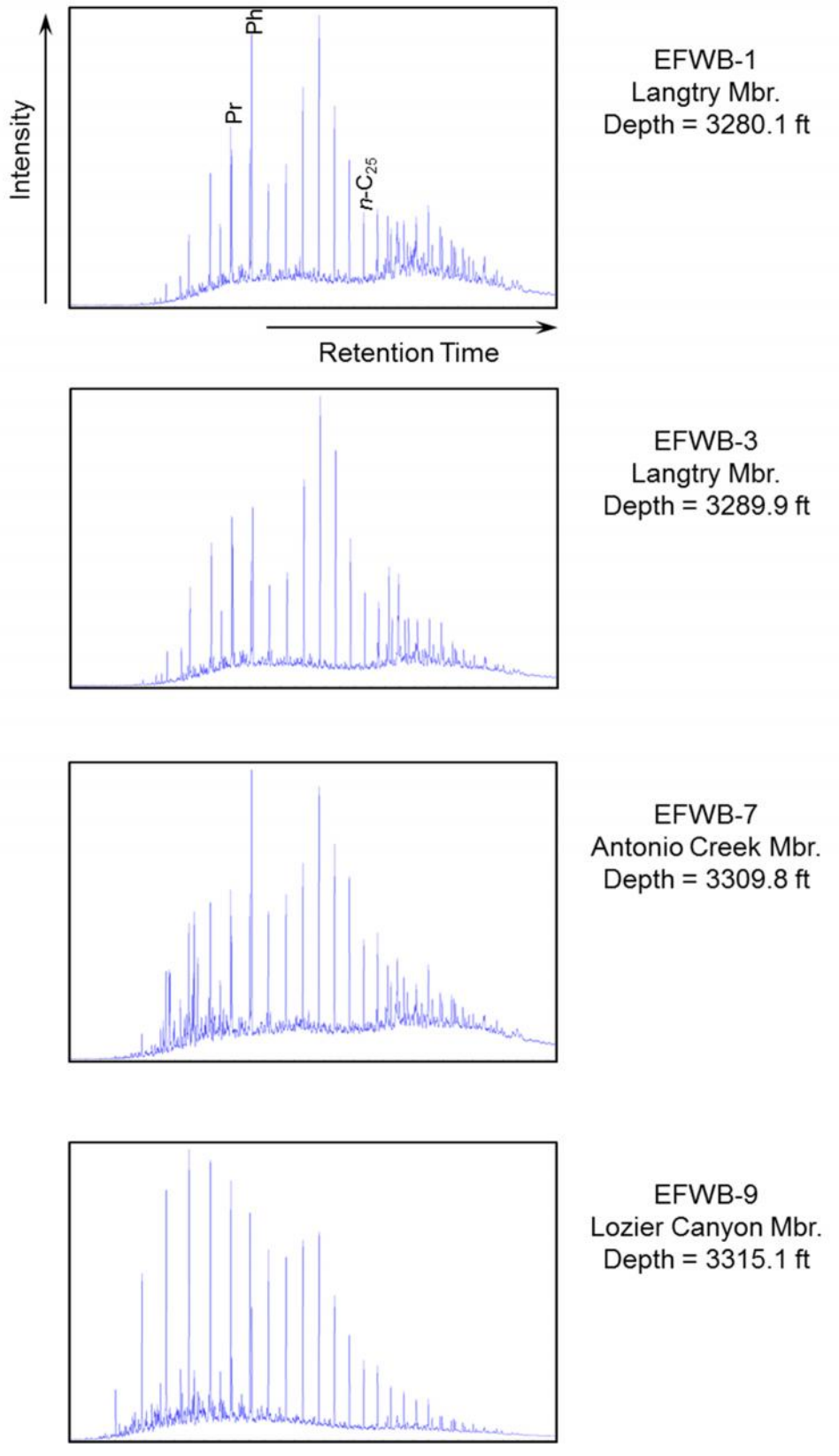

*C. J. Hendershot #1 core*

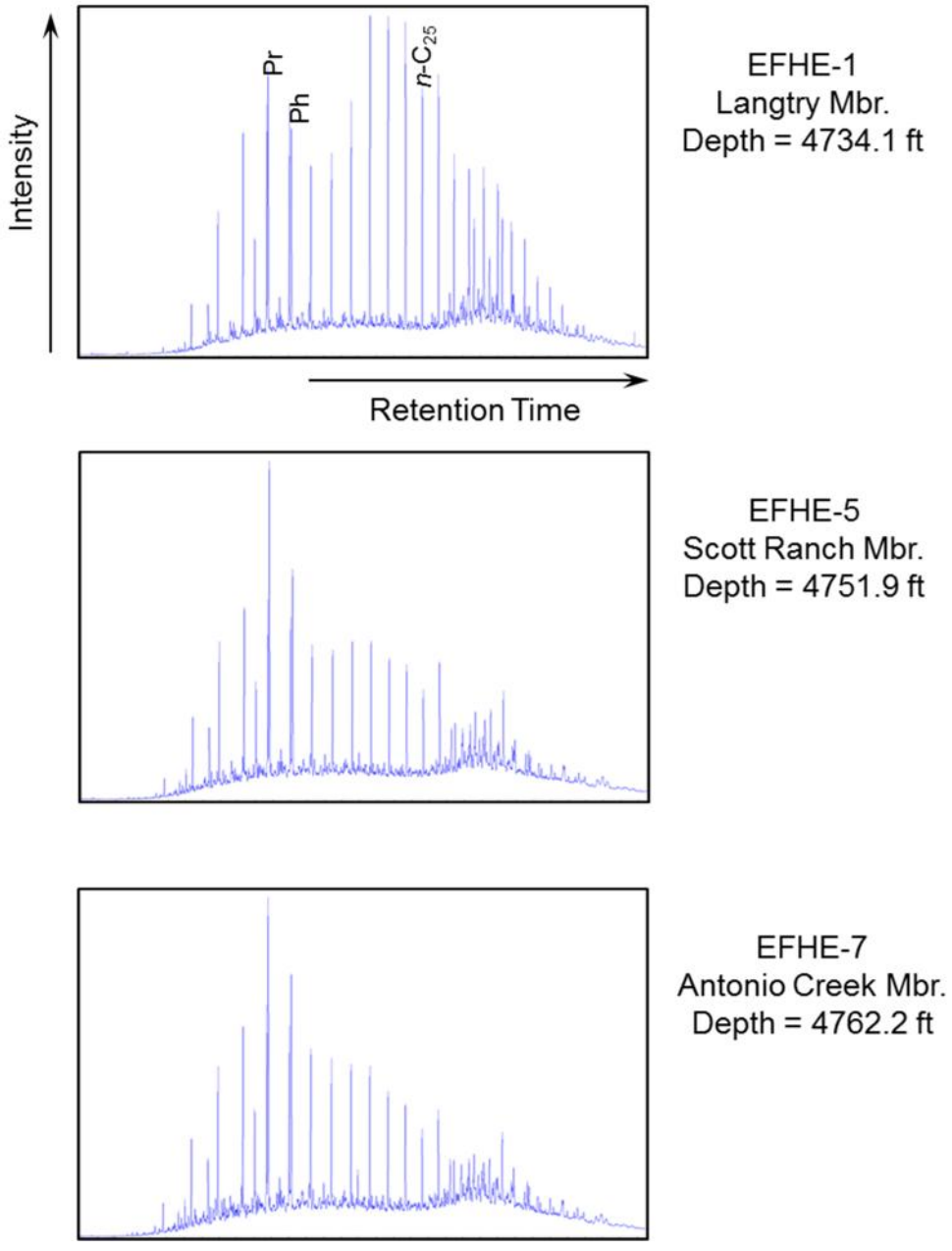

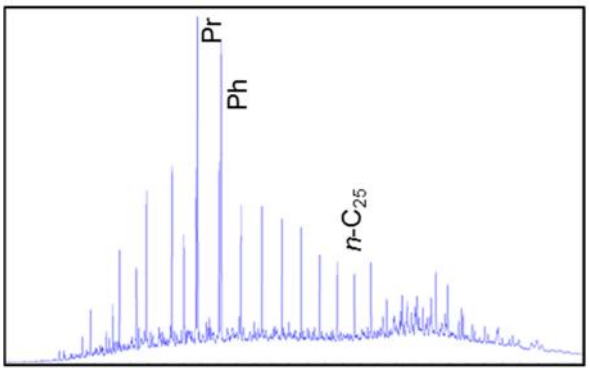


EFHE-9
Lozier Canyon Mbr.
Depth = 4771.0 ft

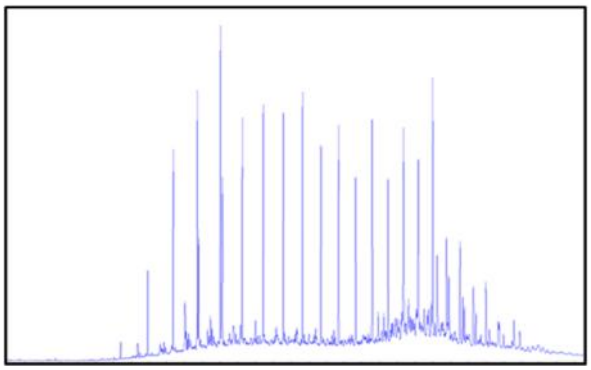

EFHE-10
Lozier Canyon Mbr.
Depth = 4773.8 ft

*Lily Hoppess #1 core*

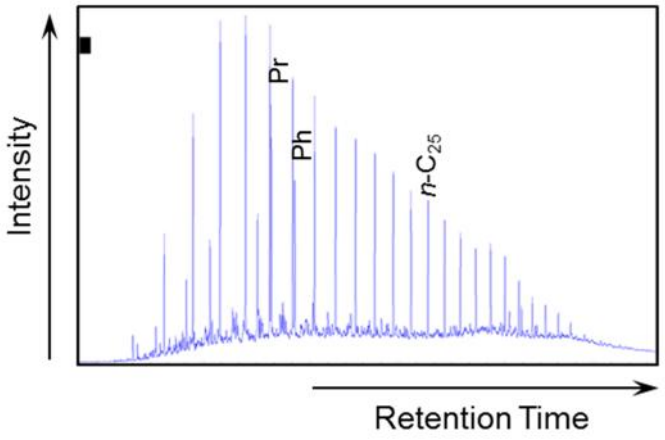


EFLH-9
Lower Eagle Ford Fm.
Depth = 6709 ft

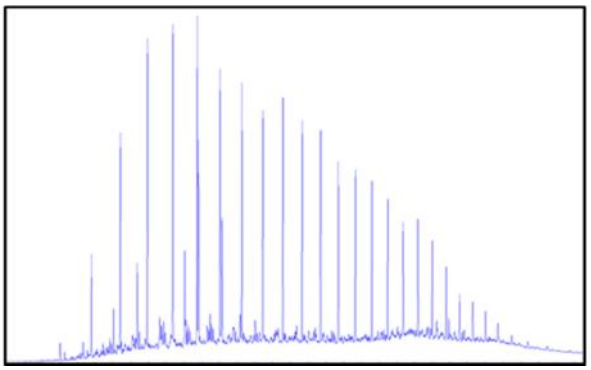

EFLH-15
Maness Shale
Depth = 6754 ft

*NWMK-533.2 oil*

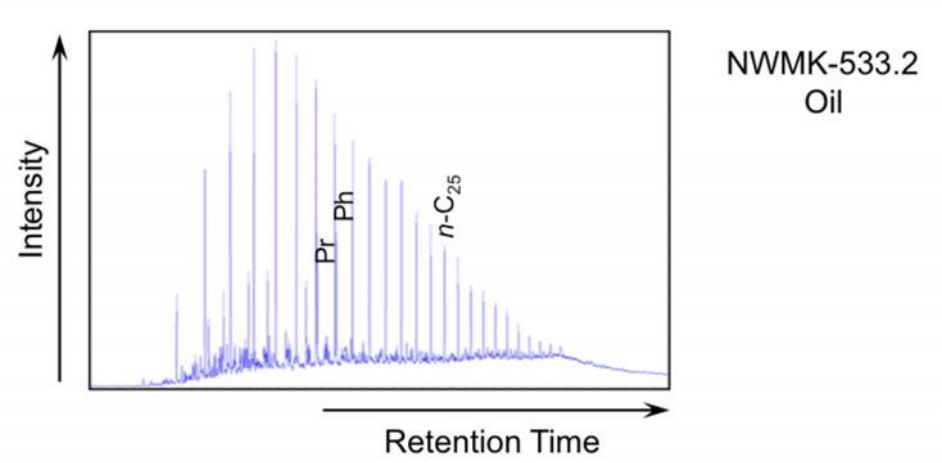


*NFMK 526-1H oil*

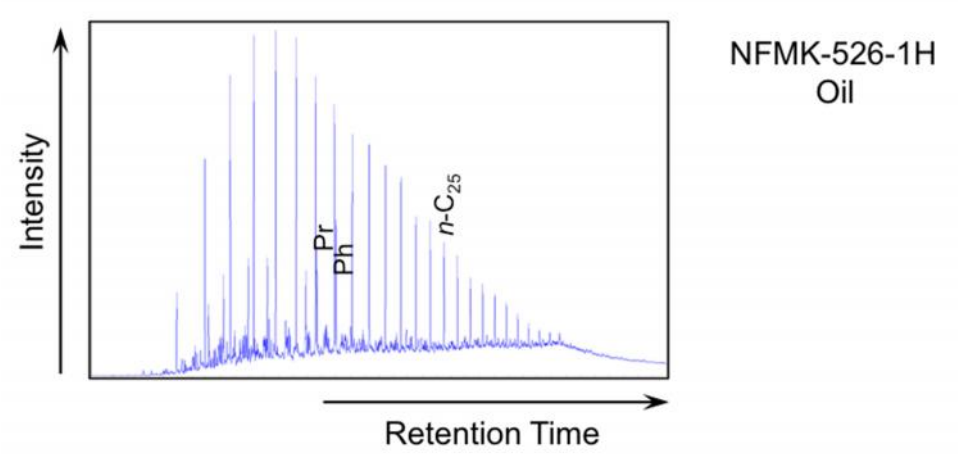

*MJOG-UEF oil*

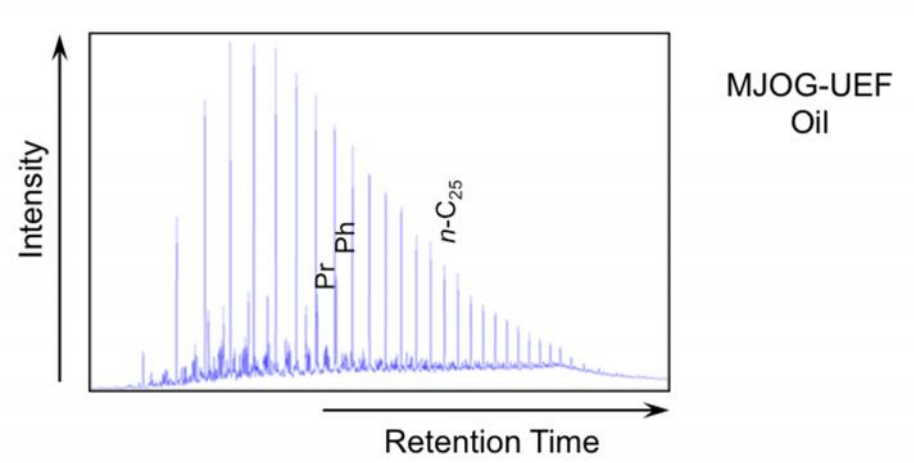


*MJOG-LEF oil*

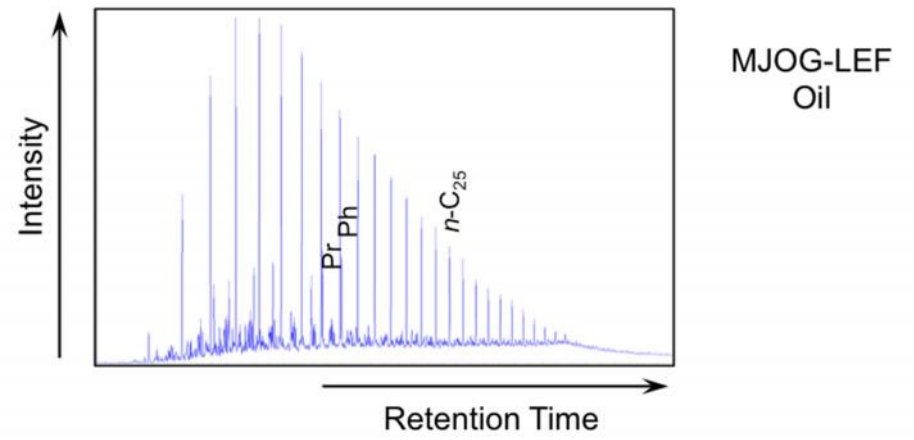

*GREF-1-110 condensate*

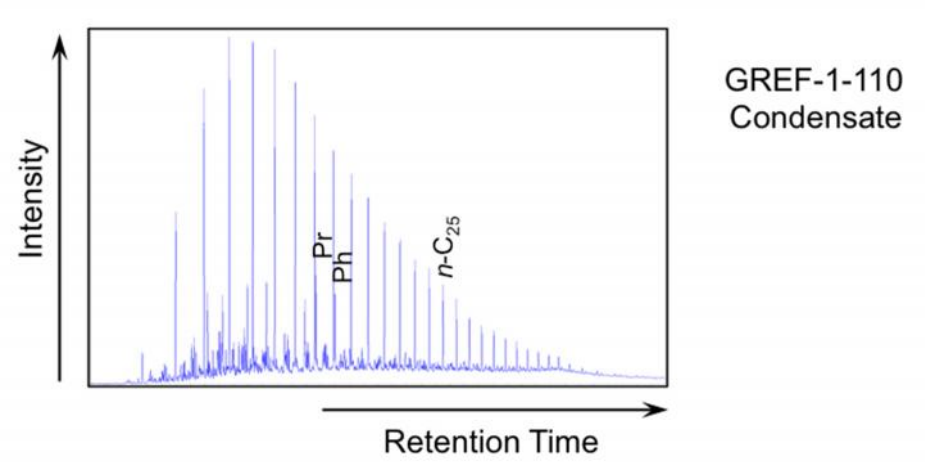

**E. Geochemical ratios of *n*-alkanes and isoprenoids for the saturate fractions of the Eagle Ford Shale bitumen, oil, and condensate samples (ND = not determined)**

*Lozier Canyon outcrop*

| Sample | Depth (ft) | Pr/Ph | Pr/ *n*-$C_{17}$ | Pr/ *n*-$C_{18}$ | Pr/ (Pr+Ph) | TAR | CPI | long/ short chain *n*-alkanes |
|---|---|---|---|---|---|---|---|---|
| EFLC-28 | 130.0 | 0.45 | 1.50 | 2.52 | 0.31 | 1.39 | 0.84 | 2.60 |
| EFLC-26 | 121.5 | 0.42 | 0.94 | 1.78 | 0.30 | 0.38 | 0.82 | 1.23 |
| EFLC-25 | 116.5 | 0.31 | 1.93 | 3.68 | 0.24 | 0.00 | 0.56 | 2.41 |
| EFLC-20 | 89.0 | ND | ND | 3.57 | ND | 1.98 | 0.41 | 5.06 |
| EFLC-19 | 85.0 | ND | ND | ND | ND | ND | 1.12 | 13.97 |
| EFLC-18 | 80.5 | ND | ND | ND | ND | ND | 1.48 | ND |
| EFLC-16 | 70.0 | ND | ND | ND | ND | 27.07 | 1.20 | 15.67 |
| EFLC-14 | 60.0 | 0.30 | 0.78 | 2.18 | 0.23 | 1.45 | 1.06 | 2.11 |
| EFLC-13 | 55.0 | ND | ND | ND | ND | ND | 0.57 | 33.61 |
| EFLC-12 | 50.0 | 0.25 | 0.88 | 2.06 | 0.20 | 3.70 | 0.86 | 4.17 |
| EFLC-11 | 45.0 | 0.25 | 1.36 | 4.08 | 0.20 | 1.86 | 1.02 | 2.52 |
| EFLC-10 | 40.0 | 0.41 | 0.45 | 1.08 | 0.29 | 0.20 | 0.93 | 0.73 |
| EFLC-9 | 35.0 | 0.35 | 0.60 | 1.59 | 0.26 | 0.51 | 1.03 | 1.13 |
| EFLC-8 | 30.0 | 0.36 | 0.40 | 1.05 | 0.27 | 0.22 | 0.95 | 0.76 |
| EFLC-7 | 25.0 | 0.39 | 0.46 | 1.06 | 0.28 | 0.23 | 1.00 | 0.77 |
| EFLC-6 | 20.0 | ND | ND | 5.67 | ND | 15.41 | 1.13 | 9.05 |
| EFLC-5 | 15.0 | 0.22 | 0.75 | 3.10 | 0.18 | 0.99 | 1.15 | 2.88 |
| EFLC-4 | 10.0 | 0.25 | 2.15 | 5.56 | 0.20 | 1.04 | 1.19 | 2.46 |
| EFLC-3 | 9.0 | 0.34 | 0.73 | 1.69 | 0.25 | 2.42 | 1.22 | 2.84 |
| EFLC-1 | 0.0 | 0.42 | 1.13 | 2.42 | 0.30 | 1.48 | 1.04 | 2.49 |

*Ferguson McKnight #526-1H core*

| Sample | Depth (ft) | Pr/Ph | Pr/ *n*-$C_{17}$ | Pr/ *n*-$C_{18}$ | Pr/ (Pr+Ph) | TAR | CPI | long/ short chain *n*-alkanes |
|---|---|---|---|---|---|---|---|---|
| EFMK-1 | 5793.0 | 1.17 | 0.53 | 0.51 | 0.54 | 0.11 | 1.01 | 0.45 |
| EFMK-3 | 5809.0 | 1.34 | 0.51 | 0.48 | 0.57 | 0.11 | 0.96 | 0.44 |
| EFMK-4 | 5817.5 | 1.30 | 0.58 | 0.58 | 0.57 | 0.16 | 0.97 | 0.54 |
| EFMK-5 | 5825.5 | 1.29 | 0.54 | 0.52 | 0.56 | 0.12 | 0.98 | 0.44 |
| EFMK-8 | 5849.0 | 1.40 | 0.55 | 0.50 | 0.58 | 0.15 | 0.98 | 0.53 |
| EFMK-10 | 5864.5 | 1.34 | 0.57 | 0.52 | 0.57 | 0.18 | 0.96 | 0.60 |
| EFMK-12 | 5881.0 | 1.30 | 0.52 | 0.51 | 0.57 | 0.10 | 0.96 | 0.41 |
| EFMK-13 | 5889.0 | 1.42 | 0.58 | 0.53 | 0.59 | 0.16 | 0.98 | 0.56 |
| EFMK-15 | 5905.5 | 1.26 | 0.58 | 0.54 | 0.56 | 0.14 | 0.98 | 0.51 |
| EFMK-16 | 5913.5 | 1.27 | 0.58 | 0.55 | 0.56 | 0.13 | 0.97 | 0.50 |
| EFMK-17 | 5921.0 | 1.14 | 0.49 | 0.51 | 0.53 | 0.10 | 0.99 | 0.41 |
| EFMK-19 | 5937.5 | 1.32 | 0.54 | 0.50 | 0.57 | 0.13 | 0.96 | 0.52 |
| EFMK-20 | 5945.5 | 1.29 | 0.54 | 0.53 | 0.56 | 0.10 | 0.97 | 0.44 |
| EFMK-22 | 5961.0 | 1.20 | 0.54 | 0.54 | 0.55 | 0.12 | 0.99 | 0.49 |
| EFMK-23 | 5969.0 | 1.22 | 0.56 | 0.56 | 0.55 | 0.13 | 0.95 | 0.51 |
| EFMK-24 | 5977.5 | 1.31 | 0.55 | 0.53 | 0.57 | 0.14 | 0.99 | 0.53 |
| EFMK-25 | 6072.0 | 0.98 | 0.54 | 0.60 | 0.50 | 0.15 | 0.95 | 0.57 |
| EFMK-26 | 6174.0 | 0.91 | 0.47 | 0.58 | 0.48 | 0.16 | 0.98 | 0.54 |

*Fasken "A" #1 core*

| Sample | Depth (ft) | Pr/Ph | Pr/ $n$-$C_{17}$ | Pr/ $n$-$C_{18}$ | Pr/ (Pr+Ph) | TAR | CPI | long/ short chain $n$-alkanes |
|---|---|---|---|---|---|---|---|---|
| EFFA-1 | 9430.5 | 0.92 | 0.30 | 0.34 | 0.48 | 0.01 | 1.47 | 0.23 |
| EFFA-3 | 9450.0 | 1.14 | 0.42 | 0.44 | 0.53 | ND | 1.44 | 0.20 |
| EFFA-5 | 9470.5 | 0.95 | 0.36 | 0.41 | 0.49 | ND | 1.55 | 0.23 |
| EFFA-7 | 9489.0 | 1.05 | 0.38 | 0.42 | 0.51 | ND | 1.50 | 0.19 |
| EFFA-11 | 9530.0 | 0.86 | 0.36 | 0.39 | 0.46 | 0.01 | 1.37 | 0.31 |
| EFFA-15 | 9570.5 | 1.23 | 0.43 | 0.43 | 0.55 | 0.01 | 1.27 | 0.20 |
| EFFA-17 | 9589.0 | 1.11 | 0.41 | 0.43 | 0.53 | ND | 1.46 | 0.22 |
| EFFA-18 | 9599.5 | 1.10 | 0.42 | 0.44 | 0.52 | ND | 1.55 | 0.20 |
| EFFA-20 | 9620.5 | 0.94 | 0.44 | 0.48 | 0.48 | 0.01 | 1.28 | 0.32 |
| EFFA-21 | 9629.5 | 1.22 | 0.43 | 0.44 | 0.55 | ND | 1.69 | 0.20 |
| EFFA-22 | 9639.5 | 1.10 | 0.39 | 0.41 | 0.52 | ND | 1.52 | 0.19 |
| EFFA-23 | 9650.5 | 1.16 | 0.38 | 0.39 | 0.54 | ND | 1.50 | 0.21 |
| EFFA-24 | 9655.5 | 1.22 | 0.43 | 0.43 | 0.55 | ND | 1.33 | 0.17 |
| EFFA-26 | 9670.5 | 1.42 | 0.45 | 0.42 | 0.59 | ND | 1.29 | 0.15 |
| EFFA-28 | 9685.5 | 1.24 | 0.42 | 0.41 | 0.55 | ND | 1.63 | 0.18 |
| EFFA-30 | 9700.5 | 1.27 | 0.43 | 0.42 | 0.56 | ND | 1.53 | 0.19 |
| EFFA-32 | 9717.0 | 1.20 | 0.40 | 0.40 | 0.55 | ND | 1.44 | 0.18 |
| EFFA-34 | 9733.5 | 1.29 | 0.44 | 0.43 | 0.56 | ND | 1.21 | 0.16 |
| EFFA-37 | 9756.5 | 1.33 | 0.45 | 0.46 | 0.57 | ND | 1.28 | 0.14 |
| EFFA-38 | 9761.5 | 1.17 | 0.43 | 0.44 | 0.54 | ND | 1.52 | 0.20 |
| EFFA-40 | 9776.0 | 1.08 | 0.42 | 0.44 | 0.52 | ND | 1.49 | 0.23 |

*Bouldin Creek outcrop*

| Sample | Depth (ft) | Pr/Ph | Pr/ *n*-$C_{17}$ | Pr/ *n*-$C_{18}$ | Pr/ (Pr+Ph) | TAR | CPI | long/ short chain *n*-alkanes |
|---|---|---|---|---|---|---|---|---|
| EFBC-5 | 28.0 | 1.00 | 4.27 | 7.12 | 0.50 | ND | 0.56 | 1.01 |
| EFBC-6 | 27.0 | 1.22 | 3.52 | 5.73 | 0.55 | ND | ND | 0.67 |
| EFBC-7 | 26.0 | 0.90 | 4.30 | 7.49 | 0.47 | ND | ND | 0.93 |
| EFBC-8 | 25.0 | 1.05 | 3.36 | 5.16 | 0.51 | ND | ND | 0.74 |
| EFBC-9 | 24.0 | 1.12 | 3.56 | 5.61 | 0.53 | ND | ND | 0.76 |
| EFBC-10 | 23.0 | 1.02 | 4.39 | 5.60 | 0.51 | ND | ND | 0.91 |
| EFBC-11 | 22.0 | 1.02 | 4.52 | 7.48 | 0.51 | ND | ND | 1.00 |
| EFBC-12 | 21.0 | 0.92 | 4.41 | 6.83 | 0.48 | ND | ND | 0.83 |
| EFBC-13 | 20.0 | 1.30 | 4.42 | 5.76 | 0.56 | ND | ND | 0.70 |
| EFBC-14 | 19.0 | 1.26 | 4.21 | 5.48 | 0.56 | ND | ND | 0.76 |
| EFBC-15 | 18.0 | 1.15 | 4.80 | 5.23 | 0.53 | ND | ND | 0.89 |
| EFBC-16 | 17.0 | 1.24 | 4.76 | 5.47 | 0.55 | ND | ND | 0.94 |
| EFBC-17 | 16.0 | 0.96 | 5.62 | 6.94 | 0.49 | ND | ND | 1.01 |
| EFBC-18 | 15.0 | 1.24 | 3.75 | 5.29 | 0.55 | ND | ND | 0.65 |
| EFBC-19 | 14.0 | 1.44 | 4.21 | 3.55 | 0.59 | ND | ND | 0.79 |
| EFBC-20 | 13.0 | 1.80 | 3.22 | 2.11 | 0.64 | ND | ND | 0.82 |
| EFBC-23 | 10.0 | 1.48 | 2.35 | 1.63 | 0.60 | ND | ND | 0.62 |
| EFBC-24 | 9.0 | 1.22 | 4.30 | 3.72 | 0.55 | ND | 0.61 | 1.09 |
| EFBC-25 | 8.0 | 1.73 | 2.59 | 2.15 | 0.63 | ND | ND | 0.55 |
| EFBC-27 | 6.0 | 1.92 | 1.97 | 1.47 | 0.66 | ND | ND | 0.52 |
| EFBC-30 | 3.0 | 1.09 | 2.23 | 3.62 | 0.52 | ND | ND | 0.47 |
| EFBC-31 | 2.0 | 0.84 | 2.80 | 6.09 | 0.46 | ND | ND | 0.49 |
| EFBC-32 | 1.0 | 0.87 | 3.02 | 5.73 | 0.46 | ND | ND | 0.47 |
| EFBC-33 | 0.0 | 0.94 | 3.51 | 6.04 | 0.49 | ND | ND | 0.43 |
| EFBC-34 | -1.0 | 0.75 | 3.33 | 6.30 | 0.43 | ND | ND | 0.41 |

*ACC#1 core*

| Sample | Depth (ft) | Pr/Ph | Pr/ *n*-$C_{17}$ | Pr/ *n*-$C_{18}$ | Pr/ (Pr+Ph) | TAR | CPI | long/ short chain *n*-alkanes |
|---|---|---|---|---|---|---|---|---|
| EFAC-1 | 80.0 | 1.08 | 1.30 | 1.49 | 0.52 | ND | 1.07 | 3.87 |
| EFAC-2 | 85.0 | 1.26 | 1.87 | 2.20 | 0.56 | ND | 0.99 | 2.33 |
| EFAC-3 | 90.0 | 1.36 | 2.18 | 3.05 | 0.58 | ND | 1.03 | 1.81 |
| EFAC-4 | 95.0 | 0.97 | 2.52 | 4.64 | 0.49 | ND | 0.98 | 2.62 |
| EFAC-5 | 100.5 | 1.53 | 1.83 | 1.91 | 0.60 | ND | 0.92 | 1.80 |
| EFAC-6 | 105.0 | 1.55 | 1.52 | 1.64 | 0.61 | ND | 0.80 | 1.06 |
| EFAC-7 | 110.0 | 0.94 | 1.57 | 3.41 | 0.49 | ND | 0.90 | 0.68 |
| EFAC-8 | 114.8 | 0.77 | 2.38 | 5.96 | 0.44 | ND | 0.92 | 0.68 |
| EFAC-9 | 120.0 | 0.91 | 0.34 | 0.46 | 0.48 | ND | 1.10 | 0.63 |
| EFAC-10 | 124.8 | 0.90 | 0.78 | 1.25 | 0.47 | ND | 1.29 | 0.61 |



*W. Brechtel #1 core*

| Sample | Depth (ft) | Pr/Ph | Pr/ *n*-$C_{17}$ | Pr/ *n*-$C_{18}$ | Pr/ (Pr+Ph) | TAR | CPI | long/ short chain *n*-alkanes |
|---|---|---|---|---|---|---|---|---|
| EFWB-1 | 3280.1 | 0.52 | 1.06 | 2.46 | 0.34 | ND | 0.67 | 1.11 |
| EFWB-2 | 3285.0 | 0.65 | 1.29 | 2.71 | 0.40 | ND | 0.83 | 1.94 |
| EFWB-3 | 3289.9 | 0.70 | 0.99 | 1.99 | 0.41 | ND | 0.78 | 1.22 |
| EFWB-4 | 3295.0 | 0.71 | 0.90 | 1.74 | 0.41 | ND | 0.77 | 1.32 |
| EFWB-5 | 3300.0 | 0.57 | 1.02 | 2.51 | 0.36 | ND | 0.76 | 1.45 |
| EFWB-6 | 3304.9 | 0.67 | 0.90 | 1.85 | 0.40 | ND | 0.76 | 1.47 |
| EFWB-7 | 3309.8 | 0.35 | 0.80 | 2.51 | 0.26 | ND | 0.64 | 0.95 |
| EFWB-8 | 3313.0 | 0.45 | 1.10 | 2.70 | 0.31 | ND | 0.61 | 0.99 |
| EFWB-9 | 3315.1 | 0.50 | 0.30 | 0.70 | 0.33 | 0.10 | 0.82 | 0.60 |

*C.J. Hendershot #1 core*

| Sample | Depth (ft) | Pr/Ph | Pr/ *n*-$C_{17}$ | Pr/ *n*-$C_{18}$ | Pr/ (Pr+Ph) | TAR | CPI | long/ short chain *n*-alkanes |
|---|---|---|---|---|---|---|---|---|
| EFHE-1 | 4734.1 | 1.25 | 1.40 | 1.10 | 0.35 | N/D | 0.66 | 1.31 |
| EFHE-2 | 4736.8 | 1.14 | 1.56 | 1.20 | 0.50 | N/D | 0.49 | 0.73 |
| EFHE-3 | 4742.1 | 1.39 | 2.01 | 1.77 | 0.48 | N/D | 0.53 | 0.63 |
| EFHE-4 | 4747.0 | 1.72 | 2.76 | 1.90 | 0.42 | N/D | 0.55 | 0.89 |
| EFHE-5 | 4751.9 | 1.48 | 2.16 | 1.75 | 0.47 | N/D | 0.56 | 0.71 |
| EFHE-6 | 4756.9 | 1.47 | 1.86 | 1.58 | 0.52 | N/D | 0.59 | 0.53 |
| EFHE-7 | 4762.2 | 1.35 | 1.85 | 1.61 | 0.49 | N/D | 0.62 | 0.61 |
| EFHE-8 | 4768.9 | 1.11 | 1.95 | 1.89 | 0.53 | N/D | 0.67 | 0.50 |
| EFHE-9 | 4771.0 | 1.06 | 2.22 | 2.08 | 0.53 | N/D | 0.67 | 0.52 |
| EFHE-10 | 4773.8 | 0.67 | 0.52 | 0.63 | 0.48 | 0.71 | 0.65 | 1.51 |

*Lily Hoppess #1 core*

| Sample | Depth (ft) | Pr/Ph | Pr/ *n*-$C_{17}$ | Pr/ *n*-$C_{18}$ | Pr/ (Pr+Ph) | TAR | CPI | long/ short chain *n*-alkanes |
|---|---|---|---|---|---|---|---|---|
| EFLH-1 | 6640.0 | 1.52 | 1.04 | 0.89 | 0.60 | 0.26 | 1.05 | 0.72 |
| EFLH-3 | 6656.0 | 1.47 | 1.04 | 0.88 | 0.59 | 0.29 | 1.10 | 0.75 |
| EFLH-5 | 6672.0 | 1.42 | 0.95 | 0.85 | 0.59 | 0.31 | 1.08 | 0.79 |
| EFLH-7 | 6688.0 | 1.54 | 0.85 | 0.72 | 0.61 | 0.25 | 1.05 | 0.68 |
| EFLH-9 | 6704.0 | 1.44 | 0.87 | 0.73 | 0.59 | 0.32 | 1.06 | 0.80 |
| EFLH-11 | 6719.0 | 1.24 | 0.70 | 0.71 | 0.55 | 0.42 | 1.05 | 0.93 |
| EFLH-13 | 6735.0 | 1.32 | 0.52 | 0.44 | 0.57 | 0.58 | 1.12 | 1.12 |
| EFLH-15 | 6754.0 | 1.54 | 0.70 | 0.55 | 0.61 | 0.43 | 1.06 | 0.97 |
| EFLH-16 | 6764.0 | 1.23 | 0.50 | 0.46 | 0.55 | 0.56 | 1.13 | 1.14 |
| EFLH-18 | 6784.0 | 1.48 | 0.62 | 0.49 | 0.60 | 0.57 | 1.12 | 1.16 |
| EFLH-20 | 6804.0 | 1.45 | 0.68 | 0.58 | 0.59 | 0.36 | 1.08 | 0.85 |



*Oils and condensates*

| Sample | Pr/ Ph | Pr/ *n*-$C_{17}$ | Pr/ *n*-$C_{18}$ | Pr/ (Pr+Ph) | TAR | CPI | long/ short chain *n*-alkanes |
|---|---|---|---|---|---|---|---|
| NWMK-533.2 | 1.07 | 0.56 | 0.64 | 0.74 | 0.23 | 0.99 | 0.71 |
| NFMK-526-1H | 0.80 | 0.46 | 0.66 | 0.74 | 0.21 | 0.98 | 0.66 |
| MJOG-UEF | 0.80 | 0.35 | 0.49 | 0.78 | 0.23 | 0.97 | 0.68 |
| MJOG-LEF | 1.14 | 0.43 | 0.46 | 0.77 | 0.21 | 1.00 | 0.65 |
| GREF-1-110 | 1.25 | 0.45 | 0.43 | 0.77 | 0.18 | 1.04 | 0.57 |

## F. Geochemical logs of biomarker ratios of steranes for the Eagle Ford Shale bitumens analyzed

*Ferguson McKnight #526-1H core*

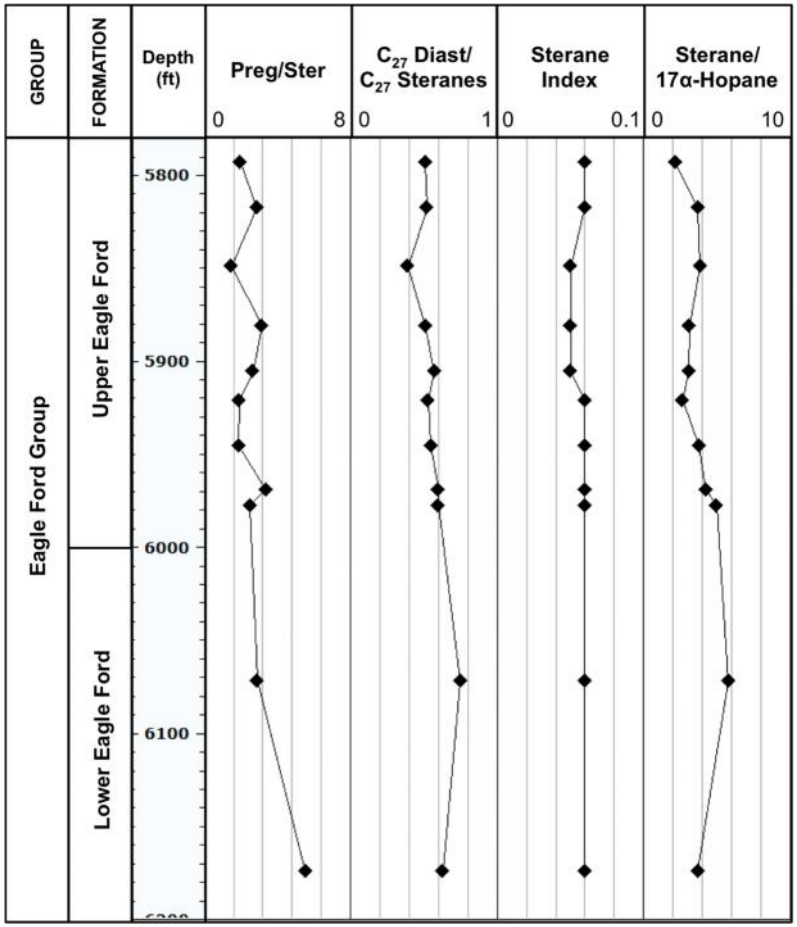

*Fasken "A" #1*

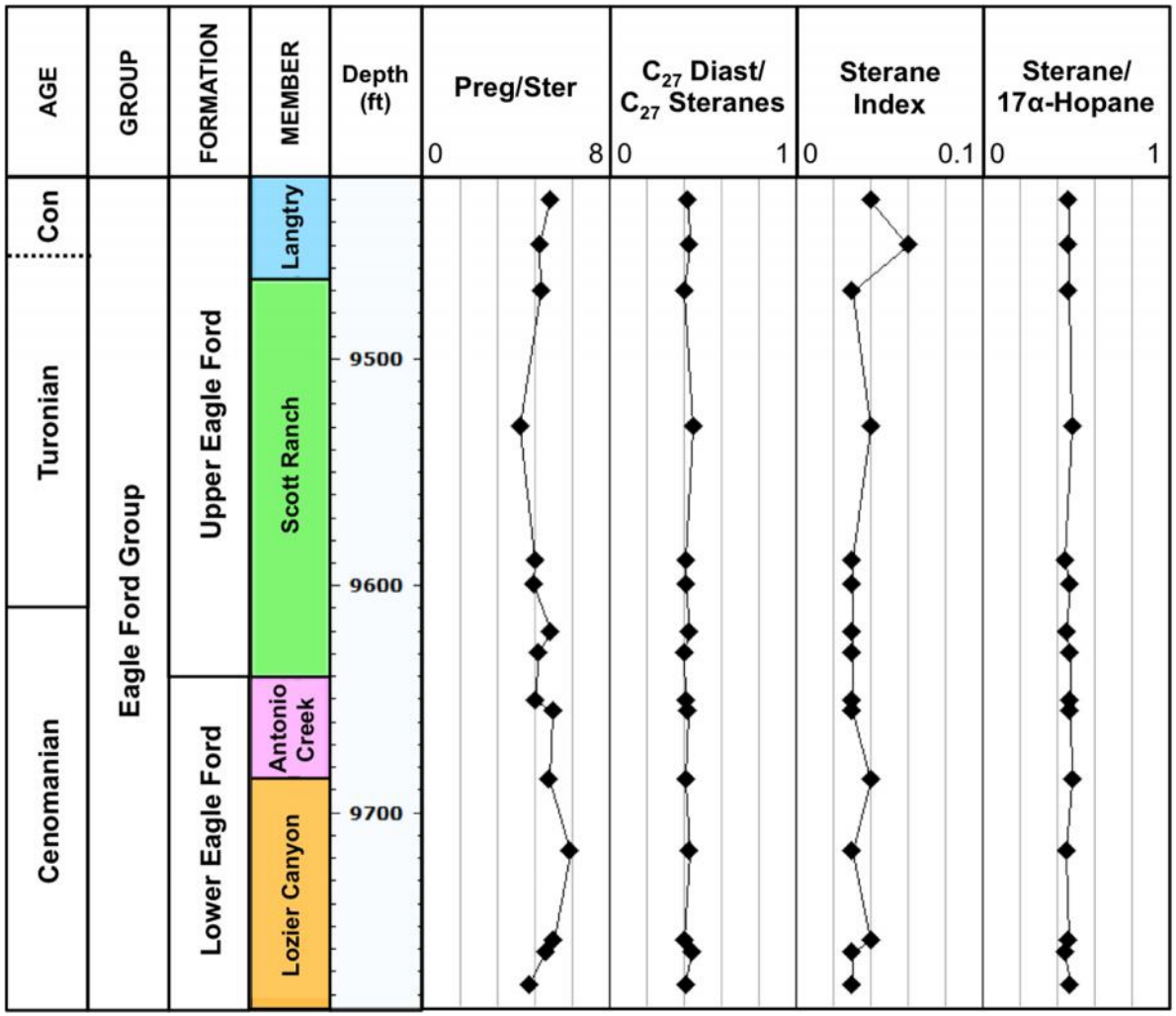
AGE
GROUP
FORMATION
MEMBER
Depth (ft)
Preg/Ster
0
8
C27 Diast/ C27 Steranes
0
1
Sterane Index
0
0.1
Sterane/ 17α-Hopane
0
1
Con
Turonian
Cenomanian
Eagle Ford Group
Upper Eagle Ford
Lower Eagle Ford
Langtry
Scott Ranch
Antonio Creek
Lozier Canyon
9500
9600
9700

*Bouldin Creek outcrop*

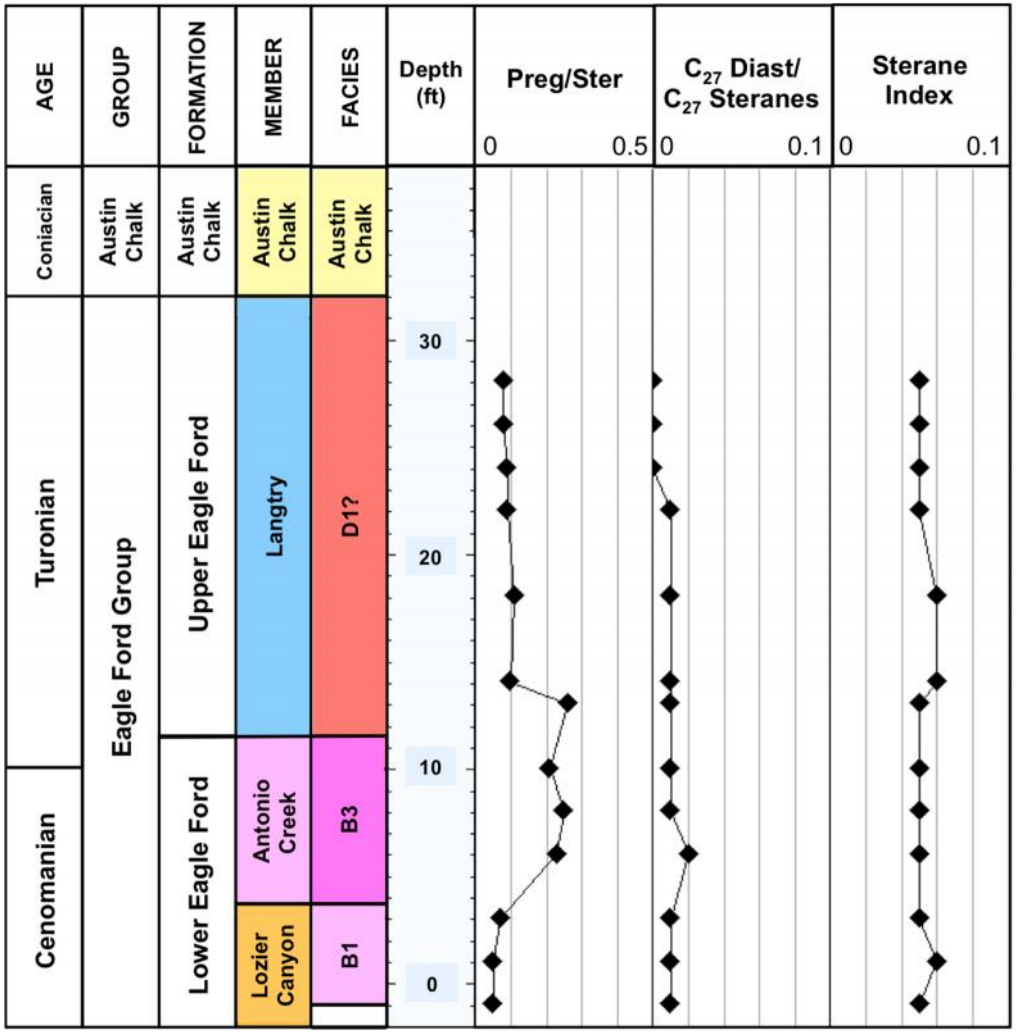

*ACC #1 core*

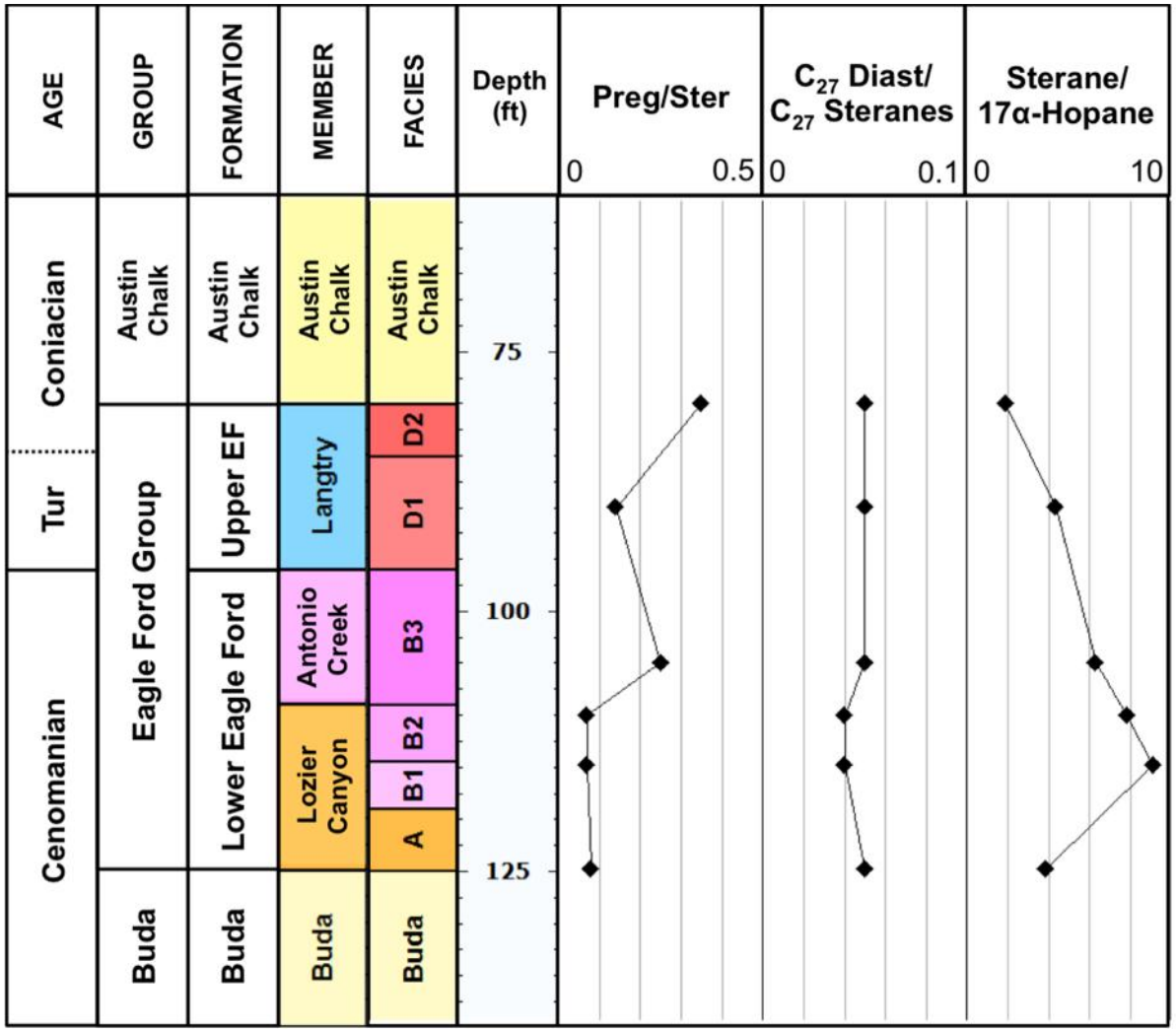
AGE
GROUP
FORMATION
MEMBER
FACIES
Depth (ft)
Preg/Ster
0
0.5
$C_{27}$ Diast/ $C_{27}$ Steranes
0
0.1
Sterane/ 17α-Hopane
0
10
Cenomanian
Coniacian
Tur
Buda
Eagle Ford Group
Austin Chalk
Lower Eagle Ford
Upper EF
Lozier Canyon
Antonio Creek
Langtry
A
B1
B2
B3
D1
D2
75
100
125

*W. Brechtel #1 core*

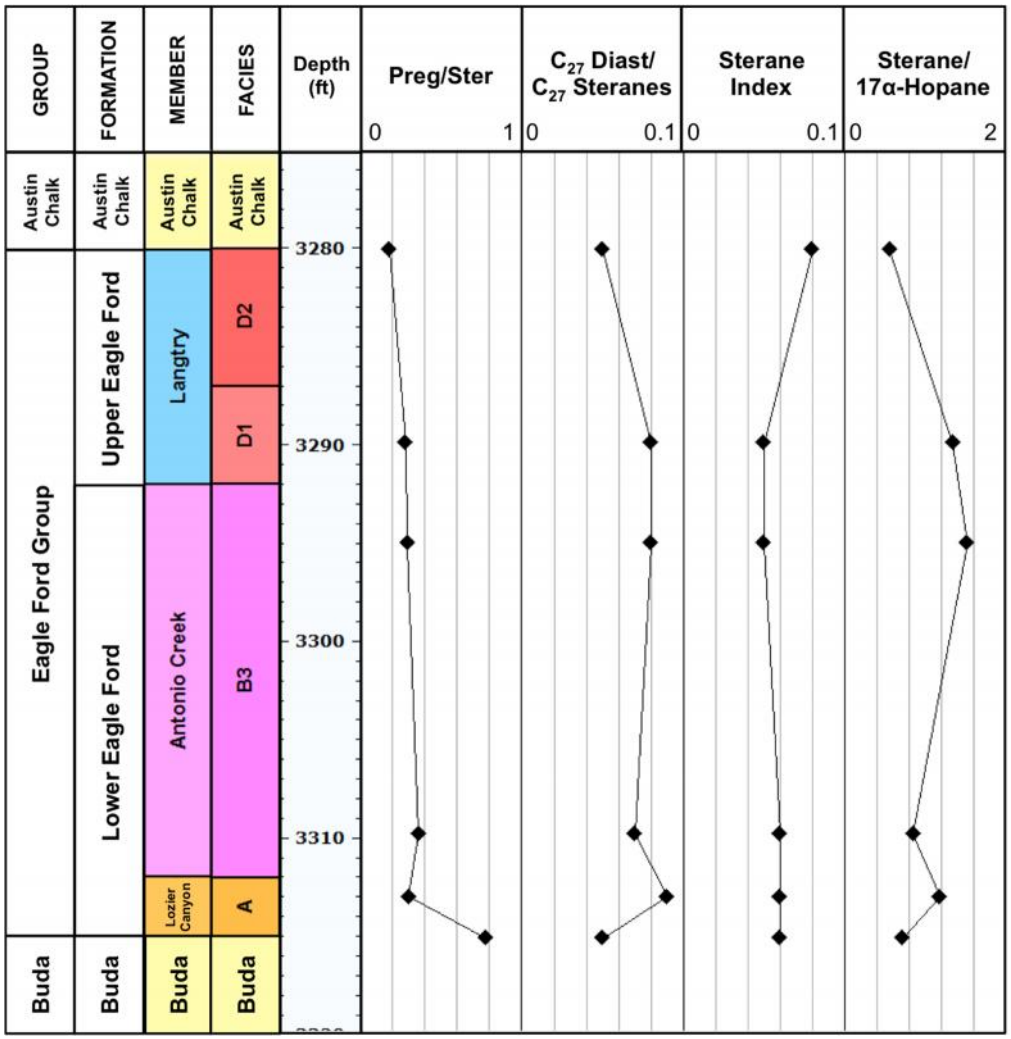

*C. J. Hendershot #1 core*

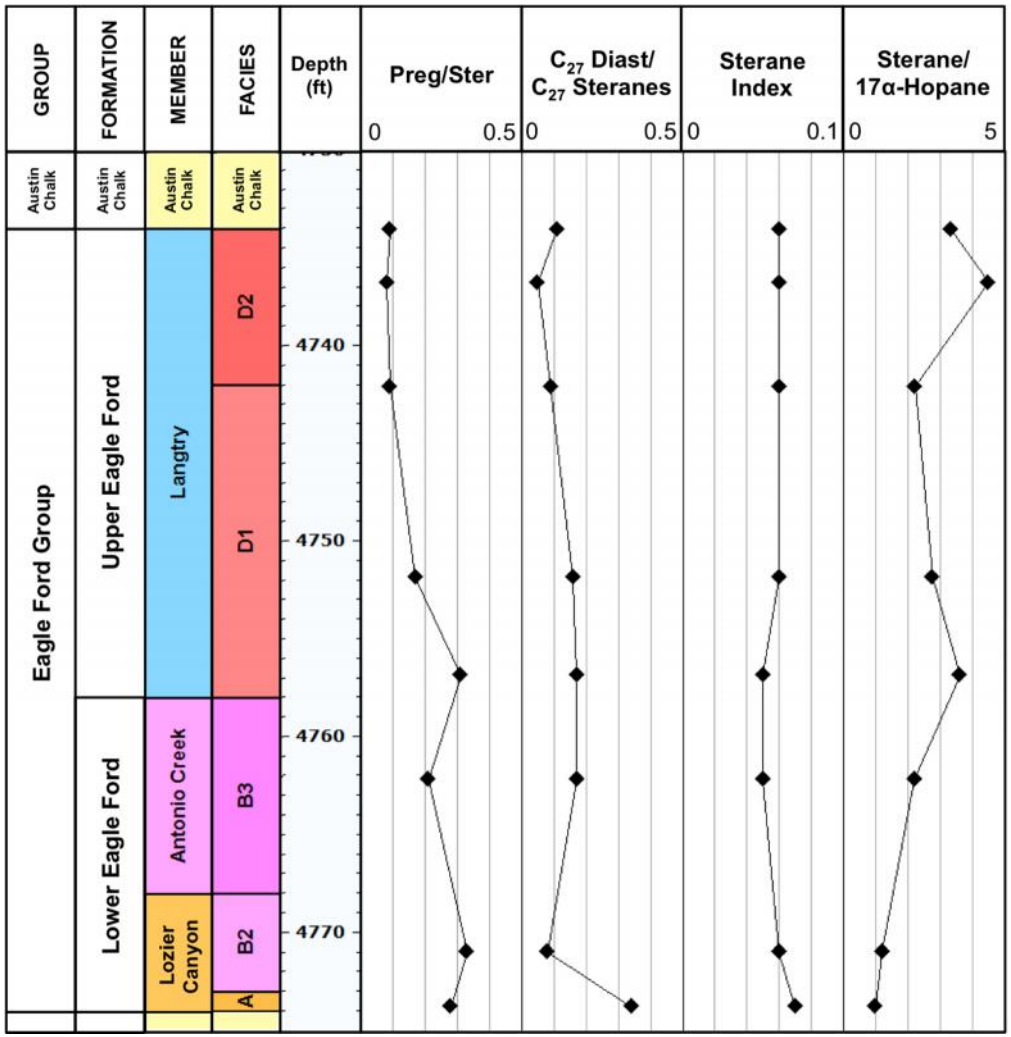

*Lily Hoppess #1 core*

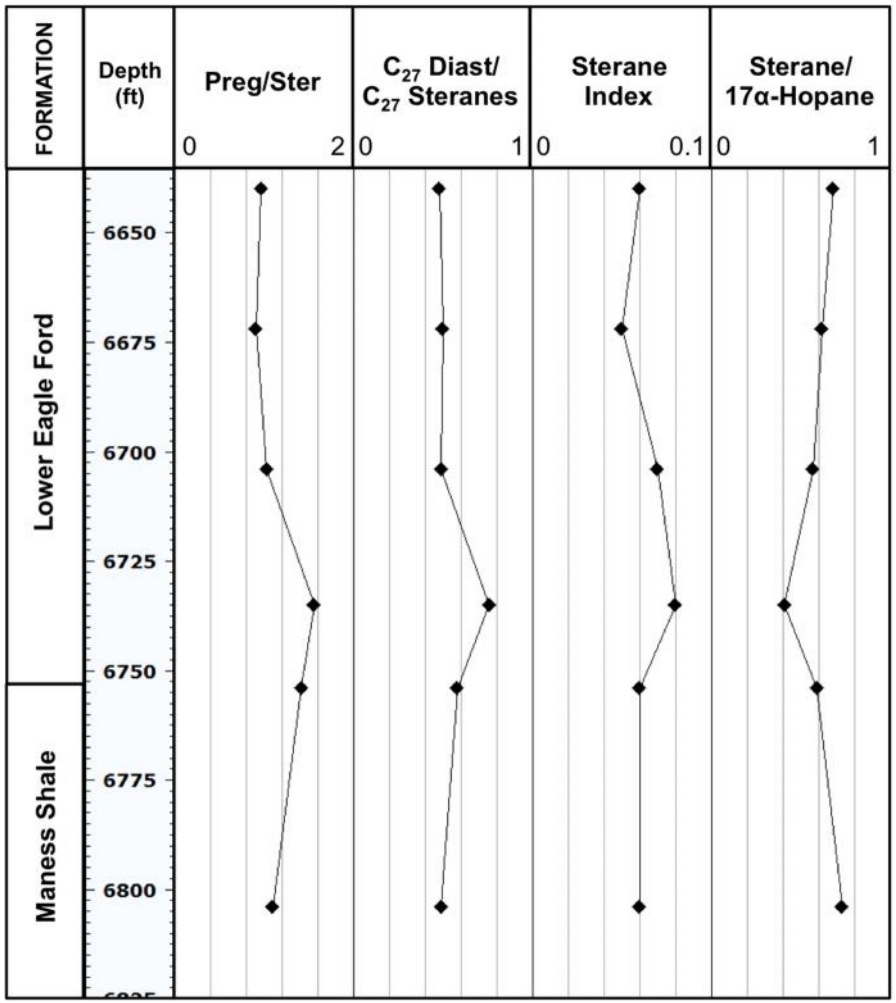

## G. Geochemical logs of biomarker ratios of terpanes for the Eagle Ford Shale bitumens analyzed

*Ferguson McKnight #526-1H core*

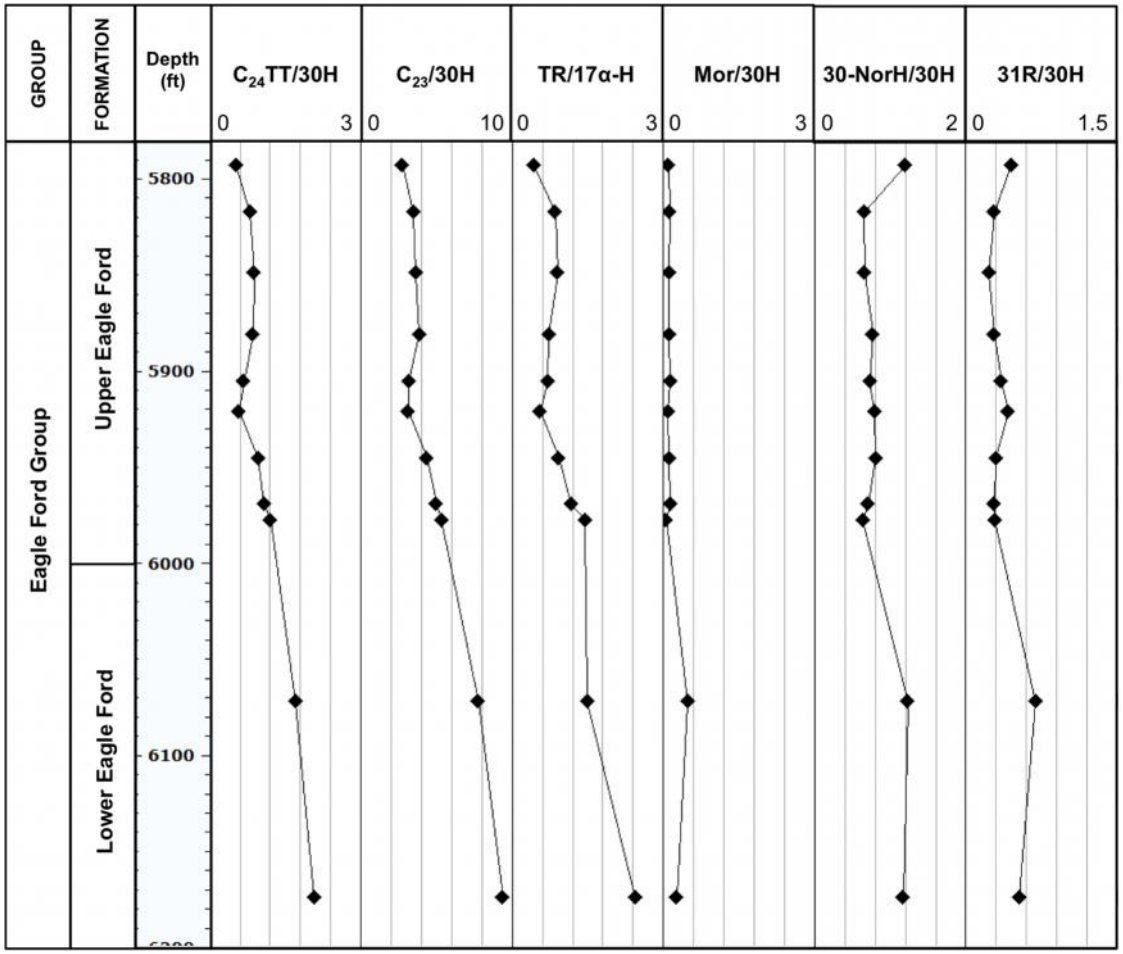

*Fasken "A" #1*

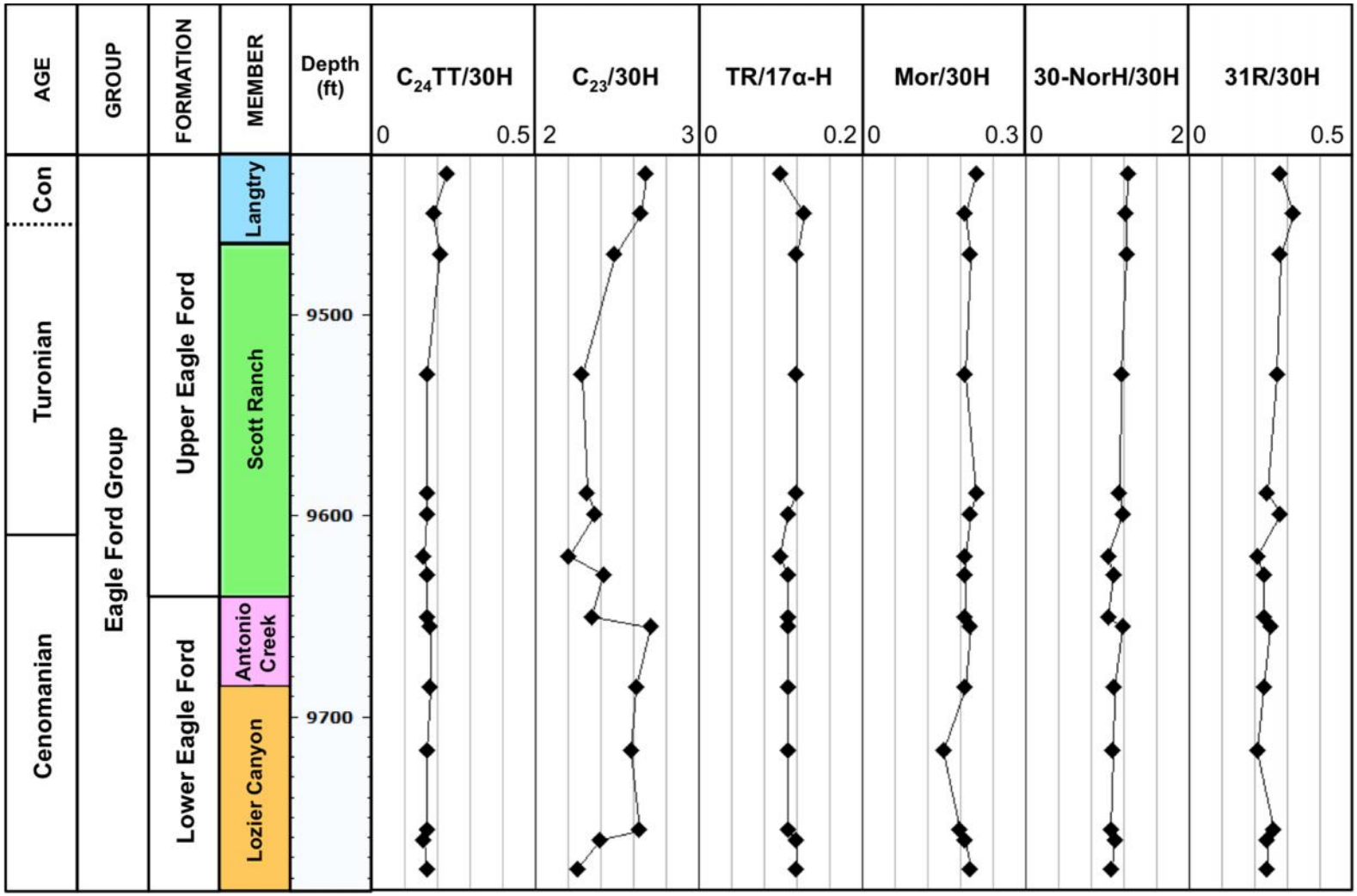
AGE
GROUP
FORMATION
MEMBER
Depth (ft)
Con
Turonian
Cenomanian
Eagle Ford Group
Upper Eagle Ford
Lower Eagle Ford
Langtry
Scott Ranch
Antonio Creek
Lozier Canyon
9500
9600
9700
C24TT/30H
0
0.5
C23/30H
2
3
TR/17α-H
0
0.2
Mor/30H
0
0.3
30-NorH/30H
0
2
31R/30H
0
0.5

*Bouldin Creek outcrop*

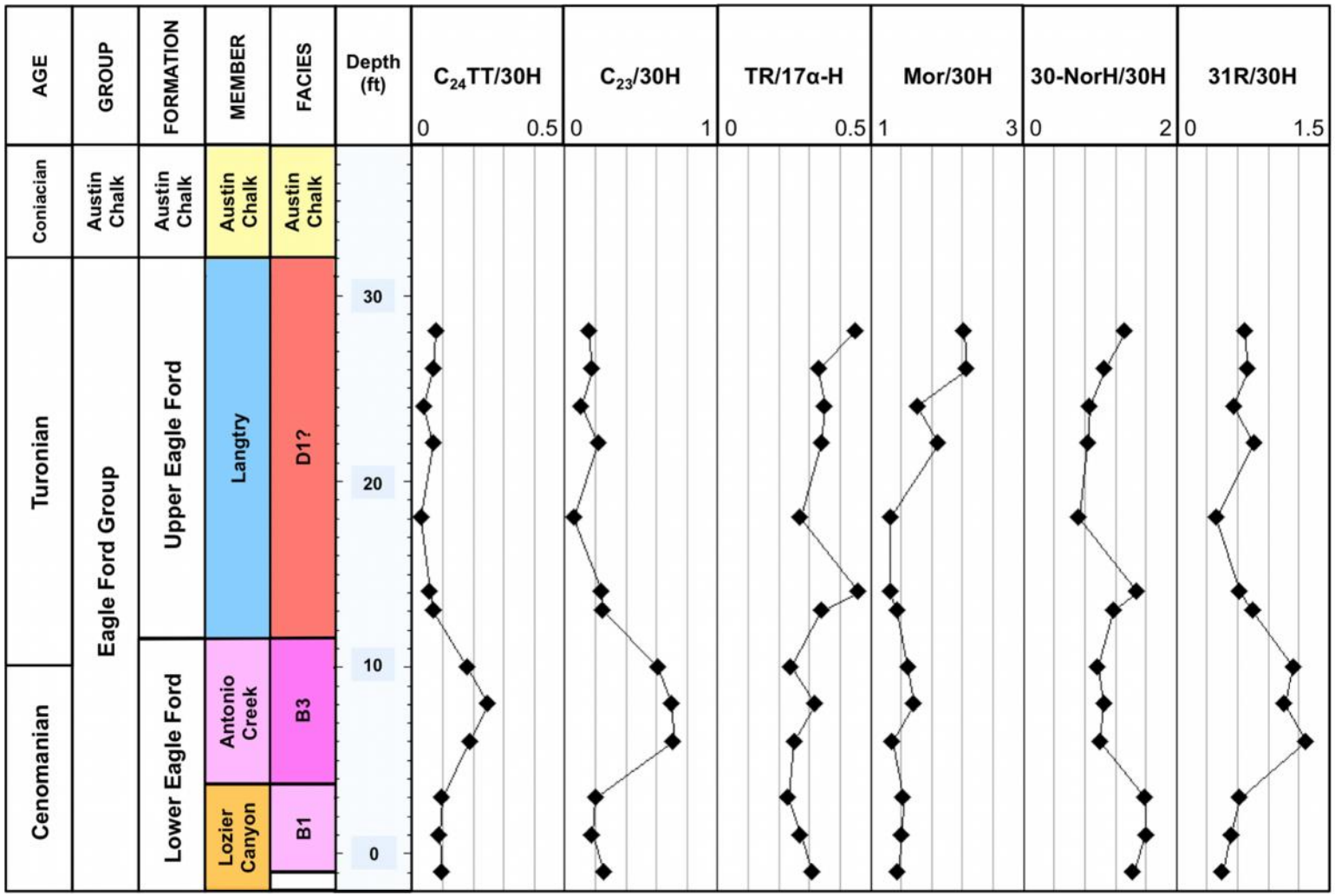

*ACC #1 core*

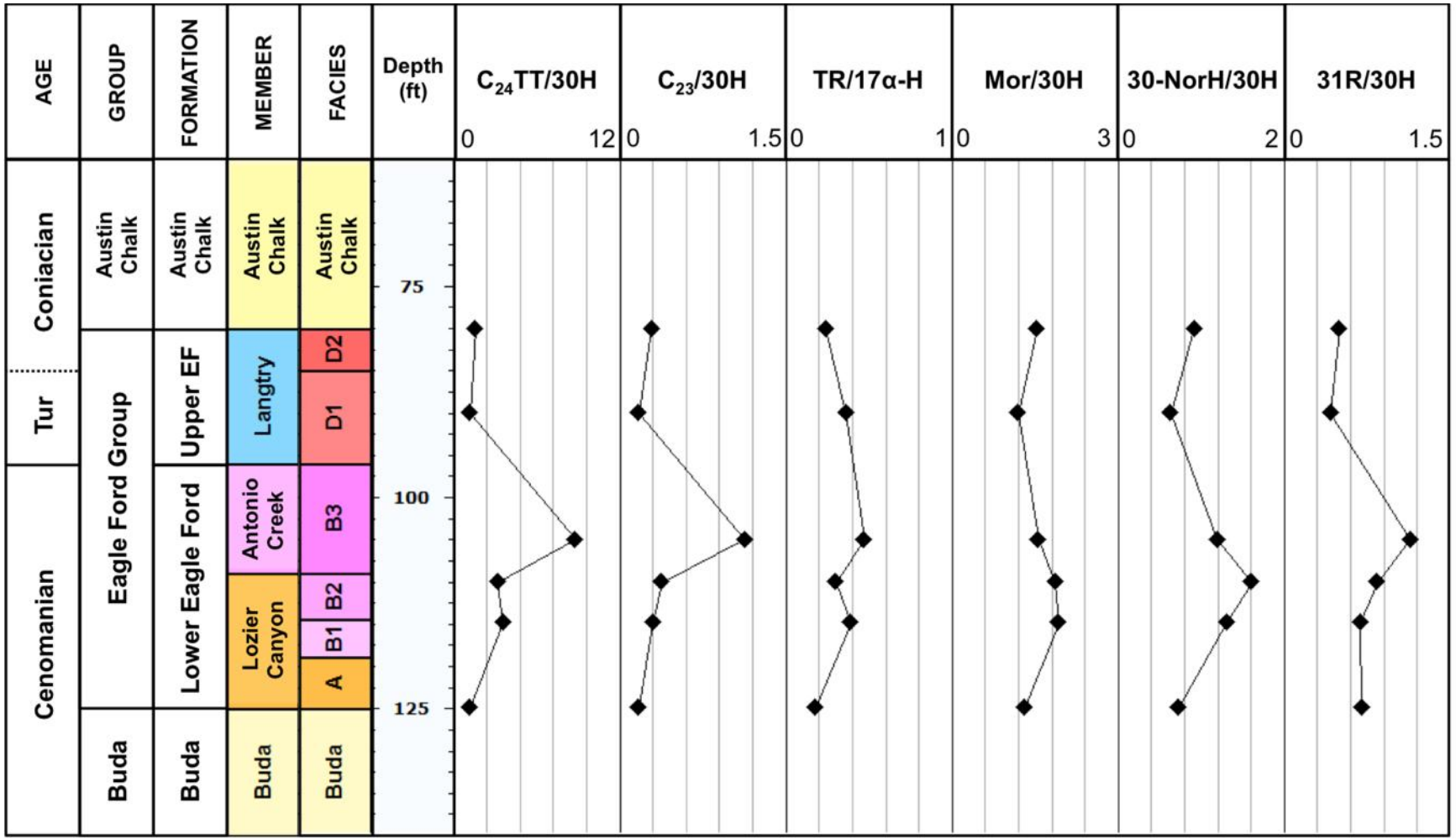
AGE
GROUP
FORMATION
MEMBER
FACIES
Depth (ft)
Cenomanian
Coniacian
Tur
Buda
Eagle Ford Group
Austin Chalk
Lower Eagle Ford
Upper EF
Lozier Canyon
Antonio Creek
Langtry
A
B1
B2
B3
D1
D2
75
100
125
$C_{24}$TT/30H
0 12
$C_{23}$/30H
0 1.5
TR/17α-H
0 1
Mor/30H
0 3
30-NorH/30H
0 2
31R/30H
0 1.5

*W. Brechtel #1 core*

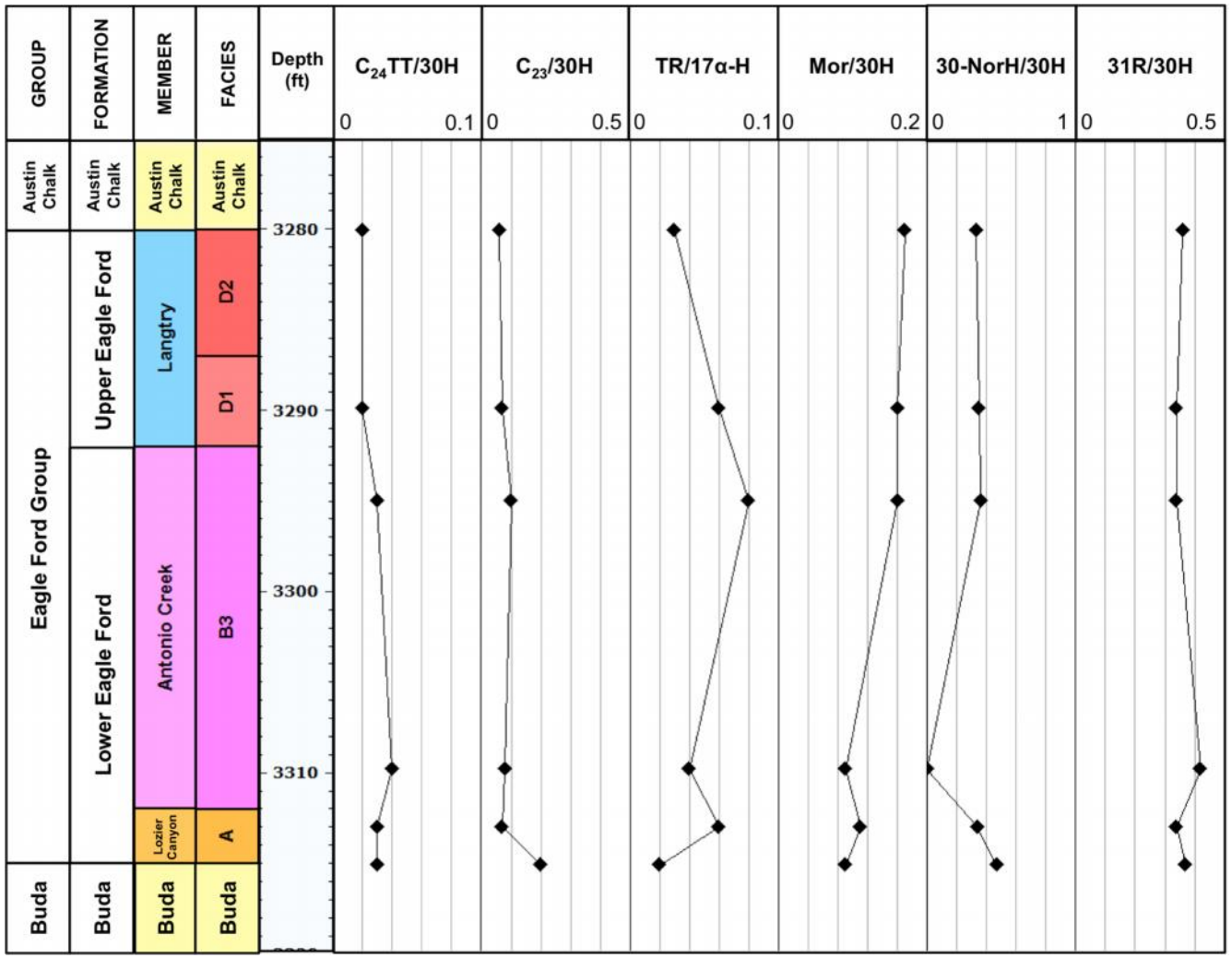

*C. J. Hendershot #1 core*

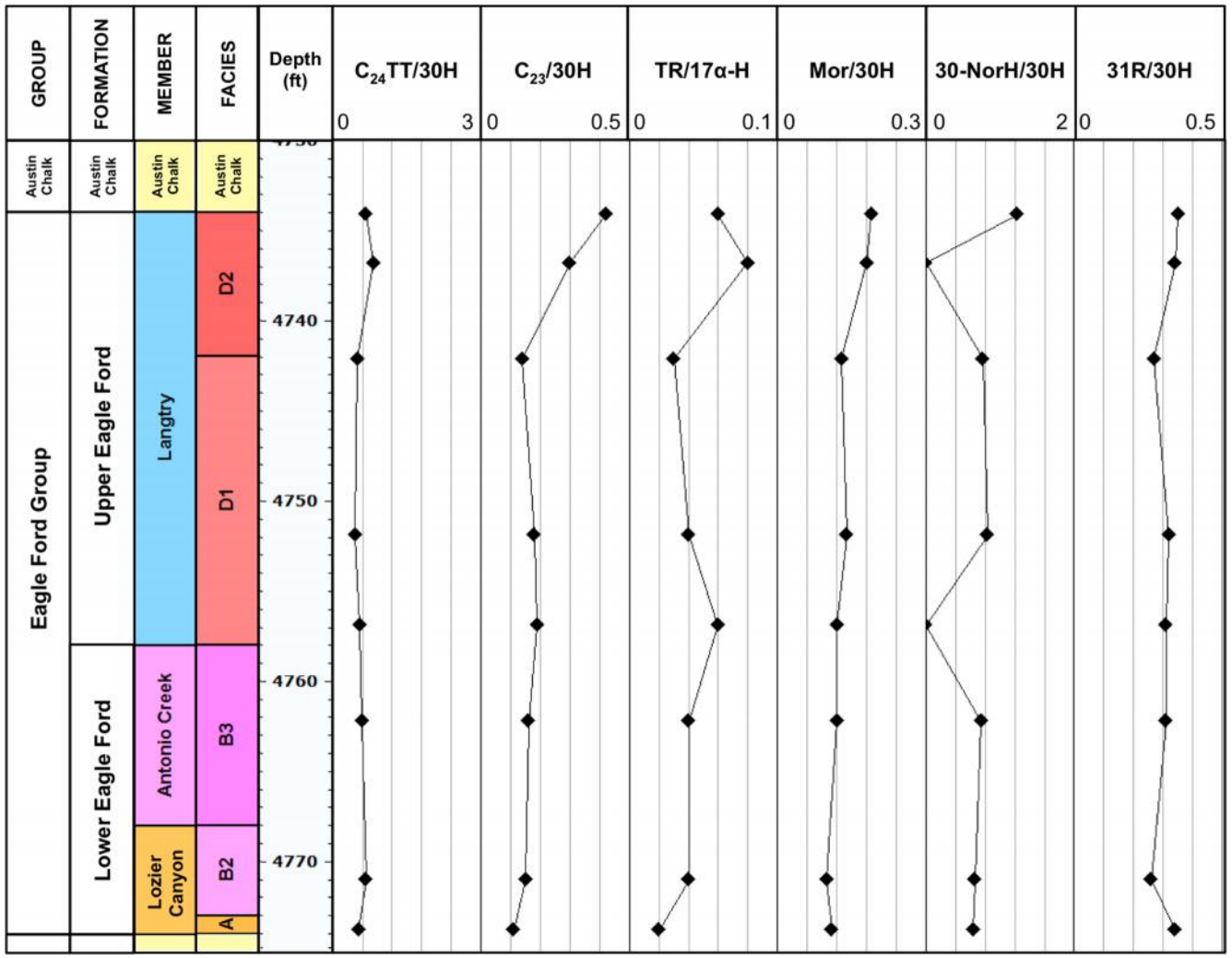

*Lily Hoppess #1 core*

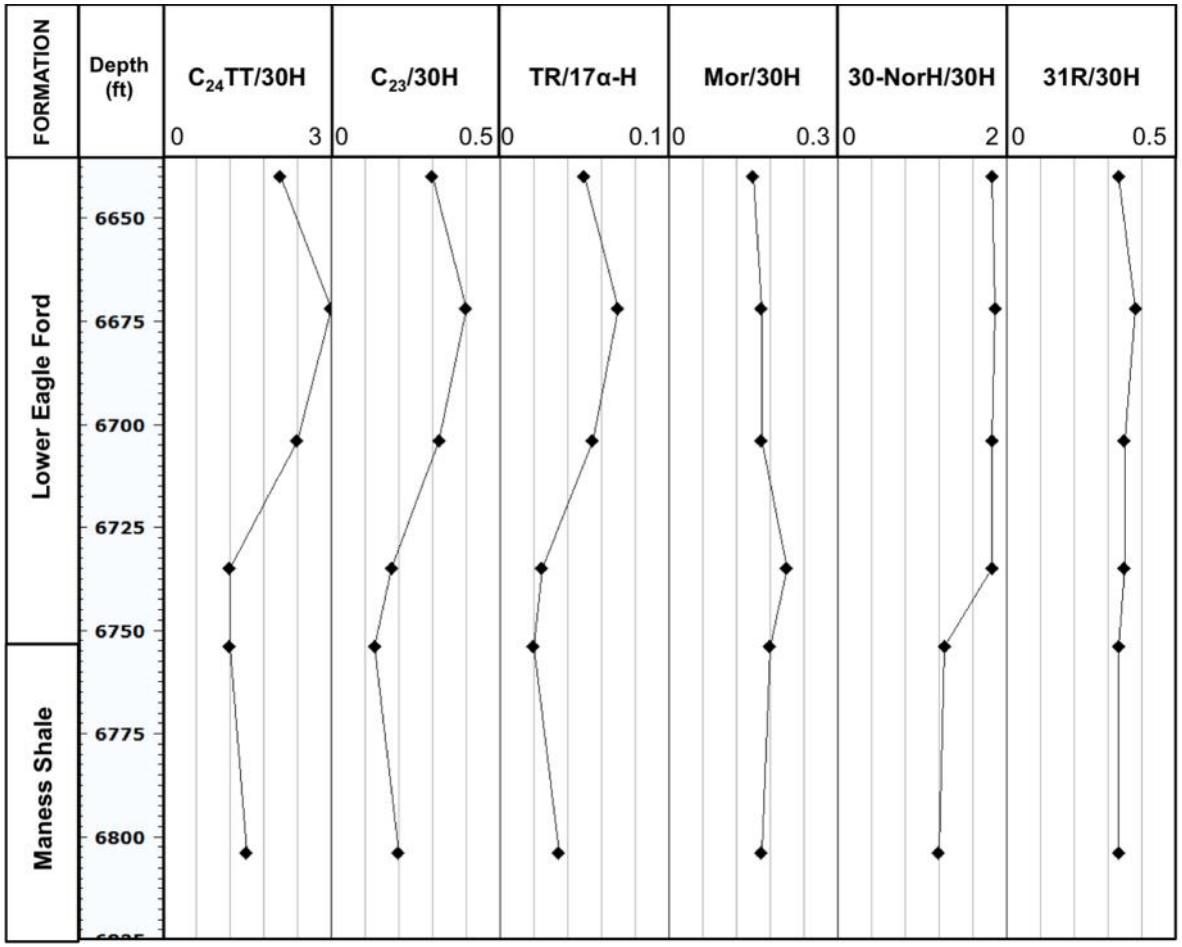

**H. Geochemical ratios of steranes for the branched and cyclic fractions (B&C) of the Eagle Ford Shale bitumen, oil, and condensate samples (ND = not determined)**

*Lozier Canyon outcrop*

| SAMPLE | $C_{27}$% | $C_{28}$% | $C_{29}$% | $C_{29}$ 20S/ (20S+20R) | $C_{29}$ ββ/ (ββ + αα) | Preg/ Steranes | $C_{27}$ Dia/ $C_{27}$ Ster | $C_{27}$ Dia/ (Dia+Reg) | Sterane Index |
|---|---|---|---|---|---|---|---|---|---|
| EFLC-28 | 43.57 | 24.24 | 32.19 | 0.48 | 0.55 | 0.67 | 0.33 | 0.31 | 0.05 |
| EFLC-26 | 42.55 | 24.17 | 33.29 | 0.48 | 0.54 | 0.70 | 0.32 | 0.31 | 0.05 |
| EFLC-25 | 42.23 | 24.22 | 33.55 | 0.48 | 0.53 | 0.46 | 0.27 | 0.27 | 0.05 |
| EFLC-20 | 37.68 | 30.06 | 32.26 | 0.49 | 0.54 | 0.61 | 0.20 | 0.23 | 0.05 |
| EFLC-18 | 36.73 | 30.98 | 32.29 | 0.49 | 0.54 | 0.66 | 0.20 | 0.23 | 0.06 |
| EFLC-14 | 36.87 | 31.62 | 31.51 | 0.48 | 0.54 | 0.67 | 0.17 | 0.21 | 0.06 |
| EFLC-12 | 39.10 | 28.22 | 32.68 | 0.49 | 0.56 | 0.98 | 0.16 | 0.19 | 0.05 |
| EFLC-10 | 39.27 | 27.22 | 33.51 | 0.51 | 0.55 | 1.03 | 0.09 | 0.11 | 0.05 |
| EFLC-8 | 38.84 | 27.79 | 33.37 | 0.50 | 0.55 | 1.14 | 0.09 | 0.11 | 0.05 |
| EFLC-6 | 38.59 | 28.35 | 33.05 | 0.51 | 0.54 | 0.95 | 0.10 | 0.12 | 0.06 |
| EFLC-4 | 40.67 | 28.52 | 30.81 | 0.46 | 0.54 | 0.00 | 0.13 | 0.16 | 0.05 |
| EFLC-1 | 38.47 | 28.11 | 33.42 | 0.52 | 0.52 | 0.07 | 0.27 | 0.27 | 0.06 |

*Ferguson McKnight #526-1H core*

| SAMPLE | $C_{27}$% | $C_{28}$% | $C_{29}$% | $C_{29}$ 20S/ (20S+20R) | $C_{29}$ ββ/ (ββ + αα) | Preg/ Steranes | $C_{27}$ Dia/ $C_{27}$ Ster | $C_{27}$ Dia/ (Dia+Reg) | Sterane Index |
|---|---|---|---|---|---|---|---|---|---|
| EFMK-1 | 44.91 | 28.47 | 26.62 | 0.44 | 0.60 | 1.99 | 0.51 | 0.43 | 0.06 |
| EFMK-4 | 43.64 | 28.67 | 27.69 | 0.44 | 0.59 | 2.88 | 0.52 | 0.45 | 0.06 |
| EFMK-8 | 48.09 | 27.22 | 24.68 | 0.47 | 0.60 | 1.49 | 0.39 | 0.38 | 0.05 |
| EFMK-12 | 44.02 | 28.94 | 27.04 | 0.46 | 0.59 | 3.16 | 0.51 | 0.44 | 0.05 |
| EFMK-15 | 45.60 | 27.88 | 26.52 | 0.43 | 0.61 | 2.67 | 0.57 | 0.47 | 0.05 |
| EFMK-17 | 48.55 | 25.85 | 25.60 | 0.41 | 0.60 | 1.93 | 0.53 | 0.46 | 0.06 |
| EFMK-20 | 48.24 | 25.72 | 26.05 | 0.41 | 0.60 | 1.88 | 0.55 | 0.46 | 0.06 |
| EFMK-23 | 47.25 | 25.63 | 27.12 | 0.43 | 0.63 | 3.37 | 0.60 | 0.48 | 0.06 |
| EFMK-24 | 47.46 | 25.95 | 26.59 | 0.42 | 0.63 | 2.50 | 0.60 | 0.48 | 0.06 |
| EFMK-25 | 49.86 | 27.15 | 23.00 | 0.36 | 0.63 | 2.92 | 0.75 | 0.53 | 0.06 |
| EFMK-26 | 44.86 | 29.52 | 25.62 | 0.48 | 0.59 | 5.52 | 0.63 | 0.48 | 0.06 |

*Fasken "A" #1 core*

| SAMPLE | $C_{27}$% | $C_{28}$% | $C_{29}$% | $C_{29}$ 20S/ (20S+20R) | $C_{29}$ ββ/ (ββ + αα) | Preg/ Steranes | $C_{27}$ Dia/ $C_{27}$ Ster | $C_{27}$ Dia/ (Dia+Reg) | Sterane Index |
|---|---|---|---|---|---|---|---|---|---|
| EFFA-1 | 44.65 | 27.48 | 27.87 | 0.40 | 0.48 | 5.46 | 0.42 | 0.40 | 0.04 |
| EFFA-3 | 44.88 | 26.65 | 28.47 | 0.37 | 0.53 | 5.00 | 0.43 | 0.39 | 0.06 |
| EFFA-5 | 45.51 | 25.89 | 28.59 | 0.39 | 0.51 | 5.08 | 0.40 | 0.37 | 0.03 |
| EFFA-11 | 44.61 | 27.43 | 27.95 | 0.36 | 0.52 | 4.18 | 0.45 | 0.41 | 0.04 |
| EFFA-17 | 43.94 | 26.29 | 29.77 | 0.38 | 0.47 | 4.82 | 0.41 | 0.38 | 0.03 |
| EFFA-18 | 42.11 | 29.24 | 28.65 | 0.41 | 0.48 | 4.73 | 0.41 | 0.38 | 0.03 |
| EFFA-20 | 42.78 | 27.62 | 29.60 | 0.38 | 0.50 | 5.49 | 0.43 | 0.38 | 0.03 |
| EFFA-21 | 43.71 | 28.29 | 28.00 | 0.39 | 0.50 | 4.96 | 0.40 | 0.36 | 0.03 |
| EFFA-23 | 43.79 | 28.93 | 27.28 | 0.39 | 0.52 | 4.82 | 0.41 | 0.37 | 0.03 |
| EFFA-24 | 42.82 | 27.74 | 29.44 | 0.40 | 0.48 | 5.59 | 0.42 | 0.36 | 0.03 |
| EFFA-28 | 44.33 | 27.18 | 28.49 | 0.42 | 0.50 | 5.42 | 0.41 | 0.36 | 0.04 |
| EFFA-32 | 42.89 | 28.89 | 28.22 | 0.36 | 0.48 | 6.32 | 0.43 | 0.39 | 0.03 |
| EFFA-37 | 43.96 | 29.96 | 26.08 | 0.36 | 0.54 | 5.62 | 0.40 | 0.36 | 0.04 |
| EFFA-38 | 45.53 | 26.16 | 28.31 | 0.37 | 0.51 | 5.27 | 0.44 | 0.39 | 0.03 |
| EFFA-40 | 45.71 | 25.90 | 28.39 | 0.37 | 0.51 | 4.56 | 0.41 | 0.37 | 0.03 |

*Bouldin Creek outcrop*

| SAMPLE | $C_{27}$% | $C_{28}$% | $C_{29}$% | $C_{29}$ 20S/ (20S+20R) | $C_{29}$ ββ/ (ββ + αα) | Preg/ Steranes | $C_{27}$ Dia/ $C_{27}$ Ster | $C_{27}$ Dia/ (Dia+Reg) | Sterane Index |
|---|---|---|---|---|---|---|---|---|---|
| EFBC-5 | 36.50 | 40.67 | 22.83 | ND | 0.31 | 0.08 | ND | 0.01 | 0.05 |
| EFBC-7 | 37.59 | 42.03 | 20.38 | ND | 0.30 | 0.08 | ND | 0.01 | 0.05 |
| EFBC-9 | 34.98 | 43.15 | 21.87 | ND | 0.31 | 0.09 | ND | 0.01 | 0.05 |
| EFBC-11 | 36.11 | 43.30 | 20.59 | ND | 0.34 | 0.09 | 0.01 | 0.01 | 0.05 |
| EFBC-15 | 36.58 | 38.78 | 24.64 | ND | 0.33 | 0.11 | 0.01 | 0.01 | 0.06 |
| EFBC-19 | 36.15 | 33.58 | 30.28 | 0.04 | 0.34 | 0.10 | 0.01 | 0.01 | 0.06 |
| EFBC-20 | 38.47 | 34.73 | 26.80 | ND | 0.35 | 0.26 | 0.01 | 0.02 | 0.05 |
| EFBC-23 | 34.05 | 42.42 | 23.54 | 0.04 | 0.36 | 0.21 | 0.01 | 0.02 | 0.05 |
| EFBC-25 | 32.88 | 44.76 | 22.36 | ND | 0.38 | 0.25 | 0.01 | 0.02 | 0.05 |
| EFBC-27 | 36.35 | 39.13 | 24.52 | ND | 0.37 | 0.23 | 0.02 | 0.02 | 0.05 |
| EFBC-30 | 38.99 | 37.58 | 23.43 | ND | 0.34 | 0.07 | 0.01 | 0.01 | 0.05 |
| EFBC-32 | 42.18 | 31.28 | 26.54 | 0.03 | 0.32 | 0.05 | 0.01 | 0.01 | 0.06 |
| EFBC-34 | 33.10 | 43.50 | 23.40 | 0.03 | 0.32 | 0.05 | 0.01 | 0.01 | 0.05 |

*ACC#1 core*

| SAMPLE | $C_{27}$% | $C_{28}$% | $C_{29}$% | $C_{29}$ 20S/ (20S+20R) | $C_{29}$ ββ/ (ββ + αα) | Preg/ Steranes | $C_{27}$ Dia/ $C_{27}$ Ster | $C_{27}$ Dia/ (Dia+Reg) | Sterane Index |
|---|---|---|---|---|---|---|---|---|---|
| EFAC-1 | 44.88 | 28.34 | 26.78 | ND | 0.28 | 0.35 | ND | ND | 0.05 |
| EFAC-3 | 38.73 | 36.51 | 24.76 | ND | 0.27 | 0.14 | ND | ND | 0.05 |
| EFAC-6 | 42.59 | 34.92 | 22.49 | ND | 0.26 | 0.25 | ND | ND | 0.05 |
| EFAC-7 | 38.98 | 38.56 | 22.46 | ND | 0.26 | 0.07 | ND | ND | 0.04 |
| EFAC-8 | 39.98 | 39.03 | 20.99 | ND | 0.26 | 0.07 | ND | ND | 0.04 |
| EFAC-10 | 36.30 | 31.90 | 31.80 | ND | 0.22 | 0.08 | ND | ND | 0.05 |

*W. Brechtel #1 core*

| SAMPLE | $C_{27}$% | $C_{28}$% | $C_{29}$% | $C_{29}$ 20S/ (20S+20R) | $C_{29}$ ββ/ (ββ + αα) | Preg/ Steranes | $C_{27}$ Dia/ $C_{27}$ Ster | $C_{27}$ Dia/ (Dia+Reg) | Sterane Index |
|---|---|---|---|---|---|---|---|---|---|
| EFWB-1 | 44.00 | 29.54 | 26.46 | 0.36 | 0.38 | 0.18 | 0.05 | 0.06 | 0.08 |
| EFWB-3 | 37.05 | 38.00 | 24.95 | 0.38 | 0.36 | 0.28 | 0.08 | 0.10 | 0.05 |
| EFWB-4 | 36.55 | 37.41 | 26.04 | 0.38 | 0.35 | 0.29 | 0.08 | 0.10 | 0.05 |
| EFWB-7 | 40.68 | 33.62 | 25.70 | 0.45 | 0.47 | 0.36 | 0.07 | 0.09 | 0.06 |
| EFWB-8 | 40.96 | 34.76 | 24.28 | 0.44 | 0.44 | 0.30 | 0.09 | 0.11 | 0.06 |
| EFWB-9 | 38.92 | 32.76 | 28.31 | 0.47 | 0.48 | 0.78 | 0.05 | 0.07 | 0.06 |

*C.J. Hendershot #1 core*

| SAMPLE | $C_{27}$% | $C_{28}$% | $C_{29}$% | $C_{29}$ 20S/ (20S+20R) | $C_{29}$ ββ/ (ββ + αα) | Preg/ Steranes | $C_{27}$ Dia/ $C_{27}$ Ster | $C_{27}$ Dia/ (Dia+Reg) | Sterane Index |
|---|---|---|---|---|---|---|---|---|---|
| EFHE-1 | 46.16 | 27.62 | 26.22 | 0.20 | 0.26 | 0.09 | 0.11 | 0.13 | 0.06 |
| EFHE-2 | 42.57 | 29.58 | 27.85 | 0.18 | 0.25 | 0.08 | 0.05 | 0.07 | 0.06 |
| EFHE-3 | 40.76 | 31.23 | 28.01 | 0.21 | 0.23 | 0.09 | 0.09 | 0.11 | 0.06 |
| EFHE-5 | 37.72 | 35.91 | 26.37 | 0.28 | 0.23 | 0.17 | 0.16 | 0.21 | 0.06 |
| EFHE-6 | 40.85 | 31.32 | 27.83 | 0.35 | 0.26 | 0.31 | 0.17 | 0.21 | 0.05 |
| EFHE-7 | 39.82 | 31.77 | 28.41 | 0.35 | 0.24 | 0.21 | 0.17 | 0.19 | 0.05 |
| EFHE-9 | 39.53 | 31.93 | 28.55 | 0.47 | 0.29 | 0.33 | 0.08 | 0.10 | 0.06 |
| EFHE-10 | 42.37 | 26.13 | 31.50 | 0.45 | 0.27 | 0.28 | 0.34 | 0.34 | 0.07 |

*Oils and condensates*



| SAMPLE | $C_{27}$% | $C_{28}$% | $C_{29}$% | $C_{29}$ 20S/ (20S+20R) | $C_{29}$ ββ/ (ββ + αα) | Preg/ Steranes | $C_{27}$ Dia/ $C_{27}$ Ster | $C_{27}$ Dia/ (Dia+Reg) | Sterane Index |
|---|---|---|---|---|---|---|---|---|---|
| NWMK-533.2 | 37.52 | 39.45 | 23.03 | 0.42 | 0.60 | 2.51 | 0.47 | 0.41 | 0.06 |
| NFMK-526-1H | 42.73 | 32.12 | 25.15 | 0.38 | 0.61 | 4.56 | 0.70 | 0.51 | 0.06 |
| MJOG-UEF | 59.99 | 19.28 | 20.74 | 0.30 | 0.65 | 2.40 | 0.76 | 0.52 | 0.01 |
| MJOG-LEF | 62.16 | 20.28 | 17.56 | 0.41 | 0.69 | 2.06 | 0.72 | 0.52 | 0.04 |
| GREF-1-110 | 54.40 | 22.71 | 22.89 | 0.26 | 0.36 | 1.36 | 0.96 | 0.58 | 0.09 |

***I.*** **Geochemical ratios of terpanes for the branched and cyclic fractions (B&C) of the Eagle Ford Shale bitumen, oil, and condensate samples (ND = not determined)**

*Lozier Canyon outcrop*

| Sample | Steranes/ 17α-H | TR/ 17α-H | $C_{22}/C_{21}$ TR | $C_{24}/C_{23}$ TR | $C_{26}/C_{25}$ TR | $C_{23}$/ 30H | $C_{24}$TT/ 30H | 30-NorH/ 30H | Mor/ 30H | 31R/ 30H | 35S/ 34S | HH Index | Ts/ Ts+Tm | $C_{31}$ 22S/ (22S+22R) |
|---|---|---|---|---|---|---|---|---|---|---|---|---|---|---|
| EFLC-28 | 0.66 | 0.03 | 0.24 | 0.57 | 0.96 | 0.23 | 0.05 | 0.6 | 0.06 | 0.46 | 1.20 | 0.11 | 0.32 | 0.62 |
| EFLC-26 | 0.63 | 0.03 | 0.32 | 0.53 | 0.76 | 0.27 | 0.04 | 0.62 | 0.06 | 0.47 | 1.01 | 0.09 | 0.20 | 0.61 |
| EFLC-25 | 0.51 | 0.02 | 0.36 | 0.59 | 0.89 | 0.14 | 0.03 | 0.58 | 0.06 | 0.46 | 1.16 | 0.11 | 0.19 | 0.61 |
| EFLC-20 | 0.7 | 0.04 | 0.54 | 0.43 | 0.71 | 0.28 | 0.04 | 0.65 | 0.06 | 0.53 | 1.46 | 0.13 | 0.19 | 0.61 |
| EFLC-18 | 0.68 | 0.04 | 0.63 | 0.33 | 0.64 | 0.39 | 0.05 | 0.69 | 0.06 | 0.57 | 1.42 | 0.14 | 0.20 | 0.62 |
| EFLC-14 | 0.56 | 0.05 | 0.84 | 0.29 | 0.52 | 0.55 | 0.06 | 0.84 | 0.06 | 0.56 | 1.44 | 0.14 | 0.21 | 0.62 |
| EFLC-12 | 0.58 | 0.07 | 0.88 | 0.29 | 0.52 | 0.77 | 0.08 | 0.83 | 0.06 | 0.52 | 1.46 | 0.14 | 0.23 | 0.61 |
| EFLC-10 | 0.42 | 0.06 | 0.92 | 0.29 | 0.59 | 0.59 | 0.06 | 0.82 | 0.06 | 0.46 | 1.39 | 0.14 | 0.21 | 0.6 |
| EFLC-8 | 0.42 | 0.06 | 0.88 | 0.29 | 0.61 | 0.65 | 0.06 | 0.84 | 0.06 | 0.46 | 1.36 | 0.13 | 0.22 | 0.61 |
| EFLC-6 | 0.42 | 0.06 | 0.9 | 0.32 | 0.62 | 0.56 | 0.07 | 0.84 | 0.06 | 0.47 | 1.42 | 0.14 | 0.22 | 0.61 |
| EFLC-4 | 0.35 | 0.05 | 0.81 | 0.26 | 0.63 | 0.75 | 0.07 | 0.88 | 0.06 | 0.49 | 1.38 | 0.15 | 0.26 | 0.61 |
| EFLC-1 | 0.82 | 0.03 | 0.35 | 0.95 | 1.11 | 0.14 | 0.04 | 0.56 | 0.08 | 0.43 | 1.44 | 0.21 | 0.27 | 0.6 |

*Ferguson McKnight #526-1H core*

| Sample | Steranes/ 17α-H | TR/ 17α-H | $C_{22}/C_{21}$ TR | $C_{24}/C_{23}$ TR | $C_{26}/C_{25}$ TR | $C_{23}$/ 30H | $C_{24}$TT/ 30H | 30-NorH/ 30H | Mor/ 30H | 31R/ 30H | 35S/ 34S | HH Index | Ts/ Ts+Tm | $C_{31}$ 22S/ (22S+22R) |
|---|---|---|---|---|---|---|---|---|---|---|---|---|---|---|
| EFMK-1 | 2.15 | 0.43 | 0.30 | 0.62 | 0.48 | 2.74 | 0.53 | 1.20 | 0.10 | 0.45 | ND | ND | 0.49 | 0.46 |
| EFMK-4 | 3.68 | 0.86 | 0.22 | 0.65 | 0.55 | 3.49 | 0.80 | 0.65 | 0.13 | 0.28 | ND | ND | 0.56 | 0.57 |
| EFMK-8 | 3.84 | 0.90 | 0.24 | 0.62 | 0.64 | 3.62 | 0.88 | 0.66 | 0.11 | 0.23 | ND | ND | 0.63 | 0.59 |
| EFMK-12 | 3.12 | 0.73 | 0.27 | 0.60 | 0.67 | 3.85 | 0.86 | 0.77 | 0.11 | 0.28 | ND | ND | 0.60 | 0.60 |
| EFMK-15 | 3.10 | 0.71 | 0.29 | 0.63 | 0.70 | 3.19 | 0.68 | 0.73 | 0.14 | 0.35 | ND | ND | 0.66 | 0.54 |
| EFMK-17 | 2.67 | 0.56 | 0.26 | 0.57 | 0.79 | 3.13 | 0.58 | 0.79 | 0.09 | 0.42 | ND | ND | 0.65 | 0.49 |
| EFMK-20 | 3.79 | 0.93 | 0.25 | 0.64 | 0.65 | 4.35 | 0.96 | 0.81 | 0.12 | 0.30 | ND | ND | 0.66 | 0.60 |
| EFMK-23 | 4.25 | 1.17 | 0.25 | 0.64 | 0.66 | 4.98 | 1.08 | 0.71 | 0.14 | 0.28 | ND | ND | 0.66 | 0.56 |
| EFMK-24 | 4.98 | 1.45 | 0.25 | 0.67 | 0.64 | 5.35 | 1.21 | 0.64 | 0.06 | 0.29 | 1.11 | 0.12 | 0.66 | 0.53 |
| EFMK-25 | 5.80 | 1.49 | 0.37 | 0.72 | 0.68 | 7.76 | 1.71 | 1.23 | 0.48 | 0.69 | ND | ND | 0.68 | 0.52 |
| EFMK-26 | 3.68 | 2.44 | 0.41 | 0.74 | 0.65 | 9.38 | 2.07 | 1.17 | 0.26 | 0.53 | ND | ND | 0.57 | 0.37 |

*Fasken "A" #1 core*

| Sample | Steranes/ 17α-H | TR/ 17α-H | $C_{22}/C_{21}$ TR | $C_{24}/C_{23}$ TR | $C_{26}/C_{25}$ TR | $C_{23}$/ 30H | $C_{24}$TT/ 30H | 30-NorH/ 30H | Mor/ 30H | 31R/ 30H | 35S/ 34S | HH Index | Ts/ Ts+Tm | $C_{31}$ 22S/ (22S+22R) |
|---|---|---|---|---|---|---|---|---|---|---|---|---|---|---|
| EFFA-1 | 0.46 | 0.10 | 0.36 | 0.45 | 0.94 | 2.68 | 0.23 | 1.26 | 0.21 | 0.28 | ND | ND | 0.53 | 0.57 |
| EFFA-3 | 0.46 | 0.13 | 0.35 | 0.44 | 0.91 | 2.65 | 0.19 | 1.23 | 0.19 | 0.32 | ND | ND | 0.41 | 0.53 |
| EFFA-5 | 0.46 | 0.12 | 0.36 | 0.45 | 0.92 | 2.49 | 0.21 | 1.24 | 0.20 | 0.28 | ND | ND | 0.37 | 0.57 |
| EFFA-11 | 0.48 | 0.12 | 0.38 | 0.45 | 0.92 | 2.29 | 0.17 | 1.18 | 0.19 | 0.27 | ND | ND | 0.40 | 0.54 |
| EFFA-17 | 0.44 | 0.12 | 0.35 | 0.47 | 0.92 | 2.32 | 0.17 | 1.15 | 0.21 | 0.24 | ND | ND | 0.38 | 0.57 |
| EFFA-18 | 0.47 | 0.11 | 0.36 | 0.43 | 0.96 | 2.37 | 0.17 | 1.19 | 0.20 | 0.28 | ND | ND | 0.38 | 0.55 |
| EFFA-20 | 0.45 | 0.10 | 0.36 | 0.43 | 0.87 | 2.21 | 0.16 | 1.02 | 0.19 | 0.21 | ND | ND | 0.40 | 0.58 |
| EFFA-21 | 0.47 | 0.11 | 0.31 | 0.44 | 1.05 | 2.42 | 0.17 | 1.08 | 0.19 | 0.23 | ND | ND | 0.41 | 0.56 |
| EFFA-23 | 0.47 | 0.11 | 0.34 | 0.43 | 0.93 | 2.35 | 0.17 | 1.02 | 0.19 | 0.23 | ND | ND | 0.39 | 0.57 |
| EFFA-24 | 0.47 | 0.11 | 0.33 | 0.42 | 0.95 | 2.71 | 0.18 | 1.19 | 0.20 | 0.25 | ND | ND | 0.37 | 0.58 |
| EFFA-28 | 0.48 | 0.11 | 0.32 | 0.43 | 0.92 | 2.62 | 0.18 | 1.09 | 0.19 | 0.23 | ND | ND | 0.35 | 0.54 |
| EFFA-32 | 0.45 | 0.11 | 0.32 | 0.44 | 0.96 | 2.59 | 0.17 | 1.07 | 0.15 | 0.21 | ND | ND | 0.40 | 0.57 |
| EFFA-37 | 0.46 | 0.11 | 0.30 | 0.43 | 0.95 | 2.64 | 0.17 | 1.05 | 0.18 | 0.26 | ND | ND | 0.40 | 0.51 |
| EFFA-38 | 0.44 | 0.12 | 0.31 | 0.45 | 0.96 | 2.40 | 0.16 | 1.10 | 0.19 | 0.24 | ND | ND | 0.34 | 0.57 |
| EFFA-40 | 0.47 | 0.12 | 0.34 | 0.45 | 0.87 | 2.26 | 0.17 | 1.06 | 0.20 | 0.24 | ND | ND | 0.38 | 0.56 |

*Bouldin Creek outcrop*

| Sample | Steranes/ 17α-H | TR/ 17α-H | $C_{22}/C_{21}$ TR | $C_{24}/C_{23}$ TR | $C_{26}/C_{25}$ TR | $C_{23}$/ 30H | $C_{24}$TT/ 30H | 30-NorH/ 30H | Mor/ 30H | 31R/ 30H | 35S/ 34S | HH Index | Ts/ Ts+Tm | $C_{31}$ 22S/ (22S+22R) |
|---|---|---|---|---|---|---|---|---|---|---|---|---|---|---|
| EFBC-5 | 13.23 | 0.45 | ND | 0.47 | 0.82 | 0.16 | 0.08 | 1.33 | 2.22 | 0.67 | ND | ND | 0.08 | 0.42 |
| EFBC-7 | 13.69 | 0.33 | ND | 0.50 | 0.98 | 0.18 | 0.07 | 1.06 | 2.26 | 0.70 | ND | ND | 0.07 | 0.31 |
| EFBC-9 | 10.01 | 0.35 | ND | 0.52 | 0.86 | 0.11 | 0.04 | 0.87 | 1.61 | 0.56 | ND | ND | 0.07 | 0.31 |
| EFBC-11 | 13.90 | 0.34 | ND | 0.40 | 0.70 | 0.22 | 0.07 | 0.84 | 1.89 | 0.76 | ND | ND | 0.06 | 0.34 |
| EFBC-15 | 7.53 | 0.27 | ND | 0.71 | 1.06 | 0.06 | 0.03 | 0.73 | 1.26 | 0.39 | ND | ND | 0.06 | 0.30 |
| EFBC-19 | 11.00 | 0.46 | ND | 0.37 | 1.16 | 0.24 | 0.06 | 1.49 | 1.26 | 0.62 | ND | ND | 0.09 | 0.35 |
| EFBC-20 | 8.03 | 0.34 | ND | 0.25 | 1.42 | 0.25 | 0.07 | 1.18 | 1.35 | 0.75 | 0.06 | 0.11 | 0.04 | 0.23 |
| EFBC-23 | 17.80 | 0.24 | ND | 0.21 | 1.10 | 0.61 | 0.18 | 0.97 | 1.49 | 1.15 | ND | ND | 0.06 | 0.15 |
| EFBC-25 | 20.06 | 0.32 | ND | 0.17 | 0.90 | 0.70 | 0.25 | 1.05 | 1.57 | 1.06 | ND | ND | 0.05 | 0.15 |
| EFBC-27 | 13.95 | 0.25 | ND | 0.15 | 0.89 | 0.71 | 0.19 | 1.00 | 1.29 | 1.27 | ND | ND | 0.07 | 0.11 |
| EFBC-30 | 10.83 | 0.23 | ND | 0.45 | 1.21 | 0.20 | 0.10 | 1.59 | 1.43 | 0.62 | ND | ND | 0.05 | 0.12 |
| EFBC-32 | 10.61 | 0.27 | ND | 0.33 | 0.87 | 0.18 | 0.09 | 1.60 | 1.41 | 0.54 | ND | ND | 0.05 | 0.10 |
| EFBC-34 | 16.68 | 0.31 | ND | 0.27 | 0.60 | 0.26 | 0.10 | 1.43 | 1.36 | 0.45 | 0.06 | 0.13 | 0.04 | 0.13 |

*ACC#1 core*

| Sample | Steranes/ 17α-H | TR/ 17α-H | $C_{22}/C_{21}$ TR | $C_{24}/C_{23}$ TR | $C_{26}/C_{25}$ TR | $C_{23}$/ 30H | $C_{24}$TT/ 30H | 30-NorH/ 30H | Mor/ 30H | 31R/ 30H | 35S/ 34S | HH Index | Ts/ Ts+Tm | $C_{31}$ 22S/ (22S+22R) |
|---|---|---|---|---|---|---|---|---|---|---|---|---|---|---|
| EFAC-1 | 1.89 | 0.24 | 0.19 | 0.50 | 1.13 | 0.29 | 0.04 | 0.92 | 1.54 | 0.50 | ND | ND | 0.05 | 0.30 |
| EFAC-3 | 4.35 | 0.36 | 0.17 | 0.52 | 0.69 | 0.17 | 0.03 | 0.63 | 1.19 | 0.42 | ND | ND | 0.07 | 0.31 |
| EFAC-6 | 6.31 | 0.47 | 0.16 | 0.34 | 0.69 | 1.13 | 0.22 | 1.19 | 1.56 | 1.14 | ND | ND | 0.09 | 0.26 |
| EFAC-7 | 7.82 | 0.30 | 0.17 | 0.38 | 0.75 | 0.38 | 0.08 | 1.61 | 1.86 | 0.84 | ND | ND | 0.04 | 0.33 |
| EFAC-8 | 9.11 | 0.39 | 0.22 | 0.59 | 0.53 | 0.30 | 0.09 | 1.31 | 1.92 | 0.69 | ND | ND | 0.03 | 0.40 |
| EFAC-10 | 3.86 | 0.18 | 0.18 | 0.36 | 1.68 | 0.17 | 0.03 | 0.73 | 1.32 | 0.70 | ND | ND | 0.08 | 0.31 |

*W. Brechtel #1 core*

| Sample | Steranes/ 17α-H | TR/ 17α-H | $C_{22}/C_{21}$ TR | $C_{24}/C_{23}$ TR | $C_{26}/C_{25}$ TR | $C_{23}$/ 30H | $C_{24}$TT/ 30H | 30-NorH/ 30H | Mor/ 30H | 31R/ 30H | 35S/ 34S | HH Index | Ts/ Ts+Tm | $C_{31}$ 22S/ (22S+22R) |
|---|---|---|---|---|---|---|---|---|---|---|---|---|---|---|
| EFWB-1 | 0.56 | 0.03 | 1.57 | 1.50 | 1.16 | 0.06 | 0.02 | 0.33 | 0.17 | 0.36 | 1.19 | 0.13 | 0.20 | 0.56 |
| EFWB-3 | 1.34 | 0.06 | 0.39 | 0.89 | 0.84 | 0.07 | 0.02 | 0.35 | 0.16 | 0.34 | 0.87 | 0.14 | 0.18 | 0.59 |
| EFWB-4 | 1.52 | 0.08 | 0.38 | 0.79 | 0.91 | 0.10 | 0.03 | 0.36 | 0.16 | 0.34 | 0.60 | 0.13 | 0.21 | 0.59 |
| EFWB-7 | 0.85 | 0.04 | 2.77 | 0.96 | 1.13 | 0.08 | 0.04 | 0.00 | 0.09 | 0.42 | 1.23 | 0.10 | 0.24 | 0.61 |
| EFWB-8 | 1.18 | 0.06 | 0.26 | 1.32 | 0.64 | 0.07 | 0.03 | 0.34 | 0.11 | 0.34 | 0.91 | 0.11 | 0.23 | 0.61 |
| EFWB-9 | 0.72 | 0.02 | 0.18 | 0.59 | 1.15 | 0.20 | 0.03 | 0.47 | 0.09 | 0.37 | 1.11 | 0.10 | 0.26 | 0.61 |

*C.J. Hendershot #1 core*

| Sample | Steranes/ 17α-H | TR/ 17α-H | $C_{22}/C_{21}$ TR | $C_{24}/C_{23}$ TR | $C_{26}/C_{25}$ TR | $C_{23}$/ 30H | $C_{24}$TT/ 30H | 30-NorH/ 30H | Mor/ 30H | 31R/ 30H | 35S/ 34S | HH Index | Ts/ Ts+Tm | $C_{31}$ 22S/ (22S+22R) |
|---|---|---|---|---|---|---|---|---|---|---|---|---|---|---|
| EFHE-1 | 3.34 | 0.06 | 0.25 | 0.68 | 0.72 | 0.42 | 0.10 | 1.23 | 0.19 | 0.35 | 1.56 | 0.19 | 0.29 | 0.53 |
| EFHE-2 | 4.51 | 0.08 | 0.15 | 0.82 | 0.69 | 0.30 | 0.10 | 0.00 | 0.18 | 0.34 | 1.40 | 0.17 | 0.25 | 0.53 |
| EFHE-3 | 2.23 | 0.03 | 0.14 | 0.50 | 0.97 | 0.14 | 0.04 | 0.77 | 0.13 | 0.27 | 0.76 | 0.12 | 0.28 | 0.56 |
| EFHE-5 | 2.77 | 0.04 | 0.18 | 0.46 | 0.68 | 0.18 | 0.04 | 0.83 | 0.14 | 0.32 | 0.94 | 0.14 | 0.21 | 0.59 |
| EFHE-6 | 3.61 | 0.06 | 0.15 | 0.55 | 0.71 | 0.19 | 0.05 | 0.00 | 0.12 | 0.31 | 0.92 | 0.13 | 0.22 | 0.61 |
| EFHE-7 | 2.20 | 0.04 | 0.16 | 0.59 | 0.38 | 0.16 | 0.04 | 0.75 | 0.12 | 0.31 | 0.94 | 0.12 | 0.24 | 0.60 |
| EFHE-9 | 1.21 | 0.04 | 0.13 | 0.68 | 0.61 | 0.15 | 0.05 | 0.66 | 0.10 | 0.26 | 0.80 | 0.10 | 0.19 | 0.61 |
| EFHE-10 | 0.99 | 0.02 | 0.27 | 0.53 | 1.34 | 0.11 | 0.03 | 0.64 | 0.11 | 0.34 | 1.41 | 0.15 | 0.39 | 0.61 |



*Lily Hoppess #1 core*

| Sample | Steranes/ 17α-H | TR/ 17α-H | $C_{22}/C_{21}$ TR | $C_{24}/C_{23}$ TR | $C_{26}/C_{25}$ TR | $C_{23}$/ 30H | $C_{24}$TT/ 30H | 30-NorH/ 30H | Mor/ 30H | 31R/ 30H | 35S/ 34S | HH Index | Ts/ Ts+Tm | $C_{31}$ 22S/ (22S+22R) |
|---|---|---|---|---|---|---|---|---|---|---|---|---|---|---|
| EFLH-1 | 0.68 | 0.10 | 0.20 | 0.46 | 0.86 | 0.30 | 0.07 | 0.55 | 0.10 | 0.20 | 0.34 | 0.05 | 0.51 | 0.57 |
| EFLH-5 | 0.62 | 0.14 | 0.23 | 0.49 | 0.72 | 0.40 | 0.10 | 0.56 | 0.11 | 0.23 | 0.41 | 0.05 | 0.48 | 0.55 |
| EFLH-9 | 0.57 | 0.11 | 0.21 | 0.48 | 0.94 | 0.32 | 0.08 | 0.55 | 0.11 | 0.21 | 0.42 | 0.06 | 0.51 | 0.58 |
| EFLH-13 | 0.41 | 0.05 | 0.29 | 0.47 | 1.40 | 0.18 | 0.04 | 0.55 | 0.14 | 0.21 | 0.40 | 0.06 | 0.61 | 0.61 |
| EFLH-15 | 0.59 | 0.04 | 0.30 | 0.54 | 1.44 | 0.13 | 0.04 | 0.38 | 0.12 | 0.20 | 0.34 | 0.05 | 0.70 | 0.60 |
| EFLH-20 | 0.73 | 0.07 | 0.22 | 0.50 | 1.02 | 0.20 | 0.05 | 0.36 | 0.11 | 0.20 | 0.40 | 0.06 | 0.64 | 0.59 |

*Oils and condensates*

| Sample | Steranes/ 17α-H | TR/ 17α-H | $C_{22}/C_{21}$ TR | $C_{24}/C_{23}$ TR | $C_{26}/C_{25}$ TR | $C_{23}$/ 30H | $C_{24}$TT/ 30H | 30-NorH/ 30H | Mor/ 30H | 31R/ 30H | 35S/ 34S | HH Index | Ts/ Ts+Tm | $C_{31}$ 22S/ (22S+22R) |
|---|---|---|---|---|---|---|---|---|---|---|---|---|---|---|
| NWMK-533.2 | 3.19 | 0.61 | 0.22 | 0.76 | 0.63 | 1.98 | 0.42 | 0.30 | 0.07 | 0.37 | 0.58 | 0.04 | 0.46 | 0.50 |
| NFMK-526-1H | 7.87 | 3.71 | 0.28 | 0.86 | 0.58 | 7.75 | 1.99 | 0.88 | ND | 0.31 | ND | ND | 0.52 | ND |
| MJOG-UEF | 13.20 | 8.13 | 0.70 | 0.66 | 0.63 | ND | ND | ND | ND | ND | ND | ND | 0.65 | ND |
| MJOG-LEF | 10.57 | 3.53 | 0.24 | 0.72 | 0.64 | 12.87 | 3.27 | 2.29 | ND | ND | ND | ND | 0.66 | ND |
| GREF-1-110 | ND | ND | ND | ND | ND | ND | ND | ND | ND | ND | ND | ND | ND | ND |

**J. Aryl isoprenoids ratio (AIR) for the branched and cyclic fractions (B&C) of the Eagle Ford Shale bitumen, oil, and condensate samples (ND = not determined)**

*Lozier Canyon outcrop*

| Sample | AIR |
|---|---|
| EFLC-28 | 1.04 |
| EFLC-26 | 1.37 |
| EFLC-25 | 0.66 |
| EFLC-18 | 0.54 |
| EFLC-14 | 0.83 |
| EFLC-12 | 0.84 |
| EFLC-10 | 1.33 |
| EFLC-8 | 1.21 |
| EFLC-6 | 0.37 |
| EFLC-4 | 0.56 |
| EFLC-1 | 0.74 |

*Ferguson McKnight #526-1H core*

| Sample | AIR |
|---|---|
| EFMK-1 | 1.72 |
| EFMK-4 | 4.61 |
| EFMK-8 | 3.72 |
| EFMK-12 | 4.25 |
| EFMK-15 | 2.95 |
| EFMK-17 | 1.90 |
| EFMK-20 | 3.88 |
| EFMK-23 | 2.24 |
| EFMK-24 | 3.48 |
| EFMK-25 | 1.68 |
| EFMK-26 | 1.65 |

*Fasken "A" #1 core*

| Sample | AIR |
|---|---|
| EFFA-1 | 1.70 |
| EFFA-3 | 3.07 |
| EFFA-5 | 2.02 |
| EFFA-11 | 1.23 |
| EFFA-17 | 2.15 |
| EFFA-18 | 2.26 |
| EFFA-20 | 1.42 |
| EFFA-21 | 2.20 |
| EFFA-23 | 1.95 |
| EFFA-24 | 3.24 |
| EFFA-28 | 4.10 |
| EFFA-32 | 2.90 |
| EFFA-37 | 4.53 |
| EFFA-38 | 3.21 |
| EFFA-40 | 2.25 |

*Bouldin Creek outcrop*

| Sample | AIR |
|---|---|
| EFBC-5 | 1.01 |
| EFBC-7 | 0.54 |
| EFBC-9 | 1.14 |
| EFBC-11 | 0.80 |
| EFBC-15 | 0.79 |
| EFBC-19 | 0.87 |
| EFBC-20 | 0.62 |
| EFBC-23 | 0.65 |
| EFBC-25 | 2.46 |
| EFBC-27 | 2.81 |
| EFBC-30 | 1.37 |
| EFBC-32 | 1.60 |
| EFBC-34 | 1.43 |

*ACC #1 core*

| Sample | AIR |
|---|---|
| EFAC-1 | 0.32 |
| EFAC-3 | 0.79 |
| EFAC-6 | 0.49 |
| EFAC-7 | 0.33 |
| EFAC-8 | 0.38 |
| EFAC-10 | 0.48 |

*W. Brechtel #1 core*

| Sample | AIR |
|---|---|
| EFWB-1 | 1.08 |
| EFWB-3 | 2.11 |
| EFWB-4 | 2.26 |
| EFWB-7 | 2.00 |
| EFWB-8 | 2.74 |
| EFWB-9 | 2.63 |

*C.J. Hendershot #1 core*

| Sample | AIR |
|---|---|
| EFHE-1 | 1.44 |
| EFHE-2 | 1.42 |
| EFHE-3 | 2.34 |
| EFHE-5 | 1.87 |
| EFHE-6 | 2.07 |
| EFHE-7 | 1.98 |
| EFHE-9 | 1.76 |
| EFHE-10 | 0.62 |

*Lily Hoppess #1 core*

| Sample | AIR |
|---|---|
| EFLH-1 | 2.43 |
| EFLH-5 | 1.90 |
| EFLH-9 | 2.19 |
| EFLH-13 | 2.65 |
| EFLH-15 | 2.95 |
| EFLH-20 | 1.99 |

*Oils and condensates*

| Sample | AIR |
|---|---|
| NWMK-533.2 | 2.80 |
| NFMK-526-1H | 2.05 |
| MJOG-UEF | 2.27 |
| MJOG-LEF | 2.21 |
| GREF-1-110 | 3.45 |

**K. Geochemical ratios for aromatic biomarkers of the Eagle Ford Shale bitumen, oil, and condensate samples (ND = not determined)**

*Lozier Canyon outcrop*

| Sample | MPI 1 | MPI 2 | MA(I)/ MA(I+II) | TA(I)/ TA(I+II) | $C_{26}$ TA (20S/20S+20R) | TA28/ (MA29+TA28) | %$C_{27}$ MAS | %$C_{28}$ MAS | %$C_{29}$ MAS |
|---|---|---|---|---|---|---|---|---|---|
| EFLC-28 | 0.22 | 0.28 | 0.06 | 0.10 | 0.17 | 0.79 | 15.58 | 70.17 | 14.25 |
| EFLC-26 | 0.13 | 0.18 | 0.10 | 0.10 | 0.17 | 0.78 | 15.68 | 69.81 | 14.51 |
| EFLC-25 | 0.18 | 0.25 | 0.07 | 0.08 | 0.17 | 0.74 | 15.28 | 69.41 | 15.31 |
| EFLC-20 | 0.18 | 0.24 | 0.04 | 0.06 | 0.16 | 0.78 | 16.04 | 70.91 | 13.05 |
| EFLC-18 | 0.10 | 0.15 | 0.10 | 0.16 | 0.15 | 0.55 | 16.26 | 68.33 | 15.41 |
| EFLC-14 | 0.16 | 0.22 | 0.18 | 0.29 | 0.15 | 0.33 | 17.72 | 68.37 | 13.91 |
| EFLC-12 | 0.52 | 0.56 | 0.13 | 0.14 | 0.16 | 0.71 | 18.27 | 70.02 | 11.71 |
| EFLC-10 | 0.56 | 0.63 | 0.18 | 0.14 | 0.17 | 0.76 | 19.03 | 68.22 | 12.75 |
| EFLC-8 | 0.39 | 0.48 | 0.21 | 0.29 | 0.18 | 0.71 | 19.05 | 68.11 | 12.83 |
| EFLC-6 | 0.43 | 0.52 | 0.14 | 0.17 | 0.19 | 0.63 | 19.59 | 66.03 | 14.38 |
| EFLC-4 | 0.12 | 0.17 | 0.16 | 0.35 | 0.17 | 0.47 | 19.39 | 68.21 | 12.40 |
| EFLC-1 | 0.59 | 0.57 | 0.05 | 0.11 | 0.21 | 0.30 | 18.49 | 71.25 | 10.26 |

*Ferguson McKnight #526-1H core*

| Sample | MPI 1 | MPI 2 | MA(I)/ MA(I+II) | TA(I)/ TA(I+II) | $C_{26}$ TA (20S/20S+20R) | TA28/ (MA29+TA28) | %$C_{27}$ MAS | %$C_{28}$ MAS | %$C_{29}$ MAS |
|---|---|---|---|---|---|---|---|---|---|
| EFMK-1 | 0.72 | 0.78 | 0.46 | 0.53 | 0.21 | 0.96 | 30.03 | 52.86 | 17.11 |
| EFMK-4 | 0.68 | 0.77 | 0.53 | 0.64 | 0.20 | 0.96 | 31.38 | 51.03 | 17.59 |
| EFMK-8 | 0.73 | 0.80 | 0.57 | 0.69 | 0.20 | 0.96 | 29.90 | 51.33 | 18.77 |
| EFMK-12 | 0.68 | 0.78 | 0.55 | 0.68 | 0.20 | 0.94 | 29.19 | 55.34 | 15.47 |
| EFMK-15 | 0.72 | 0.81 | 0.43 | 0.62 | 0.17 | 0.96 | 26.19 | 56.77 | 17.04 |
| EFMK-17 | 0.72 | 0.80 | 0.37 | 0.61 | 0.19 | 0.95 | 26.21 | 54.68 | 19.11 |
| EFMK-20 | 0.72 | 0.82 | 0.42 | 0.63 | 0.17 | 0.96 | 25.54 | 57.54 | 16.92 |
| EFMK-23 | 0.74 | 0.84 | 0.42 | 0.61 | 0.19 | 0.97 | 26.72 | 54.10 | 19.18 |
| EFMK-24 | 0.71 | 0.81 | 0.42 | 0.63 | 0.18 | 0.96 | 26.45 | 55.46 | 18.09 |
| EFMK-25 | 0.72 | 0.84 | 0.44 | 0.66 | 0.19 | 0.97 | 26.57 | 53.63 | 19.80 |
| EFMK-26 | 0.73 | 0.84 | 0.49 | 0.69 | 0.19 | 0.98 | 29.02 | 54.04 | 16.94 |

*Fasken "A" #1 core*

| Sample | MPI 1 | MPI 2 | MA(I)/ MA(I+II) | TA(I)/ TA(I+II) | $C_{26}$ TA (20S/20S+20R) | TA28/ (MA29+TA28) | %$C_{27}$ MAS | %$C_{28}$ MAS | %$C_{29}$ MAS |
|---|---|---|---|---|---|---|---|---|---|
| EFFA-1 | 0.93 | 1.03 | 0.59 | 0.74 | 0.21 | 0.50 | 45.42 | 40.05 | 14.53 |
| EFFA-3 | 0.89 | 0.93 | 0.55 | 0.70 | 0.22 | 0.63 | 25.40 | 60.54 | 14.06 |
| EFFA-5 | 0.91 | 0.96 | 0.50 | 0.72 | 0.21 | 0.62 | 26.16 | 60.05 | 13.79 |
| EFFA-11 | 0.96 | 1.04 | 0.46 | 0.71 | 0.22 | 0.65 | 24.93 | 60.99 | 14.09 |
| EFFA-17 | 0.89 | 0.95 | 0.50 | 0.71 | 0.21 | 0.60 | 25.69 | 59.85 | 14.47 |
| EFFA-18 | 0.91 | 0.97 | 0.49 | 0.76 | 0.23 | 0.58 | 26.78 | 58.71 | 14.51 |
| EFFA-20 | 0.90 | 0.97 | 0.49 | 0.75 | 0.25 | 0.41 | 23.84 | 63.85 | 12.31 |
| EFFA-21 | 0.82 | 0.86 | 0.62 | 0.66 | 0.22 | 0.58 | 26.90 | 59.66 | 13.44 |
| EFFA-23 | 0.89 | 0.95 | 0.59 | 0.72 | 0.21 | 0.59 | 27.30 | 60.39 | 12.31 |
| EFFA-24 | 0.87 | 0.88 | 0.58 | 0.67 | 0.19 | 0.62 | 25.87 | 61.83 | 12.31 |
| EFFA-28 | 0.87 | 0.89 | 0.58 | 0.70 | 0.21 | 0.61 | 24.05 | 61.25 | 14.70 |
| EFFA-32 | 0.91 | 0.94 | 0.53 | 0.69 | 0.21 | 0.64 | 26.69 | 60.82 | 12.49 |
| EFFA-37 | 0.77 | 0.82 | 0.64 | 0.73 | 0.21 | 0.59 | 25.61 | 62.11 | 12.29 |
| EFFA-38 | 0.93 | 0.95 | 0.52 | 0.66 | 0.21 | 0.62 | 25.86 | 60.97 | 13.17 |
| EFFA-40 | 0.86 | 0.90 | 0.50 | 0.71 | 0.23 | 0.59 | 26.49 | 60.92 | 12.58 |

*Bouldin Creek outcrop*

| Sample | MPI 1 | MPI 2 | MA(I)/ MA(I+II) | TA(I)/ TA(I+II) | $C_{26}$ TA (20S/20S+20R) | TA28/ (MA29+TA28) | %$C_{27}$ MAS | %$C_{28}$ MAS | %$C_{29}$ MAS |
|---|---|---|---|---|---|---|---|---|---|
| EFBC-5 | 0.44 | 0.36 | 0.03 | 0.13 | 0.11 | ND | 7.31 | 61.62 | 31.07 |
| EFBC-7 | 0.47 | 0.46 | 0.03 | 0.14 | 0.11 | ND | 7.14 | 62.56 | 30.31 |
| EFBC-9 | 0.47 | 0.43 | 0.03 | 0.12 | 0.10 | ND | 6.51 | 62.17 | 31.32 |
| EFBC-11 | 0.49 | 0.44 | 0.02 | 0.13 | 0.09 | ND | 6.15 | 63.50 | 30.35 |
| EFBC-15 | 0.41 | 0.44 | 0.03 | 0.12 | 0.11 | ND | 7.36 | 57.59 | 35.05 |
| EFBC-19 | 0.22 | 0.23 | 0.03 | 0.11 | 0.10 | ND | 7.01 | 57.90 | 35.09 |
| EFBC-20 | 0.31 | 0.31 | 0.04 | 0.10 | 0.12 | 0.01 | 7.96 | 59.44 | 32.60 |
| EFBC-23 | 0.30 | 0.31 | 0.04 | 0.11 | 0.12 | ND | 8.57 | 62.08 | 29.35 |
| EFBC-25 | 0.36 | 0.37 | 0.04 | 0.11 | 0.12 | 0.01 | 8.77 | 62.88 | 28.35 |
| EFBC-27 | 0.45 | 0.47 | 0.05 | 0.13 | 0.14 | 0.01 | 10.04 | 61.12 | 28.84 |
| EFBC-30 | 0.49 | 0.50 | 0.07 | 0.23 | 0.15 | ND | 11.62 | 55.58 | 32.80 |
| EFBC-32 | 0.55 | 0.60 | 0.05 | 0.15 | 0.17 | ND | 10.56 | 53.41 | 36.03 |
| EFBC-34 | 0.67 | 0.74 | 0.05 | 0.15 | 0.15 | ND | 9.67 | 53.50 | 36.83 |

*ACC#1 core*

| Sample | MPI 1 | MPI 2 | MA(I)/ MA(I+II) | TA(I)/ TA(I+II) | $C_{26}$ TA (20S/20S+20R) | TA28/ (MA29+TA28) | %$C_{27}$ MAS | %$C_{28}$ MAS | %$C_{29}$ MAS |
|---|---|---|---|---|---|---|---|---|---|
| EFAC-1 | 0.32 | 0.32 | 0.03 | 0.13 | 0.12 | 0.01 | 7.00 | 60.22 | 32.78 |
| EFAC-3 | 0.33 | 0.34 | 0.03 | 0.15 | 0.10 | ND | 6.46 | 58.97 | 34.57 |
| EFAC-6 | 0.39 | 0.40 | 0.05 | 0.19 | 0.13 | 0.01 | 9.57 | 63.28 | 27.15 |
| EFAC-7 | 0.37 | 0.39 | 0.06 | 0.23 | 0.13 | 0.01 | 12.60 | 53.11 | 34.29 |
| EFAC-8 | 0.42 | 0.44 | 0.05 | 0.21 | 0.13 | ND | 11.64 | 52.45 | 35.91 |
| EFAC-10 | 0.45 | 0.45 | 0.04 | 0.25 | 0.13 | 0.01 | 11.89 | 52.94 | 35.17 |

*W. Brechtel #1 core*

| Sample | MPI 1 | MPI 2 | MA(I)/ MA(I+II) | TA(I)/ TA(I+II) | $C_{26}$ TA (20S/20S+20R) | TA28/ (MA29+TA28) | %$C_{27}$ MAS | %$C_{28}$ MAS | %$C_{29}$ MAS |
|---|---|---|---|---|---|---|---|---|---|
| EFWB-1 | 0.68 | 0.79 | 0.08 | 0.09 | 0.22 | 0.17 | 26.07 | 61.47 | 12.46 |
| EFWB-3 | 0.66 | 0.77 | 0.07 | 0.07 | 0.16 | 0.13 | 24.99 | 51.28 | 23.72 |
| EFWB-4 | 0.65 | 0.74 | 0.05 | 0.07 | 0.17 | 0.22 | 20.09 | 68.54 | 11.38 |
| EFWB-7 | 0.58 | 0.67 | 0.06 | 0.09 | 0.20 | 0.26 | 23.80 | 65.21 | 10.99 |
| EFWB-8 | 0.48 | 0.56 | 0.05 | 0.08 | 0.19 | 0.19 | 21.91 | 67.22 | 10.87 |
| EFWB-9 | 0.63 | 0.74 | 0.10 | 0.34 | 0.20 | 0.35 | 28.27 | 61.19 | 10.54 |



*C.J. Hendershot #1 core*

| Sample | MPI 1 | MPI 2 | MA(I)/ MA(I+II) | TA(I)/ TA(I+II) | $C_{26}$ TA (20S/20S+20R) | TA28/ (MA29+TA28) | %$C_{27}$ MAS | %$C_{28}$ MAS | %$C_{29}$ MAS |
|---|---|---|---|---|---|---|---|---|---|
| EFHE-1 | 0.59 | 0.56 | 0.11 | 0.12 | 0.22 | 0.26 | 32.52 | 48.57 | 18.91 |
| EFHE-2 | 0.58 | 0.52 | 0.09 | 0.12 | 0.21 | 0.26 | 24.55 | 60.57 | 14.88 |
| EFHE-3 | 0.59 | 0.55 | 0.06 | 0.12 | 0.19 | 0.31 | 40.79 | 48.21 | 10.99 |
| EFHE-5 | 0.55 | 0.49 | 0.05 | 0.08 | 0.17 | 0.31 | 20.68 | 67.03 | 12.28 |
| EFHE-6 | 0.55 | 0.47 | 0.07 | 0.09 | 0.19 | 0.44 | 23.55 | 64.91 | 11.54 |
| EFHE-7 | 0.55 | 0.48 | 0.06 | 0.09 | 0.19 | 0.41 | 22.92 | 65.82 | 11.26 |
| EFHE-9 | 0.54 | 0.46 | 0.05 | 0.05 | 0.21 | 0.46 | 41.96 | 49.02 | 9.02 |
| EFHE-10 | 0.53 | 0.53 | 0.08 | 0.13 | 0.25 | 0.47 | 26.60 | 61.83 | 11.57 |

*Lily Hoppess #1 core*

| Sample | MPI 1 | MPI 2 | MA(I)/ MA(I+II) | TA(I)/ TA(I+II) | $C_{26}$ TA (20S/20S+20R) | TA28/ (MA29+TA28) | %$C_{27}$ MAS | %$C_{28}$ MAS | %$C_{29}$ MAS |
|---|---|---|---|---|---|---|---|---|---|
| EFLH-1 | 0.55 | 0.52 | 0.19 | 0.20 | 0.21 | 0.94 | 25.06 | 60.04 | 14.90 |
| EFLH-5 | 0.55 | 0.52 | 0.18 | 0.20 | 0.19 | 0.93 | 24.63 | 60.29 | 15.08 |
| EFLH-9 | 0.52 | 0.50 | 0.20 | 0.15 | 0.20 | 0.94 | 25.24 | 59.01 | 15.75 |
| EFLH-13 | 0.53 | 0.51 | 0.15 | 0.35 | 0.22 | 0.92 | 40.12 | 49.39 | 10.49 |
| EFLH-15 | 0.54 | 0.53 | 0.14 | 0.25 | 0.19 | 0.94 | 23.92 | 59.25 | 16.83 |
| EFLH-20 | 0.53 | 0.51 | 0.18 | 0.27 | 0.19 | 0.93 | 24.80 | 58.55 | 16.65 |



*Oils and condensates*

| Sample | MPI 1 | MPI 2 | MA(I)/ MA(I+II) | TA(I)/ TA(I+II) | $C_{26}$ TA (20S/ 20S+20R) | TA28/ (MA29+TA28) | %$C_{27}$ MAS | %$C_{28}$ MAS | %$C_{29}$ MAS |
|---|---|---|---|---|---|---|---|---|---|
| NWMK-533.2 | 0.63 | 0.66 | 0.44 | 0.70 | 0.16 | 0.78 | 26.46 | 56.81 | 16.73 |
| NFMK-526-1H | 0.65 | 0.73 | 0.54 | 0.79 | 0.17 | 0.76 | 26.82 | 50.03 | 23.16 |
| MJOG-UEF | 0.74 | 0.81 | 0.56 | 0.91 | 0.40 | 0.52 | 22.63 | 43.42 | 33.95 |
| MJOG-LEF | 0.81 | 0.87 | 0.64 | 0.94 | 0.50 | 0.43 | 22.83 | 40.49 | 36.68 |
| GREF-1-110 | 0.86 | 0.89 | 0.53 | ND | ND | ND | 24.29 | 48.78 | 26.93 |

**L. Quantitative biomarker analysis results for steranes (Concentrations are expressed as µg biomarkers/g TOC; ND = not determined)**

*Lozier Canyon outcrop*

| Sample Name | Diapreg | Preg | Diahomopreg | Homopreg | $C_{27}$ α-Dia (20S) | $C_{27}$ α-Dia (20R) | $C_{27}$ α -Dia (20S) | C27 α -Dia (20R) | $C_{28}$ α-Dia (20S) | $C_{28}$ α-Dia (20R) | $C_{28}$ α -Dia (20S) + $C_{27}$ αα (20S) | $C_{27}$ (20R) + $C_{29}$ α-Dia (20S) | $C_{27}$ (20S) + $C_{28}$ α -Dia (20R) | $C_{27}$ αα (20R) |
|---|---|---|---|---|---|---|---|---|---|---|---|---|---|---|
| EFLC-28 | 52 | 78 | 2 | 31 | 97 | 53 | 19 | 36 | 17 | 41 | 88 | 144 | 103 | 117 |
| EFLC-26 | 91 | 157 | 6 | 71 | 176 | 95 | 28 | 75 | 30 | 61 | 167 | 267 | 188 | 223 |
| EFLC-25 | 21 | 38 | 1 | 18 | 57 | 32 | 9 | 26 | 11 | 25 | 68 | 102 | 81 | 83 |
| EFLC-20 | 45 | 114 | 3 | 57 | 100 | 47 | 15 | 58 | 22 | 46 | 155 | 217 | 185 | 186 |
| EFLC-18 | 12 | 29 | 1 | 15 | 23 | 11 | 4 | 14 | 6 | 11 | 36 | 47 | 41 | 43 |
| EFLC-14 | 9 | 26 | 1 | 13 | 16 | 7 | 2 | 11 | 3 | 8 | 31 | 37 | 34 | 38 |
| EFLC-12 | 23 | 77 | 4 | 38 | 32 | 17 | 5 | 17 | 6 | 17 | 62 | 84 | 75 | 79 |
| EFLC-10 | 20 | 103 | 4 | 51 | 23 | 10 | 4 | 11 | 8 | 6 | 78 | 103 | 101 | 99 |
| EFLC-8 | 33 | 157 | 7 | 79 | 34 | 14 | 5 | 11 | 11 | 10 | 107 | 140 | 124 | 138 |
| EFLC-6 | 9 | 40 | 2 | 20 | 11 | 5 | 2 | 4 | 4 | 3 | 39 | 39 | 39 | 42 |
| EFLC-4 | 3 | 0 | 1 | 6 | 4 | 2 | 1 | 2 | 1 | 2 | 10 | 9 | 9 | 11 |
| EFLC-1 | 122 | 27 | 15 | 113 | 263 | 148 | 52 | 97 | 58 | 141 | 287 | 466 | 386 | 399 |

*Lozier Canyon outcrop (cont.)*

| Sample Name | $C_{29}$ α-Dia (20R) | $C_{29}$ α -Dia (20S) | $C_{28}$ αα (20S) | $C_{28}$ (20R) +$C_{29}$ α -Dia (20R) | $C_{28}$ (20S) | $C_{28}$ αα (20R) | $C_{29}$ αα (20S) | $C_{29}$ (20R) | $C_{29}$ (20S) | $C_{29}$ αα (20R) | $C_{30}$ αα (20S) | $C_{30}$ (20R) | $C_{30}$ (20S) | $C_{30}$ αα (20R) |
|---|---|---|---|---|---|---|---|---|---|---|---|---|---|---|
| EFLC-28 | 44 | 70 | 74 | 69 | 47 | 61 | 71 | 102 | 82 | 78 | 9 | 13 | 20 | 7 |
| EFLC-26 | 83 | 127 | 140 | 127 | 94 | 119 | 145 | 200 | 158 | 157 | 19 | 27 | 37 | 15 |
| EFLC-25 | 34 | 49 | 58 | 53 | 34 | 48 | 60 | 79 | 62 | 64 | 8 | 12 | 17 | 6 |
| EFLC-20 | 93 | 148 | 186 | 168 | 94 | 146 | 143 | 194 | 151 | 150 | 19 | 29 | 37 | 16 |
| EFLC-18 | 26 | 36 | 44 | 40 | 21 | 36 | 33 | 44 | 35 | 34 | 5 | 8 | 9 | 5 |
| EFLC-14 | 22 | 31 | 38 | 35 | 16 | 31 | 26 | 37 | 29 | 28 | 5 | 7 | 10 | 5 |
| EFLC-12 | 36 | 50 | 66 | 61 | 37 | 53 | 54 | 78 | 62 | 57 | 8 | 12 | 15 | 7 |
| EFLC-10 | 45 | 57 | 83 | 77 | 38 | 67 | 74 | 100 | 78 | 73 | 10 | 15 | 19 | 10 |
| EFLC-8 | 61 | 78 | 114 | 100 | 56 | 94 | 100 | 132 | 106 | 99 | 14 | 17 | 21 | 13 |
| EFLC-6 | 19 | 25 | 35 | 32 | 20 | 30 | 32 | 40 | 32 | 31 | 5 | 7 | 9 | 4 |
| EFLC-4 | 5 | 7 | 8 | 7 | 4 | 7 | 6 | 9 | 7 | 7 | 1 | 2 | 2 | 1 |
| EFLC-1 | 223 | 261 | 347 | 300 | 218 | 259 | 335 | 405 | 287 | 308 | 35 | 71 | 100 | 32 |

*Ferguson McKnight #526-1H core*

| Sample Name | Diapreg | Preg | Diahomopreg | Homopreg | $C_{27}$ α-Dia (20S) | $C_{27}$ α-Dia (20R) | $C_{27}$ α -Dia (20S) | $C_{27}$ α -Dia (20R) | $C_{28}$ α-Dia (20S) | $C_{28}$ α-Dia (20R) | $C_{28}$ α -Dia (20S) + $C_{27}$ αα (20S) | $C_{27}$ (20R) + $C_{29}$ α-Dia (20S) | $C_{27}$ (20S) + $C_{28}$ α -Dia (20R) | $C_{27}$ αα (20R) |
|---|---|---|---|---|---|---|---|---|---|---|---|---|---|---|
| EFMK-1 | 127 | 199 | 113 | 109 | 137 | 83 | 32 | 79 | 79 | 56 | 81 | 140 | 110 | 100 |
| EFMK-4 | 76 | 145 | 73 | 73 | 79 | 47 | 18 | 50 | 45 | 47 | 47 | 80 | 62 | 50 |
| EFMK-8 | 166 | 308 | 150 | 150 | 143 | 83 | 33 | 94 | 88 | 106 | 88 | 151 | 129 | 206 |
| EFMK-12 | 88 | 159 | 76 | 75 | 70 | 43 | 16 | 46 | 45 | 53 | 43 | 72 | 57 | 50 |
| EFMK-15 | 82 | 139 | 70 | 60 | 78 | 47 | 17 | 54 | 50 | 63 | 40 | 72 | 55 | 52 |
| EFMK-17 | 269 | 441 | 237 | 194 | 242 | 147 | 56 | 167 | 147 | 190 | 127 | 211 | 160 | 229 |
| EFMK-20 | 189 | 311 | 155 | 130 | 186 | 112 | 42 | 130 | 111 | 135 | 91 | 164 | 122 | 166 |
| EFMK-23 | 196 | 435 | 35 | 131 | 202 | 122 | 42 | 135 | 113 | 149 | 68 | 214 | 127 | 129 |
| EFMK-24 | 168 | 294 | 144 | 114 | 181 | 104 | 40 | 117 | 103 | 128 | 60 | 184 | 110 | 117 |
| EFMK-25 | 103 | 178 | 83 | 65 | 112 | 67 | 23 | 68 | 66 | 84 | 29 | 91 | 59 | 61 |
| EFMK-26 | 82 | 180 | 77 | 57 | 53 | 33 | 11 | 28 | 23 | 36 | 30 | 44 | 29 | 33 |

*Ferguson McKnight #526-1H core (cont.)*

| Sample Name | $C_{29}$ α-Dia (20R) | $C_{29}$ α -Dia (20S) | $C_{28}$ αα (20S) | $C_{28}$ (20R) +$C_{29}$ α -Dia (20R) | $C_{28}$ (20S) | $C_{28}$ αα (20R) | $C_{29}$ αα (20S) | $C_{29}$ (20R) | $C_{29}$ (20S) | $C_{29}$ αα (20R) | $C_{30}$ αα (20S) | $C_{30}$ (20R) | $C_{30}$ (20S) | $C_{30}$ αα (20R) |
|---|---|---|---|---|---|---|---|---|---|---|---|---|---|---|
| EFMK-1 | 98 | 73 | 84 | 67 | 53 | 69 | 45 | 84 | 68 | 58 | 13 | 14 | 19 | 10 |
| EFMK-4 | 52 | 46 | 52 | 43 | 21 | 41 | 27 | 50 | 41 | 35 | 8 | 9 | 11 | 5 |
| EFMK-8 | 105 | 87 | 96 | 93 | 65 | 71 | 56 | 96 | 81 | 63 | 15 | 16 | 21 | 10 |
| EFMK-12 | 49 | 39 | 44 | 42 | 28 | 33 | 26 | 44 | 37 | 30 | 7 | 8 | 10 | 4 |
| EFMK-15 | 49 | 40 | 43 | 34 | 25 | 32 | 22 | 42 | 35 | 28 | 6 | 8 | 8 | 5 |
| EFMK-17 | 99 | 121 | 128 | 96 | 60 | 102 | 64 | 124 | 105 | 90 | 23 | 26 | 29 | 13 |
| EFMK-20 | 69 | 88 | 90 | 70 | 61 | 69 | 48 | 97 | 80 | 68 | 16 | 18 | 22 | 10 |
| EFMK-23 | 129 | 92 | 90 | 74 | 59 | 69 | 48 | 107 | 88 | 65 | 18 | 19 | 22 | 11 |
| EFMK-24 | 60 | 81 | 78 | 64 | 58 | 59 | 41 | 92 | 74 | 58 | 14 | 18 | 18 | 9 |
| EFMK-25 | 36 | 43 | 44 | 41 | 12 | 33 | 15 | 40 | 30 | 26 | 7 | 8 | 10 | 5 |
| EFMK-26 | 35 | 25 | 28 | 23 | 16 | 23 | 15 | 27 | 19 | 17 | 3 | 7 | 6 | 3 |

*Fasken "A" #1 core*

| Sample Name | Diapreg | Preg | Diahomopreg | Homopreg | $C_{27}$ α-Dia (20S) | $C_{27}$ α-Dia (20R) | $C_{27}$ α -Dia (20S) | $C_{27}$ α -Dia (20R) | $C_{28}$ α-Dia (20S) | $C_{28}$ α-Dia (20R) | $C_{28}$ α -Dia (20S) + $C_{27}$ αα (20S) | $C_{27}$ (20R) + $C_{29}$ α-Dia (20S) | $C_{27}$ (20S) + $C_{28}$ α -Dia (20R) | $C_{27}$ αα (20R) |
|---|---|---|---|---|---|---|---|---|---|---|---|---|---|---|
| EFFA-1 | 2 | 4 | 0 | 1 | 1 | 0 | 0 | 0 | 0 | 0 | 0 | 1 | 0 | 1 |
| EFFA-3 | 0 | 0 | 0 | 0 | 0 | 0 | 0 | 0 | 0 | 0 | 0 | 0 | 0 | 0 |
| EFFA-5 | 9 | 25 | 2 | 6 | 3 | 2 | 1 | 2 | 1 | 2 | 2 | 4 | 2 | 5 |
| EFFA-11 | 14 | 30 | 2 | 8 | 5 | 3 | 1 | 3 | 1 | 3 | 4 | 5 | 3 | 7 |
| EFFA-17 | 11 | 23 | 1 | 6 | 3 | 2 | 1 | 2 | 1 | 2 | 2 | 3 | 2 | 5 |
| EFFA-18 | 11 | 28 | 2 | 7 | 4 | 2 | 1 | 2 | 1 | 2 | 3 | 4 | 2 | 6 |
| EFFA-20 | 1 | 3 | 0 | 1 | 0 | 0 | 0 | 0 | 0 | 0 | 0 | 0 | 0 | 1 |
| EFFA-21 | 3 | 7 | 0 | 2 | 1 | 1 | 0 | 0 | 0 | 0 | 1 | 1 | 0 | 1 |
| EFFA-23 | 6 | 12 | 1 | 3 | 2 | 1 | 0 | 1 | 1 | 1 | 1 | 2 | 1 | 2 |
| EFFA-24 | 34 | 68 | 4 | 17 | 8 | 5 | 1 | 3 | 3 | 4 | 6 | 8 | 5 | 12 |
| EFFA-28 | 18 | 44 | 2 | 12 | 5 | 3 | 1 | 2 | 2 | 2 | 4 | 6 | 4 | 8 |
| EFFA-32 | 38 | 95 | 6 | 23 | 12 | 7 | 3 | 6 | 4 | 6 | 9 | 12 | 7 | 15 |
| EFFA-37 | 4 | 9 | 0 | 2 | 1 | 1 | 0 | 0 | 0 | 1 | 1 | 1 | 1 | 2 |
| EFFA-38 | 21 | 43 | 3 | 12 | 6 | 3 | 1 | 3 | 2 | 2 | 4 | 6 | 3 | 8 |
| EFFA-40 | 5 | 12 | 1 | 3 | 2 | 1 | 0 | 1 | 1 | 1 | 1 | 2 | 1 | 3 |

*Fasken "A" #1 core (cont.)*

| Sample Name | $C_{29}$ α-Dia (20R) | $C_{29}$ α -Dia (20S) | $C_{28}$ αα (20S) | $C_{28}$ (20R) +$C_{29}$ α -Dia (20R) | $C_{28}$ (20S) | $C_{28}$ αα (20R) | $C_{29}$ αα (20S) | $C_{29}$ (20R) | $C_{29}$ (20S) | $C_{29}$ αα (20R) | $C_{30}$ αα (20S) | $C_{30}$ (20R) | $C_{30}$ (20S) | $C_{30}$ αα (20R) |
|---|---|---|---|---|---|---|---|---|---|---|---|---|---|---|
| EFFA-1 | 0 | 0 | 0 | 0 | 0 | 0 | 0 | 0 | 0 | 0 | 0 | 0 | 0 | 0 |
| EFFA-3 | 0 | 0 | 0 | 0 | 0 | 0 | 0 | 0 | 0 | 0 | 0 | 0 | 0 | 0 |
| EFFA-5 | 1 | 2 | 2 | 1 | 1 | 3 | 2 | 3 | 2 | 2 | 0 | 0 | 0 | 0 |
| EFFA-11 | 2 | 3 | 3 | 2 | 2 | 4 | 2 | 4 | 2 | 4 | 0 | 0 | 1 | 0 |
| EFFA-17 | 1 | 2 | 2 | 1 | 1 | 3 | 2 | 2 | 1 | 3 | 0 | 0 | 0 | 0 |
| EFFA-18 | 2 | 2 | 2 | 2 | 3 | 4 | 2 | 3 | 2 | 3 | 0 | 0 | 0 | 0 |
| EFFA-20 | 0 | 0 | 0 | 0 | 0 | 0 | 0 | 0 | 0 | 0 | 0 | 0 | 0 | 0 |
| EFFA-21 | 0 | 0 | 1 | 0 | 0 | 1 | 0 | 1 | 0 | 1 | 0 | 0 | 0 | 0 |
| EFFA-23 | 1 | 1 | 1 | 1 | 1 | 1 | 1 | 1 | 1 | 1 | 0 | 0 | 0 | 0 |
| EFFA-24 | 4 | 5 | 5 | 4 | 3 | 8 | 4 | 7 | 4 | 6 | 0 | 0 | 1 | 0 |
| EFFA-28 | 2 | 3 | 3 | 2 | 3 | 5 | 3 | 5 | 2 | 4 | 0 | 0 | 1 | 0 |
| EFFA-32 | 8 | 7 | 6 | 5 | 6 | 12 | 5 | 9 | 5 | 9 | 1 | 1 | 1 | 1 |
| EFFA-37 | 0 | 1 | 1 | 1 | 1 | 1 | 0 | 1 | 0 | 1 | 0 | 0 | 0 | 0 |
| EFFA-38 | 3 | 3 | 3 | 2 | 2 | 4 | 2 | 4 | 2 | 4 | 0 | 0 | 1 | 0 |
| EFFA-40 | 1 | 1 | 1 | 1 | 1 | 1 | 1 | 1 | 1 | 1 | 0 | 0 | 0 | 0 |

*Bouldin Creek outcrop*

| Sample Name | Diapreg | Preg | Diahomopreg | Homopreg | $C_{27}$ α-Dia (20S) | $C_{27}$ α-Dia (20R) | $C_{27}$ α -Dia (20S) | $C_{27}$ α -Dia (20R) | $C_{28}$ α-Dia (20S) | $C_{28}$ α-Dia (20R) | $C_{28}$ α -Dia (20S) + $C_{27}$ αα (20S) | $C_{27}$ (20R) + $C_{29}$ α-Dia (20S) | $C_{27}$ (20S) + $C_{28}$ α -Dia (20R) | $C_{27}$ αα (20R) |
|---|---|---|---|---|---|---|---|---|---|---|---|---|---|---|
| EFBC-5 | 0 | 1 | 2 | 0 | ND | 0 | 0 | ND | ND | 0 | 6 | 0 | 0 | 14 |
| EFBC-7 | 0 | 1 | 2 | 0 | ND | 0 | 0 | ND | ND | 0 | 7 | 1 | 0 | 16 |
| EFBC-9 | 0 | 1 | 3 | 1 | ND | 0 | 0 | ND | ND | 1 | 7 | 1 | 1 | 16 |
| EFBC-11 | 0 | 1 | 2 | 0 | ND | 0 | 0 | ND | ND | 1 | 7 | 1 | 1 | 14 |
| EFBC-15 | 0 | 1 | 2 | 0 | ND | 0 | 0 | ND | ND | 0 | 3 | 0 | 0 | 6 |
| EFBC-19 | 1 | 3 | 4 | 1 | ND | 0 | 0 | ND | ND | 1 | 16 | 2 | 0 | 33 |
| EFBC-20 | 1 | 11 | 2 | 3 | ND | 1 | 1 | ND | ND | 2 | 22 | 3 | 2 | 43 |
| EFBC-23 | 1 | 7 | 1 | 2 | ND | 0 | 0 | ND | ND | 2 | 18 | 3 | 2 | 34 |
| EFBC-25 | 1 | 6 | 1 | 2 | ND | 0 | 0 | ND | ND | 1 | 12 | 2 | 2 | 24 |
| EFBC-27 | 1 | 6 | 1 | 2 | 0 | 0 | 0 | ND | ND | 2 | 13 | 2 | 2 | 24 |
| EFBC-30 | 1 | 3 | 5 | 2 | 0 | 0 | 0 | ND | ND | 2 | 22 | 3 | 2 | 42 |
| EFBC-32 | 1 | 5 | 10 | 2 | 0 | 1 | 0 | ND | ND | 4 | 47 | 5 | 4 | 89 |
| EFBC-34 | 1 | 3 | 6 | 1 | 0 | 0 | 0 | ND | ND | 3 | 31 | 3 | 3 | 58 |

*Bouldin Creek outcrop (cont.)*

| Sample Name | $C_{29}$ α-Dia (20R) | $C_{29}$ α -Dia (20S) | $C_{28}$ αα (20S) | $C_{28}$ (20R) +$C_{29}$ α -Dia (20R) | $C_{28}$ (20S) | $C_{28}$ αα (20R) | $C_{29}$ αα (20S) | $C_{29}$ (20R) | $C_{29}$ (20S) | $C_{29}$ αα (20R) | $C_{30}$ αα (20S) | $C_{30}$ (20R) | $C_{30}$ (20S) | $C_{30}$ αα (20R) |
|---|---|---|---|---|---|---|---|---|---|---|---|---|---|---|
| EFBC-5 | 1 | ND | 8 | 1 | 0 | 15 | ND | 4 | ND | 9 | 0 | ND | 1 | 2 |
| EFBC-7 | 1 | ND | 9 | 1 | 0 | 17 | ND | 4 | ND | 9 | 0 | ND | 1 | 2 |
| EFBC-9 | 1 | ND | 10 | 1 | 0 | 19 | ND | 5 | ND | 11 | 0 | ND | 1 | 2 |
| EFBC-11 | 1 | ND | 10 | 1 | 0 | 16 | ND | 4 | ND | 8 | 0 | ND | 1 | 2 |
| EFBC-15 | 0 | ND | 4 | 0 | 0 | 6 | ND | 2 | ND | 4 | 0 | ND | 1 | 1 |
| EFBC-19 | 3 | ND | 17 | 2 | 1 | 28 | 1 | 15 | ND | 27 | 1 | ND | 4 | 5 |
| EFBC-20 | 2 | ND | 24 | 3 | 2 | 35 | ND | 17 | ND | 32 | ND | ND | 4 | 5 |
| EFBC-23 | 4 | ND | 28 | 3 | 0 | 39 | 1 | 14 | ND | 24 | 1 | ND | 3 | 4 |
| EFBC-25 | 3 | ND | 22 | 2 | 1 | 29 | ND | 10 | ND | 17 | 1 | ND | 3 | 3 |
| EFBC-27 | 3 | ND | 18 | 2 | 1 | 24 | ND | 10 | ND | 17 | 1 | ND | 3 | 3 |
| EFBC-30 | 3 | ND | 24 | 2 | 1 | 39 | ND | 14 | ND | 27 | 1 | ND | 5 | 4 |
| EFBC-32 | 8 | 4 | ND | 5 | 2 | 101 | 2 | 30 | ND | 60 | 2 | ND | 10 | 10 |
| EFBC-34 | 5 | ND | 43 | 4 | 2 | 75 | 2 | 21 | ND | 43 | 2 | ND | 7 | 7 |

*ACC #1 core*

| Sample Name | Diapreg | Preg | Diahomopreg | Homopreg | $C_{27}$ α-Dia (20S) | $C_{27}$ α-Dia (20R) | $C_{27}$ α -Dia (20S) | $C_{27}$ α -Dia (20R) | $C_{28}$ α-Dia (20S) | $C_{28}$ α-Dia (20R) | $C_{28}$ α -Dia (20S) + $C_{27}$ αα (20S) | $C_{27}$ (20R) + $C_{29}$ α-Dia (20S) | $C_{27}$ (20S) + $C_{28}$ α -Dia (20R) | $C_{27}$ αα (20R) |
|---|---|---|---|---|---|---|---|---|---|---|---|---|---|---|
| EFAC-1 | 10 | 56 | 56 | 12 | ND | ND | ND | ND | ND | ND | 61 | 4 | ND | 163 |
| EFAC-3 | 10 | 37 | 69 | 11 | ND | ND | ND | ND | ND | ND | 108 | 8 | 8 | 273 |
| EFAC-6 | 9 | 32 | 22 | 10 | ND | ND | ND | ND | ND | ND | 46 | 6 | ND | 128 |
| EFAC-7 | 3 | 13 | 17 | 4 | 1 | ND | ND | ND | ND | ND | 72 | 4 | ND | 181 |
| EFAC-8 | 2 | 14 | 21 | 4 | ND | ND | ND | ND | ND | ND | 73 | 4 | ND | 196 |
| EFAC-10 | 24 | 64 | 50 | 20 | ND | ND | ND | ND | ND | ND | 235 | 22 | ND | 790 |

*ACC #1 core (cont.)*

| Sample Name | $C_{29}$ α-Dia (20R) | $C_{29}$ α -Dia (20S) | $C_{28}$ αα (20S) | $C_{28}$ (20R) +$C_{29}$ α -Dia (20R) | $C_{28}$ (20S) | $C_{28}$ αα (20R) | $C_{29}$ αα (20S) | $C_{29}$ (20R) | $C_{29}$ (20S) | $C_{29}$ αα (20R) | $C_{30}$ αα (20S) | $C_{30}$ (20R) | $C_{30}$ (20S) | $C_{30}$ αα (20R) |
|---|---|---|---|---|---|---|---|---|---|---|---|---|---|---|
| EFAC-1 | 6 | ND | 44 | ND | ND | 100 | ND | 38 | ND | 98 | ND | ND | 10 | 17 |
| EFAC-3 | 9 | ND | 112 | ND | ND | 263 | ND | 70 | ND | 184 | ND | ND | 19 | 36 |
| EFAC-6 | 4 | ND | 44 | ND | ND | 103 | ND | 25 | ND | 70 | ND | ND | 8 | 12 |
| EFAC-7 | 6 | ND | 71 | ND | ND | 184 | ND | 38 | ND | 110 | ND | ND | 11 | 14 |
| EFAC-8 | 6 | ND | 77 | ND | ND | 189 | ND | 37 | ND | 106 | ND | ND | 12 | 15 |
| EFAC-10 | 24 | ND | 236 | ND | ND | 683 | ND | 205 | ND | 711 | ND | ND | 60 | 86 |

*W. Brechtel #1 core*

| Sample Name | Diapreg | Preg | Diahomopreg | Homopreg | $C_{27}$ α-Dia (20S) | $C_{27}$ α-Dia (20R) | $C_{27}$ α -Dia (20S) | $C_{27}$ α -Dia (20R) | $C_{28}$ α-Dia (20S) | $C_{28}$ α-Dia (20R) | $C_{28}$ α -Dia (20S) + $C_{27}$ αα (20S) | $C_{27}$ (20R) + $C_{29}$ α-Dia (20S) | $C_{27}$ (20S) + $C_{28}$ α -Dia (20R) | $C_{27}$ αα (20R) |
|---|---|---|---|---|---|---|---|---|---|---|---|---|---|---|
| EFWB-1 | 35 | 43 | 23 | 75 | 16 | 6 | ND | 10 | 12 | 5 | 144 | 57 | 51 | 233 |
| EFWB-3 | 38 | 67 | 30 | 93 | 27 | 12 | 6 | 12 | 14 | 15 | 149 | 58 | 60 | 239 |
| EFWB-4 | 29 | 44 | 14 | 70 | 19 | 8 | 4 | 9 | 10 | 11 | 103 | 42 | 50 | 154 |
| EFWB-7 | 57 | 71 | 19 | 137 | 29 | 10 | 6 | 10 | 13 | 11 | 147 | 96 | 99 | 200 |
| EFWB-8 | 27 | 34 | 9 | 65 | 18 | 8 | 3 | 7 | 7 | 9 | 83 | 46 | 48 | 111 |
| EFWB-9 | 38 | 93 | 27 | 91 | 15 | 6 | 2 | 6 | 7 | ND | 107 | 78 | 77 | 119 |

*W. Brechtel #1 core (cont.)*

| Sample Name | $C_{29}$ α-Dia (20R) | $C_{29}$ α -Dia (20S) | $C_{28}$ αα (20S) | $C_{28}$ (20R) +$C_{29}$ α -Dia (20R) | $C_{28}$ (20S) | $C_{28}$ αα (20R) | $C_{29}$ αα (20S) | $C_{29}$ (20R) | $C_{29}$ (20S) | $C_{29}$ αα (20R) | $C_{30}$ αα (20S) | $C_{30}$ (20R) | $C_{30}$ (20S) | $C_{30}$ αα (20R) |
|---|---|---|---|---|---|---|---|---|---|---|---|---|---|---|
| EFWB-1 | 24 | 48 | 101 | 63 | 21 | 140 | 65 | 66 | 45 | 115 | 25 | 12 | 30 | 24 |
| EFWB-3 | 57 | 93 | 151 | 105 | 28 | 235 | 82 | 75 | 47 | 136 | 21 | 7 | 23 | 22 |
| EFWB-4 | 39 | 61 | 100 | 73 | 25 | 159 | 62 | 55 | 31 | 100 | 15 | 5 | 17 | 16 |
| EFWB-7 | 21 | 69 | 142 | 124 | 24 | 158 | 82 | 89 | 70 | 101 | 20 | 11 | 35 | 18 |
| EFWB-8 | 26 | 41 | 74 | 66 | 14 | 91 | 42 | 42 | 32 | 54 | 11 | 6 | 18 | 10 |
| EFWB-9 | 26 | 48 | 104 | 96 | 18 | 104 | 69 | 73 | 60 | 77 | 14 | 13 | 24 | 11 |

*C.J. Hendershot #1 core*

| Sample Name | Diapreg | Preg | Diahomopreg | Homopreg | $C_{27}$ α-Dia (20S) | $C_{27}$ α-Dia (20R) | $C_{27}$ α -Dia (20S) | $C_{27}$ α -Dia (20R) | $C_{28}$ α-Dia (20S) | $C_{28}$ α-Dia (20R) | $C_{28}$ α -Dia (20S) + $C_{27}$ αα (20S) | $C_{27}$ (20R) + $C_{29}$ α-Dia (20S) | $C_{27}$ (20S) + $C_{28}$ α -Dia (20R) | $C_{27}$ αα (20R) |
|---|---|---|---|---|---|---|---|---|---|---|---|---|---|---|
| EFHE-1 | 184 | 236 | 171 | 145 | 261 | 191 | 67 | 90 | 116 | 132 | 1142 | 276 | 224 | 2487 |
| EFHE-2 | 151 | 206 | 151 | 133 | 117 | 95 | 35 | 62 | 58 | 82 | 1196 | 169 | 187 | 2528 |
| EFHE-3 | 196 | 244 | 148 | 137 | 214 | 165 | 59 | 124 | 89 | 188 | 1272 | 231 | 270 | 2657 |
| EFHE-5 | 192 | 271 | 147 | 173 | 285 | 194 | 65 | 252 | 168 | 281 | 916 | 273 | 218 | 1598 |
| EFHE-6 | 167 | 334 | 334 | 151 | 229 | 143 | 48 | 148 | 93 | 153 | 717 | 207 | 162 | 1090 |
| EFHE-7 | 186 | 253 | 128 | 160 | 248 | 160 | 55 | 95 | 107 | 194 | 789 | 232 | 188 | 1198 |
| EFHE-9 | 124 | 298 | 29 | 175 | 116 | 66 | 26 | 45 | 39 | 52 | 835 | 241 | 238 | 903 |
| EFHE-10 | 164 | 187 | 15 | 47 | 364 | 203 | 77 | 193 | 120 | 203 | 538 | 230 | 198 | 677 |

*C.J. Hendershot #1 core (cont.)*

| Sample Name | $C_{29}$ α-Dia (20R) | $C_{29}$ α -Dia (20S) | $C_{28}$ αα (20S) | $C_{28}$ (20R) +$C_{29}$ α -Dia (20R) | $C_{28}$ (20S) | $C_{28}$ αα (20R) | $C_{29}$ αα (20S) | $C_{29}$ (20R) | $C_{29}$ (20S) | $C_{29}$ αα (20R) | $C_{30}$ αα (20S) | $C_{30}$ (20R) | $C_{30}$ (20S) | $C_{30}$ αα (20R) |
|---|---|---|---|---|---|---|---|---|---|---|---|---|---|---|
| EFHE-1 | 253 | 289 | 468 | 75 | 181 | 1747 | 343 | 531 | 79 | 1392 | 143 | 26 | 98 | 266 |
| EFHE-2 | 269 | 349 | 520 | 80 | 177 | 2058 | 368 | 594 | 77 | 1629 | 160 | 48 | 105 | 305 |
| EFHE-3 | 298 | 492 | 606 | 138 | 221 | 2430 | 486 | 629 | 68 | 1860 | 190 | 39 | 124 | 313 |
| EFHE-5 | 249 | 557 | 565 | 213 | 175 | 1907 | 451 | 385 | 108 | 1156 | 128 | 43 | 101 | 216 |
| EFHE-6 | 167 | 379 | 345 | 147 | 134 | 1043 | 382 | 282 | 98 | 720 | 85 | 29 | 62 | 119 |
| EFHE-7 | 198 | 424 | 407 | 180 | 156 | 1177 | 457 | 315 | 106 | 840 | 100 | 35 | 79 | 138 |
| EFHE-9 | 28 | 454 | 421 | 255 | 149 | 966 | 541 | 294 | 163 | 604 | 104 | 46 | 92 | 102 |
| EFHE-10 | 117 | 283 | 230 | 109 | 147 | 527 | 404 | 226 | 101 | 491 | 74 | 32 | 77 | 89 |

*Lily Hoppess #1 core*

| Sample Name | Diapreg | Preg | Diahomopreg | Homopreg | $C_{27}$ α-Dia (20S) | $C_{27}$ α-Dia (20R) | $C_{27}$ α -Dia (20S) | $C_{27}$ α -Dia (20R) | $C_{28}$ α-Dia (20S) | $C_{28}$ α-Dia (20R) | $C_{28}$ α -Dia (20S) + $C_{27}$ αα (20S) | $C_{27}$ (20R) + $C_{29}$ α-Dia (20S) | $C_{27}$ (20S) + $C_{28}$ α -Dia (20R) | $C_{27}$ αα (20R) |
|---|---|---|---|---|---|---|---|---|---|---|---|---|---|---|
| EFLH-1 | 248 | 350 | 205 | 217 | 421 | 256 | 107 | 258 | 229 | 326 | 294 | 413 | 340 | 362 |
| EFLH-5 | 337 | 473 | 288 | 277 | 606 | 377 | 161 | 456 | 406 | 566 | 407 | 559 | 498 | 522 |
| EFLH-9 | 281 | 422 | 226 | 248 | 482 | 291 | 126 | 310 | 263 | 385 | 323 | 460 | 400 | 408 |
| EFLH-13 | 48 | 47 | 31 | 23 | 102 | 64 | 26 | 61 | 45 | 71 | 31 | 99 | 59 | 30 |
| EFLH-15 | 177 | 232 | 138 | 125 | 358 | 220 | 94 | 289 | 220 | 330 | 141 | 414 | 272 | 163 |
| EFLH-20 | 149 | 198 | 107 | 99 | 237 | 143 | 64 | 174 | 131 | 195 | 97 | 279 | 224 | 180 |

*Lily Hoppess #1 core (cont.)*

| Sample Name | $C_{29}$ α-Dia (20R) | $C_{29}$ α -Dia (20S) | $C_{28}$ αα (20S) | $C_{28}$ (20R) +$C_{29}$ α -Dia (20R) | $C_{28}$ (20S) | $C_{28}$ αα (20R) | $C_{29}$ αα (20S) | $C_{29}$ (20R) | $C_{29}$ (20S) | $C_{29}$ αα (20R) | $C_{30}$ αα (20S) | $C_{30}$ (20R) | $C_{30}$ (20S) | $C_{30}$ αα (20R) |
|---|---|---|---|---|---|---|---|---|---|---|---|---|---|---|
| EFLH-1 | 275 | 256 | 245 | 258 | 116 | 227 | 154 | 222 | 188 | 181 | 48 | 57 | 54 | 38 |
| EFLH-5 | 498 | 409 | 426 | 510 | 270 | 367 | 223 | 336 | 274 | 251 | 62 | 79 | 74 | 52 |
| EFLH-9 | 365 | 304 | 350 | 296 | 179 | 282 | 184 | 278 | 244 | 213 | 56 | 80 | 76 | 46 |
| EFLH-13 | 92 | 40 | 34 | 27 | 39 | 24 | 27 | 39 | 32 | 26 | 6 | 14 | 14 | 5 |
| EFLH-15 | 454 | 199 | 203 | 161 | 178 | 154 | 121 | 190 | 172 | 132 | 33 | 52 | 46 | 27 |
| EFLH-20 | 183 | 126 | 146 | 116 | 120 | 96 | 88 | 137 | 123 | 87 | 21 | 33 | 34 | 17 |

*Oils and condensates (Concentrations are expressed as µg biomarkers/g whole oil; ND = not determined)*

| Sample Name | Diapreg | Preg | Diahomopreg | Homopreg | $C_{27}$ α-Dia (20S) | $C_{27}$ α-Dia (20R) | $C_{27}$ α -Dia (20S) | $C_{27}$ α -Dia (20R) | $C_{28}$ α-Dia (20S) | $C_{28}$ α-Dia (20R) | $C_{28}$ α -Dia (20S) + $C_{27}$ αα (20S) | $C_{27}$ (20R) + $C_{29}$ α-Dia (20S) | $C_{27}$ (20S) + $C_{28}$ α -Dia (20R) | $C_{27}$ αα (20R) |
|---|---|---|---|---|---|---|---|---|---|---|---|---|---|---|
| NWMK-533.2 | 343 | 1133 | 35 | 415 | 435 | 348 | 100 | 273 | 271 | 154 | 262 | 555 | 405 | 452 |
| NFMK-526-1H | 286 | 882 | 34 | 214 | 289 | 216 | 70 | 178 | 149 | 88 | 115 | 243 | 166 | 194 |
| MJOG-UEF | 63 | 85 | 4 | 17 | 32 | 29 | 9 | 19 | 13 | 9 | 12 | 22 | 11 | 35 |
| MJOG-LEF | 115 | 175 | 8 | 14 | 95 | 57 | 26 | 50 | 41 | 30 | 26 | 67 | 34 | 85 |
| GREF-1-110 | ND | ND | ND | ND | ND | ND | ND | ND | ND | ND | ND | ND | ND | ND |

*Oils and condensates (Concentrations are expressed as µg biomarkers/g whole oil; ND = not determined; cont.)*

| Sample Name | $C_{29}$ α-Dia (20R) | $C_{29}$ α -Dia (20S) | $C_{28}$ αα (20S) | $C_{28}$ (20R) +$C_{29}$ α -Dia (20R) | $C_{28}$ (20S) | $C_{28}$ αα (20R) | $C_{29}$ αα (20S) | $C_{29}$ (20R) | $C_{29}$ (20S) | $C_{29}$ αα (20R) | $C_{30}$ αα (20S) | $C_{30}$ (20R) | $C_{30}$ (20S) | $C_{30}$ αα (20R) |
|---|---|---|---|---|---|---|---|---|---|---|---|---|---|---|
| NWMK-533.2 | 290 | 297 | 425 | 692 | 465 | 178 | 175 | 348 | 268 | 237 | 56 | 67 | 121 | 43 |
| NFMK-526-1H | 105 | 133 | 162 | 212 | 50 | 116 | 64 | 151 | 106 | 102 | 21 | 28 | 31 | 20 |
| MJOG-UEF | 6 | 8 | 8 | 7 | 6 | 6 | 3 | 8 | 10 | 7 | 1 | ND | ND | ND |
| MJOG-LEF | 11 | 22 | 17 | 14 | 23 | 15 | 8 | 25 | 16 | 11 | 3 | 5 | 3 | 4 |
| GREF-1-110 | ND | ND | ND | ND | ND | ND | ND | ND | ND | ND | ND | ND | ND | ND |

**M. Quantitative biomarker analysis results for terpanes (Concentrations are expressed as µg biomarkers/g TOC; ND = not determined)**

*Lozier Canyon outcrop*

| Sample Name | $C_{20}$ TR | $C_{21}$ TR | $C_{22}$ TR | $C_{23}$ TR | $C_{24}$ TR | $C_{25}$ TR | $C_{24}$ TT | $C_{26}$ TR | $C_{26}$ TR | $C_{28}$ TR | $C_{28}$ TR | $C_{29}$ TR | $C_{29}$ TR | $T_s$ | $T_m$ |
|---|---|---|---|---|---|---|---|---|---|---|---|---|---|---|---|
| EFLC-28 | 28 | 61 | 15 | 92 | 52 | 44 | 18 | 17 | 25 | 11 | 13 | 8 | 11 | 51 | 111 |
| EFLC-26 | 52 | 108 | 35 | 216 | 115 | 108 | 35 | 30 | 52 | 26 | 27 | 24 | 28 | 63 | 253 |
| EFLC-25 | 11 | 25 | 9 | 55 | 32 | 31 | 11 | 10 | 18 | 7 | 10 | 9 | 10 | 25 | 104 |
| EFLC-20 | 20 | 55 | 30 | 181 | 77 | 87 | 27 | 23 | 39 | 23 | 24 | 25 | 28 | 53 | 232 |
| EFLC-18 | 6 | 14 | 9 | 58 | 19 | 24 | 7 | 6 | 10 | 6 | 7 | 7 | 8 | 13 | 52 |
| EFLC-14 | 6 | 15 | 12 | 79 | 23 | 31 | 8 | 7 | 9 | 8 | 9 | 10 | 10 | 15 | 58 |
| EFLC-12 | 19 | 48 | 42 | 236 | 68 | 83 | 23 | 20 | 23 | 19 | 20 | 26 | 27 | 44 | 143 |
| EFLC-10 | 30 | 72 | 66 | 336 | 98 | 122 | 32 | 28 | 44 | 27 | 30 | 38 | 37 | 59 | 221 |
| EFLC-8 | 49 | 112 | 98 | 495 | 146 | 177 | 48 | 40 | 68 | 38 | 42 | 51 | 49 | 88 | 315 |
| EFLC-6 | 12 | 29 | 26 | 132 | 42 | 52 | 16 | 13 | 19 | 13 | 14 | 16 | 16 | 28 | 97 |
| EFLC-4 | 5 | 11 | 9 | 47 | 12 | 15 | 4 | 3 | 6 | 3 | 3 | 4 | 4 | 10 | 27 |
| EFLC-1 | 76 | 113 | 40 | 169 | 161 | 133 | 49 | 87 | 60 | 25 | 25 | 33 | 40 | 169 | 463 |

*Lozier Canyon outcrop (cont.)*

| Sample Name | $C_{29}$ αβ-30-NorH | $C_{29}$ Ts | $C_{30}$ D | $C_{29}$ βα-30-NorM | $C_{30}$ H | $C_{30}$ Mor | $C_{31}$ HH (22S) | $C_{31}$ HH (22R) | $C_{32}$ HH (22S) | $C_{32}$ HH (22R) | $C_{33}$ HH (22S) | $C_{33}$ HH (22R) | $C_{34}$ HH (22S) | $C_{34}$ HH (22R) | $C_{35}$ HH (22S) | $C_{35}$ HH (22R) |
|---|---|---|---|---|---|---|---|---|---|---|---|---|---|---|---|---|
| EFLC-28 | 236 | 44 | 8 | 18 | 392 | 25 | 300 | 182 | 183 | 121 | 97 | 60 | 72 | 40 | 86 | 48 |
| EFLC-26 | 504 | 65 | 13 | 34 | 808 | 52 | 606 | 383 | 344 | 227 | 185 | 114 | 123 | 70 | 125 | 71 |
| EFLC-25 | 231 | 28 | 6 | 15 | 401 | 24 | 286 | 183 | 172 | 116 | 97 | 60 | 68 | 39 | 79 | 45 |
| EFLC-20 | 425 | 47 | 7 | 30 | 652 | 41 | 548 | 345 | 313 | 205 | 197 | 121 | 126 | 74 | 184 | 104 |
| EFLC-18 | 101 | 10 | 2 | 7 | 147 | 9 | 133 | 83 | 75 | 49 | 50 | 31 | 33 | 19 | 48 | 27 |
| EFLC-14 | 121 | ND | 1 | 7 | 144 | 9 | 132 | 81 | 74 | 48 | 50 | 30 | 33 | 18 | 48 | 26 |
| EFLC-12 | 253 | ND | 3 | 16 | 305 | 18 | 244 | 158 | 132 | 90 | 88 | 56 | 61 | 35 | 89 | 51 |
| EFLC-10 | 464 | ND | 6 | 29 | 567 | 34 | 389 | 260 | 214 | 147 | 149 | 96 | 102 | 60 | 142 | 82 |
| EFLC-8 | 646 | ND | 9 | 39 | 766 | 49 | 540 | 351 | 287 | 197 | 204 | 130 | 140 | 82 | 190 | 108 |
| EFLC-6 | 198 | ND | 3 | 12 | 234 | 15 | 168 | 109 | 91 | 64 | 65 | 41 | 46 | 27 | 65 | 38 |
| EFLC-4 | 56 | ND | 1 | 3 | 63 | 4 | 49 | 31 | 27 | 18 | 19 | 12 | 14 | 8 | 20 | 11 |
| EFLC-1 | 696 | 171 | 47 | 68 | 1233 | 94 | 801 | 535 | 580 | 429 | 375 | 244 | 393 | 228 | 567 | 376 |

*Ferguson McKnight #526-1H core*

| Sample Name | $C_{20}$ TR | $C_{21}$ TR | $C_{22}$ TR | $C_{23}$ TR | $C_{24}$ TR | $C_{25}$ TR | $C_{24}$ TT | $C_{26}$ TR | $C_{26}$ TR | $C_{28}$ TR | $C_{28}$ TR | $C_{29}$ TR | $C_{29}$ TR | $T_s$ | $T_m$ |
|---|---|---|---|---|---|---|---|---|---|---|---|---|---|---|---|
| EFMK-1 | 209 | 216 | 65 | 331 | 205 | 184 | 64 | 43 | 46 | 44 | 45 | 52 | 50 | 79 | 81 |
| EFMK-4 | 92 | 120 | 26 | 178 | 115 | 116 | 41 | 36 | 28 | 30 | 31 | 37 | 30 | 56 | 44 |
| EFMK-8 | 244 | 272 | 65 | 393 | 243 | 237 | 96 | 83 | 68 | 73 | 68 | 77 | 61 | 160 | 94 |
| EFMK-12 | 137 | 135 | 37 | 195 | 118 | 110 | 44 | 38 | 36 | 29 | 30 | 33 | 27 | 65 | 43 |
| EFMK-15 | 111 | 111 | 32 | 158 | 99 | 93 | 34 | 36 | 29 | 28 | 26 | 31 | 25 | 82 | 42 |
| EFMK-17 | 392 | 381 | 100 | 529 | 299 | 264 | 98 | 115 | 93 | 80 | 89 | 80 | 68 | 261 | 139 |
| EFMK-20 | 254 | 280 | 69 | 402 | 256 | 241 | 88 | 92 | 64 | 66 | 65 | 81 | 65 | 188 | 95 |
| EFMK-23 | 255 | 292 | 73 | 432 | 279 | 257 | 94 | 107 | 62 | 77 | 77 | 87 | 72 | 203 | 107 |
| EFMK-24 | 223 | 243 | 60 | 365 | 243 | 234 | 82 | 95 | 55 | 73 | 69 | 78 | 68 | 183 | 94 |
| EFMK-25 | 104 | 93 | 34 | 144 | 104 | 91 | 32 | 38 | 24 | 29 | 32 | 34 | 28 | 77 | 36 |
| EFMK-26 | 145 | 153 | 63 | 257 | 190 | 150 | 57 | 64 | 34 | 53 | 46 | 54 | 47 | 99 | 73 |

*Ferguson McKnight #526-1H core (cont.)*

| Sample Name | $C_{29}$ αβ-30-NorH | $C_{29}$ Ts | $C_{30}$ D | $C_{29}$ βα-30-NorM | $C_{30}$ H | $C_{30}$ Mor | $C_{31}$ HH (22S) | $C_{31}$ HH (22R) | $C_{32}$ HH (22S) | $C_{32}$ HH (22R) | $C_{33}$ HH (22S) | $C_{33}$ HH (22R) | $C_{34}$ HH (22S) | $C_{34}$ HH (22R) | $C_{35}$ HH (22S) | $C_{35}$ HH (22R) |
|---|---|---|---|---|---|---|---|---|---|---|---|---|---|---|---|---|
| EFMK-1 | 144 | 29 | 12 | 12 | 121 | 12 | 45 | 54 | 29 | 17 | 17 | 18 | ND | ND | ND | ND |
| EFMK-4 | 33 | 33 | 4 | 6 | 51 | 7 | 19 | 14 | 12 | 8 | 8 | 5 | ND | ND | ND | ND |
| EFMK-8 | 72 | 62 | 11 | ND | 109 | 12 | 36 | 25 | 21 | 18 | 17 | 13 | ND | ND | ND | ND |
| EFMK-12 | 39 | 38 | 7 | 8 | 51 | 6 | 22 | 14 | 13 | 8 | 8 | 6 | ND | ND | ND | ND |
| EFMK-15 | 36 | 37 | 5 | 7 | 49 | 7 | 20 | 17 | 9 | 6 | 10 | 7 | ND | ND | ND | ND |
| EFMK-17 | 134 | 112 | 18 | 26 | 169 | 16 | 68 | 72 | 41 | 29 | 30 | 18 | ND | ND | ND | ND |
| EFMK-20 | 74 | 83 | 13 | 17 | 92 | 11 | 40 | 27 | 21 | 13 | 13 | 17 | ND | ND | ND | ND |
| EFMK-23 | 62 | 90 | 13 | 6 | 87 | 12 | 30 | 24 | 17 | 14 | 21 | 14 | ND | ND | ND | ND |
| EFMK-24 | 44 | 75 | 8 | 11 | 68 | 4 | 23 | 20 | 11 | 10 | 16 | 6 | 7 | 3 | 8 | 6 |
| EFMK-25 | 23 | 24 | 7 | 8 | 19 | 9 | 14 | 13 | 9 | 6 | ND | ND | ND | ND | ND | ND |
| EFMK-26 | 32 | 27 | ND | ND | 27 | 7 | 8 | 14 | ND | ND | ND | ND | ND | ND | ND | ND |

*Fasken "A" #1 core*

| Sample Name | $C_{20}$ TR | $C_{21}$ TR | $C_{22}$ TR | $C_{23}$ TR | $C_{24}$ TR | $C_{25}$ TR | $C_{24}$ TT | $C_{26}$ TR | $C_{26}$ TR | $C_{28}$ TR | $C_{28}$ TR | $C_{29}$ TR | $C_{29}$ TR | $T_s$ | $T_m$ |
|---|---|---|---|---|---|---|---|---|---|---|---|---|---|---|---|
| EFFA-1 | 7 | 6 | 2 | 7 | 3 | 2 | 1 | 0 | 1 | 0 | 0 | 0 | 0 | 1 | 1 |
| EFFA-3 | 0 | 0 | 0 | 0 | 0 | 0 | 0 | 0 | 0 | 0 | 0 | 0 | 0 | 0 | 0 |
| EFFA-5 | 39 | 36 | 13 | 46 | 21 | 10 | 4 | 3 | 6 | 2 | 2 | 2 | 1 | 5 | 9 |
| EFFA-11 | 42 | 42 | 16 | 60 | 27 | 14 | 4 | 4 | 9 | 2 | 3 | 2 | 2 | 7 | 10 |
| EFFA-17 | 39 | 35 | 12 | 44 | 20 | 9 | 3 | 3 | 6 | 2 | 2 | 2 | 1 | 5 | 8 |
| EFFA-18 | 48 | 42 | 15 | 54 | 23 | 11 | 4 | 3 | 8 | 2 | 2 | 2 | 2 | 6 | 9 |
| EFFA-20 | 5 | 5 | 2 | 6 | 3 | 1 | 0 | 0 | 1 | 0 | 0 | 0 | 0 | 1 | 1 |
| EFFA-21 | 12 | 11 | 3 | 13 | 6 | 3 | 1 | 1 | 2 | 1 | 0 | 1 | 0 | 1 | 2 |
| EFFA-23 | 20 | 18 | 6 | 23 | 10 | 5 | 2 | 1 | 3 | 1 | 1 | 1 | 1 | 2 | 4 |
| EFFA-24 | 129 | 110 | 36 | 128 | 54 | 27 | 9 | 8 | 18 | 4 | 5 | 3 | 4 | 12 | 21 |
| EFFA-28 | 81 | 72 | 23 | 86 | 37 | 17 | 6 | 4 | 12 | 3 | 2 | 3 | 2 | 8 | 15 |
| EFFA-32 | 187 | 159 | 51 | 189 | 83 | 38 | 13 | 11 | 26 | 7 | 6 | 7 | 6 | 19 | 29 |
| EFFA-37 | 20 | 16 | 5 | 19 | 8 | 4 | 1 | 1 | 2 | 1 | 1 | 1 | 0 | 2 | 3 |
| EFFA-38 | 82 | 71 | 22 | 82 | 37 | 16 | 6 | 5 | 11 | 4 | 3 | 3 | 2 | 9 | 16 |
| EFFA-40 | 18 | 17 | 6 | 22 | 10 | 5 | 2 | 1 | 3 | 1 | 1 | 1 | 1 | 2 | 4 |

*Fasken "A" #1 core (cont.)*

| Sample Name | $C_{29}$ αβ-30-NorH | $C_{29}$ Ts | $C_{30}$ D | $C_{29}$ βα-30-NorM | $C_{30}$ H | $C_{30}$ Mor | $C_{31}$ HH (22S) | $C_{31}$ HH (22R) | $C_{32}$ HH (22S) | $C_{32}$ HH (22R) | $C_{33}$ HH (22S) | $C_{33}$ HH (22R) | $C_{34}$ HH (22S) | $C_{34}$ HH (22R) | $C_{35}$ HH (22S) | $C_{35}$ HH (22R) |
|---|---|---|---|---|---|---|---|---|---|---|---|---|---|---|---|---|
| EFFA-1 | 3 | 0 | 0 | 0 | 3 | 1 | 1 | 1 | 1 | 1 | 1 | 0 | ND | ND | ND | ND |
| EFFA-3 | 0 | 0 | 0 | 0 | 0 | 0 | 0 | 0 | 0 | 0 | 0 | 0 | ND | ND | ND | ND |
| EFFA-5 | 23 | 1 | 1 | 3 | 18 | 4 | 7 | 5 | 4 | 3 | 2 | 2 | ND | ND | ND | ND |
| EFFA-11 | 31 | 1 | 1 | 3 | 26 | 5 | 8 | 7 | 4 | 4 | 3 | 3 | ND | ND | ND | ND |
| EFFA-17 | 22 | 1 | 1 | 2 | 19 | 4 | 6 | 5 | 4 | 3 | 2 | 1 | ND | ND | ND | ND |
| EFFA-18 | 27 | 1 | 1 | 3 | 23 | 5 | 8 | 6 | 4 | 4 | 2 | 2 | ND | ND | ND | ND |
| EFFA-20 | 3 | 0 | 0 | 0 | 3 | 1 | 1 | 1 | 0 | 0 | 0 | 0 | 0 | 0 | ND | ND |
| EFFA-21 | 6 | 0 | 0 | 1 | 5 | 1 | 2 | 1 | 1 | 1 | 1 | 0 | ND | ND | ND | ND |
| EFFA-23 | 10 | 0 | 0 | 1 | 10 | 2 | 3 | 2 | 1 | 1 | 1 | 1 | ND | ND | ND | ND |
| EFFA-24 | 56 | 1 | 1 | 5 | 47 | 10 | 16 | 12 | 7 | 6 | 6 | 3 | 5 | 2 | ND | ND |
| EFFA-28 | 36 | 1 | 1 | 3 | 33 | 6 | 9 | 7 | 5 | 4 | 3 | 2 | ND | ND | ND | ND |
| EFFA-32 | 78 | 1 | 2 | 8 | 73 | 11 | 20 | 16 | 12 | 10 | 8 | 5 | ND | ND | ND | ND |
| EFFA-37 | 7 | 0 | 0 | 1 | 7 | 1 | 2 | 2 | 1 | 1 | 1 | 0 | ND | ND | ND | ND |
| EFFA-38 | 37 | 1 | 1 | 5 | 34 | 7 | 11 | 8 | 5 | 4 | 3 | 2 | ND | ND | ND | ND |
| EFFA-40 | 10 | 0 | 0 | 1 | 10 | 2 | 3 | 2 | 2 | 1 | 1 | 1 | ND | ND | ND | ND |

*Bouldin Creek outcrop*

| Sample Name | $C_{20}$ TR | $C_{21}$ TR | $C_{22}$ TR | $C_{23}$ TR | $C_{24}$ TR | $C_{25}$ TR | $C_{24}$ TT | $C_{26}$ TR | $C_{26}$ TR | $C_{28}$ TR | $C_{28}$ TR | $C_{29}$ TR | $C_{29}$ TR | $T_s$ | $T_m$ |
|---|---|---|---|---|---|---|---|---|---|---|---|---|---|---|---|
| EFBC-5 | 0 | 0 | ND | 0 | 0 | 0 | 0 | 0 | 0 | ND | ND | 2 | 0 | 0 | 2 |
| EFBC-7 | 0 | 0 | ND | 0 | 0 | 0 | 0 | 0 | 0 | ND | ND | 1 | 0 | 0 | 3 |
| EFBC-9 | 0 | 0 | ND | 0 | 0 | 0 | 0 | 0 | 0 | ND | ND | 2 | 0 | 0 | 3 |
| EFBC-11 | 0 | 0 | ND | 0 | 0 | 0 | 0 | 0 | 0 | ND | ND | 1 | 0 | 0 | 2 |
| EFBC-15 | 0 | 0 | ND | 0 | 0 | 0 | 0 | 0 | 0 | ND | ND | 1 | 0 | 0 | 1 |
| EFBC-19 | 1 | 1 | ND | 1 | 0 | 1 | 0 | 0 | 1 | ND | ND | 6 | 0 | 0 | 4 |
| EFBC-20 | 1 | 2 | ND | 2 | 0 | 1 | 0 | 1 | 1 | ND | ND | 7 | 0 | 0 | 11 |
| EFBC-23 | 1 | 1 | ND | 1 | 0 | 1 | 0 | 0 | 1 | ND | ND | 2 | 0 | 0 | 5 |
| EFBC-25 | 1 | 1 | ND | 1 | 0 | 1 | 0 | 0 | 0 | ND | ND | 2 | 0 | 0 | 4 |
| EFBC-27 | 1 | 1 | ND | 1 | 0 | 1 | 0 | 0 | 0 | ND | ND | 2 | 0 | 0 | 4 |
| EFBC-30 | 1 | 1 | ND | 1 | 0 | 1 | 0 | 0 | 1 | ND | ND | 4 | 0 | 0 | 9 |
| EFBC-32 | 2 | 2 | ND | 2 | 1 | 3 | 1 | 1 | 2 | ND | ND | 9 | 0 | 1 | 16 |
| EFBC-34 | 1 | 1 | ND | 1 | 0 | 3 | 0 | 1 | 1 | ND | ND | 5 | 0 | 0 | 9 |

*Bouldin Creek outcrop (cont.)*

| Sample Name | $C_{29}$ αβ-30-NorH | $C_{29}$ Ts | $C_{30}$ D | $C_{29}$ βα-30-NorM | $C_{30}$ H | $C_{30}$ Mor | $C_{31}$ HH (22S) | $C_{31}$ HH (22R) | $C_{32}$ HH (22S) | $C_{32}$ HH (22R) | $C_{33}$ HH (22S) | $C_{33}$ HH (22R) | $C_{34}$ HH (22S) | $C_{34}$ HH (22R) | $C_{35}$ HH (22S) | $C_{35}$ HH (22R) |
|---|---|---|---|---|---|---|---|---|---|---|---|---|---|---|---|---|
| EFBC-5 | 2 | ND | 0 | 2 | 1 | 3 | 1 | 1 | ND | 0 | ND | 0 | ND | ND | ND | ND |
| EFBC-7 | 1 | ND | ND | 2 | 1 | 3 | 0 | 1 | 0 | 0 | ND | ND | ND | ND | ND | ND |
| EFBC-9 | 2 | ND | ND | 3 | 2 | 4 | 1 | 1 | 0 | 0 | ND | 0 | ND | ND | ND | ND |
| EFBC-11 | 1 | ND | ND | 2 | 1 | 3 | 1 | 1 | 0 | 0 | ND | 0 | ND | ND | ND | ND |
| EFBC-15 | 1 | ND | ND | 1 | 1 | 2 | 0 | 1 | 0 | 0 | ND | 0 | ND | ND | ND | ND |
| EFBC-19 | 5 | ND | ND | 4 | 3 | 4 | 1 | 2 | 0 | 1 | ND | 0 | ND | ND | ND | ND |
| EFBC-20 | 8 | ND | ND | 8 | 6 | 9 | 1 | 5 | 0 | 2 | ND | 0 | 1 | 0 | 0 | 1 |
| EFBC-23 | 2 | ND | ND | 4 | 2 | 3 | 0 | 3 | 0 | 1 | ND | 0 | ND | ND | ND | ND |
| EFBC-25 | 2 | ND | ND | 2 | 2 | 2 | 0 | 2 | 0 | 1 | ND | 0 | ND | ND | ND | ND |
| EFBC-27 | 2 | ND | ND | 3 | 2 | 3 | 0 | 3 | 0 | 1 | ND | 0 | ND | ND | ND | ND |
| EFBC-30 | 7 | ND | ND | 10 | 4 | 6 | 0 | 3 | 0 | 1 | ND | 0 | ND | ND | ND | ND |
| EFBC-32 | 14 | ND | ND | 17 | 9 | 13 | 1 | 5 | 0 | 2 | ND | 1 | ND | ND | ND | ND |
| EFBC-34 | 7 | ND | ND | 8 | 5 | 7 | 0 | 2 | 0 | 1 | ND | 1 | 1 | 0 | 0 | 1 |

*ACC #1 core*

| Sample Name | $C_{20}$ TR | $C_{21}$ TR | $C_{22}$ TR | $C_{23}$ TR | $C_{24}$ TR | $C_{25}$ TR | $C_{24}$ TT | $C_{26}$ TR | $C_{26}$ TR | $C_{28}$ TR | $C_{28}$ TR | $C_{29}$ TR | $C_{29}$ TR | $T_s$ | $T_m$ |
|---|---|---|---|---|---|---|---|---|---|---|---|---|---|---|---|
| EFAC-1 | 30 | 22 | 4 | 28 | 14 | 13 | 4 | 6 | 9 | 8 | 4 | 46 | 6 | 4 | 77 |
| EFAC-3 | 28 | 18 | 3 | 17 | 9 | 13 | 3 | 4 | 5 | 8 | 2 | 70 | 6 | 4 | 60 |
| EFAC-6 | 18 | 15 | 2 | 18 | 6 | 9 | 3 | 3 | 3 | 4 | 2 | 22 | 3 | 2 | 22 |
| EFAC-7 | 14 | 9 | 1 | 8 | 3 | 7 | 2 | 2 | 3 | 2 | 2 | 19 | 1 | 1 | 36 |
| EFAC-8 | 7 | 7 | 2 | 6 | 4 | 9 | 2 | 2 | 2 | 4 | 2 | 22 | 2 | 1 | 36 |
| EFAC-10 | 66 | 49 | 9 | 43 | 16 | 19 | 7 | 9 | 22 | 9 | 10 | 106 | 8 | 20 | 214 |

| Sample Name | $C_{29}$ αβ-30-NorH | $C_{29}$ Ts | $C_{30}$ D | $C_{29}$ βα-30-NorM | $C_{30}$ H | $C_{30}$ Mor | $C_{31}$ HH (22S) | $C_{31}$ HH (22R) | $C_{32}$ HH (22S) | $C_{32}$ HH (22R) | $C_{33}$ HH (22S) | $C_{33}$ HH (22R) | $C_{34}$ HH (22S) | $C_{34}$ HH (22R) | $C_{35}$ HH (22S) | $C_{35}$ HH (22R) |
|---|---|---|---|---|---|---|---|---|---|---|---|---|---|---|---|---|
| EFAC-1 | 89 | ND | 4 | 83 | 97 | 149 | 21 | 49 | 2 | 12 | ND | ND | ND | ND | ND | ND |
| EFAC-3 | 63 | ND | ND | 49 | 100 | 119 | 18 | 42 | 2 | 11 | ND | ND | ND | ND | ND | ND |
| EFAC-6 | 18 | 0 | ND | 12 | 15 | 24 | 6 | 18 | 2 | 7 | ND | ND | ND | ND | ND | ND |
| EFAC-7 | 32 | ND | 2 | 20 | 20 | 37 | 8 | 17 | 1 | 7 | ND | ND | ND | ND | ND | ND |
| EFAC-8 | 26 | ND | 2 | 14 | 20 | 38 | 9 | 14 | 1 | 6 | ND | ND | ND | ND | ND | ND |
| EFAC-10 | 186 | ND | 7 | 230 | 254 | 335 | 80 | 179 | 5 | 41 | ND | ND | ND | ND | ND | ND |

*W. Brechtel #1 core*

| Sample Name | $C_{20}$ TR | $C_{21}$ TR | $C_{22}$ TR | $C_{23}$ TR | $C_{24}$ TR | $C_{25}$ TR | $C_{24}$ TT | $C_{26}$ TR | $C_{26}$ TR | $C_{28}$ TR | $C_{28}$ TR | $C_{29}$ TR | $C_{29}$ TR | $T_s$ | $T_m$ |
|---|---|---|---|---|---|---|---|---|---|---|---|---|---|---|---|
| EFWB-1 | 78 | 41 | 64 | 37 | 56 | 29 | 16 | 14 | 19 | 34 | ND | 5 | 14 | 37 | 149 |
| EFWB-3 | 50 | 35 | 14 | 25 | 22 | 30 | 9 | 9 | 16 | 43 | ND | 5 | 16 | 24 | 106 |
| EFWB-4 | 40 | 26 | 10 | 22 | 17 | 18 | 6 | 7 | 10 | 35 | ND | 3 | 11 | 18 | 70 |
| EFWB-7 | 56 | 28 | 77 | 44 | 42 | 32 | 21 | 16 | 20 | 34 | ND | 10 | 18 | 43 | 134 |
| EFWB-8 | 25 | 20 | 5 | 14 | 19 | 18 | 6 | 6 | 6 | 19 | 1 | 6 | 10 | 18 | 60 |
| EFWB-9 | 70 | 61 | 11 | 84 | 50 | 42 | 13 | 20 | 28 | 7 | 7 | 8 | 11 | 43 | 120 |

| Sample Name | $C_{29}$ αβ-30-NorH | $C_{29}$ Ts | $C_{30}$ D | $C_{29}$ βα-30-NorM | $C_{30}$ H | $C_{30}$ Mor | $C_{31}$ HH (22S) | $C_{31}$ HH (22R) | $C_{32}$ HH (22S) | $C_{32}$ HH (22R) | $C_{33}$ HH (22S) | $C_{33}$ HH (22R) | $C_{34}$ HH (22S) | $C_{34}$ HH (22R) | $C_{35}$ HH (22S) | $C_{35}$ HH (22R) |
|---|---|---|---|---|---|---|---|---|---|---|---|---|---|---|---|---|
| EFWB-1 | 223 | ND | ND | 28 | 673 | 112 | 306 | 240 | 189 | 153 | 104 | 88 | 70 | 48 | 83 | 98 |
| EFWB-3 | 129 | 127 | ND | ND | 370 | 58 | 180 | 127 | 80 | 63 | 41 | 28 | 36 | 22 | 31 | 61 |
| EFWB-4 | 81 | ND | ND | 7 | 223 | 36 | 112 | 76 | 49 | 39 | 26 | 21 | 33 | 14 | 20 | 36 |
| EFWB-7 | ND | ND | 157 | 18 | 536 | 47 | 346 | 225 | 178 | 126 | 92 | 60 | 57 | 30 | 70 | 59 |
| EFWB-8 | 71 | ND | 2 | 5 | 209 | 23 | 110 | 71 | 56 | 36 | 26 | 19 | 21 | 14 | 19 | 25 |
| EFWB-9 | 197 | ND | ND | 17 | 418 | 36 | 247 | 156 | 138 | 93 | 70 | 44 | 48 | 25 | 53 | 42 |

*C.J. Hendershot #1 core*

| Sample Name | $C_{20}$ TR | $C_{21}$ TR | $C_{22}$ TR | $C_{23}$ TR | $C_{24}$ TR | $C_{25}$ TR | $C_{24}$ TT | $C_{26}$ TR | $C_{26}$ TR | $C_{28}$ TR | $C_{28}$ TR | $C_{29}$ TR | $C_{29}$ TR | $T_s$ | $T_m$ |
|---|---|---|---|---|---|---|---|---|---|---|---|---|---|---|---|
| EFHE-1 | 200 | 167 | 43 | 278 | 190 | 182 | 69 | 79 | 52 | 47 | 40 | 40 | 35 | 121 | 301 |
| EFHE-2 | 170 | 144 | 21 | 236 | 194 | 183 | 74 | 80 | 45 | 50 | 41 | 41 | 36 | 107 | 314 |
| EFHE-3 | 126 | 133 | 19 | 224 | 113 | 126 | 60 | 67 | 54 | 28 | 31 | 43 | 45 | 164 | 433 |
| EFHE-5 | 100 | 77 | 14 | 157 | 72 | 92 | 38 | 38 | 24 | 24 | 24 | 30 | 32 | 66 | 246 |
| EFHE-6 | 82 | 64 | 10 | 112 | 62 | 73 | 30 | 32 | 19 | 18 | 18 | 29 | 22 | 51 | 187 |
| EFHE-7 | 93 | 81 | 13 | 137 | 80 | 114 | 38 | 42 | 2 | 24 | 24 | 27 | 29 | 72 | 233 |
| EFHE-9 | 177 | 137 | 18 | 235 | 159 | 183 | 75 | 77 | 35 | 44 | 48 | 49 | 47 | 91 | 402 |
| EFHE-10 | 54 | 82 | 22 | 117 | 62 | 67 | 29 | 22 | 67 | 13 | 23 | 19 | 21 | 200 | 307 |

*C.J. Hendershot #1 core (cont.)*

| Sample Name | $C_{29}$ αβ-30-NorH | $C_{29}$ Ts | $C_{30}$ D | $C_{29}$ βα-30-NorM | $C_{30}$ H | $C_{30}$ Mor | $C_{31}$ HH (22S) | $C_{31}$ HH (22R) | $C_{32}$ HH (22S) | $C_{32}$ HH (22R) | $C_{33}$ HH (22S) | $C_{33}$ HH (22R) | $C_{34}$ HH (22S) | $C_{34}$ HH (22R) | $C_{35}$ HH (22S) | $C_{35}$ HH (22R) |
|---|---|---|---|---|---|---|---|---|---|---|---|---|---|---|---|---|
| EFHE-1 | 820 | ND | 24 | 143 | 667 | 125 | 263 | 236 | 197 | 207 | 146 | 140 | 96 | 81 | 150 | 164 |
| EFHE-2 | ND | 25 | 736 | 151 | 776 | 143 | 300 | 261 | 225 | 207 | 184 | 174 | 111 | 88 | 154 | 174 |
| EFHE-3 | 1272 | ND | 37 | 184 | 1655 | 220 | 578 | 445 | 289 | 257 | 198 | 180 | 192 | 122 | 145 | 160 |
| EFHE-5 | 701 | ND | 25 | 85 | 846 | 116 | 397 | 273 | 224 | 173 | 146 | 114 | 121 | 91 | 113 | 137 |
| EFHE-6 | ND | 480 | 9 | 57 | 591 | 73 | 282 | 183 | 149 | 113 | 92 | 65 | 77 | 50 | 71 | 85 |
| EFHE-7 | 640 | ND | 15 | 73 | 851 | 104 | 393 | 260 | 212 | 153 | 138 | 100 | 111 | 76 | 104 | 102 |
| EFHE-9 | 1071 | ND | 16 | 98 | 1620 | 159 | 660 | 427 | 302 | 212 | 199 | 134 | 160 | 93 | 129 | 122 |
| EFHE-10 | 686 | 188 | 42 | 89 | 1077 | 119 | 573 | 362 | 508 | 352 | 210 | 142 | 200 | 107 | 281 | 167 |

*Lily Hoppess #1 core*

| Sample Name | $C_{20}$ TR | $C_{21}$ TR | $C_{22}$ TR | $C_{23}$ TR | $C_{24}$ TR | $C_{25}$ TR | $C_{24}$ TT | $C_{26}$ TR | $C_{26}$ TR | $C_{28}$ TR | $C_{28}$ TR | $C_{29}$ TR | $C_{29}$ TR | $T_s$ | $T_m$ |
|---|---|---|---|---|---|---|---|---|---|---|---|---|---|---|---|
| EFLH-1 | 149 | 227 | 46 | 541 | 250 | 324 | 130 | 200 | 79 | 119 | 130 | 101 | 111 | 335 | 320 |
| EFLH-5 | 281 | 475 | 109 | 1170 | 571 | 740 | 305 | 396 | 134 | 272 | 305 | 231 | 254 | 541 | 595 |
| EFLH-9 | 218 | 352 | 75 | 795 | 381 | 477 | 194 | 310 | 136 | 179 | 183 | 151 | 166 | 491 | 477 |
| EFLH-13 | 33 | 46 | 13 | 74 | 35 | 44 | 16 | 23 | 39 | 14 | 15 | 13 | 13 | 107 | 68 |
| EFLH-15 | 101 | 156 | 47 | 210 | 113 | 116 | 55 | 75 | 92 | 43 | 48 | 38 | 43 | 444 | 190 |
| EFLH-20 | 66 | 121 | 26 | 191 | 95 | 119 | 47 | 63 | 58 | 40 | 45 | 37 | 39 | 247 | 139 |

*Lily Hoppess #1 core (cont.)*

| Sample Name | $C_{29}$ αβ-30-NorH | $C_{29}$ Ts | $C_{30}$ D | $C_{29}$ βα-30-NorM | $C_{30}$ H | $C_{30}$ Mor | $C_{31}$ HH (22S) | $C_{31}$ HH (22R) | $C_{32}$ HH (22S) | $C_{32}$ HH (22R) | $C_{33}$ HH (22S) | $C_{33}$ HH (22R) | $C_{34}$ HH (22S) | $C_{34}$ HH (22R) | $C_{35}$ HH (22S) | $C_{35}$ HH (22R) |
|---|---|---|---|---|---|---|---|---|---|---|---|---|---|---|---|---|
| EFLH-1 | 980 | 161 | 71 | 115 | 1784 | 184 | 483 | 366 | 275 | 190 | 185 | 135 | 148 | 75 | 51 | 52 |
| EFLH-5 | 1626 | 220 | 85 | 167 | 2917 | 315 | 847 | 681 | 493 | 337 | 331 | 225 | 257 | 132 | 105 | 72 |
| EFLH-9 | 1388 | 230 | 88 | 167 | 2510 | 276 | 727 | 537 | 414 | 293 | 290 | 200 | 222 | 117 | 94 | 86 |
| EFLH-13 | 223 | 51 | 45 | 32 | 403 | 57 | 132 | 86 | 101 | 71 | 75 | 51 | 51 | 27 | 20 | 16 |
| EFLH-15 | 601 | 420 | 138 | 97 | 1572 | 193 | 470 | 314 | 313 | 222 | 226 | 156 | 162 | 91 | 55 | 46 |
| EFLH-20 | 343 | 237 | 89 | 54 | 963 | 108 | 285 | 196 | 189 | 133 | 132 | 93 | 104 | 53 | 41 | 32 |

*Oils and condensates (Concentrations are expressed as µg biomarkers/g whole oil; ND = not determined)*

| Sample Name | $C_{20}$ TR | $C_{21}$ TR | $C_{22}$ TR | $C_{23}$ TR | $C_{24}$ TR | $C_{25}$ TR | $C_{24}$ TT | $C_{26}$ TR | $C_{26}$ TR | $C_{28}$ TR | $C_{28}$ TR | $C_{29}$ TR | $C_{29}$ TR | $T_s$ | $T_m$ |
|---|---|---|---|---|---|---|---|---|---|---|---|---|---|---|---|
| NWMK-533.2 | 426 | 631 | 139 | 1028 | 782 | 630 | 219 | 197 | 198 | 189 | 187 | 266 | 216 | 265 | 310 |
| NFMK-526-1H | 354 | 446 | 126 | 756 | 651 | 484 | 194 | 158 | 121 | 180 | 187 | 220 | 204 | 199 | 185 |
| MJOG-UEF | 37 | 21 | 15 | 74 | 49 | 38 | 22 | 18 | 6 | 18 | 23 | 22 | 21 | 43 | 23 |
| MJOG-LEF | 60 | 79 | 19 | 126 | 91 | 67 | 32 | 29 | 14 | 27 | 27 | 34 | 26 | 63 | 33 |
| GREF-1-110 | ND | ND | ND | ND | ND | ND | ND | ND | ND | ND | ND | ND | ND | ND | ND |

*Oils and condensates (Concentrations are expressed as µg biomarkers/g whole oil; ND = not determined; cont.)*

| Sample Name | $C_{29}$ αβ-30-NorH | $C_{29}$ Ts | $C_{30}$ D | $C_{29}$ βα-30-NorM | $C_{30}$ H | $C_{30}$ Mor | $C_{31}$ HH (22S) | $C_{31}$ HH (22R) | $C_{32}$ HH (22S) | $C_{32}$ HH (22R) | $C_{33}$ HH (22S) | $C_{33}$ HH (22R) | $C_{34}$ HH (22S) | $C_{34}$ HH (22R) | $C_{35}$ HH (22S) | $C_{35}$ HH (22R) |
|---|---|---|---|---|---|---|---|---|---|---|---|---|---|---|---|---|
| NWMK-533.2 | 156 | 1 | 26 | 38 | 520 | 38 | 197 | 194 | 118 | 83 | 78 | 53 | 44 | 27 | 26 | 11 |
| NFMK-526-1H | 85 | 9 | 17 | 15 | 98 | ND | ND | 30 | ND | ND | ND | ND | ND | ND | ND | ND |
| MJOG-UEF | 10 | 1 | 4 | ND | ND | ND | ND | ND | ND | ND | ND | ND | ND | ND | ND | ND |
| MJOG-LEF | 22 | 2 | 18 | 7 | 10 | ND | ND | ND | ND | ND | ND | ND | ND | ND | ND | ND |
| GREF-1-110 | ND | ND | ND | ND | ND | ND | ND | ND | ND | ND | ND | ND | ND | ND | ND | ND |

**N. Quantitative biomarker analysis results for aryl isoprenoids (Concentrations are expressed as µg biomarkers/g TOC; ND = not determined)**

*Lozier Canyon outcrop*

| Sample Name | $C_{13}$ AI | $C_{14}$ AI | $C_{15}$ AI | $C_{16}$ AI | $C_{17}$ AI | $C_{18}$ AI | $C_{19}$ AI | $C_{20}$ AI | $C_{21}$ AI | $C_{22}$ AI | $C_{23}$ AI | $C_{24}$ AI | $C_{25}$ AI | $C_{26}$ AI | $C_{27}$ AI | $C_{28}$ AI | $C_{30}$ AI | $C_{31}$ AI |
|---|---|---|---|---|---|---|---|---|---|---|---|---|---|---|---|---|---|---|
| EFLC-28 | 1 | 1 | 1 | 2 | 1 | 2 | 1 | 1 | 0 | 2 | ND | 2 | ND | ND | ND | ND | ND | ND |
| EFLC-26 | 3 | 2 | 3 | 6 | 2 | 3 | 2 | 2 | 1 | 3 | ND | 4 | ND | ND | ND | ND | ND | ND |
| EFLC-25 | 0 | 0 | 0 | 1 | 0 | 1 | 0 | 0 | 0 | 1 | ND | 1 | 0 | 0 | ND | ND | ND | ND |
| EFLC-20 | ND | ND | ND | ND | ND | 3 | 1 | 2 | 2 | ND | ND | ND | ND | ND | ND | ND | ND | ND |
| EFLC-18 | 0 | 0 | 0 | 0 | 0 | 0 | 0 | 0 | 0 | 0 | ND | 1 | 0 | 0 | ND | ND | ND | ND |
| EFLC-14 | 0 | 0 | 1 | 1 | 0 | 1 | 1 | 1 | 1 | 0 | ND | 1 | ND | ND | ND | ND | ND | ND |
| EFLC-12 | 13 | 22 | 44 | 45 | 12 | 48 | 40 | 39 | 19 | 15 | 4 | 18 | 6 | 4 | 4 | 9 | 4 | 5 |
| EFLC-10 | 81 | 98 | 142 | 115 | 28 | 103 | 94 | 87 | 41 | 26 | 8 | 31 | 16 | 7 | ND | 11 | ND | ND |
| EFLC-8 | 41 | 52 | 72 | 68 | 15 | 60 | 54 | 50 | 26 | 15 | 6 | 21 | 4 | 4 | ND | ND | ND | ND |
| EFLC-6 | 1 | 1 | 4 | 6 | 1 | 9 | 9 | 9 | 6 | 3 | 1 | 6 | 2 | 2 | ND | ND | ND | ND |
| EFLC-4 | 0 | 0 | 0 | 0 | 0 | 1 | 1 | 1 | 0 | 0 | ND | 0 | 0 | 0 | 0 | ND | ND | ND |
| EFLC-1 | 84 | 242 | 636 | 750 | 164 | 691 | 763 | 549 | 335 | 213 | ND | 156 | 94 | 20 | ND | 104 | ND | 53 |

*Ferguson McKnight #526-1H core*

| Sample Name | $C_{13}$ AI | $C_{14}$ AI | $C_{15}$ AI | $C_{16}$ AI | $C_{17}$ AI | $C_{18}$ AI | $C_{19}$ AI | $C_{20}$ AI | $C_{21}$ AI | $C_{22}$ AI | $C_{23}$ AI | $C_{24}$ AI | $C_{25}$ AI | $C_{26}$ AI | $C_{27}$ AI | $C_{28}$ AI | $C_{30}$ AI | $C_{31}$ AI |
|---|---|---|---|---|---|---|---|---|---|---|---|---|---|---|---|---|---|---|
| EFMK-1 | 290 | 260 | 401 | 519 | 277 | 351 | 279 | 179 | 106 | 100 | ND | ND | ND | ND | ND | ND | ND | ND |
| EFMK-4 | 330 | 200 | 193 | 263 | 104 | 53 | 67 | 51 | 34 | 33 | ND | ND | ND | ND | ND | ND | ND | ND |
| EFMK-8 | 654 | 361 | 391 | 612 | 251 | 142 | 171 | 126 | 79 | 92 | ND | ND | ND | ND | ND | ND | ND | ND |
| EFMK-12 | 441 | 273 | 264 | 362 | 139 | 85 | 104 | 69 | 42 | 49 | ND | ND | ND | ND | ND | ND | ND | ND |
| EFMK-15 | 251 | 175 | 233 | 386 | 152 | 96 | 116 | 85 | 53 | 55 | ND | ND | ND | ND | ND | ND | ND | ND |
| EFMK-17 | 1029 | 664 | 819 | 1372 | 566 | 996 | 467 | 531 | 178 | 173 | ND | ND | ND | ND | ND | ND | ND | ND |
| EFMK-20 | 1043 | 651 | 642 | 854 | 349 | 224 | 273 | 197 | 98 | 120 | ND | ND | ND | ND | ND | ND | ND | ND |
| EFMK-23 | 788 | 448 | 503 | 862 | 335 | 560 | 296 | 208 | 113 | 137 | ND | ND | ND | ND | ND | ND | ND | ND |
| EFMK-24 | 649 | 364 | 401 | 645 | 248 | 126 | 179 | 155 | 84 | 119 | ND | ND | ND | ND | ND | ND | ND | ND |
| EFMK-25 | 135 | 100 | 165 | 296 | 140 | 91 | 133 | 138 | 59 | 75 | ND | ND | ND | ND | ND | ND | ND | ND |
| EFMK-26 | 265 | 175 | 263 | 476 | 195 | 136 | 187 | 315 | 90 | 108 | ND | ND | ND | ND | ND | ND | ND | ND |

*Fasken "A" #1 core*

| Sample Name | $C_{13}$ AI | $C_{14}$ AI | $C_{15}$ AI | $C_{16}$ AI | $C_{17}$ AI | $C_{18}$ AI | $C_{19}$ AI | $C_{20}$ AI | $C_{21}$ AI | $C_{22}$ AI | $C_{23}$ AI | $C_{24}$ AI | $C_{25}$ AI | $C_{26}$ AI | $C_{27}$ AI | $C_{28}$ AI | $C_{30}$ AI | $C_{31}$ AI |
|---|---|---|---|---|---|---|---|---|---|---|---|---|---|---|---|---|---|---|
| EFFA-1 | 22 | 17 | 30 | 42 | 19 | 24 | 25 | 20 | 6 | ND | ND | ND | ND | ND | ND | ND | ND | ND |
| EFFA-3 | 0 | 0 | 0 | 0 | 0 | 0 | 0 | 0 | 0 | ND | ND | ND | ND | ND | ND | ND | ND | ND |
| EFFA-5 | 172 | 105 | 149 | 185 | 80 | 111 | 115 | 83 | 34 | ND | ND | ND | ND | ND | ND | ND | ND | ND |
| EFFA-11 | 106 | 69 | 105 | 138 | 82 | 108 | 134 | 120 | 45 | ND | ND | ND | ND | ND | ND | ND | ND | ND |
| EFFA-17 | 142 | 97 | 147 | 178 | 74 | 85 | 107 | 75 | 31 | ND | ND | ND | ND | ND | ND | ND | ND | ND |
| EFFA-18 | 188 | 127 | 197 | 232 | 87 | 108 | 129 | 93 | 38 | ND | ND | ND | ND | ND | ND | ND | ND | ND |
| EFFA-20 | 8 | 8 | 16 | 20 | 9 | 12 | 14 | 11 | 5 | ND | ND | ND | ND | ND | ND | ND | ND | ND |
| EFFA-21 | 43 | 33 | 54 | 61 | 26 | 35 | 32 | 23 | 9 | ND | ND | ND | ND | ND | ND | ND | ND | ND |
| EFFA-23 | 66 | 46 | 71 | 88 | 36 | 45 | 56 | 41 | 15 | ND | ND | ND | ND | ND | ND | ND | ND | ND |
| EFFA-24 | 910 | 520 | 623 | 626 | 241 | 271 | 310 | 232 | 88 | ND | ND | ND | ND | ND | ND | ND | ND | ND |
| EFFA-28 | 877 | 461 | 425 | 406 | 141 | 167 | 199 | 145 | 54 | ND | ND | ND | ND | ND | ND | ND | ND | ND |
| EFFA-32 | 1086 | 659 | 837 | 873 | 333 | 424 | 449 | 315 | 120 | ND | ND | ND | ND | ND | ND | ND | ND | ND |
| EFFA-37 | 190 | 116 | 131 | 121 | 37 | 43 | 46 | 31 | 11 | ND | ND | ND | ND | ND | ND | ND | ND | ND |
| EFFA-38 | 679 | 334 | 356 | 380 | 143 | 191 | 204 | 142 | 52 | ND | ND | ND | ND | ND | ND | ND | ND | ND |
| EFFA-40 | 88 | 50 | 64 | 77 | 32 | 40 | 49 | 34 | 15 | ND | ND | ND | ND | ND | ND | ND | ND | ND |

*Bouldin Creek outcrop*

| Sample Name | $C_{13}$ AI | $C_{14}$ AI | $C_{15}$ AI | $C_{16}$ AI | $C_{17}$ AI | $C_{18}$ AI | $C_{19}$ AI | $C_{20}$ AI | $C_{21}$ AI | $C_{22}$ AI | $C_{23}$ AI | $C_{24}$ AI | $C_{25}$ AI | $C_{26}$ AI | $C_{27}$ AI | $C_{28}$ AI | $C_{30}$ AI | $C_{31}$ AI |
|---|---|---|---|---|---|---|---|---|---|---|---|---|---|---|---|---|---|---|
| EFBC-5 | 0 | 1 | 0 | 1 | 0 | 0 | 1 | 0 | 0 | 1 | ND | 1 | ND | ND | ND | ND | ND | ND |
| EFBC-7 | ND | 0 | 0 | 1 | 0 | 0 | 1 | 0 | 0 | 0 | 0 | 1 | ND | ND | ND | ND | ND | ND |
| EFBC-9 | 0 | 1 | 1 | 1 | 0 | 0 | 1 | 0 | 0 | 1 | ND | 1 | ND | ND | ND | ND | ND | ND |
| EFBC-11 | 0 | 0 | 0 | 1 | 0 | 0 | 1 | 0 | 0 | 0 | ND | 1 | ND | ND | ND | ND | ND | ND |
| EFBC-15 | 0 | 0 | 0 | 0 | 0 | 0 | 0 | 0 | 0 | 0 | 0 | 0 | ND | ND | ND | ND | ND | ND |
| EFBC-19 | 0 | 2 | 1 | 2 | 1 | 1 | 3 | 1 | 1 | 1 | 0 | 2 | ND | ND | ND | ND | ND | ND |
| EFBC-20 | 0 | 1 | 1 | 3 | 1 | 2 | 4 | 2 | 1 | 2 | 0 | 2 | ND | ND | ND | ND | ND | ND |
| EFBC-23 | 0 | 1 | 1 | 3 | 1 | 2 | 3 | 1 | 1 | 2 | 0 | 2 | ND | ND | ND | ND | ND | ND |
| EFBC-25 | 3 | 6 | 3 | 4 | 1 | 2 | 2 | 1 | 1 | 1 | 0 | 1 | ND | ND | ND | ND | ND | ND |
| EFBC-27 | 3 | 8 | 4 | 4 | 1 | 2 | 2 | 1 | 1 | 1 | 0 | 2 | ND | ND | ND | ND | ND | ND |
| EFBC-30 | 3 | 12 | 6 | 11 | 1 | 6 | 10 | 3 | 2 | 3 | 0 | 2 | ND | ND | ND | ND | ND | ND |
| EFBC-32 | 10 | 34 | 12 | 24 | 2 | 10 | 23 | 6 | 6 | 6 | ND | 4 | ND | ND | ND | ND | ND | ND |
| EFBC-34 | 8 | 26 | 10 | 19 | 2 | 9 | 20 | 6 | 5 | 4 | ND | 3 | ND | ND | ND | ND | ND | ND |

*ACC #1 core*

| Sample Name | $C_{13}$ AI | $C_{14}$ AI | $C_{15}$ AI | $C_{16}$ AI | $C_{17}$ AI | $C_{18}$ AI | $C_{19}$ AI | $C_{20}$ AI | $C_{21}$ AI | $C_{22}$ AI | $C_{23}$ AI | $C_{24}$ AI | $C_{25}$ AI | $C_{26}$ AI | $C_{27}$ AI | $C_{28}$ AI | $C_{30}$ AI | $C_{31}$ AI |
|---|---|---|---|---|---|---|---|---|---|---|---|---|---|---|---|---|---|---|
| EFAC-1 | ND | 1 | 4 | 22 | 9 | 29 | 43 | 15 | 10 | 14 | ND | ND | ND | ND | ND | ND | ND | ND |
| EFAC-3 | ND | 13 | 22 | 50 | 14 | 25 | 60 | 15 | 9 | 15 | ND | ND | ND | ND | ND | ND | ND | ND |
| EFAC-6 | ND | 1 | 6 | 24 | 8 | 16 | 36 | 15 | 5 | 8 | ND | ND | ND | ND | ND | ND | ND | ND |
| EFAC-7 | ND | 1 | 7 | 34 | 8 | 30 | 70 | 18 | 18 | 15 | ND | ND | ND | ND | ND | ND | ND | ND |
| EFAC-8 | ND | 4 | 18 | 67 | 8 | 42 | 132 | 26 | 32 | 22 | ND | ND | ND | ND | ND | ND | ND | ND |
| EFAC-10 | ND | 3 | 43 | 149 | 35 | 142 | 172 | 63 | 59 | 45 | ND | ND | ND | ND | ND | ND | ND | ND |

*W. Brechtel #1 core*

| Sample Name | $C_{13}$ AI | $C_{14}$ AI | $C_{15}$ AI | $C_{16}$ AI | $C_{17}$ AI | $C_{18}$ AI | $C_{19}$ AI | $C_{20}$ AI | $C_{21}$ AI | $C_{22}$ AI | $C_{23}$ AI | $C_{24}$ AI | $C_{25}$ AI | $C_{26}$ AI | $C_{27}$ AI | $C_{28}$ AI | $C_{30}$ AI | $C_{31}$ AI |
|---|---|---|---|---|---|---|---|---|---|---|---|---|---|---|---|---|---|---|
| EFWB-1 | 17 | 91 | 151 | 214 | 90 | 149 | 171 | 89 | 46 | 66 | 8 | 46 | 9 | ND | 49 | 142 | ND | ND |
| EFWB-3 | 53 | 186 | 175 | 213 | 44 | 108 | 112 | 44 | 33 | 21 | 64 | 22 | ND | ND | 35 | 96 | ND | ND |
| EFWB-4 | 63 | 179 | 132 | 144 | 30 | 86 | 77 | 31 | 23 | 26 | 3 | 18 | ND | ND | 27 | 69 | ND | ND |
| EFWB-7 | 195 | 351 | 422 | 462 | 79 | 230 | 235 | 131 | 83 | 75 | 12 | 26 | ND | ND | 60 | 103 | ND | ND |
| EFWB-8 | 142 | 206 | 145 | 150 | 26 | 74 | 79 | 39 | 28 | 25 | 5 | 12 | ND | ND | 29 | 54 | ND | ND |
| EFWB-9 | 990 | 762 | 746 | 702 | 173 | 424 | 341 | 311 | 108 | 98 | 18 | 29 | 11 | ND | 22 | 36 | ND | ND |

*C.J. Hendershot #1 core*

| Sample Name | $C_{13}$ AI | $C_{14}$ AI | $C_{15}$ AI | $C_{16}$ AI | $C_{17}$ AI | $C_{18}$ AI | $C_{19}$ AI | $C_{20}$ AI | $C_{21}$ AI | $C_{22}$ AI | $C_{23}$ AI | $C_{24}$ AI | $C_{25}$ AI | $C_{26}$ AI | $C_{27}$ AI | $C_{28}$ AI | $C_{30}$ AI | $C_{31}$ AI |
|---|---|---|---|---|---|---|---|---|---|---|---|---|---|---|---|---|---|---|
| EFHE-1 | 152 | 286 | 357 | 410 | 141 | 314 | 257 | 143 | 103 | 121 | 23 | 64 | ND | ND | 25 | 108 | 19 | 34 |
| EFHE-2 | 128 | 246 | 303 | 360 | 117 | 281 | 236 | 126 | 84 | 88 | 58 | 64 | ND | ND | 13 | 108 | 22 | 38 |
| EFHE-3 | 312 | 485 | 434 | 441 | 133 | 296 | 226 | 92 | 60 | 95 | 56 | 54 | ND | ND | 23 | 115 | 28 | 49 |
| EFHE-5 | 315 | 507 | 426 | 490 | 97 | 321 | 309 | 150 | 99 | 103 | 43 | 53 | ND | ND | 31 | 151 | 23 | 40 |
| EFHE-6 | 252 | 422 | 369 | 401 | 85 | 246 | 235 | 112 | 78 | 67 | 27 | 39 | ND | ND | 19 | 82 | 19 | 36 |
| EFHE-7 | 338 | 541 | 462 | 495 | 106 | 340 | 302 | 154 | 97 | 86 | 97 | 44 | ND | ND | 31 | 121 | 23 | 37 |
| EFHE-9 | 558 | 969 | 806 | 869 | 155 | 634 | 610 | 318 | 190 | 158 | 76 | 91 | ND | ND | 10 | 144 | 20 | 19 |
| EFHE-10 | 27 | 68 | 150 | 288 | 78 | 319 | 288 | 167 | 106 | 101 | 23 | 31 | ND | ND | 27 | 28 | 10 | 11 |

*Lily Hoppess #1 core*

| Sample Name | $C_{13}$ AI | $C_{14}$ AI | $C_{15}$ AI | $C_{16}$ AI | $C_{17}$ AI | $C_{18}$ AI | $C_{19}$ AI | $C_{20}$ AI | $C_{21}$ AI | $C_{22}$ AI | $C_{23}$ AI | $C_{24}$ AI | $C_{25}$ AI | $C_{26}$ AI | $C_{27}$ AI | $C_{28}$ AI | $C_{30}$ AI | $C_{31}$ AI |
|---|---|---|---|---|---|---|---|---|---|---|---|---|---|---|---|---|---|---|
| EFLH-1 | 1430 | 1844 | 1362 | 1302 | 398 | 924 | 747 | 412 | 260 | 265 | 76 | 285 | ND | ND | 48 | 181 | 65 | 65 |
| EFLH-5 | 1870 | 2741 | 2472 | 2510 | 715 | 1841 | 1656 | 848 | 595 | 495 | 149 | 556 | ND | ND | 74 | 190 | 159 | 200 |
| EFLH-9 | 1695 | 2056 | 1827 | 1742 | 544 | 1235 | 1028 | 580 | 337 | 412 | 99 | 373 | ND | ND | 51 | 187 | 103 | 140 |
| EFLH-13 | 181 | 239 | 274 | 278 | 105 | 147 | 119 | 70 | 37 | 34 | 15 | 52 | ND | ND | 12 | 20 | 16 | 11 |
| EFLH-15 | 1076 | 1187 | 1076 | 1015 | 339 | 553 | 503 | 251 | 146 | 138 | 74 | 236 | ND | ND | 43 | 124 | 61 | 32 |
| EFLH-20 | 464 | 669 | 680 | 758 | 270 | 467 | 454 | 219 | 125 | 165 | 50 | 149 | ND | ND | 30 | 80 | 38 | 43 |

*Oils and condensates (Concentrations are expressed as µg biomarkers/g whole oil; ND = not determined)*

| Sample Name | $C_{13}$ AI | $C_{14}$ AI | $C_{15}$ AI | $C_{16}$ AI | $C_{17}$ AI | $C_{18}$ AI | $C_{19}$ AI | $C_{20}$ AI | $C_{21}$ AI | $C_{22}$ AI | $C_{23}$ AI | $C_{24}$ AI | $C_{25}$ AI | $C_{26}$ AI | $C_{27}$ AI | $C_{28}$ AI | $C_{30}$ AI | $C_{31}$ AI |
|---|---|---|---|---|---|---|---|---|---|---|---|---|---|---|---|---|---|---|
| NWMK-533.2 | 2716 | 1316 | 785 | 919 | 577 | 433 | 517 | 739 | 263 | 300 | ND | ND | ND | ND | ND | ND | ND | ND |
| NFMK-526-1H | 2720 | 980 | 554 | 777 | 564 | 248 | 333 | 1530 | 245 | 367 | ND | ND | ND | ND | ND | ND | ND | ND |
| MJOG-UEF | 845 | 133 | 79 | 137 | 120 | ND | 62 | 406 | 50 | 62 | ND | ND | ND | ND | ND | ND | ND | ND |
| MJOG-LEF | 658 | 97 | 95 | 171 | 195 | ND | 61 | 365 | 48 | 77 | ND | 21 | 28 | 48 | 19 | 58 | 31 | 28 |
| GREF-1-110 | ND | ND | ND | ND | ND | ND | ND | ND | ND | ND | ND | ND | ND | ND | ND | ND | ND | ND |

**O. Quantitative biomarker analysis results for monoaromatic steroids (Concentrations are expressed as µg biomarkers/g TOC; ND = not determined)**

*Lozier Canyon outcrop*

| Sample Name | Preg | 20-Mpreg | $C_{27}$ 5β-Chol (20S) | $C_{27}$ Diachol (20S) | $C_{27}$ MAS | $C_{28}$ 5β-Ergost (20S) + $C_{28}$ Diaergost (20S) | $C_{27}$ 5α-Chol (20R) | $C_{28}$ 5α-Ergost (20S) | $C_{28}$ 5β-Ergost (20R) + $C_{28}$ Diaergost (20R) | $C_{29}$ 5β-Stigmast (20S)+$C_{29}$ Diastig (20R) | $C_{29}$ 5α-Stigmast (20S) | $C_{28}$ 5α-Ergost (20R) | $C_{29}$ 5β-Stigmast (20R) + $C_{29}$ Diastigmast (20R) | $C_{29}$ 5α-Stigmast (20R) |
|---|---|---|---|---|---|---|---|---|---|---|---|---|---|---|
| EFLC-28 | 3 | 3 | 5 | 2 | 5 | 25 | 4 | 35 | 1 | 1 | 7 | 10 | 4 | 3 |
| EFLC-26 | 7 | 5 | 6 | 3 | 5 | 28 | 4 | 38 | 1 | 1 | 8 | 11 | 4 | 3 |
| EFLC-25 | 1 | 1 | 1 | 1 | 1 | 7 | 1 | 11 | 0 | 0 | 2 | 3 | 1 | 1 |
| EFLC-20 | 3 | 4 | 8 | 3 | 7 | 36 | 4 | 47 | 2 | 2 | 8 | 12 | 4 | 3 |
| EFLC-18 | 0 | 0 | 0 | 0 | 0 | 2 | 0 | 2 | 0 | 0 | 0 | 1 | 0 | 0 |
| EFLC-14 | 2 | 1 | 1 | 0 | 1 | 5 | 0 | 5 | 0 | 0 | 1 | 1 | 1 | 0 |
| EFLC-12 | 8 | 5 | 6 | 2 | 5 | 25 | 2 | 28 | 1 | 1 | 4 | 6 | 3 | 2 |
| EFLC-10 | 16 | 4 | 7 | 2 | 6 | 26 | 3 | 29 | 1 | 1 | 6 | 6 | 4 | 1 |
| EFLC-8 | 18 | 6 | 7 | 2 | 6 | 26 | 3 | 29 | 1 | 1 | 6 | 6 | 4 | 1 |
| EFLC-6 | 2 | 2 | 2 | 1 | 2 | 7 | 1 | 8 | 0 | 0 | 1 | 2 | 1 | 1 |
| EFLC-4 | 1 | 0 | 0 | 0 | 0 | 1 | 0 | 2 | 0 | 0 | 0 | 0 | 0 | 0 |
| EFLC-1 | 234 | 368 | 770 | 360 | 802 | 2825 | ND | 3665 | 100 | 91 | 489 | 856 | 337 | 155 |

*Ferguson McKnight #526-1H core*

| Sample Name | Preg | 20-Mpreg | $C_{27}$ 5β-Chol (20S) | $C_{27}$ Diachol (20S) | $C_{27}$ MAS | $C_{28}$ 5β-Ergost (20S) + $C_{28}$ Diaergost (20S) | $C_{27}$ 5α-Chol (20R) | $C_{28}$ 5α-Ergost (20S) | $C_{28}$ 5β-Ergost (20R) + $C_{28}$ Diaergost (20R) | $C_{29}$ 5β-Stigmast (20S)+$C_{29}$ Diastig (20R) | $C_{29}$ 5α-Stigmast (20S) | $C_{28}$ 5α-Ergost (20R) | $C_{29}$ 5β-Stigmast (20R) + $C_{29}$ Diastigmast (20R) | $C_{29}$ 5α-Stigmast (20R) |
|---|---|---|---|---|---|---|---|---|---|---|---|---|---|---|
| EFMK-1 | 135 | 62 | 17 | 13 | 26 | 51 | 13 | 52 | 4 | 11 | 14 | 13 | 9 | 5 |
| EFMK-4 | 75 | 36 | 8 | 5 | 11 | 21 | 6 | 21 | 2 | 5 | 6 | 5 | 3 | 2 |
| EFMK-8 | 158 | 70 | 15 | 8 | 19 | 37 | 9 | 38 | 2 | 8 | 11 | 10 | 7 | 6 |
| EFMK-12 | 72 | 35 | 7 | 4 | 9 | 20 | 5 | 20 | 2 | 4 | 6 | 7 | 2 | 2 |
| EFMK-15 | 51 | 29 | 7 | 4 | 10 | 24 | 6 | 24 | 2 | 5 | 8 | 9 | 2 | 3 |
| EFMK-17 | 166 | 92 | 30 | 16 | 44 | 102 | 24 | 104 | 7 | 19 | 34 | 23 | 18 | 12 |
| EFMK-20 | 107 | 63 | 17 | 9 | 23 | 54 | 10 | 52 | 6 | 12 | 19 | 21 | 4 | 5 |
| EFMK-23 | 109 | 62 | 18 | 8 | 26 | 50 | 11 | 51 | 6 | 14 | 21 | 21 | 5 | 6 |
| EFMK-24 | 94 | 53 | 15 | 6 | 24 | 45 | 8 | 45 | 4 | 12 | 17 | 18 | 3 | 5 |
| EFMK-25 | 56 | 30 | 7 | 3 | 13 | 27 | 6 | 21 | 3 | 6 | 9 | 6 | 4 | 2 |
| EFMK-26 | 60 | 22 | 6 | 5 | 10 | 22 | 5 | 18 | 2 | 3 | 5 | 5 | 4 | 3 |

*Bouldin Creek outcrop*

| Sample Name | Preg | 20-Mpreg | $C_{27}$ 5β-Chol (20S) | $C_{27}$ Diachol (20S) | $C_{27}$ MAS | $C_{28}$ 5β-Ergost (20S) + $C_{28}$ Diaergost (20S) | $C_{27}$ 5α-Chol (20R) | $C_{28}$ 5α-Ergost (20S) | $C_{28}$ 5β-Ergost (20R) + $C_{28}$ Diaergost (20R) | $C_{29}$ 5β-Stigmast (20S)+$C_{29}$ Diastig (20R) | $C_{29}$ 5α-Stigmast (20S) | $C_{28}$ 5α-Ergost (20R) | $C_{29}$ 5β-Stigmast (20R) + $C_{29}$ Diastigmast (20R) | $C_{29}$ 5α-Stigmast (20R) |
|---|---|---|---|---|---|---|---|---|---|---|---|---|---|---|
| EFBC-5 | 2 | 5 | 2 | 3 | 5 | 47 | 7 | 85 | 3 | 4 | 15 | 8 | 41 | 12 |
| EFBC-7 | 2 | 4 | 2 | 3 | 4 | 43 | 6 | 81 | 2 | 3 | 13 | 7 | 39 | 10 |
| EFBC-9 | 3 | 6 | 3 | 4 | 6 | 66 | 9 | 124 | 4 | 5 | 21 | 11 | 60 | 17 |
| EFBC-11 | 2 | 5 | 3 | 3 | 5 | 62 | 7 | 115 | 4 | 5 | 19 | 10 | 53 | 15 |
| EFBC-15 | 1 | 3 | 1 | 1 | 2 | 20 | 4 | 40 | 1 | 2 | 12 | 5 | 19 | 9 |
| EFBC-19 | 7 | 17 | 7 | 9 | 14 | 132 | 22 | 255 | 9 | 11 | 78 | 37 | 114 | 59 |
| EFBC-20 | 14 | 32 | 12 | 14 | 24 | 208 | 36 | 379 | 13 | 18 | 94 | 51 | 173 | 72 |
| EFBC-23 | 12 | 22 | 10 | 11 | 19 | 162 | 25 | 265 | 9 | 14 | 54 | 32 | 113 | 40 |
| EFBC-25 | 11 | 21 | 10 | 12 | 19 | 164 | 25 | 269 | 12 | 16 | 49 | 33 | 114 | 37 |
| EFBC-27 | 12 | 23 | 11 | 11 | 20 | 140 | 25 | 228 | 9 | 13 | 49 | 35 | 94 | 38 |
| EFBC-30 | 7 | 17 | 5 | 6 | 11 | 58 | 16 | 103 | 6 | 5 | 29 | 15 | 50 | 23 |
| EFBC-32 | 11 | 28 | 11 | 11 | 21 | 125 | 38 | 239 | 15 | 10 | 76 | 35 | 131 | 63 |
| EFBC-34 | 7 | 18 | 7 | 7 | 13 | 78 | 21 | 156 | 6 | 7 | 53 | 23 | 78 | 43 |

*ACC #1 core*

| Sample Name | Preg | 20-Mpreg | $C_{27}$ 5β-Chol (20S) | $C_{27}$ Diachol (20S) | $C_{27}$ MAS | $C_{28}$ 5β-Ergost (20S) + $C_{28}$ Diaergost (20S) | $C_{27}$ 5α-Chol (20R) | $C_{28}$ 5α-Ergost (20S) | $C_{28}$ 5β-Ergost (20R) + $C_{28}$ Diaergost (20R) | $C_{29}$ 5β-Stigmast (20S)+$C_{29}$ Diastig (20R) | $C_{29}$ 5α-Stigmast (20S) | $C_{28}$ 5α-Ergost (20R) | $C_{29}$ 5β-Stigmast (20R) + $C_{29}$ Diastigmast (20R) | $C_{29}$ 5α-Stigmast (20R) |
|---|---|---|---|---|---|---|---|---|---|---|---|---|---|---|
| EFAC-1 | 40 | 183 | 81 | 91 | 143 | 1382 | 237 | 3077 | 108 | 100 | 572 | 184 | 1471 | 443 |
| EFAC-3 | 72 | 216 | 72 | 91 | 139 | 1328 | 216 | 3071 | 106 | 99 | 668 | 226 | 1493 | 514 |
| EFAC-6 | 48 | 200 | 76 | 104 | 147 | 1151 | 156 | 1950 | 80 | 88 | 289 | 16 | 785 | 209 |
| EFAC-7 | 28 | 73 | 23 | 28 | 46 | 267 | 103 | 513 | 24 | 20 | 152 | 46 | 261 | 116 |
| EFAC-8 | 16 | 81 | 25 | 31 | 48 | 312 | 132 | 668 | 27 | 23 | 187 | 58 | 371 | 147 |
| EFAC-10 | 46 | 206 | 81 | 100 | 155 | 869 | 321 | 1734 | 86 | 71 | 555 | 234 | 885 | 431 |

*W. Brechtel #1 core*

| Sample Name | Preg | 20-Mpreg | $C_{27}$ 5β-Chol (20S) | $C_{27}$ Diachol (20S) | $C_{27}$ MAS | $C_{28}$ 5β-Ergost (20S) + $C_{28}$ Diaergost (20S) | $C_{27}$ 5α-Chol (20R) | $C_{28}$ 5α-Ergost (20S) | $C_{28}$ 5β-Ergost (20R) + $C_{28}$ Diaergost (20R) | $C_{29}$ 5β-Stigmast (20S)+$C_{29}$ Diastig (20R) | $C_{29}$ 5α-Stigmast (20S) | $C_{28}$ 5α-Ergost (20R) | $C_{29}$ 5β-Stigmast (20R) + $C_{29}$ Diastigmast (20R) | $C_{29}$ 5α-Stigmast (20R) |
|---|---|---|---|---|---|---|---|---|---|---|---|---|---|---|
| EFWB-1 | 941 | 1575 | 2672 | 302 | 2341 | 7283 | 2052 | 8464 | 117 | 131 | 1272 | 1503 | 1537 | 580 |
| EFWB-3 | 1041 | 2116 | 4070 | 432 | 3218 | 16606 | 3033 | 1925 | 331 | 228 | 2929 | 3202 | 6149 | 900 |
| EFWB-4 | 717 | 1466 | 2929 | 422 | 2438 | 11878 | 2449 | 13723 | 227 | 162 | 1471 | 2278 | 2313 | 719 |
| EFWB-7 | 864 | 1700 | 3315 | 456 | 2695 | 10670 | 2640 | 12025 | 188 | 126 | 1476 | 2063 | 1954 | 646 |
| EFWB-8 | 464 | 1027 | 2064 | 390 | 1774 | 7955 | 1708 | 8697 | 141 | 117 | 972 | 1414 | 1447 | 410 |
| EFWB-9 | 443 | 848 | 1267 | 163 | 1004 | 3070 | 876 | 3403 | 38 | 35 | 505 | 654 | 498 | 195 |

*C.J. Hendershot #1 core*

| Sample Name | Preg | 20-Mpreg | $C_{27}$ 5β-Chol (20S) | $C_{27}$ Diachol (20S) | $C_{27}$ MAS | $C_{28}$ 5β-Ergost (20S) + $C_{28}$ Diaergost (20S) | $C_{27}$ 5α-Chol (20R) | $C_{28}$ 5α-Ergost (20S) | $C_{28}$ 5β-Ergost (20R) + $C_{28}$ Diaergost (20R) | $C_{29}$ 5β-Stigmast (20S)+$C_{29}$ Diastig (20R) | $C_{29}$ 5α-Stigmast (20S) | $C_{28}$ 5α-Ergost (20R) | $C_{29}$ 5β-Stigmast (20R) + $C_{29}$ Diastigmast (20R) | $C_{29}$ 5α-Stigmast (20R) |
|---|---|---|---|---|---|---|---|---|---|---|---|---|---|---|
| EFHE-1 | 751 | 764 | 1125 | 263 | 1163 | 3573 | 1284 | 891 | 119 | 117 | 913 | 1147 | 769 | 432 |
| EFHE-2 | 777 | 802 | 1113 | 234 | 1161 | 3688 | 1387 | 4587 | 164 | 89 | 963 | 1173 | 836 | 472 |
| EFHE-3 | 471 | 796 | 938 | 298 | 1106 | 3881 | 6202 | 4792 | 230 | 109 | 924 | 1195 | 825 | 445 |
| EFHE-5 | 507 | 1112 | 1683 | 537 | 1719 | 8516 | 2478 | 9624 | 495 | 329 | 1407 | 2157 | 1478 | 597 |
| EFHE-6 | 424 | 1028 | 1340 | 451 | 1318 | 5683 | 1752 | 6011 | 317 | 222 | 898 | 1387 | 891 | 371 |
| EFHE-7 | 465 | 1160 | 1617 | 604 | 1650 | 7107 | 2121 | 7958 | 406 | 304 | 1099 | 1734 | 1079 | 463 |
| EFHE-9 | 363 | 853 | 1222 | 355 | 1168 | 4300 | 6046 | 4683 | 217 | 143 | 753 | 1069 | 711 | 283 |
| EFHE-10 | 210 | 464 | 591 | 208 | 596 | 1902 | 653 | 2160 | 116 | 74 | 378 | 583 | 287 | 153 |

*Fasken "A" #1 core*

| Sample Name | Preg | 20-Mpreg | $C_{27}$ 5β-Chol (20S) | $C_{27}$ Diachol (20S) | $C_{27}$ MAS | $C_{28}$ 5β-Ergost (20S) + $C_{28}$ Diaergost (20S) | $C_{27}$ 5α-Chol (20R) | $C_{28}$ 5α-Ergost (20S) | $C_{28}$ 5β-Ergost (20R) + $C_{28}$ Diaergost (20R) | $C_{29}$ 5β-Stigmast (20S)+$C_{29}$ Diastig (20R) | $C_{29}$ 5α-Stigmast (20S) | $C_{28}$ 5α-Ergost (20R) | $C_{29}$ 5β-Stigmast (20R) + $C_{29}$ Diastigmast (20R) | $C_{29}$ 5α-Stigmast (20R) |
|---|---|---|---|---|---|---|---|---|---|---|---|---|---|---|
| EFFA-1 | 4 | 1 | 0 | 0 | 0 | 1 | 1 | 0 | 0 | 0 | 0 | 0 | 0 | 0 |
| EFFA-3 | 0 | 0 | 0 | 0 | 0 | 0 | 0 | 0 | 0 | 0 | 0 | 0 | 0 | 0 |
| EFFA-5 | 14 | 5 | 1 | 1 | 2 | 5 | 1 | 5 | 0 | 1 | 1 | 1 | 1 | 0 |
| EFFA-11 | 18 | 7 | 2 | 1 | 2 | 7 | 2 | 7 | 1 | 1 | 2 | 2 | 1 | 1 |
| EFFA-17 | 14 | 4 | 1 | 1 | 2 | 5 | 1 | 4 | 0 | 1 | 1 | 1 | 1 | 0 |
| EFFA-18 | 15 | 6 | 1 | 1 | 2 | 5 | 1 | 5 | 0 | 1 | 1 | 1 | 1 | 1 |
| EFFA-20 | 3 | 1 | 0 | 0 | 0 | 1 | 0 | 1 | 0 | 0 | 0 | 0 | 0 | 0 |
| EFFA-21 | 6 | 1 | 0 | 0 | 0 | 1 | 0 | 1 | 0 | 0 | 0 | 0 | 0 | 0 |
| EFFA-23 | 10 | 2 | 1 | 0 | 1 | 2 | 0 | 2 | 0 | 0 | 0 | 1 | 0 | 0 |
| EFFA-24 | 49 | 13 | 3 | 2 | 4 | 12 | 2 | 11 | 1 | 1 | 2 | 3 | 1 | 1 |
| EFFA-28 | 34 | 9 | 2 | 2 | 2 | 8 | 1 | 8 | 1 | 1 | 2 | 2 | 1 | 1 |
| EFFA-32 | 57 | 19 | 5 | 4 | 5 | 17 | 4 | 18 | 1 | 2 | 3 | 5 | 2 | 1 |
| EFFA-37 | 9 | 2 | 0 | 0 | 0 | 2 | 0 | 2 | 0 | 0 | 0 | 0 | 0 | 0 |
| EFFA-38 | 26 | 9 | 2 | 2 | 3 | 8 | 2 | 9 | 1 | 1 | 1 | 2 | 1 | 1 |
| EFFA-40 | 7 | 2 | 1 | 1 | 1 | 2 | 1 | 2 | 0 | 0 | 0 | 1 | 0 | 0 |

*Lily Hoppess #1 core*

| Sample Name | Preg | 20-Mpreg | $C_{27}$ 5β-Chol (20S) | $C_{27}$ Diachol (20S) | $C_{27}$ MAS | $C_{28}$ 5β-Ergost (20S) + $C_{28}$ Diaergost (20S) | $C_{27}$ 5α-Chol (20R) | $C_{28}$ 5α-Ergost (20S) | $C_{28}$ 5β-Ergost (20R) + $C_{28}$ Diaergost (20R) | $C_{29}$ 5β-Stigmast (20S)+$C_{29}$ Diastig (20R) | $C_{29}$ 5α-Stigmast (20S) | $C_{28}$ 5α-Ergost (20R) | $C_{29}$ 5β-Stigmast (20R) + $C_{29}$ Diastigmast (20R) | $C_{29}$ 5α-Stigmast (20R) |
|---|---|---|---|---|---|---|---|---|---|---|---|---|---|---|
| EFLH-1 | 424 | 214 | 111 | 217 | 205 | 607 | 168 | 710 | 63 | 105 | 152 | 297 | 111 | 48 |
| EFLH-5 | 556 | 267 | 149 | 277 | 271 | 920 | 232 | 1007 | 89 | 144 | 205 | 257 | 149 | 69 |
| EFLH-9 | 446 | 208 | 111 | 212 | 202 | 600 | 150 | 708 | 62 | 102 | 159 | 207 | 98 | 62 |
| EFLH-13 | 67 | 26 | 10 | 39 | 33 | 77 | 120 | 120 | 14 | 25 | 19 | 39 | 5 | 5 |
| EFLH-15 | 221 | 126 | 59 | 170 | 138 | 431 | 121 | 543 | 66 | 108 | 127 | 172 | 65 | 44 |
| EFLH-20 | 211 | 119 | 47 | 130 | 112 | 317 | 87 | 393 | 48 | 78 | 87 | 130 | 56 | 31 |

*Oils and condensates (Concentrations are expressed as µg biomarkers/g whole oil; ND = not determined)*

| Sample Name | Preg | 20-Mpreg | $C_{27}$ 5β-Chol (20S) | $C_{27}$ Diachol (20S) | $C_{27}$ MAS | $C_{28}$ 5β-Ergost (20S) + $C_{28}$ Diaergost (20S) | $C_{27}$ 5α-Chol (20R) | $C_{28}$ 5α-Ergost (20S) | $C_{28}$ 5β-Ergost (20R) + $C_{28}$ Diaergost (20R) | $C_{29}$ 5β-Stigmast (20S)+$C_{29}$ Diastig (20R) | $C_{29}$ 5α-Stigmast (20S) | $C_{28}$ 5α-Ergost (20R) | $C_{29}$ 5β-Stigmast (20R) + $C_{29}$ Diastigmast (20R) | $C_{29}$ 5α-Stigmast (20R) |
|---|---|---|---|---|---|---|---|---|---|---|---|---|---|---|
| NWMK-533.2 | 572 | 207 | 70 | 57 | 92 | 240 | 45 | 234 | 19 | 47 | 72 | 74 | 21 | 28 |
| NFMK-526-1H | 398 | 110 | 33 | 9 | 51 | 98 | 24 | 94 | 8 | 12 | 48 | 18 | 28 | 14 |
| MJOG-UEF | 91 | 24 | 3 | 5 | 6 | 13 | 6 | 17 | 5 | 4 | 14 | 4 | 8 | 4 |
| MJOG-LEF | 163 | 33 | 5 | 5 | 9 | 17 | 6 | 20 | 4 | 11 | 16 | 4 | 10 | 4 |
| GREF-1-110 | ND | ND | ND | ND | ND | ND | ND | ND | ND | ND | ND | ND | ND | ND |

**P. Quantitative biomarker analysis results for phenanthrenes and triaromatic steroids (Concentrations are expressed as µg biomarkers/g TOC; ND = not determined)**

*Lozier Canyon outcrop*

| Sample Name | P | 3-MP | 2-MP | 9+4-MP | 1-MP | $C_{20}$ Preg | $C_{21}$ 20-Mpreg | $C_{26}$ Chol (20S) | $C_{26}$ Chol (20R) + $C_{27}$ Ergost (20S) | $C_{28}$ Stig (20S) | $C_{27}$ Ergost (20R) | $C_{28}$ Stig (20R) |
|---|---|---|---|---|---|---|---|---|---|---|---|---|
| EFLC-28 | 4004 | 262 | 472 | 505 | 597 | 32 | 33 | 41 | 194 | 115 | 117 | 117 |
| EFLC-26 | 6639 | 195 | 448 | 415 | 518 | 24 | 30 | 32 | 159 | 94 | 96 | 86 |
| EFLC-25 | 3184 | 158 | 331 | 369 | 439 | 30 | 37 | 50 | 249 | 165 | 155 | 155 |
| EFLC-20 | 5217 | 233 | 521 | 538 | 652 | 34 | 45 | 83 | 441 | 201 | 283 | 190 |
| EFLC-18 | 2940 | 61 | 166 | 123 | 189 | 18 | 15 | 12 | 68 | 28 | 38 | 22 |
| EFLC-14 | 1751 | 71 | 148 | 128 | 164 | 34 | 14 | 9 | 48 | 18 | 28 | 13 |
| EFLC-12 | 11659 | 3573 | 4252 | 6133 | 4792 | 801 | 390 | 568 | 3081 | 948 | 2024 | 799 |
| EFLC-10 | 5357 | 1597 | 2100 | 2544 | 2036 | 120 | 95 | 108 | 525 | 179 | 335 | 146 |
| EFLC-8 | 6408 | 975 | 1556 | 1673 | 1580 | 228 | 46 | 59 | 263 | 97 | 163 | 74 |
| EFLC-6 | 11033 | 2094 | 3149 | 3792 | 3298 | 274 | 161 | 192 | 819 | 279 | 525 | 238 |
| EFLC-4 | 1683 | 47 | 107 | 84 | 105 | 55 | 10 | 10 | 50 | 18 | 30 | 15 |
| EFLC-1 | 1591 | 1064 | 989 | 2465 | 1153 | 1375 | 1312 | 2423 | 8984 | 2652 | 5384 | 2566 |

*Ferguson McKnight #526-1H core*

| Sample Name | P | 3-MP | 2-MP | 9+4-MP | 1-MP | $C_{20}$ Preg | $C_{21}$ 20-Mpreg | $C_{26}$ Chol (20S) | $C_{26}$ Chol (20R) + $C_{27}$ Ergost (20S) | $C_{28}$ Stig (20S) | $C_{27}$ Ergost (20R) | $C_{28}$ Stig (20R) |
|---|---|---|---|---|---|---|---|---|---|---|---|---|
| EFMK-1 | 6280 | 3977 | 4734 | 6788 | 5027 | 462 | 622 | 82 | 311 | 182 | 206 | 175 |
| EFMK-4 | 7852 | 4257 | 5607 | 8187 | 5809 | 494 | 616 | 48 | 196 | 119 | 143 | 117 |
| EFMK-8 | 15290 | 10216 | 12489 | 19042 | 12212 | 1063 | 960 | 66 | 268 | 194 | 195 | 177 |
| EFMK-12 | 9036 | 5134 | 6768 | 9851 | 7226 | 476 | 527 | 35 | 140 | 97 | 108 | 93 |
| EFMK-15 | 3974 | 2692 | 3413 | 5070 | 3623 | 316 | 394 | 28 | 136 | 87 | 99 | 83 |
| EFMK-17 | 16140 | 10525 | 13369 | 19619 | 14079 | 1083 | 1330 | 116 | 489 | 311 | 343 | 272 |
| EFMK-20 | 11271 | 7357 | 9545 | 13832 | 9990 | 781 | 966 | 65 | 315 | 218 | 231 | 208 |
| EFMK-23 | 11624 | 7908 | 10406 | 15083 | 10664 | 853 | 1037 | 85 | 363 | 272 | 254 | 235 |
| EFMK-24 | 10489 | 7015 | 9423 | 14465 | 9922 | 768 | 901 | 66 | 294 | 226 | 210 | 196 |
| EFMK-25 | 8998 | 6077 | 8574 | 12678 | 9015 | 695 | 767 | 56 | 242 | 142 | 182 | 131 |
| EFMK-26 | 115578 | 80223 | 110884 | 161085 | 117384 | 6826 | 6771 | 432 | 1861 | 1092 | 1325 | 1322 |

*Fasken "A" #1 core*

| Sample Name | P | 3-MP | 2-MP | 9+4-MP | 1-MP | $C_{20}$ Preg | $C_{21}$ 20-Mpreg | $C_{26}$ Chol (20S) | $C_{26}$ Chol (20R) + $C_{27}$ Ergost (20S) | $C_{28}$ Stig (20S) | $C_{27}$ Ergost (20R) | $C_{28}$ Stig (20R) |
|---|---|---|---|---|---|---|---|---|---|---|---|---|
| EFFA-1 | 1598 | 659 | 805 | 419 | 338 | 2 | 1 | 0 | 0 | 0 | 0 | 0 |
| EFFA-3 | 2364 | 1013 | 1123 | 734 | 506 | 7 | 4 | 0 | 2 | 1 | 1 | 1 |
| EFFA-5 | 2872 | 1348 | 1524 | 1042 | 832 | 11 | 4 | 1 | 2 | 1 | 1 | 1 |
| EFFA-11 | 2748 | 1435 | 1678 | 1161 | 951 | 15 | 7 | 1 | 3 | 2 | 2 | 1 |
| EFFA-17 | 1945 | 909 | 1023 | 759 | 538 | 7 | 3 | 0 | 1 | 1 | 1 | 1 |
| EFFA-18 | 2864 | 1358 | 1569 | 1132 | 845 | 12 | 6 | 1 | 2 | 1 | 1 | 1 |
| EFFA-20 | 453 | 203 | 239 | 163 | 122 | 1 | 1 | 0 | 0 | 0 | 0 | 0 |
| EFFA-21 | 909 | 347 | 385 | 254 | 175 | 2 | 1 | 0 | 0 | 0 | 0 | 0 |
| EFFA-23 | 1178 | 530 | 605 | 430 | 305 | 3 | 1 | 0 | 1 | 0 | 0 | 0 |
| EFFA-24 | 3833 | 1864 | 1910 | 1616 | 1058 | 15 | 5 | 1 | 3 | 2 | 2 | 2 |
| EFFA-28 | 3107 | 1485 | 1540 | 1241 | 851 | 12 | 4 | 1 | 2 | 2 | 1 | 1 |
| EFFA-32 | 4203 | 2179 | 2310 | 1912 | 1271 | 18 | 8 | 1 | 4 | 3 | 2 | 2 |
| EFFA-37 | 1642 | 552 | 627 | 389 | 261 | 2 | 1 | 0 | 0 | 0 | 0 | 0 |
| EFFA-38 | 2828 | 1542 | 1632 | 1347 | 954 | 10 | 4 | 1 | 3 | 2 | 1 | 1 |
| EFFA-40 | 1043 | 449 | 493 | 361 | 245 | 3 | 2 | 0 | 1 | 0 | 0 | 0 |

*Bouldin Creek outcrop*

| Sample Name | P | 3-MP | 2-MP | 9+4-MP | 1-MP | $C_{20}$ Preg | $C_{21}$ 20-Mpreg | $C_{26}$ Chol (20S) | $C_{26}$ Chol (20R) + $C_{27}$ Ergost (20S) | $C_{28}$ Stig (20S) | $C_{27}$ Ergost (20R) | $C_{28}$ Stig (20R) |
|---|---|---|---|---|---|---|---|---|---|---|---|---|
| EFBC-5 | 15 | 7 | 5 | 16 | 12 | 3 | 1 | 2 | 13 | 4 | 7 | 3 |
| EFBC-7 | 11 | 4 | 4 | 8 | 7 | 2 | 1 | 1 | 9 | 3 | 5 | 2 |
| EFBC-9 | 15 | 6 | 5 | 12 | 10 | 2 | 1 | 1 | 13 | 4 | 7 | 3 |
| EFBC-11 | 7 | 4 | 3 | 8 | 7 | 2 | 1 | 1 | 11 | 3 | 6 | 2 |
| EFBC-15 | 19 | 5 | 6 | 10 | 10 | 2 | 2 | 2 | 12 | 5 | 7 | 3 |
| EFBC-19 | 53 | 6 | 6 | 15 | 13 | 2 | 1 | 1 | 10 | 5 | 6 | 4 |
| EFBC-20 | 19 | 4 | 4 | 11 | 12 | 2 | 1 | 1 | 9 | 4 | 5 | 4 |
| EFBC-23 | 27 | 4 | 5 | 10 | 9 | 2 | 1 | 1 | 9 | 3 | 5 | 3 |
| EFBC-25 | 17 | 4 | 5 | 11 | 9 | 2 | 1 | 1 | 10 | 4 | 6 | 3 |
| EFBC-27 | 11 | 6 | 7 | 18 | 13 | 3 | 1 | 2 | 11 | 5 | 6 | 3 |
| EFBC-30 | 6 | 3 | 4 | 9 | 6 | 1 | 1 | 1 | 3 | 1 | 2 | 2 |
| EFBC-32 | 7 | 5 | 6 | 13 | 9 | 2 | 1 | 1 | 7 | 3 | 4 | 3 |
| EFBC-34 | 11 | 8 | 9 | 17 | 10 | 2 | 1 | 1 | 7 | 3 | 4 | 2 |

*ACC #1 core*

| Sample Name | P | 3-MP | 2-MP | 9+4-MP | 1-MP | $C_{20}$ Preg | $C_{21}$ 20-Mpreg | $C_{26}$ Chol (20S) | $C_{26}$ Chol (20R) + $C_{27}$ Ergost (20S) | $C_{28}$ Stig (20S) | $C_{27}$ Ergost (20R) | $C_{28}$ Stig (20R) |
|---|---|---|---|---|---|---|---|---|---|---|---|---|
| EFAC-1 | 90 | 15 | 16 | 25 | 31 | 3 | 2 | 2 | 14 | 5 | 8 | 4 |
| EFAC-3 | 65 | 11 | 12 | 17 | 23 | 2 | 3 | 1 | 12 | 5 | 7 | 3 |
| EFAC-6 | 35 | 8 | 8 | 14 | 12 | 4 | 2 | 2 | 11 | 4 | 7 | 3 |
| EFAC-7 | 56 | 10 | 11 | 16 | 17 | 2 | 3 | 1 | 7 | 3 | 4 | 2 |
| EFAC-8 | 25 | 7 | 8 | 12 | 16 | 2 | 2 | 1 | 6 | 3 | 4 | 2 |
| EFAC-10 | 155 | 39 | 38 | 41 | 59 | 4 | 3 | 1 | 9 | 4 | 5 | 3 |

*W. Brechtel #1 core*

| Sample Name | P | 3-MP | 2-MP | 9+4-MP | 1-MP | $C_{20}$ Preg | $C_{21}$ 20-Mpreg | $C_{26}$ Chol (20S) | $C_{26}$ Chol (20R) + $C_{27}$ Ergost (20S) | $C_{28}$ Stig (20S) | $C_{27}$ Ergost (20R) | $C_{28}$ Stig (20R) |
|---|---|---|---|---|---|---|---|---|---|---|---|---|
| EFWB-1 | 572 | 200 | 272 | 215 | 247 | 45 | 70 | 106 | 387 | 119 | 242 | 285 |
| EFWB-3 | 699 | 215 | 306 | 242 | 248 | 77 | 110 | 207 | 1054 | 244 | 715 | 451 |
| EFWB-4 | 530 | 169 | 227 | 197 | 191 | 67 | 100 | 194 | 916 | 232 | 611 | 348 |
| EFWB-7 | 9181 | 3431 | 4616 | 6977 | 4599 | 135 | 154 | 258 | 1061 | 289 | 695 | 555 |
| EFWB-8 | 4264 | 1092 | 1526 | 2211 | 1630 | 82 | 105 | 205 | 887 | 232 | 579 | 372 |
| EFWB-9 | 6754 | 2980 | 4187 | 6302 | 4020 | 297 | 217 | 90 | 356 | 120 | 228 | 186 |

*C.J. Hendershot #1 core*

| Sample Name | P | 3-MP | 2-MP | 9+4-MP | 1-MP | $C_{20}$ Preg | $C_{21}$ 20-Mpreg | $C_{26}$ Chol (20S) | $C_{26}$ Chol (20R) + $C_{27}$ Ergost (20S) | $C_{28}$ Stig (20S) | $C_{27}$ Ergost (20R) | $C_{28}$ Stig (20R) |
|---|---|---|---|---|---|---|---|---|---|---|---|---|
| EFHE-1 | 219 | 89 | 79 | 121 | 84 | 29 | 24 | 41 | 150 | 48 | 82 | 46 |
| EFHE-2 | 172 | 78 | 62 | 110 | 77 | 26 | 20 | 35 | 132 | 41 | 74 | 40 |
| EFHE-3 | 186 | 80 | 70 | 114 | 80 | 29 | 21 | 34 | 148 | 40 | 88 | 50 |
| EFHE-5 | 162 | 71 | 57 | 110 | 79 | 45 | 40 | 91 | 452 | 108 | 263 | 104 |
| EFHE-6 | 115 | 54 | 41 | 84 | 60 | 42 | 39 | 84 | 348 | 85 | 206 | 79 |
| EFHE-7 | 157 | 72 | 56 | 115 | 80 | 53 | 48 | 106 | 450 | 111 | 257 | 105 |
| EFHE-9 | 223 | 93 | 69 | 131 | 93 | 3 | 45 | 105 | 391 | 92 | 225 | 91 |
| EFHE-10 | 588 | 231 | 232 | 427 | 289 | 36 | 24 | 54 | 162 | 48 | 84 | 47 |

*Lily Hoppess #1 core*

| Sample Name | P | 3-MP | 2-MP | 9+4-MP | 1-MP | $C_{20}$ Preg | $C_{21}$ 20-Mpreg | $C_{26}$ Chol (20S) | $C_{26}$ Chol (20R) + $C_{27}$ Ergost (20S) | $C_{28}$ Stig (20S) | $C_{27}$ Ergost (20R) | $C_{28}$ Stig (20R) |
|---|---|---|---|---|---|---|---|---|---|---|---|---|
| EFLH-1 | 1905 | 883 | 780 | 1519 | 1087 | 186 | 152 | 127 | 468 | 304 | 244 | 250 |
| EFLH-5 | 1722 | 788 | 707 | 1366 | 1025 | 143 | 115 | 89 | 378 | 217 | 204 | 174 |
| EFLH-9 | 3044 | 1257 | 1147 | 2181 | 1685 | 59 | 140 | 91 | 371 | 247 | 197 | 203 |
| EFLH-13 | 906 | 382 | 353 | 628 | 529 | 42 | 28 | 12 | 41 | 30 | 23 | 24 |
| EFLH-15 | 2158 | 883 | 848 | 1441 | 1195 | 100 | 77 | 41 | 168 | 130 | 91 | 101 |
| EFLH-20 | 2170 | 894 | 826 | 1524 | 1174 | 127 | 87 | 42 | 183 | 151 | 99 | 114 |

*Oils and condensates (Concentrations are expressed as µg biomarkers/g whole oil; ND = not determined)*

| Sample Name | P | 3-MP | 2-MP | 9+4-MP | 1-MP | $C_{20}$ Preg | $C_{21}$ 20-Mpreg | $C_{26}$ Chol (20S) | $C_{26}$ Chol (20R) + $C_{27}$ Ergost (20S) | $C_{28}$ Stig (20S) | $C_{27}$ Ergost (20R) | $C_{28}$ Stig (20R) |
|---|---|---|---|---|---|---|---|---|---|---|---|---|
| NWMK-533.2 | 8110 | 4994 | 5447 | 10290 | 6419 | 686 | 628 | 38 | 198 | 119 | 111 | 87 |
| NFMK-526-1H | 4123 | 3144 | 3984 | 7703 | 4513 | 335 | 292 | 12 | 59 | 33 | 35 | 24 |
| MJOG-UEF | 5738 | 4506 | 5535 | 8830 | 5914 | 180 | 110 | 4 | 6 | 7 | 9 | 3 |
| MJOG-LEF | 8507 | 6263 | 7283 | 9639 | 6863 | 234 | 166 | 4 | 4 | 6 | 6 | 3 |
| GREF-1-110 | 13775 | 7404 | 8028 | 7589 | 5555 | 50 | 62 | ND | ND | ND | ND | ND |

**Q. $\delta^{13}C$ values for *n*-alkanes of Eagle Ford Shale bitumens and oils analyzed in this study. $\delta^{13}C$ values are expresses in per mil (‰) relative to the Vienna Pee Dee belemnite (VPDB) standard**

*Lozier Canyon outcrop*

| | $C_{12}$ | $C_{13}$ | $C_{14}$ | $C_{15}$ | $C_{16}$ | $C_{17}$ | Pr | $C_{18}$ | Ph | $C_{19}$ | $C_{20}$ | $C_{21}$ | $C_{22}$ | $C_{23}$ | $C_{24}$ | $C_{25}$ | $C_{26}$ | $C_{27}$ | $C_{28}$ | $C_{29}$ | $C_{30}$ | $C_{31}$ |
|---|---|---|---|---|---|---|---|---|---|---|---|---|---|---|---|---|---|---|---|---|---|---|
| **EFLC-28** | | | | | -29.3 | -29.4 | -29.6 | -29.3 | -30.5 | -29.4 | -28.7 | -29.7 | -30.1 | -30.1 | -28.8 | -29.2 | -29.5 | -29.1 | -27.5 | | | |
| **EFLC-26** | | | | -23.3 | -26.7 | -27 | -27.5 | -26.7 | -28.7 | -26.8 | -28.2 | -27.8 | -27.3 | -28.3 | -27.9 | -28 | -27.7 | -27.3 | -25.6 | | | |
| **EFLC-20** | | | | | | | | | | | | | | | | | -32.7 | | -34 | | | |
| **EFLC-14** | | | -31.2 | -30.4 | -30.6 | -29.9 | -30.2 | -30.1 | -30.7 | -30.1 | -30 | -30.3 | -30.6 | -30.7 | -30.6 | -31.3 | -30.3 | -30.1 | -30.8 | -31.4 | | |
| **EFLC-10** | | -31.5 | -32.4 | -30.7 | -31 | -31 | -31.1 | -30.6 | -31.9 | -32.5 | -30.5 | -31.5 | -31.6 | -31.7 | -31.2 | -32 | -31.6 | -32 | -31.3 | -31.3 | | |
| **EFLC-8** | | -31.5 | -31.7 | -30.8 | -31 | -31.1 | -30.7 | -31.2 | -32 | -31.6 | -31.1 | -31.5 | -31.1 | -31.3 | -31.2 | -30.5 | -31.7 | -31 | -30.8 | -28.1 | | |

*Ferguson McKnight #526-1H core*

| | $C_{12}$ | $C_{13}$ | $C_{14}$ | $C_{15}$ | $C_{16}$ | $C_{17}$ | Pr | $C_{18}$ | Ph | $C_{19}$ | $C_{20}$ | $C_{21}$ | $C_{22}$ | $C_{23}$ | $C_{24}$ | $C_{25}$ | $C_{26}$ | $C_{27}$ | $C_{28}$ | $C_{29}$ | $C_{30}$ | $C_{31}$ |
|---|---|---|---|---|---|---|---|---|---|---|---|---|---|---|---|---|---|---|---|---|---|---|
| **EFMK-1** | | | | -29.2 | -29.0 | -29.4 | -31.0 | -30.1 | -30.0 | -29.6 | -30.2 | -30.0 | -29.7 | -30.7 | | | | | | | | |
| **EFMK-24** | | -31.0 | -30.5 | -30.1 | -29.8 | -29.6 | -30.3 | -29.8 | -30.4 | -30.2 | -30.1 | -30.3 | -29.3 | -30.8 | -30.5 | -29.3 | -30.6 | -31.6 | | | | |
| **EFMK-25** | | | -29.9 | -29.8 | -30.2 | -29.7 | -30.2 | -29.8 | -30.2 | -30.0 | -29.7 | -30.1 | -30.3 | -30.6 | -31.4 | -27.8 | -31.1 | | | | | |

*Fasken "A" #1 core*

| | $C_{12}$ | $C_{13}$ | $C_{14}$ | $C_{15}$ | $C_{16}$ | $C_{17}$ | Pr | $C_{18}$ | Ph | $C_{19}$ | $C_{20}$ | $C_{21}$ | $C_{22}$ | $C_{23}$ | $C_{24}$ | $C_{25}$ | $C_{26}$ | $C_{27}$ | $C_{28}$ | $C_{29}$ | $C_{30}$ | $C_{31}$ |
|---|---|---|---|---|---|---|---|---|---|---|---|---|---|---|---|---|---|---|---|---|---|---|
| **EFFA-3** | -31.2 | -30.0 | -30.9 | -29.3 | -29.3 | -29.5 | -30.5 | -29.4 | -31.3 | -30.2 | -30.1 | -30.6 | -30.7 | -30.1 | -29.9 | -30.2 | | | | | | |
| **EFFA-18** | | -30.2 | -30.7 | -29.3 | -29.2 | -29.3 | -30.2 | -29.3 | -31.3 | -30.6 | -30.4 | -30.1 | -29.8 | -30.2 | -30.5 | -29.9 | | | | | | |
| **EFFA-21** | | -29.8 | -29.3 | -29.2 | -29.9 | -29.3 | -29.9 | -30.2 | -30.2 | -29.6 | -30.4 | -30.2 | -29.6 | -30.3 | -30.0 | -32.3 | | | | | | |
| **EFFA-24** | -28.9 | -30.2 | -30.6 | -30.1 | -30.2 | -29.7 | -30.6 | -30.0 | -30.8 | -30.6 | -29.7 | -30.2 | -30.1 | -30.3 | -29.8 | -30.6 | -29.7 | -30.2 | -30.7 | -30.0 | -29.9 | -30.4 |
| **EFFA-40** | | | -29.9 | -29.6 | -29.6 | -29.3 | -29.8 | -29.4 | -30.6 | -30.4 | -29.4 | -29.7 | -29.5 | -29.9 | | | | | | | | |

*Bouldin Creek outcrop*

| | $C_{12}$ | $C_{13}$ | $C_{14}$ | $C_{15}$ | $C_{16}$ | $C_{17}$ | Pr | $C_{18}$ | Ph | $C_{19}$ | $C_{20}$ | $C_{21}$ | $C_{22}$ | $C_{23}$ | $C_{24}$ | $C_{25}$ | $C_{26}$ | $C_{27}$ | $C_{28}$ | $C_{29}$ | $C_{30}$ | $C_{31}$ |
|---|---|---|---|---|---|---|---|---|---|---|---|---|---|---|---|---|---|---|---|---|---|---|
| **EFBC-5** | | | | | | -33.7 | -31.8 | -33.1 | -30.7 | -34.5 | -32.2 | -32.3 | -31.3 | -29.7 | -32.5 | -32.1 | | | | | | |
| **EFBC-20** | | | | | | -32.2 | -32.3 | -33.2 | -31.3 | -33.0 | -32.1 | -32.0 | -30.8 | -30.3 | -31.2 | -30.6 | | | | | | |
| **EFBC-25** | | | | -34.4 | -33.0 | -33.5 | -32.2 | -33.5 | -31.3 | -34.2 | -31.6 | -32.8 | -31.1 | -29.9 | -32.0 | -32.0 | | | | | | |

*ACC #1 core*

| | $C_{12}$ | $C_{13}$ | $C_{14}$ | $C_{15}$ | $C_{16}$ | $C_{17}$ | Pr | $C_{18}$ | Ph | $C_{19}$ | $C_{20}$ | $C_{21}$ | $C_{22}$ | $C_{23}$ | $C_{24}$ | $C_{25}$ | $C_{26}$ | $C_{27}$ | $C_{28}$ | $C_{29}$ | $C_{30}$ | $C_{31}$ |
|---|---|---|---|---|---|---|---|---|---|---|---|---|---|---|---|---|---|---|---|---|---|---|
| **EFAC-1** | | | | | | -31.2 | -32.4 | -31.5 | -31.4 | -32.2 | -31.4 | -30.1 | -29.9 | -30.2 | -30.3 | -30.8 | -30.4 | | | | | |
| **EFAC-7** | | | | | -30.6 | -31.7 | -32.7 | -31.9 | -31.6 | -32.9 | -31.8 | -31.7 | -30.4 | -30.9 | -30.3 | -32.3 | | | | | | |
| **EFAC-10** | | | | | -31.2 | -32.0 | -32.1 | -32.4 | -31.6 | -34.0 | -33.3 | -32.5 | -31.5 | -31.7 | -32.3 | -32.2 | | | | | | |

*W. Brechtel #1 core*

| | $C_{12}$ | $C_{13}$ | $C_{14}$ | $C_{15}$ | $C_{16}$ | $C_{17}$ | Pr | $C_{18}$ | Ph | $C_{19}$ | $C_{20}$ | $C_{21}$ | $C_{22}$ | $C_{23}$ | $C_{24}$ | $C_{25}$ | $C_{26}$ | $C_{27}$ | $C_{28}$ | $C_{29}$ | $C_{30}$ | $C_{31}$ |
|---|---|---|---|---|---|---|---|---|---|---|---|---|---|---|---|---|---|---|---|---|---|---|
| **EFWB-1** | | | | | -31.3 | -30.2 | -30.7 | -30.8 | -31.3 | -31.8 | -30.4 | -30.0 | -29.9 | -31.3 | -31.2 | -31.8 | -30.5 | | | | | |
| **EFWB-3** | | | | | -31.9 | -31.1 | -32.4 | -32.0 | -32.7 | -34.0 | -30.7 | -31.2 | -30.7 | -32.9 | -30.8 | -31.4 | -30.7 | | | | | |
| **EFWB-7** | | | | | -33.2 | -31.7 | -32.1 | -32.3 | -33.1 | -34.0 | -31.1 | -31.1 | -30.2 | -30.4 | -30.9 | -31.9 | -32.6 | | | | | |
| **EFWB-8** | | | | | -31.4 | -30.4 | -31.8 | -31.0 | -32.8 | -31.9 | -31.0 | -30.3 | -29.9 | -30.7 | -29.8 | -30.5 | -29.6 | | | | | |

*C.J. Hendershot #1 core*

| | $C_{12}$ | $C_{13}$ | $C_{14}$ | $C_{15}$ | $C_{16}$ | $C_{17}$ | Pr | $C_{18}$ | Ph | $C_{19}$ | $C_{20}$ | $C_{21}$ | $C_{22}$ | $C_{23}$ | $C_{24}$ | $C_{25}$ | $C_{26}$ | $C_{27}$ | $C_{28}$ | $C_{29}$ | $C_{30}$ | $C_{31}$ |
|---|---|---|---|---|---|---|---|---|---|---|---|---|---|---|---|---|---|---|---|---|---|---|
| **EFHE-1** | | | -30.6 | -30.5 | -29.7 | -30.3 | -30.7 | -31.8 | -29.9 | -30.7 | -31.6 | -33.0 | -30.2 | -30.1 | -30.0 | -30.0 | -30.1 | | | | | |
| **EFHE-5** | | | -32.2 | -30.7 | -31.9 | -31.4 | -32.2 | -31.5 | -32.3 | -32.6 | -30.8 | -32.1 | -31.6 | -32.6 | -31.8 | -31.0 | -31.8 | | | | | |
| **EFHE-7** | | | -31.7 | -31.4 | -33.4 | -31.1 | -32.0 | -31.6 | -32.3 | -34.2 | -31.8 | -32.1 | -31.8 | -33.7 | -31.5 | -31.9 | -32.3 | | | | | |
| **EFHE-9** | | | -32.2 | -32.5 | -33.6 | -32.5 | -31.8 | -32.0 | -32.1 | -33.3 | -32.0 | -33.1 | -32.2 | -34.4 | -32.1 | -33.1 | -32.8 | | | | | |
| **EFHE-10** | | | | -32.4 | -31.9 | -31.7 | -32.0 | -32.1 | -32.3 | -33.1 | -32.5 | -33.2 | -33.1 | -34.4 | -32.6 | -32.5 | -32.3 | -32.4 | -32.0 | -32.0 | -34.3 | |

*Lily Hoppess #1 core*

| | $C_{12}$ | $C_{13}$ | $C_{14}$ | $C_{15}$ | $C_{16}$ | $C_{17}$ | Pr | $C_{18}$ | Ph | $C_{19}$ | $C_{20}$ | $C_{21}$ | $C_{22}$ | $C_{23}$ | $C_{24}$ | $C_{25}$ | $C_{26}$ | $C_{27}$ | $C_{28}$ | $C_{29}$ | $C_{30}$ | $C_{31}$ |
|---|---|---|---|---|---|---|---|---|---|---|---|---|---|---|---|---|---|---|---|---|---|---|
| **EFLH-5** | | | -31.9 | -31.4 | -30.1 | -31.2 | -29.9 | -31.3 | -29.7 | -33.6 | -32.0 | -32.3 | -32.4 | -31.5 | -30.9 | -30.9 | -31.1 | -27.1 | -30.0 | | | |
| **EFLH-13** | | | | -32.0 | -32.2 | -32.0 | -31.9 | -32.1 | -31.8 | -31.9 | -32.3 | -32.7 | -32.4 | -32.6 | -32.2 | -31.6 | -31.7 | -32.8 | -31.1 | -31.8 | -30.6 | |
| **EFLH-20** | | -31.3 | -32.7 | -31.7 | -32.0 | -32.2 | -32.0 | -32.2 | -31.6 | -32.0 | -32.5 | -33.4 | -32.8 | -33.3 | -32.5 | -32.3 | -32.7 | -34.3 | -32.3 | -32.1 | -32.4 | -35.0 |

*Oils and condensates*

| | $C_{11}$ | $C_{12}$ | $C_{13}$ | $C_{14}$ | $C_{15}$ | $C_{16}$ | $C_{17}$ | Pr | $C_{18}$ | Ph | $C_{19}$ | $C_{20}$ | $C_{21}$ | $C_{22}$ | $C_{23}$ | $C_{24}$ | $C_{25}$ | $C_{26}$ | $C_{27}$ | $C_{28}$ | $C_{29}$ |
|---|---|---|---|---|---|---|---|---|---|---|---|---|---|---|---|---|---|---|---|---|---|
| **NWMK-533.2** | | -29.6 | -31.7 | -32.3 | -31.6 | -30.1 | -32.5 | -31.1 | -32.2 | -31.0 | -31.0 | -30.7 | -31.3 | -30.6 | -31.2 | -31.7 | -31.8 | -31.8 | -29.7 | -32.0 | |
| **NFMK-526-1H** | | -28.6 | -31.8 | -32.7 | -30.7 | -30.0 | -31.3 | -29.6 | -31.6 | -30.2 | -29.7 | -30.2 | -31.2 | -30.0 | -31.3 | -31.4 | -28.7 | | | | |
| **MJOG-UEF** | -28.8 | -28.1 | -31.3 | -31.1 | -30.0 | -30.4 | -30.5 | -30.6 | -30.2 | -31.2 | -31.1 | -30.2 | -30.3 | -30.1 | -30.5 | -30.0 | -30.5 | -29.8 | -28.9 | -30.1 | |
| **MJOG-LEF** | -30.4 | -27.7 | -29.4 | -31.2 | -29.9 | -30.4 | -31.6 | -32.0 | -31.2 | -31.5 | -30.7 | -31.3 | -30.6 | -30.0 | -30.8 | -30.7 | -30.7 | -30.8 | -30.0 | -31.3 | -29.4 |
| **GREF-1-110** | -28.5 | -26.6 | -28.4 | -30.4 | -28.9 | -29.6 | -29.4 | -30.1 | -30.5 | -29.3 | -28.3 | -29.7 | -29.9 | -29.6 | -29.9 | -30.2 | -29.6 | -30.5 | -28.2 | | |